Aerospace Engineering 483
Aerospace System Design

*/N-/8-CR*

*73934*

Atmospheric, Oceanic &
Space Sciences 605
Satellite System Design

*P. /99*

The University of Michigan

# Project MEDSAT

## The Design of a Remote Sensing Platform for Malaria Research and Control

NASA/USRA
April 1991

# TABLE OF CONTENTS

# ABSTRACT

Last year the World Health Organization reported that the threat of vector-borne diseases is worsening and that nearly half a billion people -- one in every ten -- in the world suffer from such diseases. Malaria is the largest contributor with about 270 million cases this year. Thus, project MEDSAT was proposed with the specific goal of designing a satellite to remotely sense pertinent information useful in establishing strategies to control malaria.

The 340 kg MEDSAT satellite is to be inserted into circular earth orbit aboard the Pegasus Air-Launched Space Booster at an inclination of 21 degrees and an altitude of 473 km. It is equipped with a synthetic aperture radar and a visible/thermal/infrared sensor to remotely sense conditions at the target area of Chiapas, Mexico. The orbit is designed so that MEDSAT will pass over the target site twice each day. The data from each scan will be downlinked to Hawaii for processing resulting in maps indicating areas of high malaria risk .These will be distributed to health officials at the target site.

A relatively inexpensive launch by Pegasus and a design using mainly proven, off-the-shelf technology permit a low mission cost, while innovations in the satellite controls and the scientific instruments allow a fairly complex mission.

Preface

## FOREWORD

Aerospace Engineering 483, "Aerospace System Design", is one of a number of design courses available to students in Aerospace Engineering at The University of Michigan. In this course, each year a different topic is selected for the preliminary design study, which is carried out by the entire class as a team effort. There are no exams or quizzes in this course, but the total output of the study consists of three parts: a) a formal oral presentation at the end of the semester, b) a scale model of the design, and c) a final report. The MEDSAT satellite system is one of two designs completed this term and the thirty-fifth in the series, started in 1965 by the late Professor Wilbur C. Nelson.

The specific goal of the MEDSAT satellite is its ability to remotely sense pertinent information useful in establishing strategies to control malaria. In March of 1990 the World Health Organization reported that the threat of vector-borne diseases is worsening and that nearly half a billion people -- one in every ten -- in the world suffer from such diseases. Malaria is the largest contributor with about 270 million cases this year. Thus the goal of MEDSAT is well justified and the potential payoff is very large indeed.

Inspiration for the MEDSAT concept was provided by scientists from the Earth System Science Division of the NASA Ames Research Center who, encouraged by the results of the Biological Monitoring and Disease Control Program (DI-MOD), suggested a preliminary design study of a MEDSAT-type satellite. On the other hand, the Aerospace Engineering design class, intrigued by the recently proven capability of the Pegasus Air-Launched Space Booster, was looking for a good application for a light satellite, so launched into a low earth orbit.

Project MEDSAT was carried out in a truly interdisciplinary spirit. In addition to the Aerospace Engineers (who were primarily responsible for the spacecraft engineering: its configuration, launch, and management) the design team included students enrolled in Atmospheric, Oceanic & Space Science (AOSS) 605, "Satellite System Design", who hailed from such varied backgrounds as Engineering Physics, Electrical-, Computer-, and Aerospace Engineering, Public Health, Remote Sensing, Biology, as well as AOSS. Their responsibilities included the space science: sensors, their requirements and operation.This design team was directed by Professor John Vesecky with support provided by NASA's Ames Research Center and particularly that of Drs. Jim G. Lawless and Byron L. Wood.

During the three and a half months of the Winter Term, students from this wide variety of disciplines participated, working closely with faculty from the University and receiving much help from scientists and engineers within NASA, particularly the Ames and Lewis Research Centers. The efforts of this group have produced a design with many exciting, new features. The use of a Pegasus-launched 'lightsat' makes launch cost low, but puts severe constraints on power, weight and volume, forcing new ideas and design concepts. This has required design of very light weight, low power sensors, namely a synthetic aperture radar and a visual / IR imaging device. Data compression and high capacity memory chips allow onboard storage of image data for later downlink. The ground segment has the difficult task of receiving, interpreting and distributing data to the local public health community for malaria control. This requires the use of both satellite and local information within a geographical information system. We plan to use a mobile van as the terminal point of data interpretation and the production of a malaria risk map as the output data product.

As is customary , the students in each course elected a Project Manager and Assistant Project Manager at the beginning of the semester and subsequently organized themselves in

technical groups, one for each of the major subsystems of the design; the work of each group is directed by a Group Leader. The Managers direct and control the team activity and integrate the group inputs into a single, coherent design. The concept of a system approach to design was carried throughout the design process.

A Final Report Committee, with representatives from each group, was assigned the major task of integrating the team inputs into this document, to be published in June, 1991.

We gratefully acknowledge support from NASA in two forms. The continuation of the Grant from the NASA/USRA University Advanced Design Program. This Grant provides funding for a graduate teaching assistant, for travel, for reproduction and distribution of the final report, for construction of the scale model, and for various other operational costs. Special recognition is due Ms. Carol Hopf, Deputy Director, Division of Educational Programs, and Ms. Barbara Rumbaugh, Senior Project Administrator of the Advanced Design Program, both of USRA, Houston TX. We also acknowledge with thanks financial support from the NASA Ames Research Center. Joan Salute of NASA Ames has been especially helpful in making arragements at short notice.

As an integral part of the Grant, NASA's Lewis Research Center gave support of key lecturers and other technical resources. NASA Lewis also hosted the mid-term design review in early March. Ms. Lisa Kohout and Ms. Barbara McKissock provided technical guidance and maintained contact with the team during the year. We are thankful to them for their support and friendship.

The excitement and enthusiasm of the students and faculty at Michigan, the many contributors from NASA, and a large group of contributors from government, industry and academia has made the course both interesting and rewarding. We are looking forward to the success of MEDSAT as a project within NASA and are proud to have been part of its beginning.

Professor Harm Buning, Ae.Eng. 483
Professor John Vesecky, AOSS 605            April , 1991

# MEDSAT Design Team

## Aerospace 483:

Professor:     Harm Buning
Teaching Assistant:     Jon Friedman

Project Manager:     R. Jeffrey Benko
Assistant Project Manager:     Brian A. Renga

### Communications &Control
Lorrie E. Francis
Jeanne M. Happe
Andrew J. Wu

### Mission Analysis
Walter N. Meier
Brett A. Stottlemyer

### Scientific Payload
Anna M. Boda
Scott W. Hause

### Structures/Spacecraft Integration
Howard Bowersox
Christopher J. Cirves
Howard H. Horng
Sabine A. Vermeersch

### Power
Peter D. Jennings
Glen A. Sapilewski

## Atmospheric, Oceanic & Space Sciences 605:

Professor:     Dr. John Vesecky
Teaching Assistant:     Lorelle Meadows

Project Manager:     Ruben De La Sierra
Assistant Project Manager:     Larry Morris

### Data Management/Communications
Chris Nonis(Group leader)
Hong Chou
Ron Rojewski

### Mission/Ground Segment
Serena Schwartz(Group leader)
Bryan Dayton
Andrew Humphrey
Ya-Ching Lin
Hanli Liu
Dan Matusiewicz
Dongliang Wu

### Visible/IR Sensor
Joe Bartlo(Group leader)
Fred Tanis
Bill Charmly
Jian Wu
Weiping Zhao
Jae Lee

### Synthetic Aperture Radar Sensor
Jim Slawski(Group leader)
Eric Ericson
Greg Horlacher
Allen Larar

# Ad-Hoc Committee for the Final Report

Chairman: Pete Jennings

Anna Boda
Howard Bowersox
Jeanne Happe
Howard Horng
Larry Morris
Brett Stottlemyer

# Ad-Hoc Committee for the Model

Chairman: Chris Cirves

Pete Jennings

**Aerospace Engineering 483**
**Aerospace System Design**

**The University of Michigan**
**Winter, 1991**

Front row, left to right:

Brian Renga
Jeff Benko

Second row:

Howard Horng
Sabine Vermeersch
Andy Wu
Walt Meyer
Brett Stottlemyer

Third row:

Chris Cirves
Howard Bowersox
Scott Hause
Jeanne Happe
Anna Boda
Lorrie Francis
Glen Sapilewski
Pete Jennings

At top:

Professor Harm Buning

**Atmospheric, Oceanic, and
Space Sciences 605
Satellite System Design**

**The University of Michigan
Winter, 1991**

Front row, left to right:

Dongliang Wu
Jian Wu
Greg Horlacher
Bryan Dayton
Bill Charmly
Jae Lee

Second row:

Joe Bartlo
Serena Schwartz
Professor John Vesecky
Hong Chou

Third row:

Hanli Liu
Weiping Zhao
Allen Larar
Ruben De La Sierra
Jim Slawski
Dan Matusiewicz
Larry Morris
Ya-Ching Lin
Eric Ericson
Andrew Humphrey
Chris Nonis
Ron Rojewski

# Chapter 1

# INTRODUCTION

## 1.1    Summary

During the winter term of 1991, two design courses at the University of Michigan worked on a joint project, MEDSAT. The two design teams consisted of the Atmospheric, Oceanic, and Space Sciences 605 (AOSS 605) "Satellite System Design" and Aerospace Engineering 483 (Aero 483) "Aerospace System Design". Collaborating with each other, they worked to produce MEDSAT, a satellite and scientific payload whose purpose was to monitor environmental conditions over Chiapas, Mexico. Information gained from the sensing combined with regional data would be used to determine the potential for malaria occurrence in that area. The responsibilities of AOSS 605 consisted of determining the remote sensing techniques, the data processing, and the method to translate the information into a usable output. Aero 483 developed the satellite configuration and the subsystems required for the satellite to accomplish its task. The MEDSAT project is an outgrowth of work already being accomplished by NASA's Biospheric and Disease Monitoring Program and Ames Research Center. NASA's work has been to develop remote sensing techniques to determine the abundance of disease carriers and now this project will place the techniques aboard a satellite. MEDSAT will be unique in its use of both a Synthetic Aperture Radar and visual/IR sensor to obtain comprehensive monitoring of the site. In order to create a highly feasible system, low cost was placed as a high priority. To obtain this goal, a light satellite configuration launched by the Pegasus launch vehicle was used. The Pegasus is a recently developed launch vehicle designed by Orbital Sciences Coporation and the Hercules Aerospace Company. It uses the advantages of an unique air launch to lift small payloads into orbit for a cost of approximately $8 million.

## 1.2    Atmospheric, Oceanic, and Space Sciences Team

### 1.2.1    The MEDSAT Concept's History

While numerous space projects seem only to explore the outer frontiers of space, there are a number of projects that are actually aimed at exploring and helping the planet earth itself. NASA's Biospheric and Disease Monitoring Program is one of these projects, examining the earth's biosphere and the interaction between humans and the environment. One area of their research has been dealing with vector-borne diseases. A vector-borne disease is a illness that is transmitted by an outside vehicle, such as a mosquito with malaria. The full cycle of the disease involves a host, a vector, and a guest. While a lot of these diseases are not common place in first world countries like the United States, they do pose a serious health problem in tropical countries. In fact, vector-borne diseases, such as malaria, affect approximately half a billion people worldwide. Control measures for the diseases have not been shown to be effective. This can be seen in the fact that there have been an increasing tendency in the number of malaria cases worldwide.

Due to this need to find other methods in controling vector-borne diseases, NASA has been developing methods to assess the potential for these diseases in a specific area. They are using the fact that the vectors are the carriers of the diseases. By correlating the environmental conditions and habitat to vector abundancy, they are trying to find a measurable condition for the potential for the disease. NASA's efforts have been to develop remote sensing methods to determine high vector abundancy. This information combined with additional facts about the population and region can provide a determination for the risk of the disease spreading. The Biospheric Monitoring program is intended to have worldwide spatial coverage as well as monitoring a spectrum of diseases. For initial stages, though, the disease of malaria and specific areas of the world are the topics of concern. NASA Ames Research Center, during the 1980's, has been starting the work in

this area by carrying out remote sensing and ground truth experiments in California rice fields. These experiments were done in order to correlate biomass and standing water on the fields with the abundance of *Anopheles,* the genus of mosquito known to transmit malaria. Once the relationship between these conditions was established, the testing was moved to Chiapas, Mexico. Here the general patterns of disease transmission, local conditions, abiotic cycles, and population dynamics of malaria in disease infected localities were examined. Visible-infrared scanners, synthetic aperture radar overflights, and ground truth measurements were conducted to determine how these factors contribute to the spread of the disease.

## 1.2.2 The MEDSAT Concept

The next step of the work is to place these remote sensing techniques on a space platform and that is the project of MEDSAT. MEDSAT is a satellite whose purpose is to monitor environmental conditions. This information combined with additional facts can be used to determine the potential for vector-borne diseases in an area. The scope of the initial MEDSAT mission will be limited to the disease of malaria and one primary site in Chiapas, Mexico, with other secondary sites within coverage of the system. The project was divided between two design courses at the University of Michigan. The two design teams consisted of the Atmospheric, Oceanic, and Space Sciences 605 (AOSS 605) "Satellite System Design" and Aerospace Engineering 483 (Aero 483) "Aerospace System Design". AOSS 605 dealt with the sensing instruments and the handling of the data, while Aero 483 designed the satellite and its subsystems.

AOSS 605 desired to create a very feasible system so that low cost was placed as a high priority. To reach this goal, a light satellite design was chosen in order to minimize cost. Miniaturization of structures, data storage devices and electronics in general will make light weight sensors systems possible and affordable. Low cost, light satellites make future satellite constellations possible; thus, intensive, global monitoring of diseases and other environmental phenomena can be performed.

Another important aspect that MEDSAT will achieve is a comprehensive spatial and temporal coverage of a region where biological, human, and biochemical cycles are in a complex intertwining. In this complex situation, a detailed analysis is necessary. Under these conditions, use of ground based techniques alone (although potentially quite detailed) could become very inefficient. On the other hand, current space-borne surveillance systems are either too infrequent in coverage or at this moment nonexistent. For some systems scheduled to be deployed in the near future, the critical repeated coverage with both SAR and visual/IR sensors attainable by MEDSAT would be unavailable. Therefore, MEDSAT will provide intensive coverage of an area while still keeping cost low to provide a feasible and accurate system for future deployment.

## 1.2.3 MEDSAT Mission Science Overview

MEDSAT will be equipped with two imaging sensors, a Synthetic Aperture Radar (SAR) and a four visual /infrared scanner. The SAR is an active sensor working at a frequency of about one gigahertz (GHz). It can operate all the time under any atmospheric conditions being able to image in any type of weather. SAR is also very efficient at discriminating standing waters, soil and vegetation moisture, due to water's high dielectric coefficient. The four visual/infrared scanner, in contrast to the SAR, is weather and daytime dependent. It does possess other capabilities making it very valuable, though. By using two or more channel brightness ratios, vegetation indices can be obtained, as well as, an accurate mapping of human activities in the region.

These combined systems will give MEDSAT something that no other present system is able to produce, and that is a synergistic compatible set of data. This set of data on its own is of legitimate scientific interest, but once applied to a situation where socioeconomic conditions are involved, the data set will give space-borne research another dimension which at the current time does not have a precedent.

Intensive repeated coverage is how MEDSAT will make possible timely and accurate monitoring of the state of the habitat where the disease is endemic. This will provide the background necessary to issue risk maps and the eventual forecast of the disease spread. In order to accomplish this, the MEDSAT mission will include two stages. The first will serve to develop algorithms to implement a malaria risk model based on both spacecraft and ground-based data. The second stage will help predict and direct control efforts where needed.

### 1.2.3.4    Innovations and contributions of MEDSAT

MEDSAT can become a unique civilian satellite by leading the way in the vector-borne disease control effort. MEDSAT will be the first light satellite equipped with synergistically compatible sensors, which shows great promise in future use. Using this different system, MEDSAT can provide complementary information for other satellite systems. Thus MEDSAT will be providing a new way to sense a region; adding to a more comprehensive look than what current satellites can provide.

## 1.3    Aerospace Team

### 1.3.1    Background

The satellite era started on October 4, 1957 with the Soviets launching into orbit a 83.6 kg satellite called Sputnik I. Since this humble beginning, there has been a tremendous increase in the size and weight of the satellites used by the aerospace industry. Satellites having the mass of several thousand kilograms are now easily lifted into low earth orbit. The large weight and size was needed to house bulky monitoring equipment and larger numbers of instruments. Recently, there has been an increased interest in lighter and smaller satellites referred to as lightsats. Advancements in microelectronics and computers have allowed subsystems and sensors to shrink in size and weight. Missions accomplished previously only by large satellites were now falling into the lightsats' realm. Industry analysis support the existence of this trend of increased use of lightsats. A study completed in January, 1990 indicated that thirty-six corporations and universities were seriously working on lightsat projects. In addition, industry analysts predict a one hundred million dollar annual market for these satellites within the next ten years [1.1]. The aerospace market is obviously heading towards using these satellites in a more pronounced manner.

One obstacle in the use of lightsats has been the lack of a good launch vehicle. The current launch vehicles are geared towards much heavier payloads. The Delta and Titan series of rockets can carry thousands of kilograms into low earth orbits [1.2]. These vehicles are too large for launching a single lightsat, so multiple lightsats or lightsats combined with larger satellites have typically been placed aboard these vehicles to provide for a cost effective launch. To complement the industry trend toward the use of lightsats, a launch vehicle designed specifically for lightsats is needed. One solution to this dilemma is Pegasus, a launch vehicle recently developed by the Orbital Sciences Corporation and Hercules Aerospace Company. The Pegasus uses the unique approach of air launch to

send payloads ranging from 136 kgs to 410 kgs up to altitudes of 278 km to 834 km [1.3]. It provides this launch at the relatively low cost of eight million dollars.

### 1.3.2    Design Parameters

The launch vehicle, Pegasus, and this growing industrial trend to use lightsats became the parameters for the aerospace design class. Aero 483 wanted to capture the future trend that the aerospace industry was making for two reasons. First, team members could use the new technology that is being created for the lightsats, such as Pegasus, and second, designing a lightsat would allow students to become more aware of future industrial concerns. This design would also be a greater challenge due to the stricter requirements of the lightsat: the lower weight and volume allowances. The Pegasus launch vehicle parameter was selected for its benefits gained from the air launch. The Pegasus allowed launching from non-government areas and this would place less restrictions on the uses for the satellite.

With these parameters in mind, a suitable purpose for the satellite was needed. The MEDSAT project as mentioned in section 1.2 was brought to our attention. It was desired to keep the MEDSAT low in cost to increase the feasibility of its implementation. The lightsat, by its very nature of its size and weight, kept the satellite relatively low in cost. The Pegasus also kept with this low cost philosophy, only costing approximately $8 million, but still capable of launching a suitable design.

These parameters and mission led to the formulation of Aerospace 483's objective:

Aero 483's objective is to work with AOSS 605 to create a satellite or space platform for a scientific payload that would determine environmental conditions over a designated area. This satellite would be placed into orbit by the Pegasus launch system.

## 1.4    Team Organization and Interaction

### 1.4.1    Organization

To accomplish each team's objective, each design team was led by a Project Manager and an Assistant Project Manager. The rest of the team members were divided up into groups, each dealing with a different aspect of the design.

#### 1.4.1.1    AOSS 605's Group Responsibilities

AOSS 605's groups included Ground Segment, Synthetic Aperture Radar (SAR) and Visual/Infrared Sensors, and Data Communication and Management.

Ground Segment's responsibilities were related to the conducting and coordinating of all ground related issues. The scope of its tasks ranged from disease pathology issues to downlink and data analysis to the potential development of disease risk maps.

Synthetic Aperture Radar and Visual/Infrared Sensors determined and developed specifications necessary to deploy and implement the onboard sensors to conduct the actual monitoring of the sites, habitats, and conditions in question.

Data Communication and Management responsibilities included the compilation, compression, downlink, storage, and postprocessing of the digital data involved in the monitoring of the study areas.

### 1.4.1.2    Aero 483's Group Responsibilities

Aero 483's groups were Scientific Payload, Mission Analysis, Structures and Spacecraft Integration, Power, and Controls and Communications.

Scientific Payload served as the intermediary link between Aerospace 483 and AOSS 605, helping to convey the goals, interests, and information provided by each class to the other design class. They also performed the cost analysis on the satellite design.

Mission Analysis determined the optimal orbit for the satellite and the launch window for the Pegasus. They also calculated the orbital maneuvers and necessary fuel requirement needed to increase the lifetime of the satellite.

Structure and Spacecraft Integration constructed the structure of the satellite, the thermal cooling system, and integrated all the sensors and subsystems into a coherent shape that met the Pegasus' launch requirements.

Power oversaw the production and storage of power to meet the needs of the scientific payload and the satellite's subsystems.

Controls and Communication determined the systems needed to control the satellite's attitude, measure the satellite's position, produce orbital maneuvers, and enable uplink and downlink of information between earth and the satellite.

### 1.4.2    Design Team Interaction

The MEDSAT project is unique from past Aerospace 483 design projects because it required expertise of persons outside of the Aerospace Department (Aero). The Synthetic Aperture Radar and Visual/Infrared sensors required specific approaches to design that the Aero students had not be exposed to. To help design the remote sensing instruments, the Aero department enlisted the aid of the Atmospheric, Oceanic and Space Sciences Department (AOSS). This is the first time that a joint effort, such as this, has been attempted by the Aero and AOSS departments.

The design classes were separated into nine distinct groups, each responsible for a specific aspect of the satellite design. The Aero 483 class was assigned the task of structure design, launch and operation of the satellite, while AOSS 605 was concerned with the acquisition, storage and downlink of remote sensing data. In order to achieve the goals of the project, extensive communication was required.

To specifically address the challenge of communication in a project of this complexity, the Scientific Payload Group was formed. The responsibility of the Scientific Payload Group was to facilitate the flow of information between the Aero 483 and AOSS 605 classes. By serving as project liaisons, the Scientific Payload Group was able to keep all of the design groups abreast of changing information, at all times.

The communication and cooperation needed to undertake this mission was enormous. We are also certain that the situation was very much like those present in industry today. In industry, different groups with different ideas and languages are asked to communicate effectively and reach a common goal. Analogously, the teams were expected to work together to complete the design in the semester allotted.

Through biweekly scheduled meetings, the two departments transferred information unofficially. Officially, the departments released intermittent progress reports to keep others updated concerning the current information. The individual groups also met outside of class to work on their specific task. The groups brought the results of outside work to the biweekly meetings for comment. After receiving the results, observations and suggestions were made in order to improve the design. In this way, two seemingly unrelated departments could work together to reach the common goal.

This first time joint effort between the two departments has worked well. It has provided insight into real world situations where cooperative efforts, such as these, are commonplace.

## 1.5    The Pegasus Launch Vehicle

Produced by the Orbital Sciences Corporation and the Hercules Aerospace Company, the Pegasus is a small launch system designed to place small payloads (136 to 410 kgs) into orbit. Using the unique approach of an air assisted launch, the system is able accomplish its mission relatively inexpensively at $8 million for the entire launch cost. The Pegasus Launch vehicle is pictured in Figure 1.1.
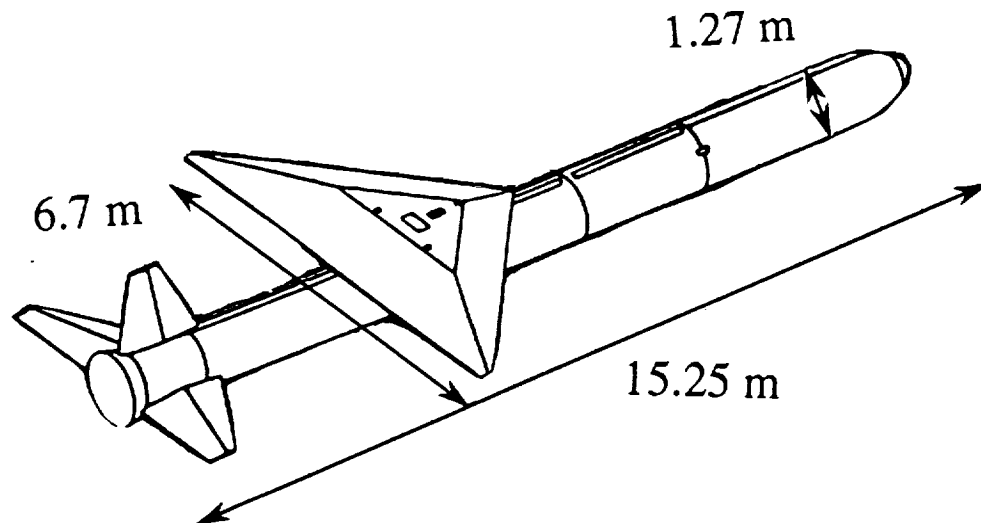


**Figure 1.1 Pegasus Launch Vehicle**

The Pegasus' basic shape is a uniform cylinder with a length of 15.25 m and diameter of 1.27 m. The delta wing is mounted 7.25 m from the front of the vehicle and has a span of 6.7 m. In addition, there are fin actuators in the rear to assist in control. The three stage solid rocket assembly and delta wing lifts the payload into orbit. Figure 1.2 shows a cut away drawing of the rocket motors. The Pegasus also takes advantage of the use of graphite composite in the wing, fins, and fuselage fillet to improve performance.

As mentioned before, the Pegasus is air launched. The Pegasus is fired from a special pylon under the wing of a B-52 or other similar size airplane. At launch, the airplane is in cruise flight conditions, flying at about Mach 0.8 and at an altitude of 12,000 m. A more detailed launch procedure is described in section 7.3.
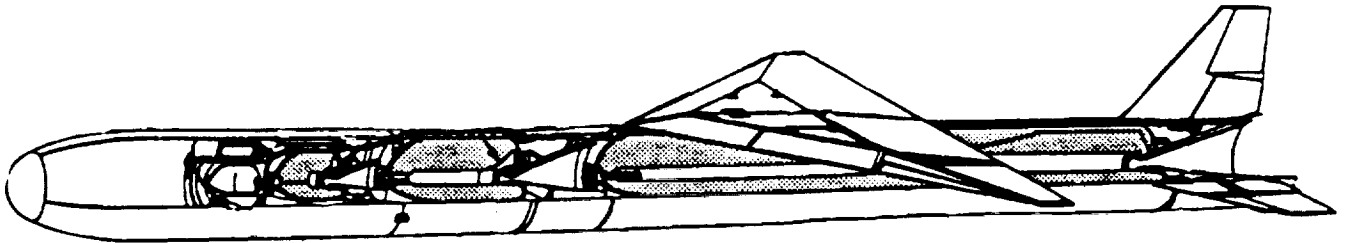
**Figure 1.2 Pegasus Launch Vehicle - Cut Away Drawing**

The advantages of this configuration compared to a land based launch are:

1) The launch vehicle gains the potential and kinetic energy of the airplane.
2) The lower density of the air at higher altitudes contributes to lower aerodynamic drag.
3) The rockets can obtain higher nozzle expansion ratios leading to a higher propulsion efficiency.
4) A flat trajectory and the wing's aerodynamic lift cause less gravity losses.
5) The airplane can provide a flexible launch site.
6) The vehicle experiences lower acceleration and dynamic pressure which lead to lower structural and thermal stresses.
7) The launch can increase the range of orbital inclinations without out of plane maneuvering.

All of these advantages allow the Pegasus launch vehicle to carry into orbit 136 kgs to 410 kgs in orbits of 278 km to 834 km [1.3] at a reduced cost than land based launch systems. The cost for a Pegasus Launch at $8 million dollars is relatively inexpensive compared to the launch cost of other launch vehicles. For example the cost of a Delta 2 launch is $55 million. Of course, the Delta launches a much larger payload, but the Pegasus offers the opportunity to launch a small payload without incorporating itself with other payloads during launch.

# Chapter 2

# GROUND SEGMENT
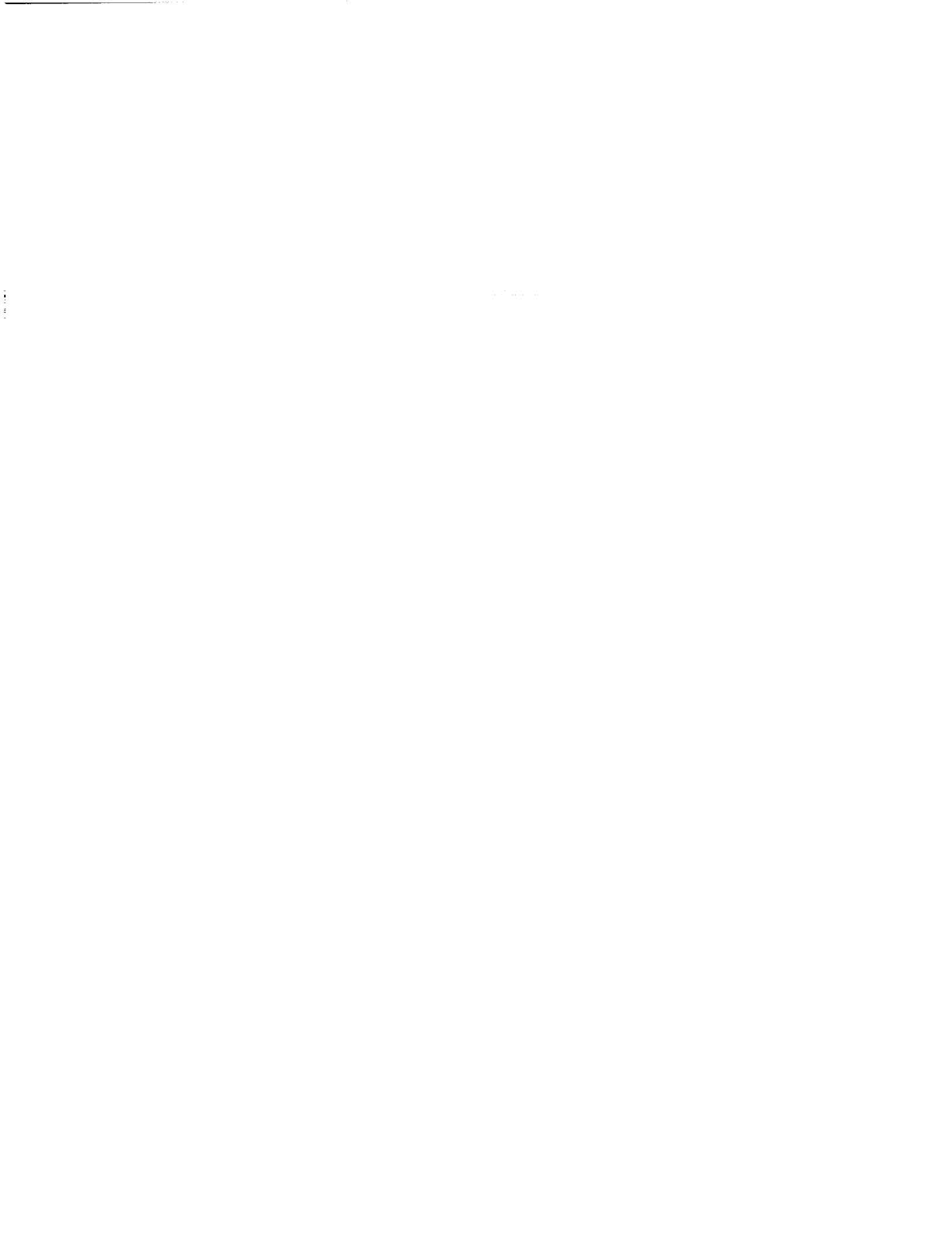
## 2.1    Introduction

"All epidemiology, concerned as it is with the variation of disease from time
to time or place to place, must be considered mathematically, however many
variables are implicated, if it is to be considered scientifically at all. To say
that a disease depends on certain factors is not to say much, until we can
also form an estimate as to how largely each factor influences the whole
result. And the mathematical model of treatment is really nothing but the
application of careful reasoning to the problems at issue." [2-1]

Sir Ronald Ross, a pioneer in research on malaria, was unaware that he was describing the
need for the MEDSAT system, when he spoke these words in 1911. He probably never
envisioned a capability to effectively monitor the variations in malaria over time and space
remotely from space. However, Sir Ronald Ross understood the potential for the
mathematical model in disease control, and laid the groundwork for the MEDSAT approach
presented here. We have the many advantages of modern technology, which allow us to
explore the use of a geographical information system (GIS) to manipulate the numerous
sources of data within a mathematical model of malaria risk for a given region. Although
much basic research has been accomplished and is currently under way within NASA's
Biospheric Monitoring and Disease Prediction program, we predict that the volume and
complexity of information, both ground and satellite collected, will require that the
MEDSAT mission have a research phase of approximately one year, in which time an
appropriate model could be developed and implemented in the application phase of the
project. The research phase would also serve to distinguish the most pertinent data to
production of a daily malaria risk map for user access. The primary purpose of the
application phase would be the actual production of this map, in the context of a regularly
updated control program. The strength of the MEDSAT system will lie in its ability to
devise a flexible plan of control that can change and reintegrate strategies as the factors
affecting malaria transmission change; this is precisely where traditional strategies have
failed time and time again [2-2]. The ground segment activities of the MEDSAT project at
the University of Michigan have involved consideration of characteristics of malaria, site
selection, data types, plans for ground station development, and the potential MEDSAT
output. We have also attempted to consider the global context in which the MEDSAT
concept was originally conceived.

## 2.2    Summary of Malaria Characteristics

Malaria is a generic term used to describe the pathological manifestations of a group of
protozoan parasites of the genus Plasmodium. Four of the species in this genus are
recognized as human parasites: *Plasmodium falciparum, Plasmodium vivax, Plasmodium
malariae and Plasmodium ovale*. Each of these four types are known to cause a unique
etiology in human hosts with distinct case fatality rates, incubation periods, extrinsic cycles
and pattern of symptoms. Symptoms commonly observed in the human hosts of all four
species include fever, chills, sweats, headache, icterus, coagulation defects, shock, renal
and liver failure, acute encephalopathy and coma [2-3].
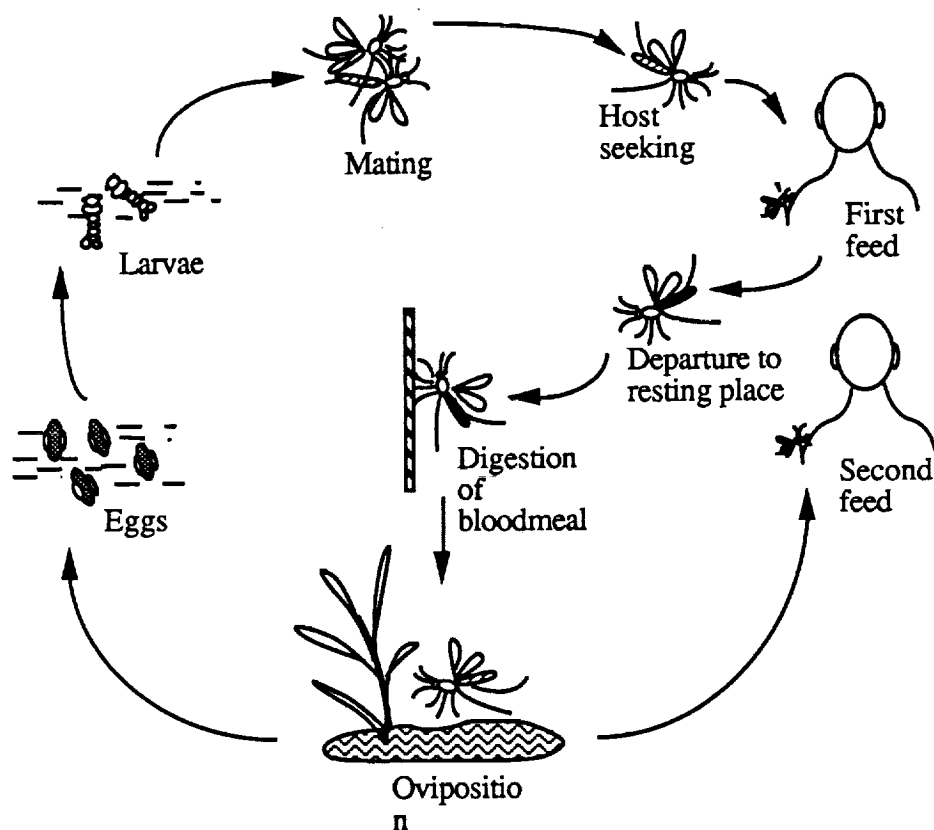
**Figure 2.1:   Transmission cycle of malaria**

Aside from the human hosts, malaria parasites require an extrinsic period within a mosquito host in order to complete their life cycle successfully. The most common of these insect hosts are mosquitoes of the genus Anopheles. Although there exist approximately 400 species within this genus, only about a fifth of these are capable of actively transmitting malaria between human hosts [2-4]. These vary widely as to their geographical distribution, length of life cycle and reproductive and feeding habits. A detailed study of the environment and life-cycle of these vectors (Figure 2.1) is essential to any program that seeks to reduce the incidence of malaria. The density of the insect vector population and their pattern of contact with infected and non-infected individuals are the main factors in determining the severity of the malaria problem in a specific area. This was first stated by Sir Ronald Ross, the individual credited with identifying the mosquito as the disease vector, in 1911 when he devised the following Threshold Theorem for malaria [2-1]:

1) The amount of malaria in a locality tends towards a fixed limit determined by the number of malaria-bearing mosquitoes and by other factors.

2) If the number of malaria-bearing Anophelines is below a certain figure, that limit will be zero.

Few, if any, health authorities currently consider it a realistic goal to push this limit to zero, but the same principles can just as well be applied to the reduction and control of the disease.

## 2.3    Site Selection

Selection of the primary site for the MEDSAT project was a two-stage process involving different selection criteria at each stage.

### 2.3.1    Country Selection

Various countries were considered as possible locations for the research site before Mexico was settled upon as the final choice. This location was determined to be the one most likely to satisfy the set of conditions deemed essential for the successful completion of this initial MEDSAT mission. These conditions can be roughly divided into two basic types: humanly induced and natural.

The humanly induced conditions are linked to anticipated constraints of political or economical nature. These include factors such as political stability of the current government, level of socio-economic development, primary health care infrastructure, status of current malarial control programs, and the probability of obtaining political access for a NASA project. The ideal country would be one with a stable government which would not only be receptive to the idea of participating in a project with NASA, but also one which would possess the necessary resources to enable both the collection of ancillary data and the useful application of the project output once it is produced.

The natural conditions are related to anticipated constraints of biological and environmental nature. These would encompass factors such as the identity, number and life cycle of the malarial vectors, the extent and nature of the malarial problem as well as accessibility of the proposed research sites. There was an attempt to locate a country with a well-defined and well-documented malarial problem in at least one area.

Of the nine countries selected for final evaluation, Mexico was the one that came closest to fulfilling the conditions stated. Other countries that came close to satisfying the criteria were Costa Rica, Brazil and Turkey. Costa Rica was subsequently selected as a secondary site.

Mexico currently accounts for 14% of all the malaria reported in the Americas. According to 1986 estimates, approximately 43 million people in Mexico live in malarious areas, resulting in 131,000 new cases annually [2-5]. Despite being one of the first countries to adopt an active malaria eradication campaign in the 1950s, Mexico has had little success in the long-term management and control of this disease. With the abolishment of the National Campaign for the Eradication of Malaria a decade ago and the rechanneling of resources to other areas of health, the magnitude of the problem has increased manyfold and has once again become a primary public health concern [2-6]. As of June, 1989, there was a steady increase in the number of reported cases of malaria in Mexico. Based upon data gathered between January and June of that same year, it was calculated that the number of cases was increasing at the rate of 41% per year [2-7].

The majority of malarial transmission in Mexico occurs along the Pacific coast, particularly in the Southern part of the country. The states of Oaxaca, Guerrero, Michoacán and Chiapas together account for 67% of of the total annual incident cases. The majority of cases of malaria in Mexico are caused by *P. vivax*, with the deadlier *P. falciparum* accounting for somewhat less than 1%. There is serious concern that the latter may be increasing more rapidly in incidence due to the high proportion of cases in the population of migrant workers from Guatemala, a country with four times the malaria prevalence of

Mexico. *P. falciparum* was reported in the states of Chiapas, Veracruz, Tabasco and Quintana Roo in 1988, with Chiapas having the highest number of cases (Fig. 2.2 ) [2-8].
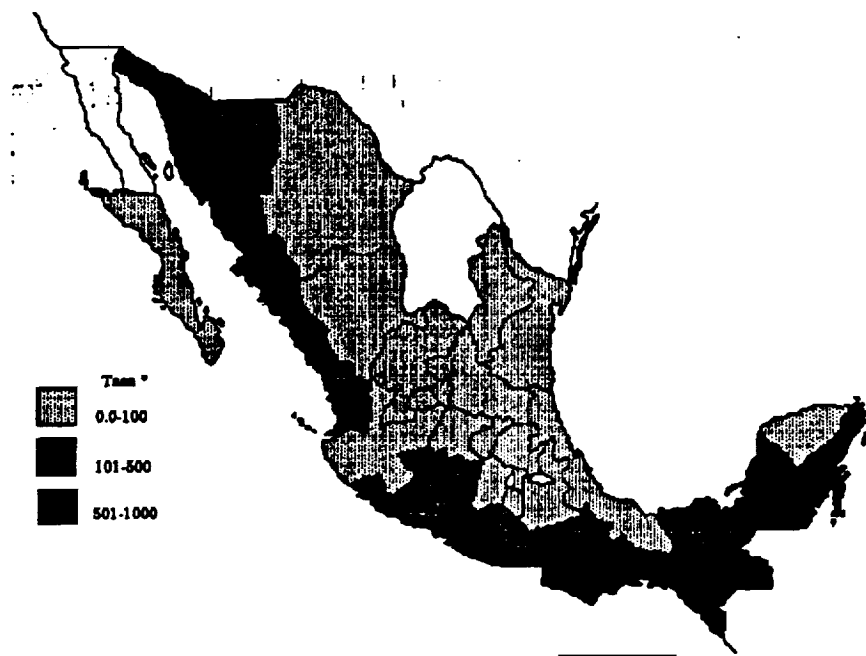


**Figure 2.2:    Malaria morbidity in the Republic of Mexico, 1988 [2-6]**

**2.3.2    Primary Site Selection**

In order to select our primary research site, a more detailed evaluation of the pattern of malaria incidence and prevalence within the selected country was completed. Particular attention was given to the factors mentioned in the natural criteria part of the section on country selection. The final decision to select the county of Soconusco in the state of Chiapas was based upon several factors which determine a unique and urgent malarial problem in this region.

Historically a site known for its persistant malaria problem, [2-9] Soconusco is located along the Pacific ocean, at the southernmost tip of Mexico, along the Guatemalan border. It is characterized by an economy rich in agriculture, producing bananas, corn, cotton and soybeans, as well as coffee in the northern foothills. Most of these crops are export-oriented and are cultivated in large plantations requiring correspondingly large quantities of seasonal labor [2-10]. This demand for labor has resulted in the large-scale influx of Guatemalan migrant workers into the region. These were estimated to total 120,000 individuals in 1986 alone [2-11]. Although Chiapas does not possess the highest numbers or rates of malaria transmission in Mexico, it is notable in that it has the highest rates of incidence of *Plasmodium falciparum.* in the country. This species of malaria is known for having the highest case-fatality rates, killing up to 10% of untreated victims. The high number of cases of this type of malaria is most likely due to this population of migrant workers who originate mostly from the highlands of Guatemala. A study of political refugees originating from the same region in Guatemala showed a prevalance rate of 1220 cases of *Plasmodium falciparum.* per 100,000 population, a number that is several times higher than the overall rate for the state of Chiapas (5.04 per 100,000) [2-12]. By
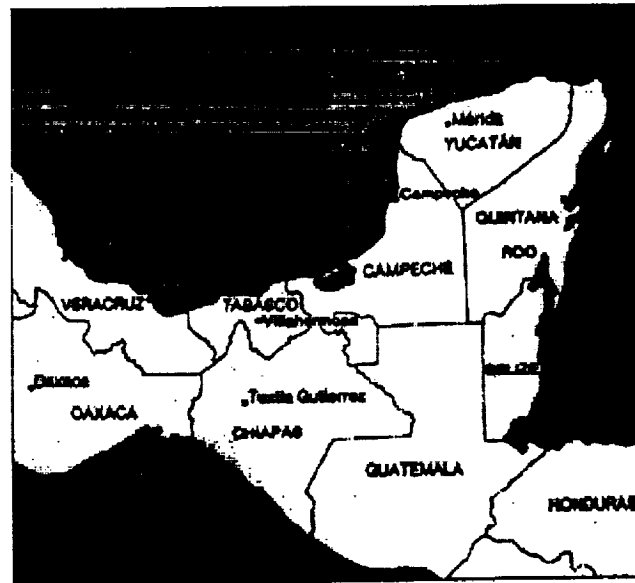
**Figure 2.3:    Relief map of the State of Chiapas, Mexico.    [2-7]**

concentrating surveillance and control efforts on the localities in Soconusco where these migrants are concentrated we can effectively target the foci of this growing problem.

There are two anopheline vectors responsible for malarial transmission in Soconusco: *Anopheles pseudopunctipennis pseudopunctipennis* Theobold and *Anopheles albimanus* Wiedemann. Although mosquito breeding occurs year-round, the type and density of vectors vary in a cyclical manner with the season of the year. In Chiapas *A. albimanus* is generally the most common species along the coast in the rainy season, although *A. pseudopunctipennis* is also present during this season. The climate in Chiapas is mostly too dry,however, to accommodate the year-round reproduction of *A. albimanus* and this
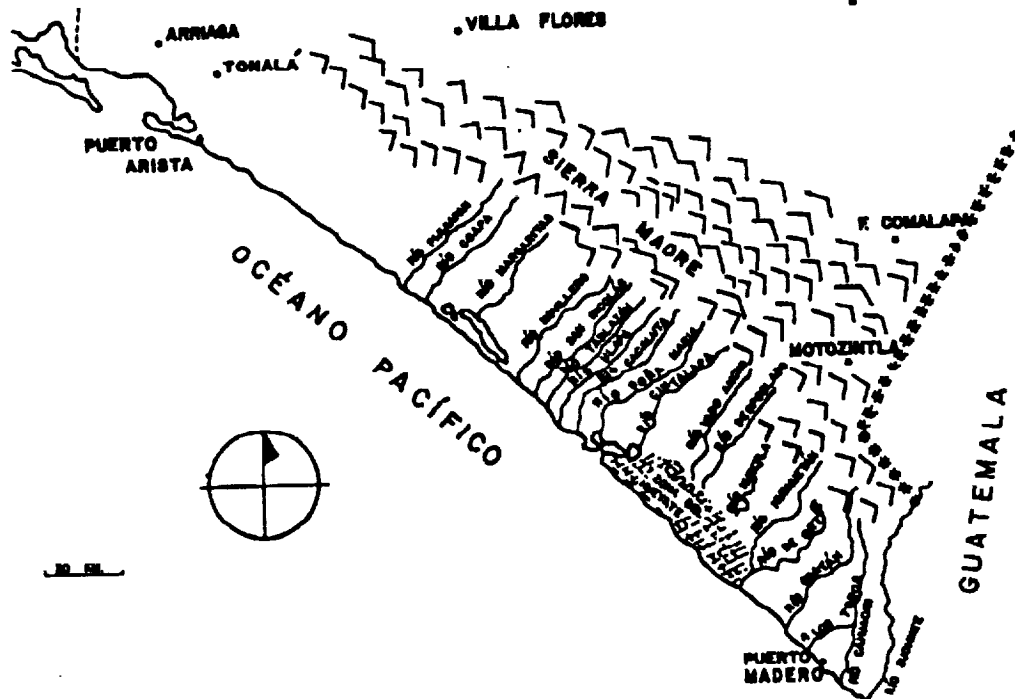
**Figure 2.4    Soconusco region in southern Chiapas**

species ceases to be of medical importance in the transmission of malaria during the dry season. Starting in October, *A.pseudopunctipennis* assumes prominance in disease transmission, persisting in this position until the start of the rains in April [2-13]. The following is a brief description of the life cycle and environmental requirements of each species:

*Anopheles albimanus* Wiedemann-This is a species of mosquito that occurs in humid lowland areas ranging up to 600m in altitude [2-13]. It is a zoophilic and moderately anthropophilic vector, often entering houses to feed on humans and has a preference for bloodmeals from large mammals [2-6,2-14]. Its flight range averages 2km [2-6]. This species has a preference for breeding in lagoons and pastures near the sea where the water is slightly saline (survive in up to 80% sea water) [2-14], but it will settle for anything from small rain-filled depressions to hoofprints and wheel ruts as long as they are not densely shaded [2-15]. This is the species studied and characterized by NASA Ames in their Phase II studies.

*Anopheles pseudopunctipennis pseudopunctipennis* Theobold-Although rarely encountered in the densities characteristic of *A. albimanus*, it has a wider distribution and is responsible for almost all of the malarial cases in the Mexican highlands [2-5]. Despite a general preference for higher terrains, it can be encountered at all altitudes between sea level and 2300m [2-16]. Studies of the vector's behavior in Mexico show it to be zoophilic and weakly anthropophilic, with specific bloodsource preferences varying from country to country [2-15]. It has an average flight range of 6km [2-7]. The larvae of this mosquito are strongly associated with clear, sunlit bodies of still or slowly running water which permit the growth of extensive *Spirogyra* algae mats [2-14]. They are often encountered in drying streams where the slower flow of water permits the development of the algae or in the pools left behind in stream beds in the dry season [2-15, 2-16].

### 2.3.3 Secondary Site

Given the uncertainty associated with the lack of field studies in the current phase of this project, it is recommended that Costa Rica be selected as a secondary site for this research project. Should conditions in Mexico prove inappropriate for the needs of the researchers, Costa Rica is a country that would be an attractive alternative to the current site. Even if the current site should prove to be fruitful, Costa Rica, with its geographical proximity to Chiapas, would be an ideal complement of data for the project.

Costa Rica is notable in that it is one of the few developing countries not located on an island that has succeeded in controling its malarial problem. Although some degree of transmission still occurs in areas along the Pacific coast [2-17], malaria has been reduced to an insignificant threat through means of an extensive health care system and constant surveillance [2-18]. The potential for a malaria problem exists however, and the current government's plans to initiate several large-scale rice development projects threaten to increase the likelihood of a return of the problem. A surveillance plan in this country would concentrate on the problems of vector increase associated with environmental and ecological disruption resulting from these projects.

## 2.4 Data Types

In order to renew the fight against malaria and to choose optimal strategies for malaria control in Chiapas, Mexico, it would be helpful to develop a mathematical model describing malaria dynamics. Before such a model can be developed, scientists, working during a research phase of the MEDSAT project, must determine the parameters which play an integral role in the population dynamics of malaria. An approximate quantitative analysis of the principal epidemiological factors involved in the transmission and maintenance of malaria led Sir Ronald Ross in 1909 to distinguish eight such parameters. MEDSAT scientists can incorporate these parameters into the development of a model. They include [2-4]:

1. average population in the locality;
2. average proportion of the population infected with malaria;
3. average number of mosquitoes per person in the locality, per month;
4. average number of mosquitoes which feed on man;
5. proportion of infectious mosquitoes which feed on man;
6. proportion of mosquitoes which survive through the extrinsic incubation period;
7. proportion of infectious mosquitoes which feed on man;
8. recovery-rate of infected individuals, per month.

Other parameters which will contribute to the development of more sophisticated models will have to be determined during a research phase of the MEDSAT project. A few of these parameters will, perhaps, be:

1. humidity;
2. temperature;
3. rainfall.

The purpose of this section of the report is to describe the various sources that biomathematicians and other scientists can access in order to obtain information about parameters which are important to the development of a malaria model for Chiapas, Mexico.

Model parameters can be determined and accessed through both ground and satellite sources. Ground sources, which are presently available in Chiapas, include agencies such as the Center for Malaria Investigation, the Ministry of Health, and the Mexican Weather Service. Another ground source called a transponder network is not yet available but could also be helpful in the collection of parameter information. The primary satellite source will be MEDSAT.

## 2.4.1 Ground Sources

Before beginning a research phase of the MEDSAT project, it would be advantageous to examine the possibility of obtaining free or low cost information concerning malaria model parameters from private or governmental agencies in Chiapas. By doing this, fewer onsite workers would need to be hired for data gathering, helping to keep project costs to a minimum. It may be possible to receive information from the Ministry of Health and/or the Center of Malaria Investigation about the following model parameters:

1. average proportion of the population infected with malaria;
2. proportion of infected individuals who are infectious;
3. recovery-rate of infected individuals, per month.

Inevitably, some malaria parameters will need to be gathered by hired workers at various sites around Chiapas during the research phase of the MEDSAT project. Parameters such as the average number of mosquitoes per person per month and the proportion of infectious mosquitoes which feed on man are most likely not readily available from existing agencies.

Parameters which consider where mosquitoes are likely to live and breed such as water availability and certain temperature and humidity values can be determined with the help of the Mexican Weather Service and more importantly with the aid of a transponder network. A transponder is a device which is composed of instruments such as thermometers, anemometers, barometers, and rain gauges. A network of transponders is capable of cost-effective collection of surface information such as rainfall, temperature, and humidity at many locations in Chiapas. This information can then be simultaneously relayed, along with a signal marking its location, to a synthetic aperture radar (SAR) on MEDSAT. With the incorporation of surface information from selected locations, accurate and timely interpretation of SAR image information can be achieved. Information on what SAR can do to establish model parameters will be discussed in the next section on satellite sources.

## 2.4.2 Satellite Sources

Satellite sources have an advantage over ground sources because information can be gathered more effectively. The first advantage is cost effectiveness. Satellites, and more specifically MEDSAT, can significantly reduce the number of onsite workers who need to be hired to gather ground data. The second advantage is the ability of gathering information for all types of locations. MEDSAT has the capability to gather data from remote locations not easily accessible to humans. The third advantage is the ability of gathering information in a timely manner. One scan completed by MEDSAT can effectively gather data over a large portion of Chiapas in a matter of seconds. A large science team on the ground would take months or years to cover the same region.

A SAR (Synthetic Aperture Radar) is one of the instruments which will exist on MEDSAT. The SAR has many favorable capabilities which scientists can take advantage of in gathering parameter information specific to Chiapas and other areas as well. The SAR is capable of observing:

1. variations in water bodies over both time and space;
2. types of vegetation;
3. changes in vegetation density;
4. where human settlements are located;

during all types of weather conditions and throughout both day and night. Variations in water bodies over time and space is an important consideration because mosquitoes need water for breeding purposes. Research scientists at NASA-Ames have discovered that changes in vegetation density are important in predicting when and where mosquito populations might reach their maximum in California rice fields [2-19]. It remains to be seen what impact this study could have on Chiapas, and research needs to be conducted in Chiapas to see if vegetation density is a significant factor in the population dynamics of malaria. Knowing the locations of human settlements, especially migrant worker camps, and how many people live in those settlements are important model parameters in Chiapas. SAR is likely to be able to distinguish migrant worker camps from surrounding areas because the camp dwellings form a distinctive pattern and have roofs which are constructed of dried palm leaves.

A visible and infrared instrument will also appear on MEDSAT. Unlike SAR, visible and infrared instruments can only be used effectively during the daytime in conditions which are relatively cloud free. Capabilities that visible and infrared instruments have include:

1. differentiation of vegetation/crop types;
2. detection of standing ground water;
3. temperature estimates.

Differentiation of vegetation/crop types is important in determining where human settlements are located. Detection of standing ground water helps to determine where mosquito breeding sites are likely to be located. Temperature strongly affects larvae production and mosquito lifetimes.

## 2.5    Ground Station

Our design for the MEDSAT ground station includes the following capabilities: data collection, image processing, data management, archiving and analysis, for both research and application purposes, and station maintenance. We foresee using existing facilities at NASA Ames for satellite flight control.

Flight control of the satellite will follow typical NASA operations procedure. Playback data from an observatory (e.g. Hawaii) are relayed through a communication satellite to NASA Ames Research Center (NARC) using NASA communication circuits. The tracking data are received by NASA flight dynamics facilities where predicted and definitive orbit calculations are made.

The data from the satellite will ultimately be downlinked to two ground targets (see Chap.6 Data Management and Communications for more information): the control center at NARC and a location close to the primary site (Chiapas) in Mexico. Figure 2.5 shows the flow of data between the satellite and the ground stations, and figure 2.6 shows the data flow diagram in our MEDSAT ground station. A high-gain antenna will be necessary for the

# MEDSAT SYSTEM OVERVIEW

MALARIA RISK REGION

STATE OF CHIAPAS

DATA COLLECTION SWATHS

GUATEMALA

GULF OF MEXICO

JFV 4/91

SATELLITE ORBIT

VISUAL/IR & SAR SENSING

NASA AMES

CHIAPAS, MEXICO FIELD SITE

DATA TRANSFER LINKS

COMMUNICATIONS SATELLITE

PACIFIC OCEAN

COMMAND-UP AND DATA-DOWN LINKS

HAWAII GROUND STATION
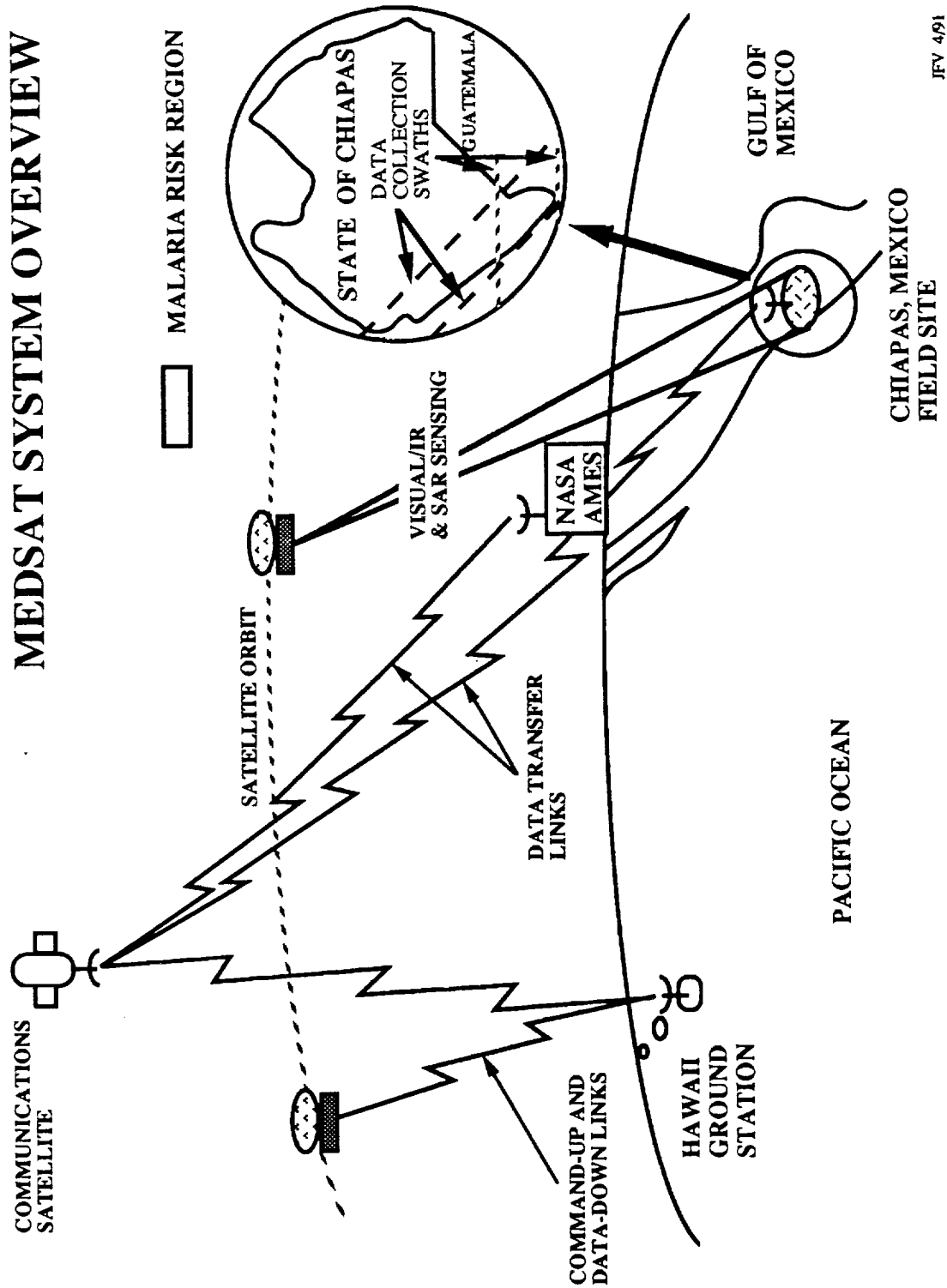
**Figure 2.5: MEDSAT data flow**

station to receive data from the satellite. The received data from a communication satellite are read in a compressed form. Once read, the data need to go through a decompressor for data processing to yield a computer readable format. Archiving will be done at NASA Ames throughout the lifetime of the project and a fixed site in Chiapas during the research phase. Raw image signals will then go to a geographical information system (GIS) for image processing. During first step processing, the SAR and Visible-Infrared images will be created, rectified, registered, classified, and finally stored. As a result, a quick-look image will be ready for display. The second step processing generally involves a lot of CPU time for modeling and statistical analyses based on scientific requirements.
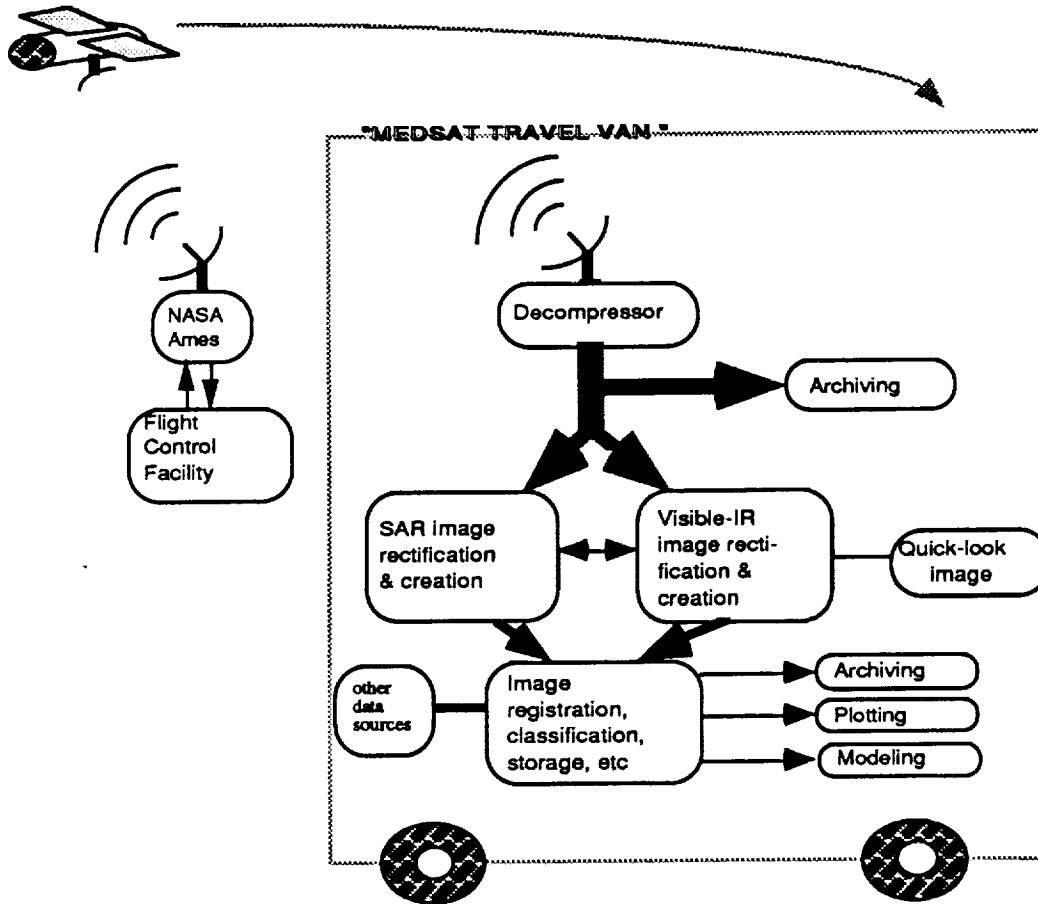


**Figure 2.6: MEDSAT ground station configuration**

The entire processing procedure will repeat every two days. In the research phase, the Chiapas ground station will require a fixed location with fairly extensive computer facilities. The staffing for this ground station will include individuals with expertise in diverse areas. Some examples of these areas include epidemiology, modeling, computer technology, and public health. This staff will be responsible for the operation of the station, data analysis, and continued field work. The archiving for research purposes will be updated every 2 to 7 days. In the application phase, the receiving and processing components will be integrated in a mobile ground station, providing greater site flexibility in applying a malaria control program. This system will be independent in its daily

functions. It is expected that most of the data manipulation, management, analysis and modeling will be done by using a GIS. The MEDSAT archives, a growing record of all the data types, will be housed in the fixed stations, one of which will be NARC.

## 2.5.1 Strategy

Several considerations are crucial to our design:

- The data levels should be limited to the smallest number possible (for example, the telemetry data and the GIS format data). This will increase the efficiency of data communication and management in a small mobile ground station.

- The MEDSAT GIS must be able to perform vector-raster image manipulation as well as house-keeping functions such as image correction, classification and registration.

- The hardware system where GIS resides will be an open structure distributed processing system such as a workstation-micro computer system. This will allow the system to be expandable in terms of its processing ability, database, and user access.

- To make a mobile station feasible in the application phase, the receiving and processing component will need to be as small as possible. This requirement will necessitate careful consideration of the configuration for different components of the MEDSAT ground station system.

## 2.5.2 Ground Station Requirements

Incoming data from a communications satellite will initially be received by a communications antenna in a compressed form. Figure 2.7 is a block diagram that shows how the ground station is supported by a workstation-micro computer system. The data are then decompressed and formatted into a code the computer can understand. The formatted data will then be put onto Computer Compatible Tape. Data archiving will take place at this step and can be achieved with a workstation.

Ground data will also require transformation into the same computer code as described above. This data will include information from the past history (maps, statistics, etc.) of the region under surveillance. Depending on the type of information, there are two potential solutions which perform the same function. One option is a digitizer, which is specifically designed for maps; input is digitized into a computer format. Once digitized, the data can be combined with other forms of data (i.e. satellite data). The other option is a flatbed scanner. This is a piece of hardware that can handle any type of input (maps, literature, statistics, etc.). The usage will be determined as the needs of MEDSAT continue to unfold.

The satellite information, now in computer code, will proceed through a workstation for first step processing. The MEDSAT GIS, workstation-based, should be able to handle the image processing. Through our studies on the latest GIS developments, we think that the following objectives can be achieved with this GIS:

- Rectification and creation of SAR and Visible-IR images
- Image enhancement
- Primitive image processing (e.g. sharpening, noise reduction, scaling/rotation, etc )
- Site identification and image registration
- Image classification

- Quick-look data processing and display
- Distributed processing system and extendable database providing read and write privileges for scientific research and data management
- Image storage and archiving using an optimal combination of hierarchical directory structures

At the workstation(s), information from the digitizer or flatbed scanner, along with satellite images, will go through the GIS management system to produce a GIS digital image of a malaria risk map in either vector or raster form.

This image is ready to be printed, which can be accomplished by a postscript printer. There are three types of printers: standard, high performance, and high resolution. We will probably opt for a high performance printer because it provides better quality performance than a standard printer, yet is less expensive than a high resolution printer. In addition, a separate printer for literature will be required. The output from the digitizer, flatbed scanner and workstation will remain in a buffer that can be accessed by all processors on the bus line. The buffer is a part of the workstation(s) that provides an efficient system of access to data by any hardware component of the ground station.

When new data enters the system, the buffer will be available and allocated for next round processing. We have the option of using an expandable hard drive at any time, to take the load off other components, thereby enhancing and extending our computer power and capability when needed. An optical drive may also be incorporated in the future, if we decide to perform our own archiving, particularly in the research phase. Once our application phase commences, we will set up the independent mobile ground station which will have its own staff of technicians. Archiving will then occur solely at NASA-Ames, in an attempt to develop a tool that is very site-flexible.

We are considering Sun workstations for the second step processing. Since the image processing at this stage involves complex scientific modeling and statistical analyses, significant computational power is required. For such operations we plan to utilize an array processor. For the simple modeling, workstation-based GIS software packets and scientific language ( e.g. FORTRAN) subroutines will be able to handle it. The simple modeling probably includes a set of basic analytic functions such as:

- Proximity: calculate the distance and identify the nearest element among the features of two coverages
- Overlay: use Boolean operators (AND, OR, NOT) to register one coverage to another to establish a new coverage.
- Buffer: establish a user-specified distance around a selected feature.
- Clip: make a subset of a coverage using a user-specified boundary or another coverage
- Network: use lines and polygons to establish a topological network and perform operations such as routing, allocation, and districting.
- Surface modelling and contouring: given continuous data, produce surface models and develop contours at user-specified intervals

Combinations of such simple GIS functions enable one to program and execute complex tasks in image analyses and interpretation.

Ground Segment

Project MEDSAT

Bus Line/Buffer

Digitizer

Antenna

Flatbed scanner

Receiver

PC

Workstation

High speed array processor

Workstation
(Image Processing)

PC

GIS Database

Printer
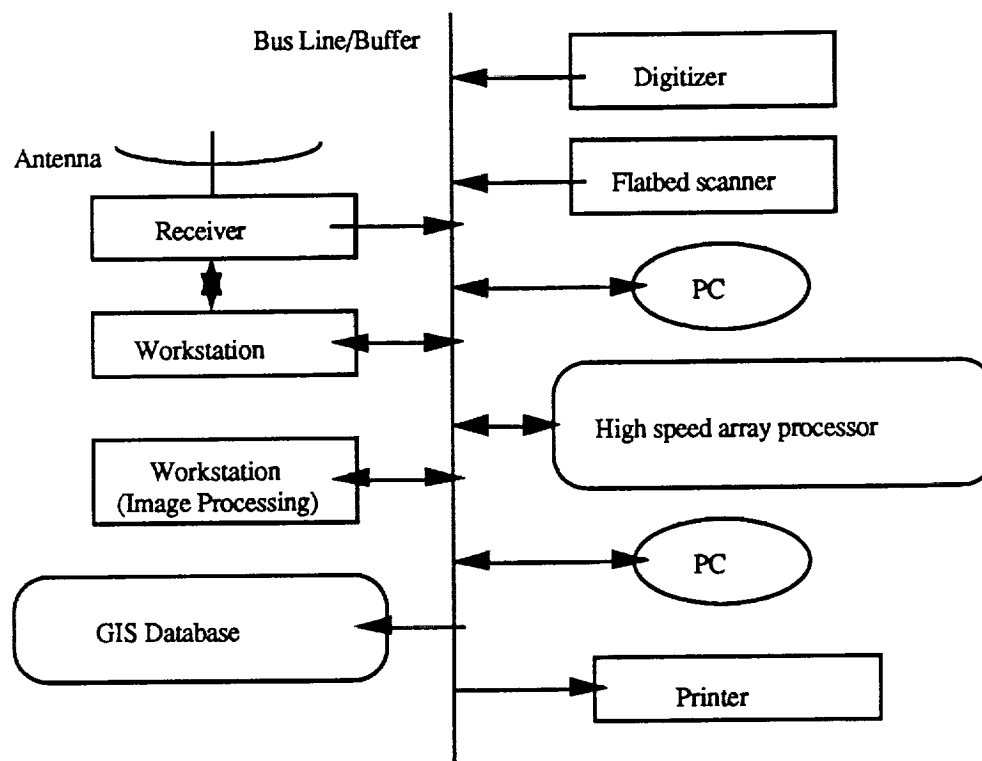
**Figure 2.7    Block Diagram of Ground Station Hardware**

## 2.6    Conclusion

Once the combination of ground and satellite data is received and processed at the ground station, the output of this project will be determined by the specific goals of the research and application phases. The research phase will involve gathering data from the satellite and correlating this data with ground information. Ground truths such as actual malaria cases will be part of the basis for testing the predictability of our malaria risk model, a primary goal of the research phase.

In our particular study we hypothesize that there may be correlations between mosquito habitats and human population areas, particularly regarding vegetation and regions of standing water. However, such hypotheses need to be tested. In the research phase ground data in the form of known mosquito habitats and actual malaria cases will be collected and utilized in collaboration with remotely sensed data in order to generate a model that can be used to map and predict those areas that are most prone to malaria outbreaks. Research within the NASA-Ames program will help in accomplishing these objectives. However, we believe a research phase during the Medsat mission will still be required.

Concurrently, data archives will be set up and organized in-situ at a fixed site within Chiapas. These archives will be repeated at NASA-AMES throughout the lifetime of MEDSAT for the purpose of monitoring progress and continued research. The archived data at Chiapas will be dissolved once the malaria risk model has been developed and

validated for implementation in the application phase. Archives are very space consuming and expensive to maintain particularly where extensive facilities do not exist.

A mobile ground station requires that only the most pertinent data be received and directly applied towards the production of a malaria risk map. Hence, the application phase will involve combining very specific pre-determined data types, both ground and remotely sensed, and feeding them into the MEDSAT GIS to be modeled and mapped.

The output is envisioned as an accurate prediction device supplied to public health officials in Mexico as often as every day. A malaria risk map may for instance provide the ability to predict where and when mosquito populations will reach their maximum density allowing for the effective allocation of malaria control measures. In the long term more and more data will be gathered and mathemetically manipulated. From this process we will learn more about the behavioral and habitational characteristics of malaria transmitting mosquitoes as well as the people they infect. With these developments this satellite will become more applicable to other areas of the world which are suffering from malaria.
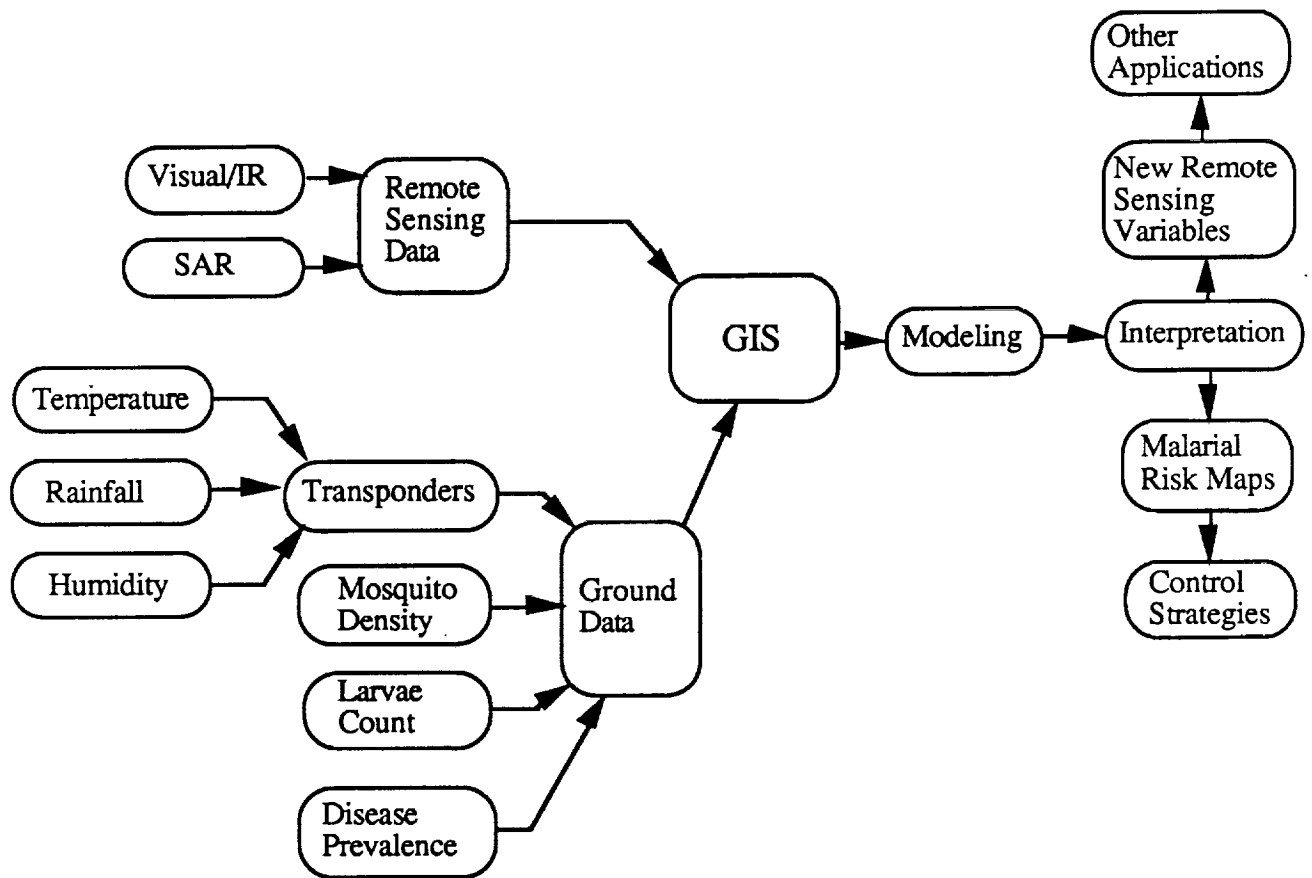


**Figure 2.8    Overview of MEDSAT mission**

Through the development of a systematic approach to monitoring malaria, it is very feasible that other vectorborne diseases may also be within the scope of the MEDSAT project. Among those to consider are Schistosomiasis (intermediate carriers are snails), Lymphatic Filariasis, Chagas' Disease, Onchocerciasis ("river blindness"), Leishmaniasis and African Sleeping Sickness, listed in order of

prevalence [2-21]. All of these are tropical diseases which have eluded traditional measures of treatment or control, making them ideal candidates for a MEDSAT approach. The global applications of the MEDSAT system will quickly evolve upon commencement of an active and orbiting satellite; it will be a matter of time and practice before the proper techniques are developed and mastered for the monitoring and control of diseases defined by factors that can be profiled from space.

# Chapter 3

# SYNTHETIC APERTURE RADAR SENSOR

## 3.1 Summary

In order for the MEDSAT satellite to be an effective tool used in determining areas of high malaria risk in the region of Chiapas, Mexico, it must possess a sensor capable of remotely sensing mosquito habitats and human habitation through rain and clouds independent of solar illumination conditions. The all-weather and day/night operational attributes of a synthetic aperture radar (SAR) system, coupled with the ability to utilize the output imagery in identifying, classifying, and measuring the terrain parameters that are of key importance to the this project, make the SAR ideal for use on the MEDSAT sensing platform. This chapter presents the design of the MEDSAT synthetic aperture radar sensor.

## 3.2 Introduction

The synthetic aperture radar (SAR) design was a two step process that consisted of determining the feasibility of using a SAR to remotely sense mosquito habitats, and, if proven feasible, the specification of a SAR system capable of being placed aboard the small MEDSAT satellite. In order to accomplish the first step, a feasibility assessment of the SAR sensor, which also included an investigation into current and planned satellite SAR designs, was completed. After determining the feasibility of placing a SAR sensor aboard the MEDSAT satellite, the second step was undertaken which entailed research into both the geometric imaging requirements and system design specifications of the SAR system. The rest of this introduction discusses the results of the feasibility assessment, while the remainder of the chapter presents and discusses the SAR system designed for placement aboard the MEDSAT satellite.

The feasibility assessment consisted of research into the possible remote sensing capabilities of a synthetic aperture radar (SAR) system to determine if it could be used to fulfill the remote sensing task of the MEDSAT project. The MEDSAT remote sensing task is defined by both imaging and environmental factors. The imaging factors consist of the ability to distinguish two target classes, mosquito habitats and human habitation, on the resulting imagery. These imaging factors are discussed in more detail in the next section. The two environmental factors consist of the ability to remotely sense the two target classes discussed above through any weather condition and independent of solar illumination. The malaria problem is worst in the tropical parts of the world--like Chiapas, Mexico-- where there tends to be long rainy seasons. This means that having at least one sensor with the ability to penetrate through clouds and rain is important to the remote sensing task. The orbit of the MEDSAT satellite will bring the sensor over the target area at various times in the day or night. Meaning that having at least one sensor which does not depend on solar illumination, in order to remotely sense the target area, is important to the remote sensing task.

The remote sensing ability of the MEDSAT project can be greatly enhanced through use of a synthetic aperture radar system. In addition to being operationally independent of either solar illumination or weather conditions, SAR systems can be employed to create imagery used to: remotely classify and measure vegetation; identify and measure soil moisture/standing water, even through moderate vegetation canopies; and identify man-made structures.

As mentioned earlier, the feasibility assessment also included an investigation into the attributes of other current and planned satellite SAR systems. The goal of this research was to determine if these systems were capable of completing the above mentioned remote sensing task. The efficient design of the MEDSAT project required that an on-board SAR complement existing and planned systems and not duplicate their coverage. The

investigation of these other SAR systems was concerned with their radar frequency band(s), resolution, polarization, and, most importantly, the time between successive overflights of the target.

Since an outbreak of mosquitos is possible within seven days of a rainfall, MEDSAT's mission of malaria control dictates that the system have coverage of the test site every 1 to 3 days to be effective. Existing and planned systems have repeat cycles in the range of 7 to 44 days [3-76]. These coverage frequencies were deemed inadequate for the MEDSAT project, and were the driving reason for placing a SAR sensor aboard the MEDSAT satellite, rather than depending on other satellite SAR systems, to fulfill the remote sensing task.

The selection of a light satellite platform for MEDSAT placed strict limitations upon the synthetic aperture radar system's power, volume, mass and data rate. The rest of this chapter describes the various design parameters of the MEDSAT SAR sensor. First, the detection question is addressed. From the need to detect vegetated areas with underlying standing water and to identify human habitation, the SAR system's frequency band (wavelength) is chosen. Then, the determination of the geometric imaging requirements (e.g., resolution, ground swath size, incidence angle) and the design specifications of the system, restricted by the limitations mentioned above, are presented. The chapter is concluded with a summary of the MEDSAT SAR design, and a short discussion of additional research and possible technical innovations that would improve this preliminary MEDSAT SAR sensor design .

## 3.3    Detection

This section discusses the imaging factors of the remote sensing task in more detail, and also describes the various parameters that affect the detection characteristics of a synthetic aperture radar system. In particular, the focus of this section is on the influence that the frequency band of a SAR has on the ability of the system to fulfill the MEDSAT remote sensing objective. In order for the SAR sensor to be a successful tool in detecting and monitoring the mosquito habitats, these mosquito breeding areas (typically vegetated areas with underlying standing water) must be distinctive on the resulting imagery. The identification of human habitation (typically migrant worker camps) from the images was also considered an important factor in order to provide some measure of the human population spatial distribution in the region. Based on these considerations, the optimum frequency band for the MEDSAT SAR has been determined to be L-band (1.275 GHz /   ·  0.23 m), as is described in this section.

### 3.3.1    Detection of Mosquito Habitats Using SAR

Fundamental to the success of the MEDSAT project is a detailed knowledge of the spatial distribution of population densities of the malaria transport vector, the mosquito, to enable efficient implementation of appropriate disease control methods. This can be accomplished through knowledge of locations where the environmental variables are favorable for mosquito larvae development. SAR data can be used to sense these environmental variables since it can provide the image interpreter with the ability to identify the aquatic habitats and vegetation associated with mosquito breeding within the MEDSAT target area. As mentioned in the beginning of this chapter section, the mosquito habitats of interest will consist primarily of wet grasslands or marshes in coastal regions to areas of partially or heavily shaded water in forest regions further inland. All of these conditions are observable using SAR, as has been demonstrated in previous work by many researchers [3-74].

Another aspect of the mosquito habitat remote sensing problem that must be addressed is the temporal nature of the imagery. Since MEDSAT is a pioneer with regard to this type of satellite SAR application, there is uncertainty as to when the best time is for collecting the SAR image data (i.e., time of day or time after a rain fall). MEDSAT's orbit will actually help in this determination. The orbit, besides having a period of 90 minutes and a repeat cycle of 24 hours, has a precession rate, which will cause the satellite to pass over the test site of Chiapas, Mexico 20-30 minutes earlier each day. This precession rate will help in the determination of the optimum time of day, and hopefully the best time after a rain fall, to collect the SAR image data.

## 3.3.2 Detection of Migrant Worker Camps Using SAR

Malaria is not a "problem" unless humans are present to get infected by the mosquitos and complete the disease spreading cycle. Within the MEDSAT target area of southern Mexico, migrant workers are believed to be at highest risk due to the high incidence of malaria among such workers and their close proximity to the mosquito habitats. Therefore, in addition to knowledge pertaining to locations of mosquito habitats, spatial distribution of migrant worker camps is also highly desirable.

The building construction practices and materials used in constructing living quarters in these migrant worker camps is very primitive compared with a modern "urban center" composed of concrete and steel, for which radar detectability is well established. Nevertheless, SAR data can still be very useful in either directly detecting the camp sites or inferring their locations through indirect means. Camps of sufficient size (or dwelling density) should be directly identifiable with their radar signature (intensity and pattern) being different than that of surrounding areas; they will not be composed of living vegetation, and their vertical structure will be different than that of the environment. A more indirect approach can also be used to locate camps that are difficult to identify directly; migrant worker camps should be situated in close proximity to agricultural regions where the workers are needed, so their positions can be estimated by locating crops using the SAR (see Section 3.3.3) and visual/IR sensor.

## 3.3.3 Radar Return Parameters

Five radar and surface parameters affect the intensity of the radar return signal. These are: frequency (wavelength), polarization, target surface dielectric constant, target surface roughness and incidence angle. The radar frequency determines the wavelength of microwave radiation that interacts with the reflecting surface. A particular surface can be rough with respect to a short radar wavelength (e.g., X-band, see Section 3.3.4), yielding large radar backscatter, and it can be smooth with respect to a longer wavelength (e.g., P-band), producing negligible backscatter (this concept is discussed in more detail in Section 3.3.4). Thus, the radar frequency directly affects the return signal from a surface. The polarization of the transmitted and return microwave radiation can provide information on variations in the surface topography and can assist in target classification (e.g., agricultural crops, human dwellings, swamps, flooded areas, etc.). A more detailed discussion of polarization is included in the SAR Geometric Requirements section (Section 3.4). The complex dielectric constant is a measure of the electrical properties of the surface and determines the amount of radar energy that is absorbed, reflected, or dissipated upon incidence with the surface. Materials with higher dielectric constants reflect more of the incident microwave radiation. Water has a high dielectric constant, which makes wet soils reflect more radar energy than dry soils; and thus enables inferal of soil moisture content. The Rayleigh roughness criteria states that a surface is rough when the small scale height

Synthetic Aperture Radar

condition ($\Delta$h) in equation (3-1) is met.

$$\Delta h > \lambda / (8 \sin \psi) \tag{3-1}$$

where:

$\Delta$h = terrain small scale height

$\psi$ = grazing angle

$\lambda$ = wavelength of radiation

The surface roughness directly controls the amount of backscattered radiation; this quantity is a measure of how rough a surface is relative to the wavelength of incident microwave radiation. The rougher the surface the higher the backscatter. Lastly, the incidence angle controls the direction of maximum reflected energy. All of these parameters must be carefully chosen to achieve best results, as is discussed in latter sections of this report.

Synthetic aperture radars have been used to study the microwave backscatter dependence on soil moisture, surface roughness, and vegetation cover [3-68]. The results show a positive correlation between scattering coefficient and soil moisture content. Also, the surface roughness and vegetation type are known to strongly affect the microwave backscatter. There have also been studies where SAR images have been used in delineation of standing water boundaries [3-68 & 3-27]. These results suggest that observations with a synthetic aperture radar system of appropriate frequency (see Section 3.3.4) can be used to infer soil moisture content, surface roughness, and type of vegetation cover, as well as to locate swamps or flooded areas. MEDSAT SAR has a particular advantage in that repeated observations at frequent intervals are made and hence the SAR signature history is known with daily samples; changes can then be observed and used in interpretation.

### 3.3.4 . Radar Frequency Considerations

The choice of a radar frequency for MEDSAT was a difficult task, since different frequencies provide maximum information content in varying locations of the remote sensing parameter spectrum (i.e., soil moisture, type of vegetation, vegetation canopy penetration, etc.). Ideally, one would like to combine the advantages of multiple frequencies into one instrument. However, this becomes merely a desire when conforming to the constraints of a small satellite (i.e., power, mass, volume, data rate, etc.); due to these constraints, MEDSAT will employ only one microwave frequency band in the SAR design. The frequency/wavelength bands considered for MEDSAT consist of the following: X (9.35 GHz/3.2 cm), C (5.30 GHz/5.6 cm), L (1.25 GHz/24.0 cm) and P (0.5 GHz/60.0 cm).

Out of the bands considered, the surface roughness is highest in the X-band since it has the smallest wavelength; thus X-band images tend to be brighter because of increased backscatter due to roughness. X-band SAR images enable determination of vegetation canopy vertical structure. This frequency band is ideally suited for agricultural crop classification [3-34]. Using a range of incidence angles, along with vertical and horizontal polarizations, some researchers [3-60] have found that X-band can not only be used to find rice crops, but can actually be used to infer the stage of plant development. Rice paddies are very popular mosquito breeding sites in many parts of the world, and knowledge of the stage of crop development has been found to be directly related to mosquito population densities [3-72]; this would probably make X-band a very attractive choice. However, the mosquito habitats in the MEDSAT target region of southern Mexico do not consist of rice fields. Also, some of the mosquito habitats will be located under vegetation canopies,

through which X-band would provide very little penetration and not be very useful. An X-band antenna would be desirable since it is 1/3 width of an L-band antenna, however, the corresponding power requirements would be excessively high.

C-band SAR images have the desirable feature of being very sensitive to soil moisture. As with the X-band, C-band has a high backscatter return signal (i.e., most surfaces appear rough) due to the relatively small wavelength. However, this implies a low penetration ability and would probably not enable identification of standing water (mosquito habitats) underneath a forest canopy. The C-band, as with the X-band, would be very helpful in locating and differentiating between standing water and a vegetated swamp or flooded grassland.

A radar system operating at a frequency below 5 GHz is necessary to penetrate the crop canopy in order to measure soil moisture under a dense vegetation cover; L-band (1.25 GHz/24.0 cm) can accomplish this task [3-49]. The ability of L-band to detect pools of standing water and determine soil moisture content through a dense forest canopy with minimum effect from the vegetation canopy has been demonstrated [3-68]. Also, a strong correlation has been observed between microwave backscatter and soil moisture content using L-band. L-band has limited vegetation classification potential, but can be used to successfully identify and distinguish among various target classes (crops, forests, swamps, flooded forests, etc.). Overall, frequencies less than 5 GHz--such as L-band--and angles of incidence less than 20 degrees are desirable for remotely sensing soil moisture in order to minimize both the direct backscattering by vegetation and the effective attenuation loss related to the two-way transmission through the vegetation canopy. L-band should work well for observing the water in pastures which are important in the Chiapas, Mexico region. Jack Paris of California State (Fresno campus), who is currently working with multi-frequency--P, L, and C-bands--and multi-polarization (fully polarimetric) data from the Chiapas, Mexico region, has indicated [3-8] that employing L-band on the MEDSAT SAR would most likely produce the best all-around images for this remote sensing application. Also worth noting is the fact that the SEASAT, SIR-A, and SIR-B projects have all been successful applications of L-band.

P-band was also considered for potential use on MEDSAT. Having the longest wavelength of the bands considered, P-band would provide the greatest vegetation canopy penetration ability; correspondingly, it would require the largest antenna--an antenna too large for the MEDSAT satellite. Initially, it was believed that P-band could do everything that L-band could plus an additional advantage due to the greater penetration ability; however, our opinion changed after further research. First of all, the surface may appear too smooth due to the relatively long wavelength. Thus, decreasing the ability to distinguish between dry ground and open water, as well as short vegetated ground and swamp in the resulting imagery. However, most importantly, P-band has not been "space proven" like L-band. Researchers in the microwave remote sensing field have significant concern over the feasibility of using multi-polarization P-band on a space platform [3-8, 3-2 & 3-3]. The concern is regarding whether or not ionospheric interference (e.g., phase distortions from Faraday rotation) would destroy the polarimetric information content of the return signal [3-63]. Also, radio interference would likely decrease the signal-to-noise ratio since P-band is located inside the UHF and VHF radio frequencies. It is the team's opinion that more research needs to be done with this frequency band before it can be considered for application on an operational satellite.

As mentioned earlier, constraint permitting, multiple frequency bands would be most desirable for the MEDSAT application. In fact, multiple frequencies (e.g., L-band and X-band or C-band) would probably be essential for a MEDSAT type of satellite to be simultaneously operational for all malaria prone areas of the world, with the varying

mosquito habitats which exist. However, due to constraints we must choose one frequency; for the mosquito habitats in the MEDSAT target area of southern Mexico, L-band appears to be the optimum choice enabling the MEDSAT goals and objectives to be achieved; L-band will enable the most important features of the Chiapas target region (i.e., migrant worker camps and flooded regions both in pastures and beneath vegetation canopies) to be observed.

## 3.4 Geometric Imaging Requirements

One of the most difficult aspects encountered in the design of a synthetic aperture radar system is the determination of the geometric imaging requirements. This is because the geometric imaging requirements must be chosen so that the physical phenomena of interest--discussed in the previous section on detection--will be distinctive on the resulting SAR imagery. The geometric imaging requirements consist of altitude, range to target, image ground swath size, resolution cell size, incidence angle, and polarization of the transmitted microwave radiation. All of these parameters are interrelated with one another--changing one will effect the value of the others--and all are ultimately constrained by the restrictive volume, mass, power and data rate allotments of the MEDSAT project's small satellite design (see Figure 3.1).

Of the constraints mentioned above, the power is the most important in determining the geometric imaging requirements and system design specifications of the SAR design. Equations (3-2) and (3-3) below are intended to give the reader a feel for the interrelatedness of the various parameters. These equations are simplified theoretical antenna average and peak radiating power formulas for a synthetic aperture radar with the azimuth and range compression factors included:

$$P_{ave} = \{(S/N)(\lambda R^3 8\pi L k T_s v_g)\} / \{A^2 \sigma_0 \rho_{R(ground)}\} \qquad (3-2)$$

$$P_{peak} = P_{ave} / (\tau PRF) \qquad (3-3)$$

where:

$P_{ave}$ = average antenna radiating radio frequency (RF) power
$P_{peak}$ = peak antenna radiating radio frequency (RF) power
$A$ = antenna area = $d_h d_v$
$d_v$ = antenna vertical (elevation) dimension
$d_h$ = antenna horizontal (azimuth) dimension

$\sigma_0$ = system noise floor (the system's minimum detectable average radar cross section normalized to the illuminated surface area)

$\lambda$ = microwave wavelength used by the system

$v_g$ = equivalent ground velocity of the satellite SAR antenna

$k$ = Boltzman's constant ($1.38 \times 10^{-23}$ J/K)
$R$ = range to target
$S/N$ = signal to (thermal) noise ratio
$PRF$ = pulse repetition frequency of transmitter

$\tau$ = actual transmitted pulse length
$L$ = system loss factor (dependent on wavelength)
$T_s$ = system noise temperature (dependent on wavelength)

$\rho_{R(ground)}$ = range resolution (as measured in ground range)
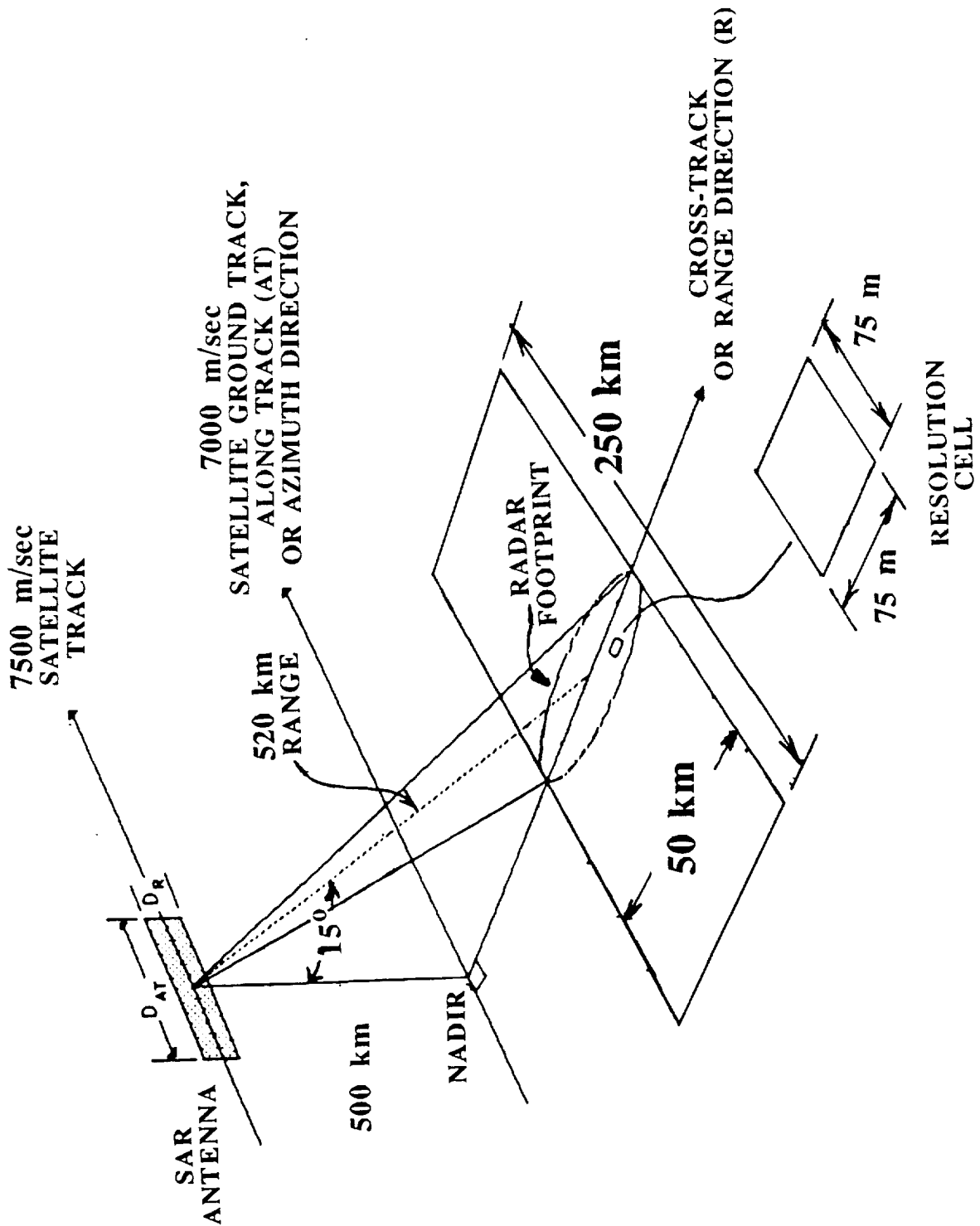
**Figure 3.1: Sketch of MEDSAT SAR geometric imaging requirements.**

Synthetic Aperture Radar

Some of the variables that go into the power calculation are determined primarily by other factors. The wavelength, velocity and range to target are good examples of this other factor determination. The wavelength ($\lambda$) of operation has been decided upon primarily due to the target detection ability, and the parameters of equivalent ground velocity (v) and range to target (R) are determined by the altitude (h) of the satellite.

From equation (3-2) above, the geometric parameter changes that could be made to reduce the antenna radiating power include increasing the resolution cell size ($\rho_R, \rho_A$) or reducing the range swath which is inversely related to the antenna's vertical dimension $R_{swath}=$ $R_{far} - R_{near} = (\lambda R_{boresight})/d_v$. The system specification changes would include increasing antenna dimensions (A = $d_h d_v$), raising the noise floor ($\sigma_0$), or reducing the signal-to-noise ratio (S/N).

This section of the report presents the geometric imaging requirements that we have determined along with the supporting reasons for the various choices, while the next section describes the system specifications (section 3.5).

### 3.4.1 Altitude and Range to Target

The MEDSAT satellite operational altitude of 475 km is low compared to the typical 600 to 800 km altitudes employed by other previous or planned satellite SAR systems. The low altitude is actually an advantage for the synthetic aperture radar sensor. From equation (3-2), it can be seen that the antenna radiating power is directly proportional to the cube of the range to target. This means that a substantial savings in power can occur by simply having as low an operational altitude as possible.

The radar geometric and system parameters were calculated using a nominal altitude (h) of 500 km. This corresponds to a boresight range to target (R) of 520 km for a 15 degree incidence angle ($\theta_i$) at antenna boresight (see equation (3-4) and Figure 3.1).

$$R_{boresight} = h / \cos\theta_i \qquad (3\text{-}4)$$

$$R_{boresight} = (500 \text{ km}) / \cos(15^\circ) = 517.6 \text{ km}$$

$$R_{boresight} \approx 520 \text{ km}$$

The nominal altitude of 500 km also corresponds to an orbital velocity of about 7500 m/s, and an equivalent satellite ground speed of 7000 m/s (see equations (3-5) to (3-8) below).

$$F = m a = (G m M) / r^2$$

$$a = (G M) / r^2 = 8.3294 \text{ m/s}^2 \qquad (3\text{-}5)$$

since: $\qquad a \approx v_{so} / r$

then: $\qquad v_{so} = [ a r ]^{1/2} \qquad (3\text{-}6)$

where:

$F =$ gravitational force of attraction

$m =$ mass of satellite

$a =$ acceleration of gravity at a distance r from Earth's center

$M =$ mass of earth ($5.98 \times 10^{24}$ kg)

$h =$ altitude of satellite ($500 \times 10^3$ m))

$R_E =$ radius of earth ($6.37 \times 10^6$ m)

$r =$ distance of satellite from the earth's center $= h + R_E = 6.87 \times 10^6$ m

$G =$ universal gravitational constant ($6.67 \times 10^{-11}$ m$^3$ / s$^2$kg)

$v_{so} =$ satellite orbital velocity

Solving for the orbital velocity with equation (3-6):

$$v_{so} = [(8.3294 \text{ m/s}^2)(6.87 \times 10^6 \text{ m})]^{1/2}$$

$$v_{so} = 7564.58 \text{ m/s} \approx 7500 \text{ m/s}$$

The equivalent satellite ground speed is approximated by the following equation (this equation does not take into account the rotational speed of the surface of the Earth):

$$v_g = v_{so} (R_E / r) \qquad (3\text{-}7)$$

$$v_g = (7564.58 \text{ m/s})(6.37 / 6.87)$$

$$v_g = 7014.02 \text{ m/s} \approx 7000 \text{ m/s}$$

### 3.4.2    Ground Swath Size

The SAR sensor's maximum ground swath range dimension or width ($S_R$) is 50 km, and the maximum ground swath azimuth dimension or length ($S_L$) is 250 km (see Figure 3.1). The main restrictions for the ground swath size are power and data rate. The ground swath size determination is a compromise between the requirements of having enough of the area imaged to complete the remote sensing task and the restrictions of the small satellite design. The SAR system is envisioned as being fully programmable which will allow the user to modify (reduce) the swath length from the maximum value stated above. This design will theoretically allow two or more smaller swath lengths (the total length not to exceed 250 km) to be imaged before the data needs to be downlinked.

The time over the target area determines the length of time of a sensing session. The longest sensing session time is 36 sec., and is given by the maximum swath length divided by the equivalent ground speed:

$$T_{sensing} = S_L / v_g \qquad (3\text{-}8)$$

$$T_{sensing} = (250,000 \text{ m}) / (7000 \text{ m/s})$$

$$T_{sensing} = 35.7 \text{ s} \approx 36 \text{ s}$$

### 3.4.3    Resolution

The MEDSAT SAR design incorporates a ground resolution cell size of 75 m by 75 m (see Figure 3.1). This cell size has been determined as a trade-off between achieving the

maximum possible system resolution and keeping within the power and data rate constraints. Higher system resolution (i.e., smaller resolution cell size) corresponds to better target detection and classification in the resulting images. The higher system resolution also increases the data rate, as compared to a lower resolution system, since there is a larger amount of information in a given image scene. Increasing the azimuth resolution of the system also directly effects the length of time the radar must be operational in the burst mode. This discussion is concerned more with the geometric reasoning behind choice of the resolution cell size. The relationships between the geometry and system design, as indicated in the above sentences, will be covered more thoroughly in the section on system design specifications (section 3.5).

The choice of square resolution cells means the resulting image pixels will be square. This increases the ease of image manipulation. This is especially important in the MEDSAT application since the images will most likely be geocoded (geographically referenced) to a map base prior to insertion into the geographic information system (GIS) [3-1, 3-26, 3-32, & 3-48].

Synthetic aperture radar employs the Doppler principle and data processing techniques to synthetically lengthen the antenna by coherently integrating the target echo signals. The synthetic lengthening of the antenna creates a high system resolution [3-6, 3-9, 3-10, 3-16, 3-20, 3-21, 3-22, 3-31, 3-35, 3-38, 3-44, 3-54, 3-55, 3-58, 3-62, 3-63, 3-64, & 3-69].

The unfocused SAR design appeared to be attractive since it would greatly simplify the design, and even possibly allow on-board processing [3-10 & 3-62]. In this mode, the azimuth resolution is obtained by a synthetic antenna lengthening process which does not correct for phase errors in range. The calculation of the theoretical azimuth resolution for the unfocused SAR is shown below. From the calculation, it can be seen that the unfocused SAR design would not give good enough resolution (about 175 m) at the range to target experienced by the MEDSAT satellite. This was the basis for the decision to design a fully focused SAR system.

$$\rho_{A(unfocused)} = (1/2) (R \lambda)^{1/2} \qquad\qquad (3-9)$$

where:

$\rho_A$ = azimuth resolution
R = range to target (520 km)
$\lambda$ = microwave wavelength of SAR L-band (0.23 m)

$$\rho_{A(unfocused)} = (1/2) \{ (520,000 \text{ m})(.23 \text{ m})\}^{1/2}$$

$$\rho_{A(unfocused)} = 172.9 \text{ m}$$

In the focused SAR design, the azimuth resolution is obtained by a synthetic antenna lengthening process in which all the phase errors in range are corrected. As seen in the calculation below, the MEDSAT SAR with a 6 m horizontal antenna length, could theoretically achieve 3 m resolution in azimuth. The drawbacks to the fully focused SAR design are that the processing is made more complicated and the data rate is higher. These problems are manageable by having the processor on the ground and applying various

techniques to reduce the final data rate. The data reduction techniques are presented in detail within the section on system design specifications (section 3.5.5).

$$\rho_{A(focused)} = \rho_{azimuth} = d_h / 2 \qquad\qquad (3\text{-}10)$$

$$\rho_{A(focused)} = 6\,m / 2 = 3\,m$$

where:

$d_h$ = antenna horizontal dimension

In the operation of the SAR sensor, the fundamental measurement is echo time delay, hence, the range to target determined from the radar echo is in slant range coordinates. The final image is typically corrected to ground range coordinates during processing, where the image data is converted from slant range coordinates to ground range coordinates. However, this conversion must be taken into account when designing a SAR system so that the appropriate ground range resolution is attained. The conversion from slant range to ground range is given in equation (3-11) below and the geometry is shown in Figure 3.2. From this equation the slant range resolution of the MEDSAT SAR system is about 19 m at an incidence angle of 15 degrees.

$$\rho_{R(slant)} = \rho_{R(ground)}\,\sin\theta_i \qquad\qquad (3\text{-}11)$$

where:

$\rho_{R(slant)}$ = range resolution measured in slant range)

$\rho_{R(ground)}$ = range resolution measured in ground range (75 m)

$\theta_i$ = incidence angle at target surface (15°)

$$\rho_{R(slant)} = (75\,m)\,\sin(15°) = 19.41\,m$$
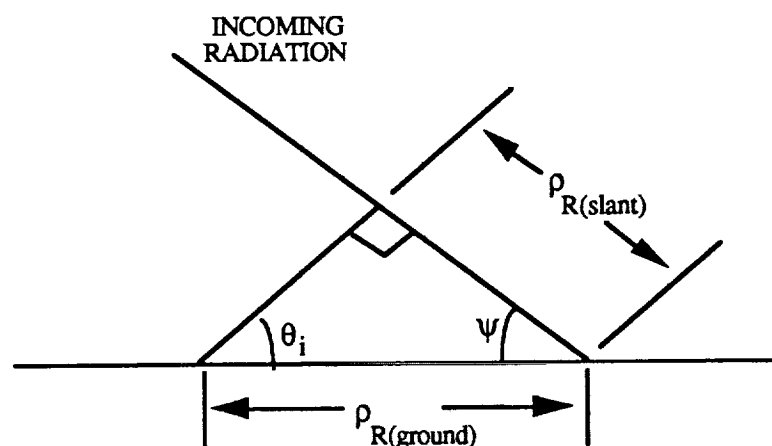


**Figure 3.2:** **Sketch showing the relation between the ground range and slant range dimensions.**

## 3.4.4　Incidence Angle

The look angle ($\theta_N$) of the radar system is defined as the angle that the main antenna beam (boresight) makes with respect to the local perpendicular to the ground (i.e., the Nadir). The depression angle ($\theta_d$) of the system is defined as the angle that the boresight makes with respect to the local horizontal. The incidence angle ($\theta_i$) is the angle, relative to the surface normal of target/ground, with which the incident radiation strikes the target/ground. The grazing angle ($\psi$) is defined as the complement of the incidence angle ($90 - \theta_i$). The latter two angles are dependent upon the earth curvature as seen in Figure 4.3.
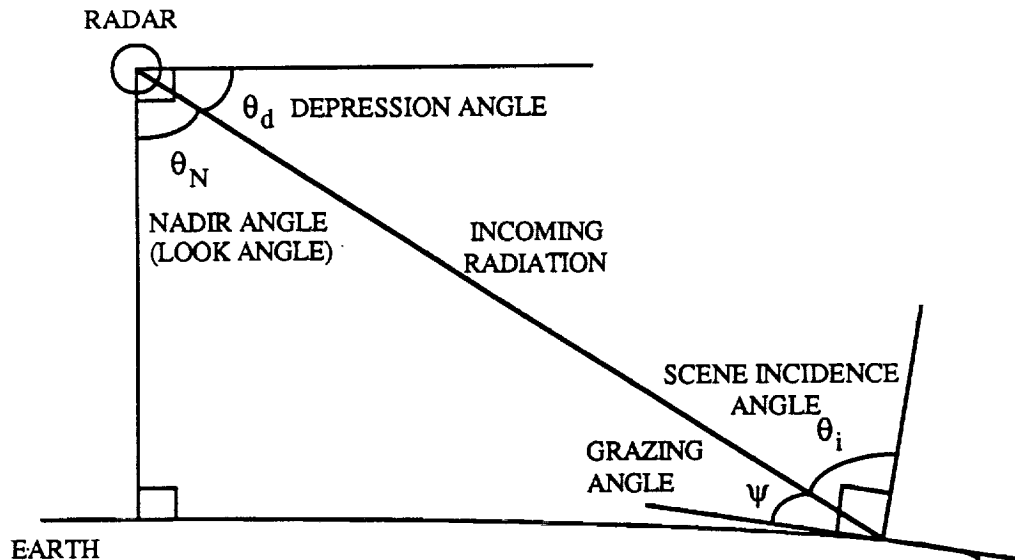


**Figure 3.3:　Radar/target scene geometry [3-20,p.126].**

The MEDSAT synthetic aperture radar will employ a small look angle. At small look angles, the surface of the earth can be approximated as flat. In this case, the depression and grazing angles can be considered equal, and the look angle and incidence angles can be considered equal. All of the radar parameters in this report were calculated using the flat earth assumption stated above. Although, some variation in the above angle equalities is expected when imaging large sloping targets like mountains and skyscrapers, these variations do not effect the calculations of the radar parameters.

The major reason for going to a small incidence angle radar system is the correspondingly lower antenna radiating power requirement, as compared to larger incidence angle systems. There are two reasons for the lower radiating power requirement, both being related to the imaging geometry. First, the smaller incidence angle corresponds to a closer range to target (R). As mentioned previously in the discussion about the satellite altitude, as the range is reduced, the radiating power is reduced because the antenna radiating power is directly proportional to the cube of the range to target (see equation 3-2 and Figure 3.4). The second reason for the lower radiating power requirement comes from the fact that as the illuminating radiation direction approaches the surface normal of the target/ground, the intensity of the radar backscatter (return echo strength) increases [3-49] (see Figures 3.5 and 3.6). Simply stated, as the incidence angle of the radar system decreases, more of the incident microwave radiation is reflected back to the antenna. Since the microwave

backscatter is higher at smaller incidence angles--as compared to larger angles--the required antenna radiating power is correspondingly reduced.
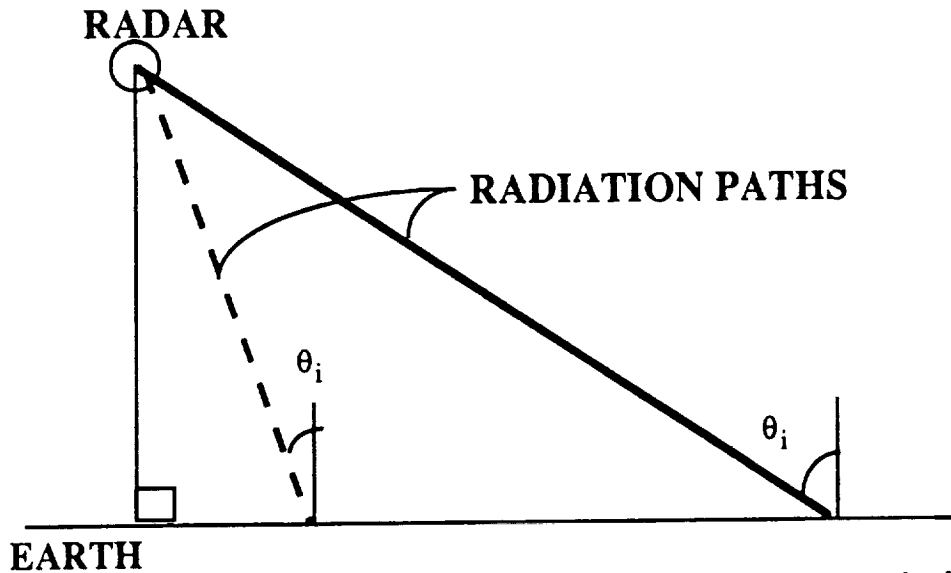


**Figure 3.4:** Sketch showing the reduction in range to target as incidence angle ($\theta_i$) is made smaller.
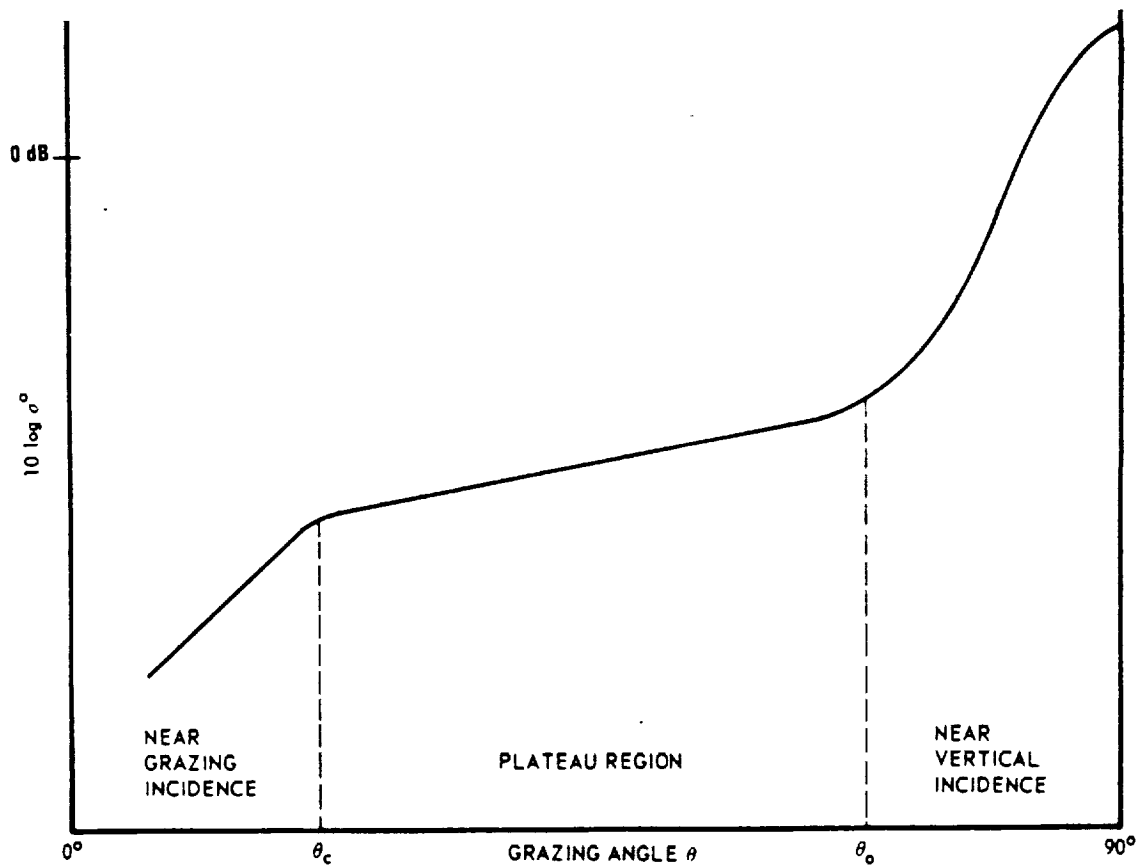


**Figure 3.5:** General target backscatter intensity (measured as $\sigma_0$) as a function of the grazing angle. Notice that MEDSAT will be operating in the near vertical incidence angle region [3-49,p.213].

σ°(θ) vs. θ
f = 415 Mc.
A - Water, Lake Bemidji, Minn.
B - Water, Salton Sea, Calif.
C - Apt.Bldgs., K.C., Mo.
D - Forest, Presque, Isle, Me.
E - Industrial areas, Minn., Minn.
F - Residential area, Minn., Minn.
G - Farmland, Cameron, Mo.
H - Snow Cov.farmland, Wahpeton,N.D.
I - Farmland, Sioux City, Iowa
J - Woods, Pine Island, Minn.

RELATIVE PLOTS OF
σ° VS. θ FOR VARIOUS
TERRAIN TYPES

σ°(θ) vs. θ
f = 3800 Mc.
A - Water, Salton Sea, Calif.
B - Water, Lake Bemidji, Minn.
C - Farmland, Cameron, Mo.
D - Apt. Bldgs., K.C., Mo.
E - Indust.area, Minn., Minn.
F - Snow cov. farmland,
    Wahpeton, N.D.
G - Res. area, Minn.,Minn.
H - Forest, Presque Isle,
    Maine
I - Farmland, Sioux City,
    Iowa
J - Woods, Pine Island,Minn.

**Figure 3.6:** **Backscatter intensity (measured as $\sigma_0$) as a function of the incidence angle for various target classes at P and S-band [3-49,p.246].**

One of the advantages of using a small incidence angle radar system is in the ability to discriminate various types of target classes. Comparison of image data from Seasat and the Shuttle Imaging Radars (SIR) A and B has shown that smaller incidence angle images (less than 35 degrees), as compared to larger incidence angle images, allow an image interpreter to discriminate between more geologic features [3-18]. There is also an indication that a similar relationship exists between incidence angle and separation of vegetation types. From a study completed using multiple incidence SIR-B data on forested regions in Argentina, the smaller incidence angle images were determined more useful for separating vegetation types [3-23]. As mentioned earlier in the section on detection, the smaller incidence angle (less than 20 degrees) is also desirable for the detection and measurement of soil moisture content through vegetation canopies [3-10, 3-27, 3-37, & 3-68].

The small incidence angle radar system also has the advantage that the Brewster angle criterion for vertically polarized transmit pulses will never be met within the swath [3-49]. The Brewster angle effect can be seen in Figure 3.7 where the reflectance coefficient curves dip toward zero. The criterion for the reduction in reflectance is that the angle of incidence equals the Brewster angle, where the Brewster angle is a function of the ratio of the dielectric constants of the target to that of air. When the criterion is met, most of the vertically polarized incident microwave energy penetrates the target/ground surface reducing the backscatter and hence the image brightness. The typical value of the Brewster angle for most terrain is about 62 degrees [3-6], and the value of the Brewster angle increases as the dielectric constant of the target/ground increases. Since the malaria problem is most acute in tropical parts of the world where there tends to be an abundance of rain/dampness, and moist soils tend to have fairly high dielectric constants, the Brewster angle will only get larger and the SAR imagery will not be effected.

Another advantage of the small incidence angle radar is that the images produced will provide the interpreter with information about the topography of the imaged target/ground. This is because smaller incidence angle images highlight the terrain surface slopes. Comparison of Seasat and SIR-A images indicates that terrain surface slope sensitivity is increased in the small (20 degrees) incidence angle images, while sensitivity to surface roughness is enhanced in images utilizing an intermediate (40 degrees) incidence angle [3-2 & 3-49]. The topographic sensitivity comes about due to the way the backscatter intensity is modulated by the surface slopes. In the small incidence angle images, the foreslopes tend to be brighter and backslopes are darker. The topographic information provided by these images is comparable to that normally provided by shadows in high incidence angle airborne radar images [3-18]. However, it must be kept in mind that when the target is very tall vertically (e.g., mountains or skyscrapers) image detail may be lost due to image layover which is discussed in the following paragraph.

The disadvantage of a smaller incidence angle radar system is the increase in amount of image layover for tall vertical targets like mountains and skyscrapers. Since the primary target area is the coastal plain area of Chiapas, Mexico--which is outside the mountainous region--this disadvantage should be negligible for the present imaging interests of the MEDSAT project. However, this disadvantage should be kept in mind if the MEDSAT satellite is to be used to provide images of other regions.

There are two possible cases of image layover, yet both may result in a loss of image detail on the sides of tall vertical targets. In the less severe case, when the angle of the foreslope or backslope of the tall vertical target is smaller than the look angle, the top of the target is displaced toward the satellite's line of flight in the image [3-42 & 3-54]. The foreslope in the image of this less severe case will appear to be steeper than actual due to a compression or foreshortening effect (see Figure 3.7), while the backslope will appear less steep than
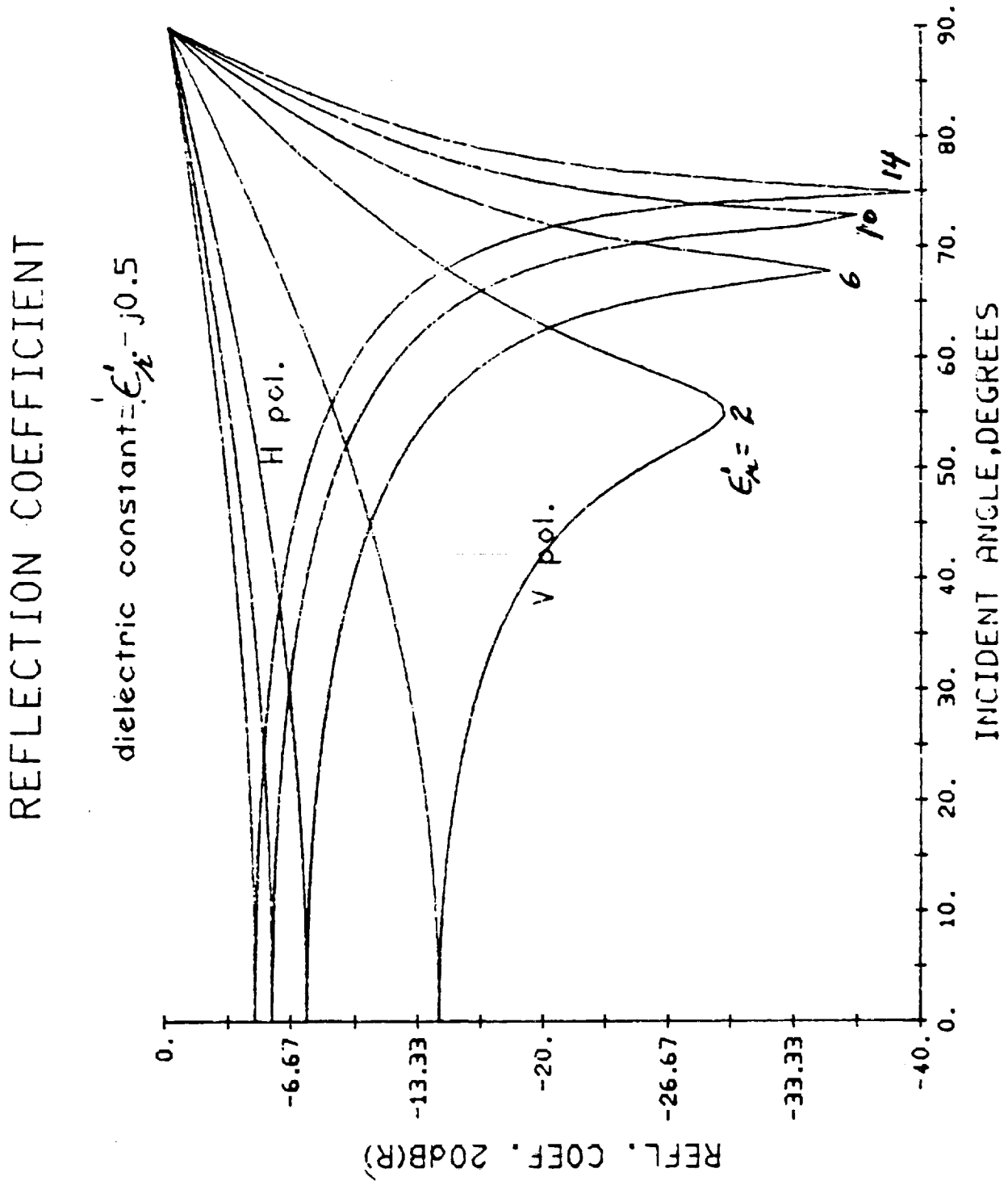
Figure 3.7: Magnitude of the reflection coefficient (ρ) as a function of the incidence angle for targets with various dielectric constants. Graph shows results for transmitted vertical (V) and horizontal (H) polarizations [3-6].

actual due to a stretching or lengthening effect [3-36]. The layover factor for the foreshortening, or lengthening, of the image slopes is given approximately by equation (3-12):

$$L_{f/l} = \sin(\theta_N - \alpha) \qquad\qquad (3\text{-}12)$$

where:

$\theta_N$ = look angle

$\alpha$ = angle of the surface slope (positive for foreslope and negative for backslope)

The extreme case of image layover occurs when the angle of the foreslope or backslope is greater than the look angle. When the foreslope angle is greater than the look angle, the top of the tall vertical target is actually closer to the radar antenna than the base of the target, so the return echo from the top of the target will reach the antenna before the return echo from the target's base. In the resulting image, the top of the target will again be displaced toward the satellite's line of flight. When the backslope angle is greater than the look angle, the backside of the tall vertical object will not be illuminated by the transmitted microwave radiation and a radar shadow will appear in the image.
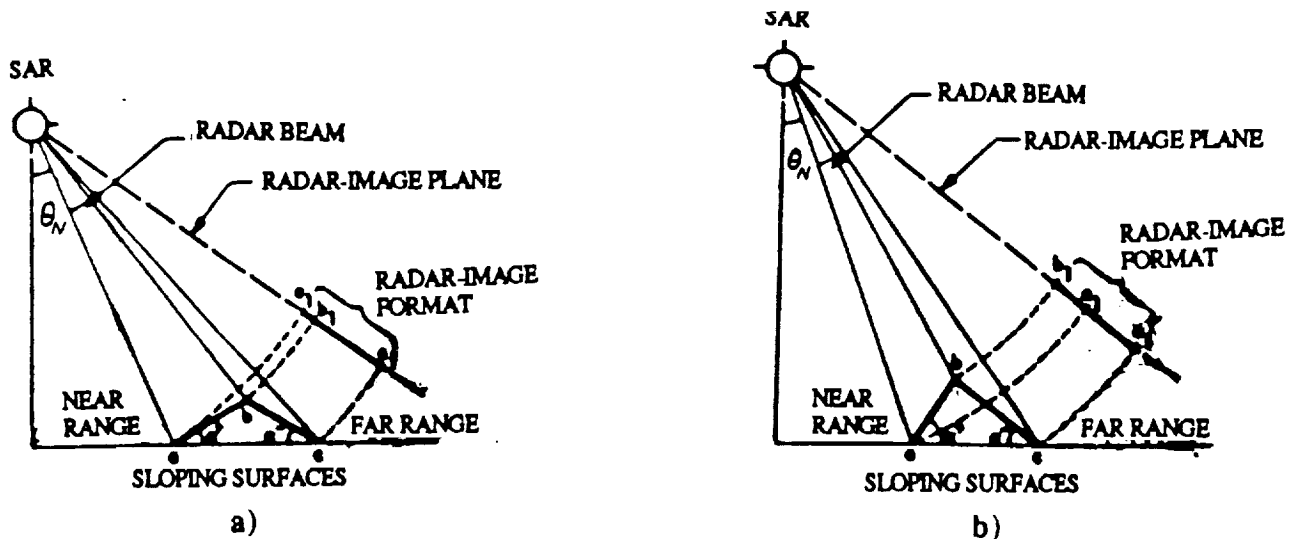


Figure 3.8: Sketch showing image layover for the two cases: a) less severe case; b) severe case [3-36].

Synthetic Aperture Radar

## 3.4.5    Polarization

The best discrimination of target classes on images would be obtained by using a synthetic aperture radar sensor that employs two or more frequency bands (e.g., a high frequency like X-band along with a lower frequency like L-band). The second best attribute that a SAR sensor could have to improve the target class distinction problem would be the ability to exploit the multipolar return signatures of the target/ground [3-2, 3-3, 3-8 & 3-10]. The MEDSAT SAR design is constrained--due to the power and size requirements of present technology devices--to employing only one frequency band. However, the increase in system power, data rate, and antenna complexity associated with going to a fully polarimetric SAR design is manageable with present technology devices [3-7, 3-14, 3-15, 3-24 & 3-53]. In the above sentence, a fully polarimetric SAR is a synthetic aperture radar system that has the ability to measure all the possible multipolar returns from the target/ground.

Therefore, the MEDSAT SAR sensor will be fully polarimetric in order to gain an increased ability to distinguish various target classes from each other in the resulting imagery. The polarimetric information will help to fill the image interpretation gap created by having to use only one frequency band in the SAR design [3-49, 3-54 & 3-58]. For example, one of the more important applications of the polarimetric information will be to help distinguish between short grass type flooded and open water areas. Discrimination of these two target classes would be very difficult using an image created from L-band, single polarization data. However, examination of multipolarization, L-band images with Steve Durden at JPL, has shown that L-band will give high phase shifted data (i.e., a brighter image for the cross polarized return) for short grass type flooded areas as compared to open water areas [3-3 & 3-29].

In active microwave remote sensing applications--like the MEDSAT SAR--part of the reflected microwave energy field from the target returns with polarization different than the incident field. This polarimetric information can be recorded using a SAR system designed to measure the magnitude and the phase of the multipolarized return echoes. The polarimetric radar information is typically characterized by the parallel-polarized returns HH and VV, and the cross-polarized returns HV and VH. The first letter indicates the transmitted polarimetric orientation of the microwave radiation, and the second letter indicates the received polarimetric orientation of the return echo from the target. In this notation, H stands for horizontal and V stands for vertical polarization with respect to the local horizontal of the target/ground.

In general, at any incident angle, echo strength of HH and VV returns tend to be about equal (1 to 2 db fluctuation) as seen in Figures 3.9 and 3.10, while VH and HV returns can be 3 to 10 db lower in magnitude than their corresponding parallel-polarized returns as depicted in Figure 3.11 [3-49, 3-50 & 3-57].

Cross polarization images tend to bring out the geometric or architectural differences in the target /ground. In an image scene, what is typically observed is that depolarizing scatterers tend to be small (twigs, ripples, leaves, grass), while the nondepolarizing scatterers tend to be large (tree trunks, limbs, waves, buildings) [3-49]. Scatterers that depolarize contribute equally to the cross-polarized returns HV and VH. These same scatters also contribute to the parallel-polarized returns HH and VV. However, the nondepolarizing scatterers contribute to parallel-polarized returns only (HH and VV).

Another factor that effects the return polarization is multipath reflections from the target. Multipath reflections occur when the incident microwave radiation experiences multiple bounces at the target surface before returning to the sensor. The multipath polarization
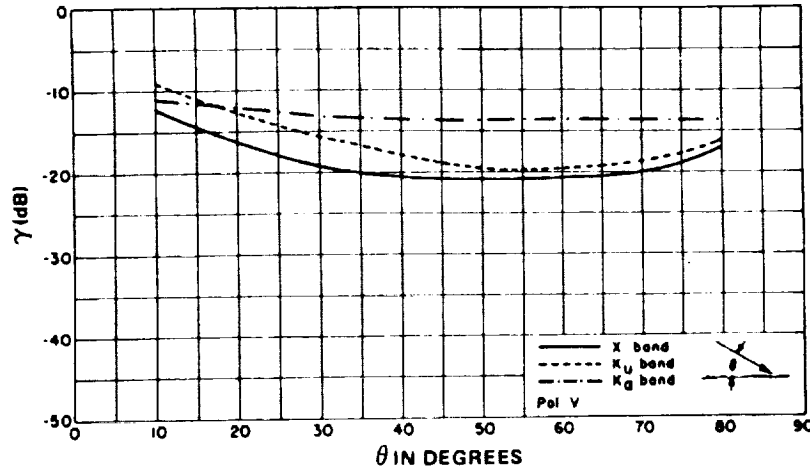


Source: Cosgriff, Peake, and Taylor (1960).

**Figure 6-12.** $\gamma_{vv}$ for 15-inch Green Grass in Head at $X$, $K_u$ and $K_a$ Bands, Where $\sigma°$ Equals $\gamma$ Sin $\theta$.
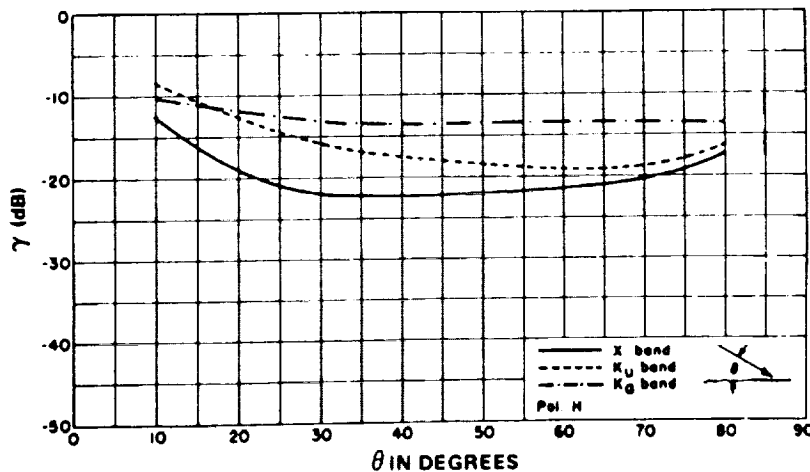


**Figure 3.9:** Backscatter intensity (measured as $\gamma = \sigma_0$ / sin$\theta$) as a function of the grazing angle ($\theta$) for 15 inch green grass in head at X, $K_u$ and $K_a$-bands: a) VV backscatter return; b) HH backscatter return. Notice the minimal difference between the magnitudes of the two backscatter intensities at grazing angles used in the MEDSAT design (around 75 degrees) [3-49,p.233].
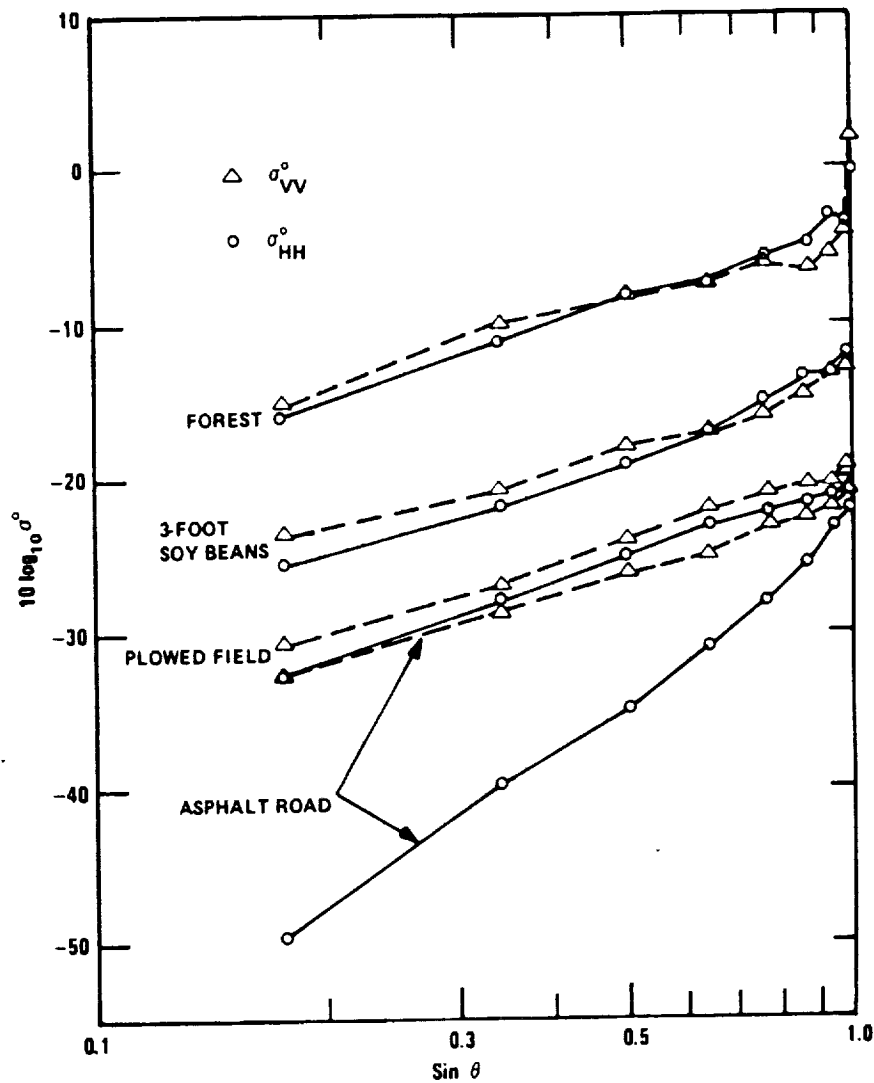
Figure 3.10: Horizontal and vertical backscatter intensity (measured as $\sigma_{oHH}$ and $\sigma_{oVV}$) as a function of the sine of grazing angle ($\theta$) for various target classes at X-band. Notice that the backscatter intensities are about equal for all target classes, except the (radar smooth) road, through the full range of grazing angles [3-49,p.237].
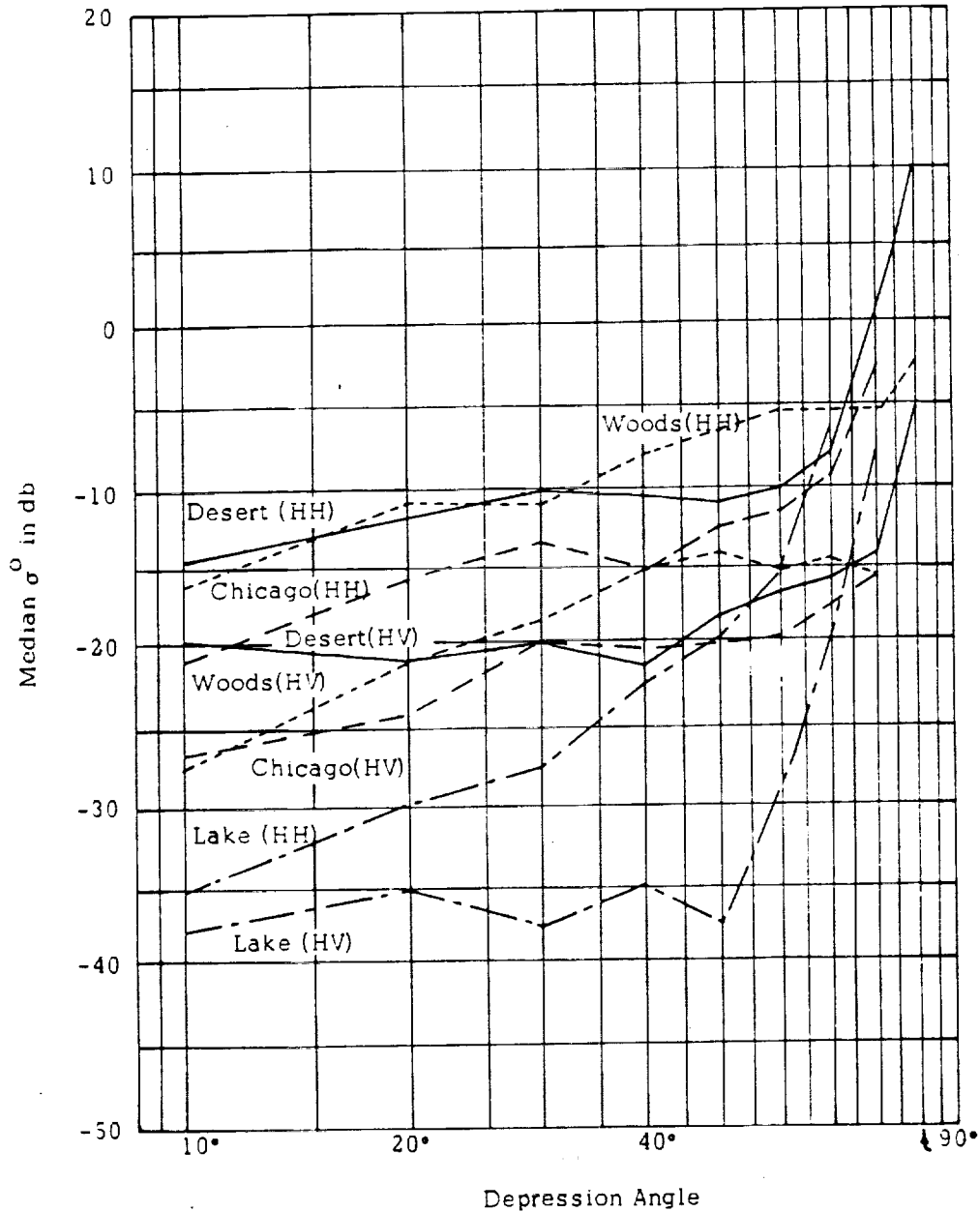
Figure 3.11: Backscatter intensity (measured as $\sigma_0$) as a function of the grazing (depression) angle comparing parallel-polarized and cross-polarized returns for various target classes. Notice that the cross-polarized backscatter intensities are always 3 to 10 db lower than their corresponding parallel-polarized backscatter intensity [3-50,p.75].

effect is important in the situation of flooded and nonflooded vegetated areas. When standing water is present under the vegetation, the double bounce interaction dominates making the HV and VH returns low, while making the HH and VV returns fairly high. When dry ground is present under the vegetation, single or multiple (more than two) bounce interaction occurs making the HV and VH returns fairly high [3-8]. In support of these ideas, it has been shown, in a polarimetric scattering model created at JPL, that the multipath reflection effect is the most important in determining the polarimetric return signature of dry ground forested areas [3-29].

Within the last five years, various techniques have also been developed for analysis of the polarimetric properties of SAR images [3-57 & 3-61]. One of the simplest techniques for examining the polarization characteristics of natural targets in the SAR data is to create ratios of normalized radar cross sections (i.e., ratio of the image power intensity) due to the various polarimetric returns and compare them [3-49].

## 3.5 System Design Specifications

This section describes the system design specifications of the MEDSAT synthetic aperture radar. The determination of these SAR design parameters is influenced not only by both the geometric imaging requirements--discussed in the previous section--and the power, size, and data rate constraints of the small satellite design, but also by the image quality requirements. The system design specifications that have a direct effect on the radiating power of the SAR system include: pulse repetition frequency (PRF), pulse length ($\tau$), system losses (L), noise temperature ($T_s$), signal-to-noise ratio (S/N), antenna area (A), and noise floor ($\sigma_0$). Equations (3-2) and (3-3) are repeated below in order to demonstrate how all these parameters are related to the radiating power:

$$P_{ave} = \{(S/N) \, (\lambda \, R^3 \, 8\pi \, L \, k \, T_s \, v_g)\} / \{A^2 \, \sigma_0 \, P_{R(ground)}\} \qquad (3-2)$$

$$P_{peak} = P_{ave} / (\tau \, PRF) \qquad (3-3)$$

The antenna is the SAR design parameter most heavily restricted by the size constraints of the MEDSAT satellite. The rest of system design specifications tend to have a more direct effect on the system data rate. These parameters include: burst repetition frequency (BRF), burst length, range chirp bandwidth, dynamic range and number of looks. The SAR design parameters that influence the quality of the resulting imagery are: signal-to-noise ratio, noise floor, dynamic range, number of looks, and range resolution. The rest of this section discusses each of these MEDSAT SAR system design specifications in more detail.

### 3.5.1 Pulse Length and Chirp Pulse Bandwidth

The actual system pulse length ($\tau$) was chosen as 20 $\mu$sec. This pulse length is similar to that used in various other terrain imaging satellite SAR systems. In order to obtain the 75 m resolution in ground range dimension, as determined from the previous section on geometric imaging requirements (section 3.4.3), the transmitted pulse is coded with a linear frequency modulation. The resultant coded pulse is called a chirp pulse. The equation and calculation involved in determining the frequency bandwidth of the chirp pulse for the MEDSAT SAR are given below, along with the equations for determining the resulting SAR system pulse compression factor and effective pulse length [3-38 & 3-20].

$$BW_{chirp} = c / (2 \, \rho_{R(slant)})$$ (3-13)

where:

$BW_{chirp}$ = chirp pulse bandwidth
c = speed of light ($300 \times 10^6$ m/s)
$\rho_{R(slant)}$ = slant range resolution = 19.41 m (see section 3.4.3)

$BW_{chirp}$ = 7.727 MHz

This corresponds to a pulse compression factor of:

$$C_p = \tau \, BW_{chirp} = 154.55$$ (3-14)

and an effective pulse length of:

$$\tau_{eff} = 1 / BW_{chirp} = 0.1294 \, \mu s$$ (3-15)

## 3.5.2  Pulse Repetition Frequency

The nominal pulse repetition frequency (PRF) for the Medsat SAR, has been determined to be 5047.95 Hz. This value was calculated assuming the SAR to be in quad polar (i.e., fully polarimetric) operation at 500 km altitude and 15 degree incidence angle with a range swath of 50 km. Application of the PRF value given above allows for the interleaving of the transmit an receive pulses along with a blockage of the Nadir return pulses.

The PRF has an upper bound value determined by range ambiguity which occurs when return echoes from different transmit pulses overlap in the radar's data window. This maximum limit is the inverse of the echo duration time [3-20, 3-30, 3-63 & 3-69]. As shown in the calculations below [3-69], the PRF upper bound for MEDSAT is about 9375 Hz.

$$PRF_{max} = 1 / \tau_e$$ (3-16)

$$\tau_e = \tau + \{2R_{swath} / c\}$$ (3-17)

where:

$\tau_e$ = echo return signal period
$\tau$ = actual transmitted pulse length (20 $\mu s$)
$R_{swath}$ = swath range = $R_{far} - R_{near}$ = 12,955 m
c = speed of light ($300 \times 10^6$ m/s)

$\tau_e = 20 \, \mu s + [2(12,955 \, m) / (300 \times 10^6 \, m/s)]$
$\tau_e = 106.366 \, \mu s$

$PRF_{max} = 9375.58$ Hz

The pulse repetition frequency also has a lower bound value determined by the Doppler ambiguity. Doppler ambiguity occurs when the transmitter does not pulse before the SAR satellite moves a distance of one-half the length of the real antenna [3-20, 3-63 & 3-69].

This minimum PRF for the MEDSAT SAR is about 2338 Hz, as shown in the calculation below:

$$PRF_{min} = (2\ v_g)\ /\ d_h = 2338.01\ Hz \tag{3-18}$$

where:

$v_g$ = equivalent ground velocity of SAR
$d_h$ = horizontal real antenna dimension

When operating in quad polar mode, the system transmits alternately polarized (H and V) pulses (see Figure 3.12). In order to adequately sample the Doppler bandwidth to create unambiguous polarimetric images (HH,VV,HV,VH) each sequence of horizontal and vertical pulses must meet the Doppler ambiguity constraint of $PRF_{min}$ calculated above [3-15 & 3-53]. This means the MEDSAT system's minimum PRF is twice that calculated above:

$$PRF_{min(quad\ system)} = 2\ (PRF_{min}) = 4676.02\ Hz \tag{3-19}$$

## polarized transmit pulses



## polarimetric receive pulses
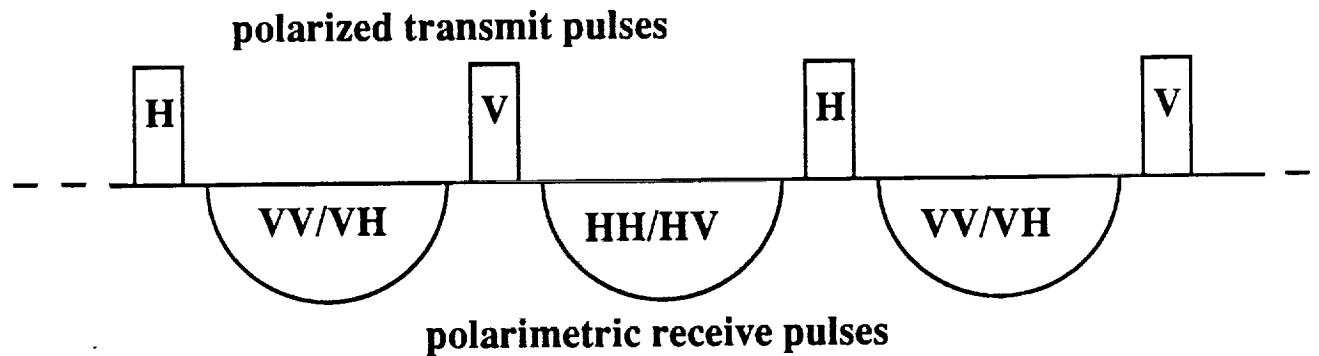
**Figure 3.12:** **Sketch showing the alternately polarized transmit pulses, and the polarimetric receive pulses.**

The PRF actually used by the system is determined as the value between the upper and lower bounds that will allow for interleaving of the transmit and receive pulses and, at the same time, not allow Nadir returns to enter the receive data window. The sketch in Figure 3.13 shows the timing that was arrived at in order to achieve the interleaving and Nadir blockage mentioned above. The time periods involved in this determination are defined below:

$$\tau_i = \tau_{sf} + \tau_e + \tau_{sb} = T_p - \tau \tag{3-20}$$

$$T_p = 1\ /\ PRF \tag{3-21}$$

$$\tau_{far} = (2\ R_{far})\ /\ c \tag{3-22}$$

$$\tau_{near} = (2\ R_{near})\ /\ c \tag{3-23}$$

$$\tau_{Nadir} = (2\ R_{Nadir})\ /\ c = (2\ h)\ /\ c \tag{3-24}$$

$$\tau_e = (\tau_{far} + \tau) - \tau_{near} = \tau + \{(2\ R_{swath})\ /\ c\} \tag{3-25}$$

where:

$\tau$ = transmitted pulse length = 20 $\mu$sec

$\tau_i$ = interpulse period = 178.1002 $\mu$sec

$T_p$ = pulse period = 1 / 5047.95 Hz = 198.1002 $\mu$sec

$\tau_{far}$ = time of first far field return = 3.4984 msec

$\tau_{near}$ = time of first near field return = 3.412 msec

$\tau_{Nadir1}$ = time of first Nadir return = 3.333 msec

$\tau_e$ = echo return period = 106.366 $\mu$sec

$\tau_{sb}, \tau_{sf}, \tau_{Nf}, \tau_{Nb}$ = safety factors for front and back of the receive pulse

The start time of transmission for the nth, first, eighteenth and nineteenth pulses is given by:

$$T_n = (n-1) \, T_p \qquad\qquad (3\text{-}26)$$

$T_1 = 0 \, T_p = 0$
$T_{18} = 17 \, T_p = 3.368$ msec
$T_{19} = 18 \, T_p = 3.566$ msec

From the above calculations, at PRF = 5047.97 Hz, it can be seen that the echo for the first transmit pulse returns at time $\tau_{near}$, after 18 pulses have been transmitted by the radar.

The time of next Nadir return is given by:

$$\tau_{Nadir2} = \tau_{Nadir1} + T_p = 3.531 \text{ msec} \qquad\qquad (3\text{-}27)$$

For PRF = 5047.95 Hz, proper interleaving occurs and the safety factors shown in Figure 3.13 have the following values:

$\tau_{sf}$ = 24.3 $\mu$sec

$\tau_{sb}$ = 47.4 $\mu$sec

$\tau_{Nf}$ = 58.7 $\mu$sec

$\tau_{Nb}$ = 13.0 $\mu$sec
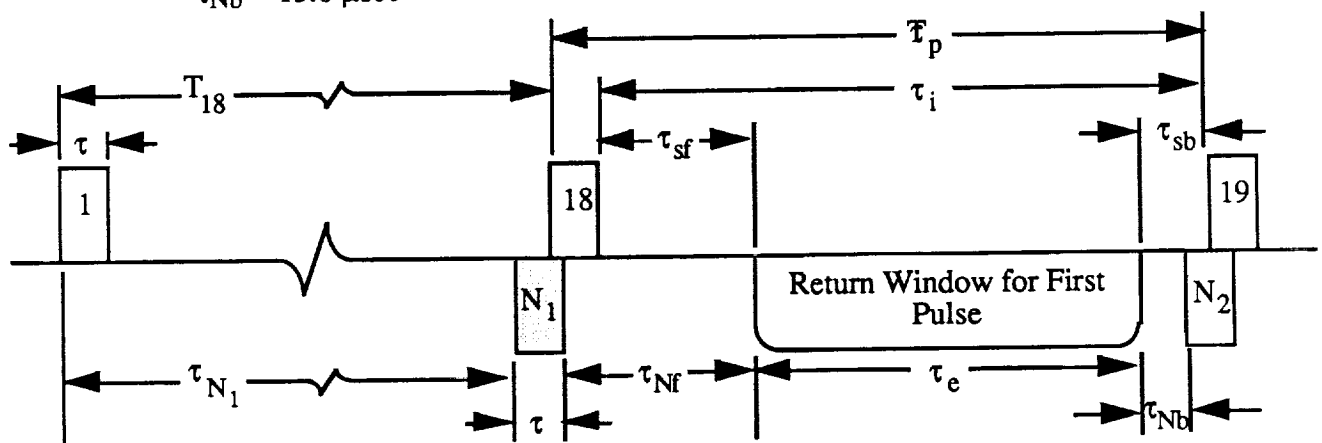


**Figure 3.13: Sketch of MEDSAT SAR transmit/receive pulse interleaving.**

The MEDSAT SAR system very sensitive to changes in the range to target (i.e., altitude), because of the small size of the antenna. Since the MEDSAT satellite will have altitude fluctuations, on-board, real-time PRF control will be required to deal with the range sensitivity of the SAR system. This could be accomplished by sending a test pulse out just before the sensing session to accurately determine the altitude [3-4]. After the altitude is known, the PRF of the system can be calculated by the on-board computer controller using a preprogrammed algorithm.

### 3.5.3    Number of Looks

Synthetic aperture radar image quality is reduced by speckle noise--small bright and dark spots on the image--which is caused by the fact that the radar illuminates the target with coherent radiation. Reduction of the speckle noise is typically accomplished by averaging independent estimates or "looks" of the imaged target area, since the signal-to-speckle noise ratio increases (image quality gets better) proportionally as the square root of the number of looks [3-69]. However, this noise reduction occurs at the expense of the system's azimuth resolution, since the azimuth resolution is inversely proportional to the number of looks.

The MEDSAT SAR will be incorporating four look image processing ($N_L$ = 4) in order increase the signal-to-speckle noise ratio. Four look image processing is typically used for terrestrial imaging with space-based SAR systems [3-35, 3-55, 3-62 & 3-69].

A single "look" in the MEDSAT design, like those of Cassini and Magellan, corresponds to one of the active "burst on" times of the SAR system [3-4, 3-12, 3-30, 3-43, 3-55, 3-70 & 3-71]. This means, assuming the resolution is kept constant, an increase in the number of looks corresponds to an increase in the number of active "burst on" times for the radar, which results in a higher operational data rate and power draw for the MEDSAT SAR system. The relation between the number of bursts and the system power and data rate is discussed in more detail in the next section.

### 3.5.4    Burst Mode Operation

The MEDSAT SAR will be employing burst mode operation, in order to reduce the operational data rate and power draw of the sensor. This mode of operation has been well developed by JPL on the Magellan and Cassini SAR systems [3-4, 3-12, 3-30, 3-43, 3-55, 3-70 & 3-71]. This technique works by simply turning the radar on and off in specific timed bursts during the imaging time over the target. The duration of the "burst on" time is calculated to create a synthetic aperture (antenna lengthening) of sufficient length to satisfy the azimuth resolution specification. A sketch qualitatively showing two cycles of the burst mode operation is shown in Figure 3.14.

**BRF = 1.4 Hz**          **PRF = 5050 Hz**
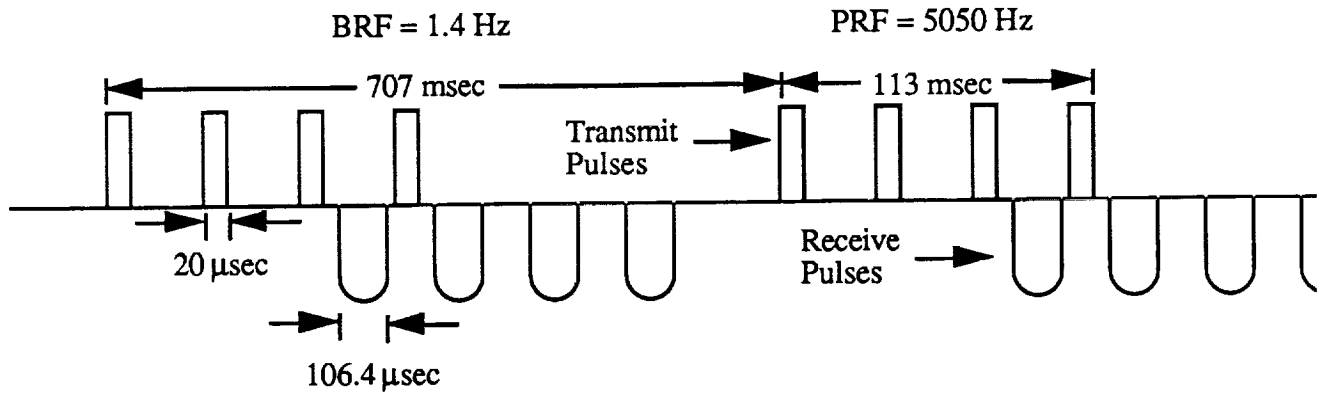
Figure 3.14: Sketch of MEDSAT SAR burst mode operation showing two burst cycles.

In the MEDSAT design, the "burst on" duty cycle works out to be 17%. This corresponds to an 83% reduction in the number of transmitted pulses as compared to a traditional continuous mode SAR. The reduction in the number of transmitted pulses for the MEDSAT SAR results in a lower operational power draw and a smaller amount of data per image, since the amount of return echoes is also reduced.

The following calculations show how the parameters of burst length, number of pulses per burst, point target dwell time, burst repetition frequency (BRF), data reduction ratio ($M_D$), and power reduction ratio (Mp) are determined.

As mentioned above, the length of the "burst on" time ($\tau_b$) is determined primarily by the azimuth resolution of the system (see the equation below) [3-4 & 3-71]. For the MEDSAT SAR, the "burst on" time is about 113 msec.

$$\tau_b = (R\,\lambda)\,/\,(2\,v_g\,\rho_A) = 113.16 \text{ ms} \qquad (3\text{-}28)$$

where:

variables are as defined previously

The number of pulses per burst (Np) is simply given by the burst length times the pulse repetition frequency [3-4 & 3-71]. As seen in the calculation below, the number of pulses per burst is 571 for the MEDSAT SAR design.

$$N_p = \text{integer value of } [\tau_b\,\text{PRF}] \qquad (3\text{-}29)$$

$$N_p = \text{integer value of } [571.226] = 571$$

The point target dwell time ($\tau_d$), also known as the integration time, is the time that it takes the satellite to move the length of the synthetic aperture [3-20 & 3-71]. The MEDSAT SAR design, as determined below, has an integration time of approximately 3 sec.

$$\tau_d = (R\,\lambda)\,/\,(v_g\,d_h) \qquad (3\text{-}30)$$

$$\tau_d = 2.829 \text{ s}$$

The burst repetition frequency is a function of the point target dwell time and the number of looks per image as shown in the equation below [3-71]. The meaning of this equation for the MEDSAT SAR system is that each point target will be illuminated by four bursts in order to create the resulting 4-look image. This will require a burst repetition frequency of 1.4 Hz, and corresponds to a burst period of about 707 msec.

$$BRF = N_L / \tau_d = 1.4139 \text{ bursts/s} \qquad (3-31)$$

$$T_b = 1 / BRF = 707.25 \text{ ms} \qquad (3-32)$$

The data reduction ratio is used in the calculation of the amount of image data received by the SAR (section 3.5.5), and is given by the "burst on" time divided by burst period (see equation below). In the MEDSAT SAR design, the data rate reduction ratio is 0.16000 (or 16%).

$$M_D = \tau_b / T_b \qquad (3-33)$$

$$M_D = 113.16 \text{ ms} / 707.25 \text{ ms} = 0.16000$$

The power reduction ratio is used to calculate the average power draw required from the satellite power supply while in burst mode (section 3.5.5). Since power draw is required during the transmission and reception of signals, the time for the return of the last pulse from the burst must be added to the burst time before the power reduction ratio is computed (as shown in the equation below). For MEDSAT SAR, this works out to be 0.16497 (or 17%).

$$M_P = (\tau_b + \tau_{far} + \tau) / T_b \qquad (3-34)$$

$$M_P = (113.16 \text{ ms} + 3.4984 \text{ ms} + 20 \text{ } \mu s) / 707.25 \text{ ms}$$

$$M_P = 0.16497$$

### 3.5.5    Data Rate

The MEDSAT design will incorporate an adaptive quantization scheme similar to that used by the Magellan and Cassini SAR systems. This approach allows the system to retain a large dynamic range while using fewer bits. This quantization scheme provides a data compression to compliment the data reduction obtained by the burst mode operation. Applying these two techniques to decrease the amount of SAR data means that the system will operate at a much lower data rate and require substantially less memory than traditional SAR systems.

Modeling the MEDSAT design after those of the above mentioned JPL designs, the incoming data will be initially quantized to 8-bits per sample (i.e., 8-bit dynamic range). This 8-bit data is then passed through a device similar to Magellan's block adaptive quantizer where the input 8-bit data is returned in 2-bit form [3-46, 3-43, 3-55 & 3-71].

Since the MEDSAT SAR will be operating in fully polarimetric mode two sets of polarized return data will be present in a single receive window (i.e. HH and HV or VV and VH). These parallel-polarized and cross-polarized returns will be separated into two channels, each of which will be initially quantized to 8-bits [3-43 & 3-53]. This addition of one more channel to the data stream is offset by the subtraction of one channel due to the elimination

of the on-board separation of the receive signal into its two component signals with the formats of in-phase and quadrature (I-Q). The transformation of the return signal to in-phase and quadrature (I-Q) format is planned to be completed during the digital processing on the ground using Hilbert or Fourier transform techniques [3-35].

Sampling theorem states that in order to be able to reconstruct the original continuous time signal (analog signal) from its samples (digital signal) the sampling rate (A to D sampling frequency) must be greater than the Nyquist rate of the input signal. Where the Nyquist rate is defined as twice the highest frequency contained in the analog signal [3-35]. For the MEDSAT SAR system, this means that the sampling rate must be greater than two times the range chirp bandwidth. A sampling rate of $\gamma=2.2$ was chosen for MEDSAT based on the value used for Seasat [3-35].

The following calculations show how the very large instantaneous data rate of the MEDSAT SAR is reduced to a more manageable value by time expansion buffering (stretch processing) [3-20], burst mode operation [3-43], and block adaptive quantization [3-43]. This process is also depicted in Figure 3.15.

The first step is the calculation of the instantaneous data rate [3-20 & 3-43]. From the calculation below, the instantaneous data rate for the MEDSAT SAR is about 272 Mbits/sec.

$$DR_I = (BW_{chirp}) \gamma Q C \qquad\qquad (3-35)$$

where:

$C$ = number of channels (2)
$Q$ = system dynamic range (8 bits/sample)
$BW_{chirp}$ = range chirp bandwidth (7.727 MHz)

$\gamma$ = sampling rate (2.2 samples/cycle)

$DR_I = 271.99$ Mbits/s

The next step is to calculate the data rate reduction (inherent in all satellite SAR systems) due to the fact that the length of the receive pulse is not equal to the interpulse period. This reduction is called time expansion buffering or stretch processing [3-20 & 3-43]. The MEDSAT SAR data rate (as calculated below) after applying this time expansion buffering is about 163 Mbits/sec.

$$DR_P = DR_I (\tau_e / \tau_i) \qquad\qquad (3-36)$$

where:

$\tau_e$ = echo return period (106.366 $\mu$s)

$\tau_i$ = interpulse time (178.100 $\mu$s)

$DR_P = 162.43$ Mbits/s

In the third step (as shown below), the data rate reduction due to the burst mode operation (section 3.5.5) is calculated resulting in a data rate of about 26 Mbits/sec for the MEDSAT SAR [4-43].

$$DR_B = DR_P (\tau_b / T_b) = DR_P M_D \qquad\qquad (3-37)$$

$DR_B = 25.99$ Mbits/s

The final step is the calculation of the data compression due to the block adaptive quantization [3-43]. From the calculation below, the final MEDSAT SAR data rate to the recorders is about 6.5 Mbits/sec.

$$DR_{BAQ} = DR_B (2/8) = DR_B (.25) = 6.497 \text{ Mbits/s} \qquad (3\text{-}38)$$

As determined in the calculation below, the total recorder memory capacity needed for an image of 250 km by 50 km is about 234 Mbits.

$$\text{total memory (one image)} = DR_{BAQ} T_{sensing} \qquad (3\text{-}39)$$

$$\text{total memory (one image)} = (6.497 \text{ Mbits/s})(36 \text{ s})$$

$$\text{total memory (one image)} = 233.91 \text{ Mbits}$$

## 3.5.6 Signal to Noise and System Noise Floor

The thermal signal-to-noise ratio (S/N) of 8 db for MEDSAT was chosen to assure image quality after applying 2-bit block adaptive quantization to the data (as discussed in the previous section). The decision to use the 8 db value was based on the results of simulation studies, performed at JPL for the Cassini and Magellan SAR systems, with terrestrial radar images at various S/N's and quantization levels. These simulation results indicated that for a 2-bit quantization level, and more than four looks, the images showed no apparent changes in quality at S/N values higher than 8 to 8.5 db, but lower values of S/N degraded the images [3-43, 3-55 & 3-71].

This choice of thermal signal-to-noise ratio also agrees with the S/N values used by other SAR systems (4.7 to 7.7 db, without data compression) to successfully create terrestrial imagery applied to detect wetlands, crops, and other target types.

The system noise floor is the minimum detectable normalized radar cross section of the SAR. The normalized radar cross section ($\sigma_0$) is the parameter typically used to specify the target return echo strength (see equation (3-40)). The normalized radar cross section ($\sigma_0$) is defined as the the target's average radar cross section, within a ground resolution cell, normalized to the illuminated surface area (i.e., area of the ground resolution cell). The radar cross section (RCS or $\sigma$) is a measure of the backscattering properties of the target, and is defined as the effective area--as seen by the radar--of a target (for a more detailed discussion of RCS the reader is referred to [3-45, 3-58 & 3-64]).

$$\sigma_0 = \sigma / A_g \qquad (3\text{-}40)$$

$$A_g = \rho_{R(ground)} \rho_A \qquad (3\text{-}41)$$

where:

$\sigma$ = average radar cross section in units of $m^2$
$A_g$ = ground resolution cell area

$A_g$ = (75 m)(75 m) = 5625 $m^2$

As mentioned earlier in the section on detection (section 3.2), the radar target return is a function of various scattering mechanisms within the resolution cell of a radar system.
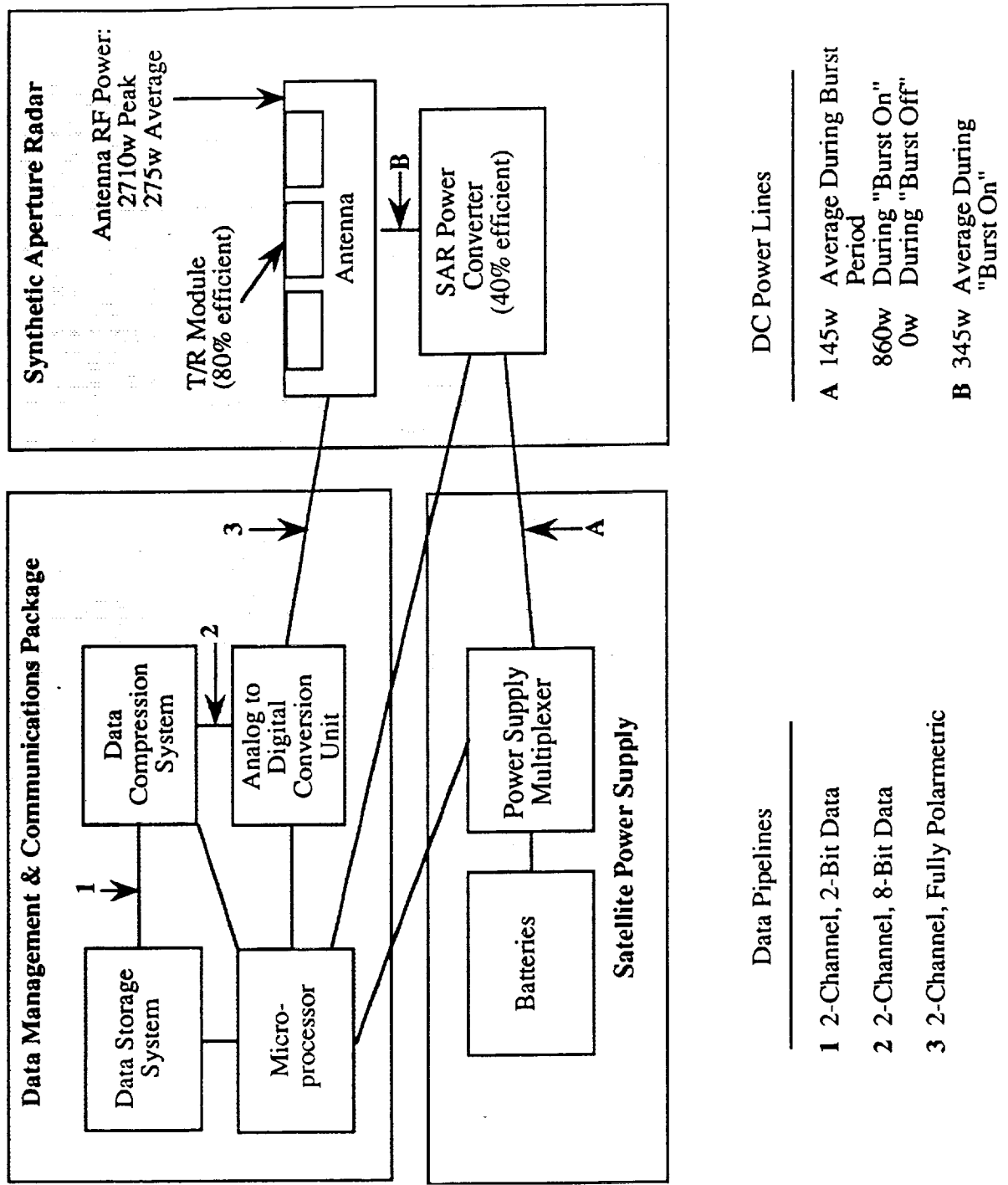
Figure 3.15: Block diagram showing the MEDSAT SAR system's power and data paths.

Thus, the value obtained for the normalized radar cross section ($\sigma_0$) is dependent upon both the properties of the radar system and target. The radar system variables that determine $\sigma_0$ are: wavelength, incidence angle, and polarization. The target properties of importance to $\sigma_0$ are: complex dielectric constant, architecture, gross size, and surface roughness. Most of the target properties are dependent upon the radar system variables as well as on environmental conditions. For example, the microwave surface roughness is dependent upon the wavelength and incidence angle (see equation (3-1)), and the complex dielectric constant is dependent on all three radar variables mentioned above.

Environmental conditions (seasons, rain, snow, temperature, time of day) have a big effect on the target properties that determine the value of $\sigma_0$ measured by a given radar system. For instance, the complex dielectric constant for rocks, soils and vegetation changes with the temperature and the amount of water present (both internal and external moisture content). An example of the somewhat random nature of environmental effects on $\sigma_0$ is the situation of a plowed field before and after a rain. The plowed field will tend to have less surface roughness after the rain, but the moisture content of the soil will be greatly changed, and--in the case of a very heavy rain--errosion may even cause the larger scale surface roughness to increase.

Another factor that enters into the determination of $\sigma_0$ is target surface penetration. The depth of penetration is dependent upon the wavelength, polarization, and complex dielectric constant (i.e., moisture content) of the target surface. Thin covering materials (about 1 to 10 cm thick) may be penetrated and the resultant radar scattering becomes a sum of the scattering from the various layers of the target (surface, volume, and sub-surface scattering). Thus, when significant penetration occurs, the return echo is no longer providing information about the target surface alone, and the true value of $\sigma_0$ for the surface can not be determined without having previous knowledge of the backscatter from the other layers of the target [3-6 & 3-49]. This penetration phenomena is typically most severe in very dry snow or soils where the dielectric constant is very low, and as mentioned before in the section on geometric imaging requirements (section 3.4.4), there tends to be an abundance of rain/dampness in the regions where the malaria problem is most acute (i.e., the tropics) resulting in moist soils with fairly high complex dielectric constants. Therefore, when choosing the noise floor value the very dry, high penetration types of targets did not have to be considered.

In the MEDSAT SAR design, the choice of the minimum detectable value of $\sigma_0$ (noise floor) is determined by considering the radar system and target properties that produce a minimum in the return echo strength. The following sentences refer to the graph in Figure 3.11. At a wavelength of .23 m and incidence angle of 15 degrees (i.e., depression or grazing angle of 75 degrees), the backscatter will be least for a smooth surface with a relatively high complex dielectric constant. This combination is met by the lake surface. The data for the parallel-polarized return for the lake only goes to 70 degrees, the measurement is made from this value and should actually make the determination of the noise floor for the system more accurate, since this grazing angle is closer to the local grazing angle experienced at the far range of the swath. As expected from the previous discussion on polarization, the plot shows that the cross-polarized $\sigma_0$ for the lake ($\approx$ -20 db) is lower than the parallel-polarized $\sigma_0$ ($\approx$ -7 db) by about 13 db. Since the system will be fully polarized, the noise floor choice is based on the cross-polarized value of $\sigma_0$.

The MEDSAT SAR system is designed with a noise floor of $\sigma_0 = -23db$. The value of $\sigma_0 = -23$ db for the noise floor was chosen to give a margin of error to the measurement taken from the graph of Figure 3.11, since the calibration between the system that took the measurement and the MEDSAT system will most likely not be the same. The value of $\sigma_0 = -23$ db for noise floor was also indicated as an example value for a space-based terrestrial imaging SAR system in [3-63]. From the graphs in Figures 3.6, 3.16 & 3.17, it can be seen that this value of noise floor is well below the normalized radar cross sections for most target classes at the wavelength and incidence angle of the MEDSAT SAR. This noise floor value is also below (i.e., better than) the values of noise floor used in most other planned or existing satellite SAR systems.
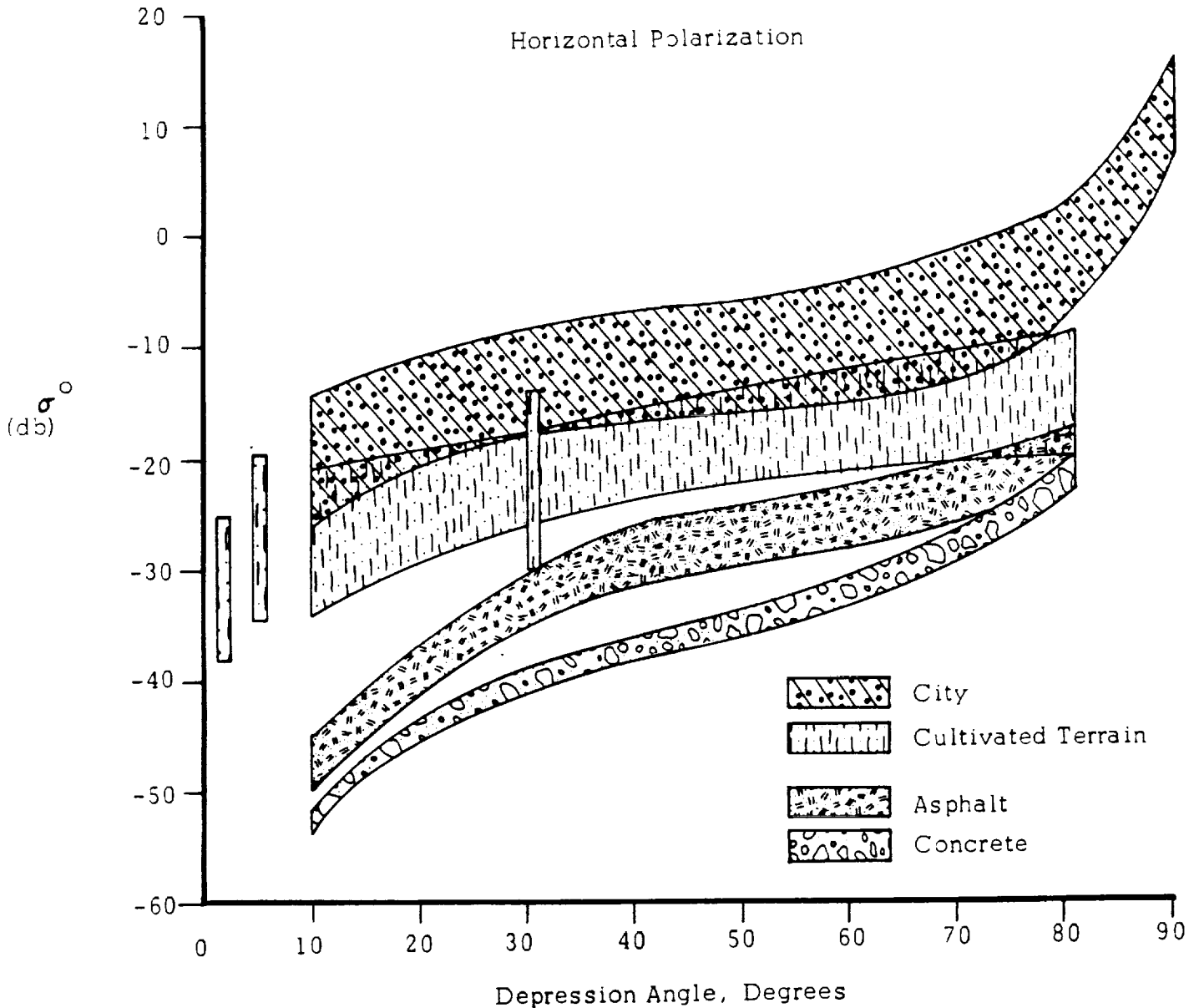


Figure 3.16: Backscatter intensity (measured as $\sigma_0$) as a function of the grazing (depression) angle for various target classes [3-50,p.65].
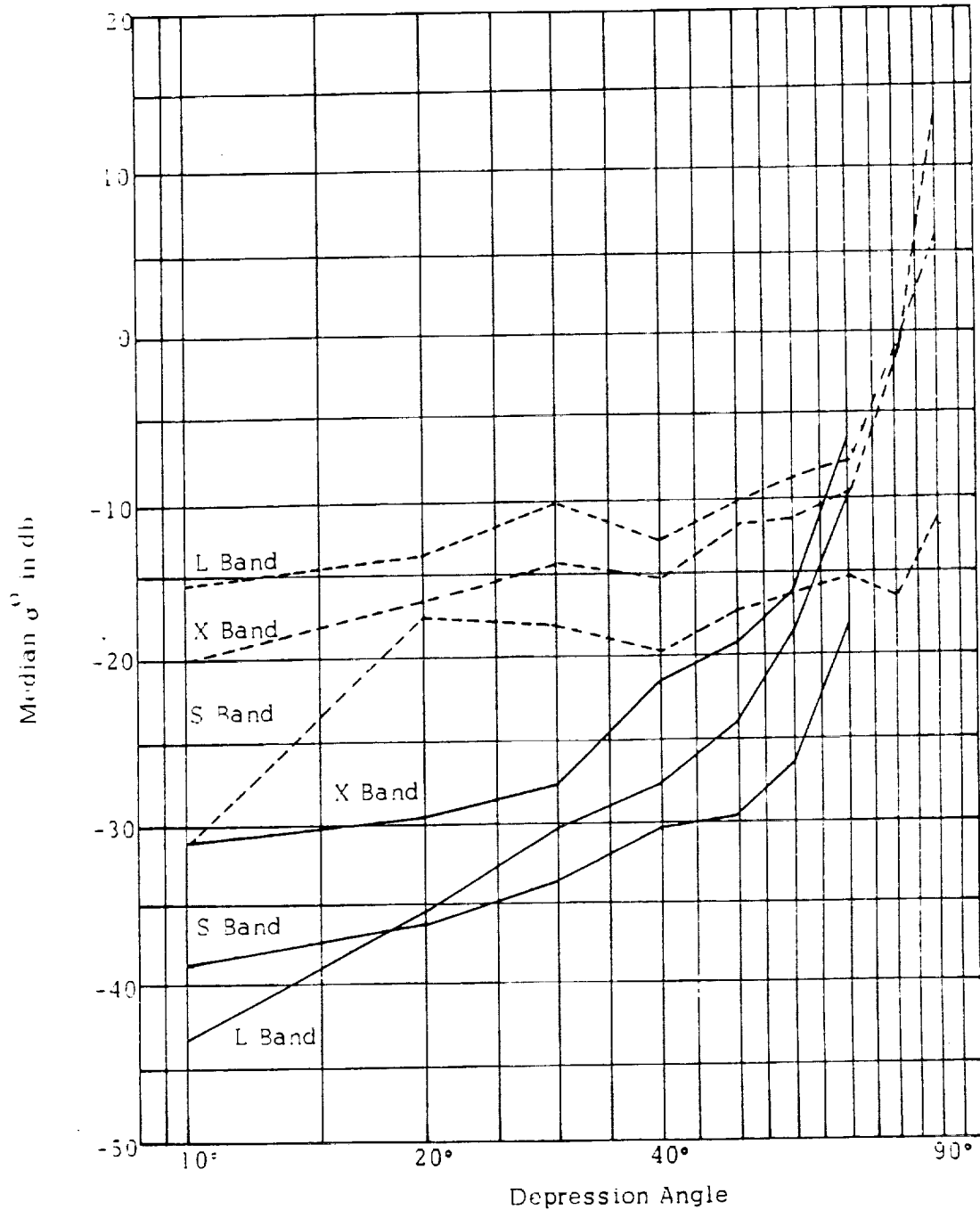
Figure 3.17: Backscatter intensity (measured as $\sigma_0$) as a function of grazing (depression) angle for two target classes at different wavelengths [3-50,p.71].

### 3.5.7    System Loss Factor and Noise Temperature

Once the radar frequency band (wavelength) is chosen, the system loss factor and noise temperature can be approximated. In general, as the SAR system's wavelength increases the system losses and noise temperature decrease. A large percentage of the SAR system noise temperature is due to the surface temperature of target/ground being imaged (typically 290 K), with the rest coming from receiver noise/losses and antenna temperature.

For the MEDSAT SAR which operates at L-band (1.275 GHz / 0.23 m), the noise temperature $(T_s)$ is about 500 K and the system loss factor (L) is around 4 db [3-16, 3-20 & 3-58].

### 3.5.8    Radiating Power Calculation

Now that the all the parameters for the power equations (3-2) and (3-3) are defined, a calculation can be made to determine the radiating power required by the MEDSAT SAR antenna (assuming a 6 m by 1 m antenna size, see discussion in next section). Substituting into the power equations, as shown below, gives an average radiating power for the antenna of about 275 w which corresponds to a peak radiating power of about 2710 w (see Figure 3.15).

Using equation (3-2) to determine average radiating power:

$$P_{ave} =$$

$$\frac{(6.30957)(.23m)(1.3870 \times 10^{17} m^3)(8\pi)(2.511886)(1.38 \times 10^{-23} J/K)(500K)(7014.02\ m/s)}{(6\ m^2)(5.01187 \times 10^{-3})(75\ m)}$$

$$P_{ave} = (20450.733\ w\ m) / \rho_{R(ground)} = 272.68\ w$$

averaging up to allow for errors we get:

$$P_{ave} = 275\ w$$

Using equation (3-3) to determine the peak radiating power:

$$P_{peak} = P_{ave} / (20 \times 10^{-6}\ sec)\ (5047.95\ Hz) = P_{ave} / .100959 =$$

$$P_{peak} = P_{ave}\ (9.905011) = 2700.86\ w$$

averaging up to allow for errors we get:

$$P_{peak} = 2710\ w$$

Knowing these antenna radiating power values, the antenna design can now be determined. This design step is addressed in the next subsection.

### 3.5.9 Antenna Design

In order to meet both the budget and launch vehicle constraints of MEDSAT, the synthetic aperture radar's antenna needs to satisfy the following requirements:

- be relatively inexpensive
- have low mass
- have the ability to fold into a compact size
- possess beam steering capability
- use minimal amounts of power
- have the ability to operate in quad polarized mode

Aperture antennas are unable to fulfill these requirements because of their manufacturing complexity, which results in higher costs, and their large size. The most feasible method of meeting the SAR's design specifications is through the use of distributed active phased array microstrip technology. Microstrip antennas have been space-proven on many previous satellite SAR systems.

The small satellite design places severe limitations upon the antenna's size and mass. Therefore, the overall size of the MEDSAT's SAR antenna will be only 6 m x 1m. Drawbacks of such a small antenna include decreased antenna gain, increased power requirements, a higher PRF requirement, and larger chirp/receive bandwidths.

To meet the payload specifications of the launch vehicle, the antenna will be subdivided into 10 identical panels, each 51 cm x 100 cm. These panels will be separated by 10 cm and will be supported by a foldable epoxy-graphite truss. This will allow for folding into the necessary stowed configuration. A basic layout of the extended antenna is shown in Figure 3.18.

The minimum number of Transmit/Receive (T/R) modules needed on the antenna is derived from the peak radiated antenna power and the peak RF transmitting power of these modules as shown [3-7]:

$$N_{modules} = P_{peak} / P_{module} \qquad\qquad (3\text{-}42)$$

where:

$P_{peak}$ = peak radiated antenna power (2710 w)
$P_{module}$ = peak RF transmitting power of T/R modules (12 w)

With a required peak power of 2710 w, this equation shows that a minimum of 226 T/R modules operating at 12 w will be needed. By using multiple T/R modules, the SAR gains advantageous beam steering capabilities. This will allow for the optimization of the main and side lobes of the antenna. In the actual design, a total of 250 modules should be used. This redundancy will help to protect against possible equipment failures, since the antenna will remain operational as long as 90% of the radiating elements are still working.

Each T/R module will drive a single patch element which is orientated for either horizontal or vertical polarization. Patch elements of the two orientations are positioned alternately along the antenna's azimuth and elevation dimensions. In order to obtain quad polarized operation, the peak antenna radiating power must be obtained for both the horizontal and vertical transmit pulses. This means the number of patch elements, and corresponding T/R modules, must be doubled--resulting in a total of 500 patch elements required on the antenna. Each of the 10 panels will contain identical groups of 50 elements. They will be placed in an array with 10 elements in the elevation direction and 5 elements in the azimuth

direction (see Figure 3.18). The minimum spacing from the center of one element to the center of its neighbor can be determined with the following equations [3-25]:

$$x_{elevation} = (2.65 \, \lambda_o) / \{(M+1) \, \pi \, \beta_{elevation}\} \qquad (3\text{-}43)$$

$$x_{azimuth} = (2.65 \, \lambda_o) / \{(N+1) \, \pi \, \beta_{azimuth}\} \qquad (3\text{-}44)$$

where:

$x_{elevation}$ = the element spacing along the elevation axis

$x_{azimuth}$ = the element spacing along the azimuth axis

$\lambda_o$ = the nominal free-space wavelength of microwave radiation (25 cm)

$M+1$ = the number of elements along the elevation axis (10)

$N+1$ = the number of elements along the azimuth axis (50)

$\beta_{elevation}$ = the half-power elevation beamwidth = $\lambda_o / d_v$ = .25 radians

$\beta_{azimuth}$ = the half-power azimuth beamwidth = $\lambda_o / d_h$ = .04167 radians

These formulas yield an elevation spacing of at least 8.5 cm and an azimuth spacing of at least 10.2 cm. The patch elements will have rectangular shapes with the longer edge being the direction of polarization. The length of the long edge is approximately $(1/2)\lambda_m$, where $\lambda_m$ is the wavelength in the patch's dielectric material. This can be found using:

$$\lambda_m = \lambda_o / (\epsilon_r)^{1/2} \qquad (3\text{-}45)$$

where:

$\epsilon_r$ = relative permitivity of the dielectric material

Using a typical value for $\epsilon_r$, such as 2.3 [3-59, 3-73 & 3-75], the long edge's length is found to be 8.24 cm. The short side of the patch needs to have a length of only about $(1/3)\lambda_m$ to insure that the patch is polarized in only one direction. Thus, this side is 5.6 cm long. As shown in Figure 3.18, it is possible to satisfy these spacing requirements by placing the patches every 3 cm in the elevation direction while spacing them every 4 cm in the azimuth direction.

The required DC input power from the satellite's power supply to the antenna is about 860 w during the "burst on" time, and 0 w during the "burst off" time. This is found by assuming a 40% efficiency from the satellite's power supply to the T/R modules and an 80% efficiency from the modules to the radiating elements as shown below (also see Figure 3.15):

$$P_{DC} = P_{ave} / \{(\eta_{ps}) (\eta_{sr})\} \qquad (3\text{-}46)$$

where:

$P_{ave}$ = the average power radiated by the antenna (275 w)

$\eta_{ps}$ = the power efficiency from the power supply to the T/R modules (40%)

$\eta_{sr}$ = the power efficiency from the T/R modules to the radiating elements (80%)

The average power supply draw over the burst period is calculated using the power reduction ratio calculated in section 3.5.4. From the calculation below, the average power draw from the satellites power supply is about 145 w (see Figure 3.15).

$$Ps = P_{DC} \, Mp \qquad (3\text{-}47)$$

$$Ps = 860 \, (0.16497) = 141.878 \text{ w}$$
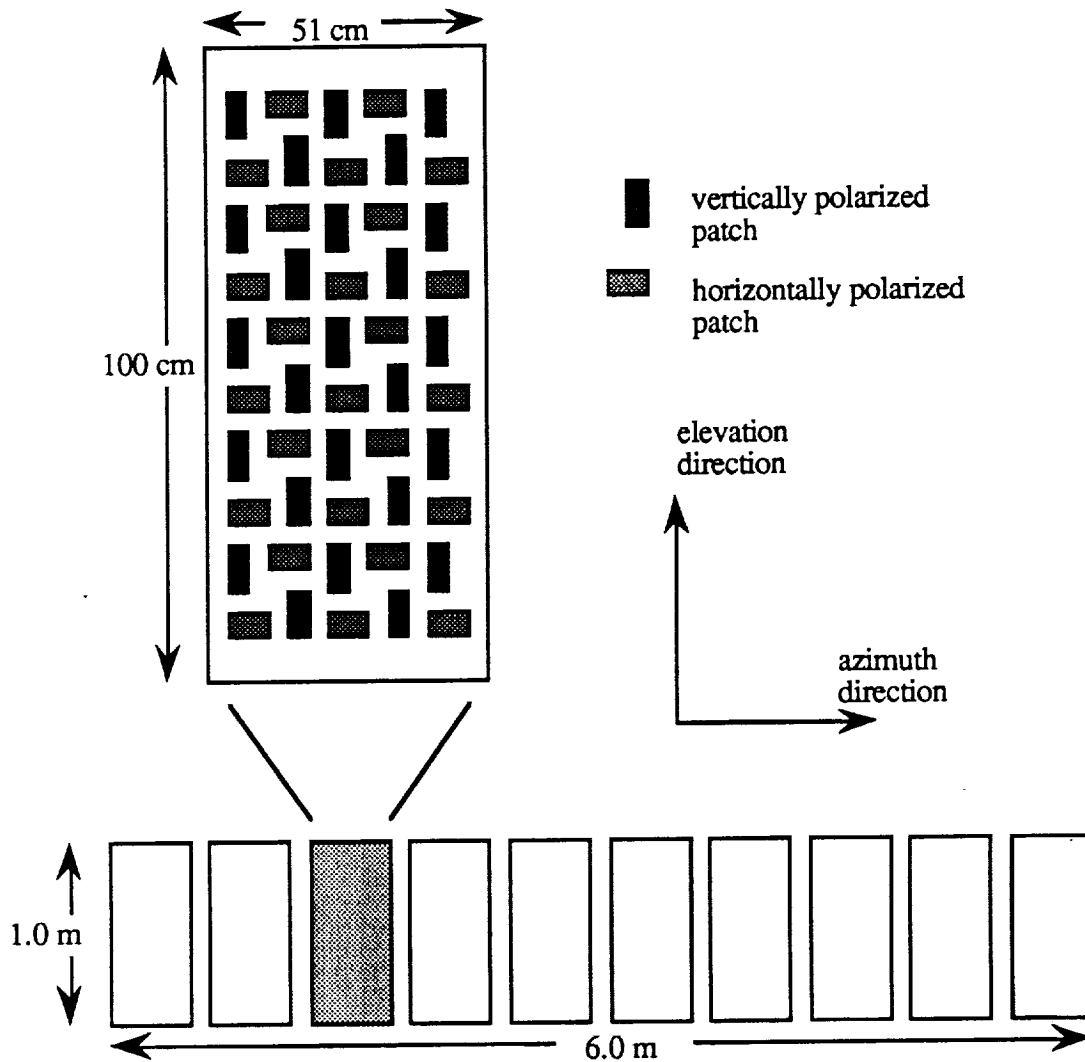


Figure 3.18: Basic layout of the MEDSAT SAR antenna

## 3.6    Conclusions

The MEDSAT project can be greatly enhanced by the application of a synthetic aperture radar system to perform the remote sensing task. In addition to being operationally independent of either solar illumination or weather conditions, SAR systems can be employed to create imagery used to detect and measure the mosquito habitats and human habitation of interest to the MEDSAT project.

Existing and planned SAR systems will not provide the required 1 to 3 day coverage frequency of the target area. Hence, the decision to place a SAR system aboard the MEDSAT satellite. The small satellite design places severe constraints on the power, mass, volume and data rate of the SAR sensor. However, this investigation has shown that it is technologically feasible to design a SAR sensor to meet all of restrictions inherent to the small satellite and still fulfill the remote sensing task of the MEDSAT project. This chapter has presented the various MEDSAT SAR sensor design parameters, and the reasons behind choosing specific values for those parameters.

The following tables summarize this preliminary design of the MEDSAT SAR system. Included in the last table are estimates of mass and cost for research and development of the system. The mass estimates, of the antenna and electronics, were based on the Seasat and another advanced SAR design [3-20 & 3-53]. The mass estimates for the antenna correspond to estimates received from Ball Aerospace, which is also who provided the cost estimate of the antenna. We were unable to confirm the mass and cost estimates of the MEDSAT SAR system electronics package.

<div align="center">

Geometric Imaging Requirements

</div>

| | |
|---|---|
| Radar Frequency (wavelength) | 1.275 GHz (0.23 m) |
| Nominal Range to Target | 520 km |
| Satellite Altitude | 500 km |
| Satellite Altitude | 520 km |
| Ground Equivalent Velocity | 7000 m/s |
| Azimuth Resolution | 75 m |
| Range Resolution | 75 m |
| Incidence Angle | 15 degrees |
| Ground Swath | 250 km X 50 km |
| Polarization | HH, VV, HV, VH |

**Figure 3.19: Table of Geometric Imaging Requirements.**

SAR System Specifications

| | |
|---|---|
| Signal-to-Noise Ratio | 8 db |
| System Losses | 4 db |
| Noise Temperature | 500 K |
| Noise Floor | -23 db |
| Pulse Repetition Frequency | 5047.95 Hz |
| Transmitted Pulse Length | 20 μsec. |
| Chirp Pulse Bandwidth | 7.727 MHz |
| Burst Repetition Frequency | 1.4 Hz |
| Number of Pulses per Burst | 571 |
| "Burst On" Time | 113 msec. |
| Integration Time | 3 sec. |
| Data Reduction Ratio | 16 % |
| Power Reduction Ratio | 17 % |
| Final Average Data Rate to Data Storage System. | 6.5 Mbits/sec |
| Number of Looks | 4 |
| Antenna Dimensions | 6 m X 1m |

**Figure 3.20:  Table of SAR System Specifications**

SAR Power, Mass and Cost

| | |
|---|---|
| Antenna  Radiating Peak Power | 2710 w (RF) |
| Antenna Radiating Average Power | 275 w (RF) |
| "Burst On" Power Draw From Power Supply | 860 w (DC) |
| "Burst Off" Power Draw From Power Supply | 0 w (DC) |
| Average Power Draw From Power Supply Over the Burst Period | 145 w (DC) |
| Antenna Mass | 40 kg |
| Electronics Mass | 30 kg |
| Antenna Cost | $ 5 - 7 million |
| Electronics Cost (including R & D) | $ 8 - 12 million |

**Figure 3.21:  Table of SAR Power, Mass, and Cost**

## 3.6.1    Possible Design Improvements

A means of obtaining space-based SAR imagery of the Chiapas, Mexico region was suggested by Rolando Jordan [3-5]. The suggestion was to see if imagery of the region could be obtained when the SIR-C/X-SAR project is operational. This SAR system would be able to collect multi-frequency image data of the region.  Such imagery would be helpful in a final determination of the best frequency band to employ in a space-based SAR system in order to create imagery useful in the detection and measurement of the mosquito habitats and human habitation of the region.

Another method of obtaining information to help in the final determination of the best frequency band to employ in the MEDSAT SAR system would be to use some form of

terrain backscatter simulation model. Researchers from the Department of Electrical Engineering and Computer Sciences, at the University of Michigan, have developed a computer model to simulate the backscatter from a vegetation canopy, which can be used to predict the radar's return given a simplified set of assumptions defining the target environment. The Michigan Microwave Canopy Scattering Model (MIMICS) uses a radiative transfer intensity approach, which accounts for inhomogeneity in the canopy layer by averaging the Stokes matrix over the statistical distributions of sizes, shapes, and orientation of the canopy elements [3-28]. Parameters for the model include the total biomass and its apportionment; the distributions of trunk and branch diameters, lengths, densities and orientation; leaf thickness and area; and total tree and canopy heights [3-2]. In addition, data on the soil's roughness and moisture content are also required. Since these parameters vary in nature, a range of data is acceptable and even desirable. Once this data has been obtained, it is suggested that MIMICS be used to simulate the radar's return under the dry, saturated, and flooded conditions. The results of these simulations can then be combined and weighted by area to determine the minimum percentage of standing water that can be detected. Additionally, simulations with MIMICS will indicate the contributions of direct canopy, canopy-ground and trunk-ground components to the total backscatter under the different polarizations.

Future advances in satellite technologies could result in a much more effective SAR. Perhaps the most important of these would be the development of cheaper launch vehicles with greater payload allowances. This would allow for more scientific payload to be placed aboard the satellite. This in turn would put fewer constraints on the SAR's design and enable a larger antenna, possibly with multiple frequency capabilities, to be used. The resulting advantages would include increased ground resolution and coverage area, further increasing the amount of image data acquired by the SAR.

Lower mass antenna materials could also make the SAR more effective. As already stated above, decreasing the mass of the antenna makes it easier to meet the limits of the launch vehicle. This would give the designers more latitude when determining the antenna's size and operational wavelength(s).

Another possible area of improvement is in the power efficiency from the satellite's power supply to the T/R modules. The development of more efficient microstrip materials used in combination with innovative antenna design techniques could result in a more efficient system thus decreasing power losses. This would make more power available to the SAR leading to improved sensor performance.

## 3.7    Acknowledgements

# Chapter 4

# VISIBLE AND INFRARED SENSING

# 4.1    Introduction

A visible and infrared sensing system is proposed to be included in the MEDSAT scientific payload. There are several reasons why this is desirable:

1. To detect changes in the characteristics of vegetation, as they may relate to mosquito density.

2. To help in determining locations of pasture and marsh areas, which may be high-producing mosquito regions.

3. To detect the movements and settlements of residents and migrant workers in Chiapas.

4. To sense ground temperature characteristics of various sites in and around Chiapas.

In addition, there are other possible uses of the visual and infrared (VIS/IR) sensor that may not be clear at the moment, and only will be learned after some experimentation.

# 4.2    Visible and Infrared Sensor Team Goals

The goals of the VIS/IR sensor team were to determine which ground features were most important in determining mosquito populations and their changes in Chiapas, and to look into the design of an appropriate VIS/IR sensing system for a light satellite which can accomplish 1 - 4 above. Since it is not possible, at present, to sense the regions of high mosquito density themselves, it is necessary to indirectly infer how changes in vegetation, grassland, forest, and marsh areas may affect the mosquito population. Thus by measuring the reflectance from specific channels in the solar spectrum, finding the vegetation index, and perhaps finding "continuous" reflectance spectra of solar radiation over various wavelength intervals, one can determine how changes in the mosquito population vary with changing ground status. Also, a thermal infrared sensor is desirable, since the mosquitoes prefer a known range of temperatures.

One of the most difficult tasks facing the VIS/IR sensing team is to find a sensing device that can accomplish the purposes 1 - 4 above and still meet the stringent satellite payload mass and volume constraints. A sensor system mass of 33kg, excluding a radiator cooling device was set, due to the use of the Pegasus system to launch this satellite. Thus, with the need for a sensor in the visible and near infrared (VNIR) range of the solar spectrum, one in the shortwave infrared (SWIR) range of the solar spectrum, and the desire for one or more in the mid-wave infrared (MWIR) or thermal infrared (THIR) ranges of the terrestrial spectrum, lightweight components and small size and reliability is a must. The sensor must also contend with the synthetic aperture radar (SAR), and interference between the two sensors must be avoided. To detect changes in vegetation and local ground status using the VNIR and SWIR sensors, a pixel resolution of 100m or less is desired, and one of 50m or less is preferred. For the THIR sensor, a higher resolution of a few hundred meters could be used. The power required to operate the sensor is expected to be on the order of tens of Watts. Also, the data communications team noted that data volume should not be a problem for the desired data resolution over the area of study with 2 overhead orbits per day.

## 4.3 Visible and Infrared Sensor Requirements

The visible and infrared sensor will have two main functions. First, to detect regions in Chiapas where habitats are ideal for mosquito production. Second, to track the location of migrant workers from Guatemala, who are the source of much of the malaria. In addition to these, other functions of the sensor will be to locate geographical indicators, both natural and man-made, which with ground truth observations can aid in specifying which portion of Chiapas is being portrayed, and perhaps to study malaria and other tropical diseases in other areas of the globe.

### 4.3.1 Detection

Detection of the various objects mentioned above is determined by the requirements given for the project, the sensor requirements mentioned above, and by knowledge gained from previous workers in this field (of which there are few).

### 4.3.1.1 Mosquito Habitat

Before a discussion of mosquito habitat, it is worthwhile to mention the related work done in the central valley of California. In the study, an airborne multispectral scanner was used to look at rice fields, the purpose of which was to see if remote sensing could be used to detect fields with high populations of the *Annopheles Freeborni* mosquito. The researchers used five VNIR and SWIR channels in their analysis. In this study, the Normalized Difference Vegetation Index (NDVI) was used. The NDVI is

$$NDVI = (IR - RED) / (IR + RED)$$

The NDVI is well documented as an indicator for deliniating vegetation. By using the NDVI in conjunction with information on the location of the blood meal source for mosquitoes, the authors were successful in distinguishing between high and low-producing rice fields. Students from the University of California at Davis went to the rice fields, dipped, and counted the mosquitoes present in each field under study.

The two types of Annopheles mosquitoes found in Chiapas that act as malaria vectors are *Annopheles albimanus* and *Annopheles psuedopunctipennis*:

*Annopheles albimanus* prefers to breed in lagoons and pastures near the ocean. It enjoys slightly saline waters. Lagoons are open bodies of water which can often be detected because of water's low reflectivity of solar radiation. A pasture can also be detected due to its plant life, mostly grasses, if the pasture size is larger than or comparable to the pixel resolution size, which is expected to be about 50m. Around Chiapas, three species of grass, *Cynodon*, *Echimochloa*, and *Fimbristylis* are known to be positively correlated with *albimanus* mosquitoes.

*Annopheles psuedopunctipennis* larvae develop in sunlit bodies of still or slowly moving water, often associated with Spiragyric algae mats. Around Chiapas, these are mainly found above an altitude of 200m along the southern slopes of the Sierra Madres mountain range, during the dry season. A VIS/IR system is very good at detecting sunlit bodies of water. The link between the algae mats and the mosquitoes will increase the ability of the sensor to find the *psuedopunctipennis* habitat. Once field work is done to determine a reflectance signature for the algae, then locating the habitat is quite possible.

Both of the mosquito species prefer certain temperatures for breeding. Optimal temperatures are in the 25 - 27°C range. Development is arrested for temperatures of less than 10°C or greater than 40°C. This information can be very useful in determining mosquito habitat. The types of habitat for the mosquitoes makes detection by the VIS/IR system possible. However, it should be stressed that the data collected by the sensor will have to be verified on the the ground in Chiapas during the experimental phase of the satellite's life.

### 4.3.1.2    Migrant Workers

As has been discussed previously in the report, the malaria in Mexico is closely linked to migrant workers from Guatemala. If the location of the migrant workers could be determined, it would be useful information for combating the malaria problem. It is possible that a VNIR and/or SWIR sensor could be used to determine the position of the migrant workers. However, it should first be recognized that information on the migrant workers is limited. Part of what will be said here is speculation which will need to be confirmed in the future. It is known that workers live in temporary camps. They live in groups and usually in huts made of thatched palm roofs and bamboo. They tend to live near the agricultural fields at which they work. Neither the size of these camps, nor their configuration are known. Therefore, it will be estimated that the camps have a population of approximately 1000 people, and that they live in close proximity to one another. This would imply that the huts are within about 15m of each other. If each hut contains an average of 5 people, then there would be about 200 huts per camp, and thus the camp should be about 200m on a side. Thus, the VNIR sensor may be able to pick up a characteristic signature of these campsites, and since the workers are likely to leave cut wood and bamboo outside their huts, which will become very soggy during the wet season, the SWIR sensor, which detects leaf moisture quite well, should be useful in detecting this. Once these signatures and signals have been recognized and confirmed by the ground observations, the identification of these camps should be possible.

An additional use of the VIS/IR system will be in the identification of agricultural fields. The state of Chiapas produces bananas, corn, cotton, soybeans, and coffee. Since the characteristic signatures of these crops have largely been determined, locations of these crops can be sensed and also can give further information on the locations of migrant workers, which can be the victims of the vicious *Annopheles* vectors.

### 4.3.1.3    Reflectance Characteristics of Vegetation

Remote sensing of vegetation obviously depends greatly upon reflectance characteristics over the solar spectrum (figure 4.1). In the visible region of the spectrum, pigmentation dominates the spectral response of the plant; chlorophyll being particularly important. In the near infrared region of the spectrum, the reflectance rises considerably because the green leaves absorb very little energy. In the middle infrared region, water absorbs energy strongly, and since green leaves have a very high moisture content, the water absorption bands dominate the spectral response. As the moisture content of a leaf increases, the reflectance decreases markedly. In figure 4.1, the solar EM spectrum bands that we prefer for remote sensing are indicated, and these will be discussed in more detail below. In the MWIR, the reflectance of solar radiation is comparable to the emission of terrestrial radiation by the earth and atmosphere itself, and thus this spectral region is best used only at night. The THIR signal is due to emitted terrestrial radiation almost exclusively, thus both this region and the MWIR (at night) can be useful in determining surface temperature.
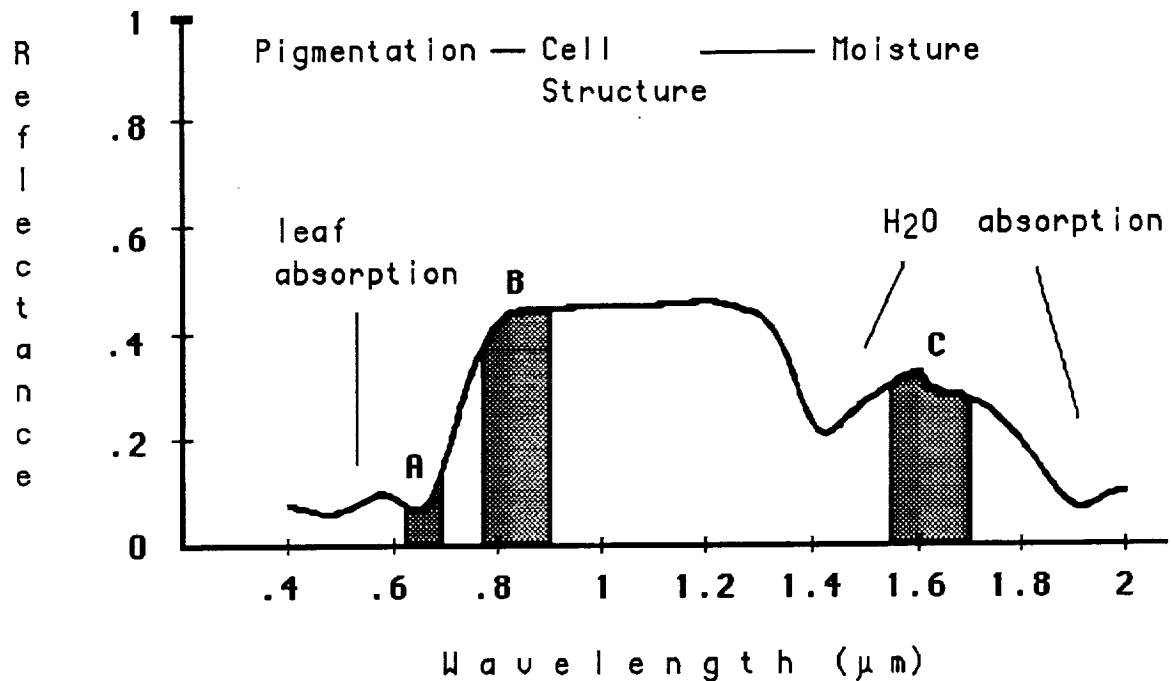
Figure 4.1: Reflectance characteristics of vegetation

## 4.3.1.4 Geographical Reference Corregistration

The final requirement of the sensor is that it detect reference locators on the ground. Often times it is difficult to tell which geographical area a given satellite image is portraying. With the VIS/IR system, the location of cities and large bodies of water can be used to pin down the area of Chiapas being imaged. Also, streams and roads can give recognizable reflectance spectra, if the pixel resolution is 50m or less.

## 4.3.2 Geometric Requirements

Certain geometric requirements are necessary for the operation of the VIS/IR system. In order to match the SAR's field of view, a deformation of the cone angle is expected. To account for this distortion, we must allow for the slant view angle and the different pixel size which results from it. Once these factors are integrated into the adjusting algorithm, the appropriate correction can be made.

## 4.3.2.1 Matching the SAR

Since the synthetic aperture radar will operate at an off-nadir viewing angle of 15°, the VIS/IR remote sensing device must be pointed at the equivalent direction off the satellite. Figure 4.2 illustrates this. Thus, when calculations are done on reflectance data, the oblique view of the ground features must be taken into consideration.

MEDSAT

15° off nadir

~ 250 km

1000 pixels / scan

STUDY REGION

50 km
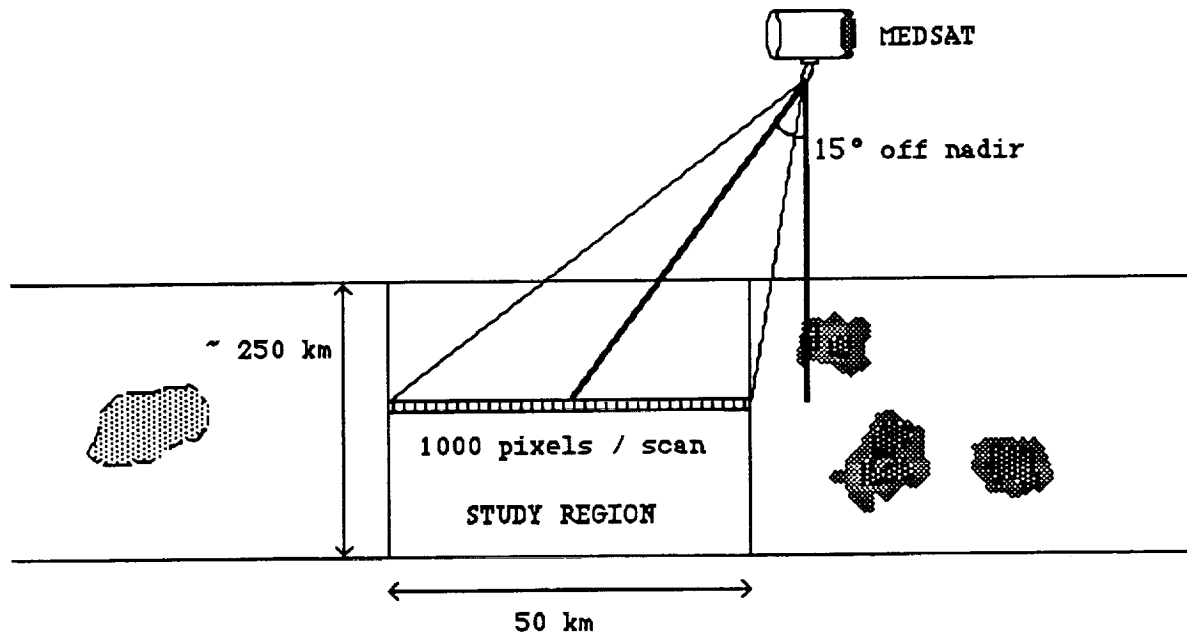
**Figure 4.2:  Off - nadir viewing angle for VIS/IR sensor**

## 4.3.2.2    Resolution

For the detection of streams and roads, the sensor will be expected to detect these with any resolution of greater than 20-30m. For marshlands and breeding grounds in the highlands, a spectral resolution of 50m may be used, but smaller areas of breeding in these areas may indeed go undetected unless contrast makes up for the lack of resolution. For crop areas, the 50 - 100m resolution should be appropriate, and for pastures and grassland, most of these should yield quite useable reflectance spectra. It is in the pastures that many cattle are found, which are the main blood meal sources for the mosquitoes.

Considering the THIR sensor, spatial resolution should be little problem, since the temperature ranges at which the mosquitoes breed most readily are greater than the likely variation of temperature over an area of a kilometer or more. This is certainly true for daytime cases, where winds tend to be stronger, and is likely to be true even for nighttime cases with light winds, for which radiative cooling differences of the various ground surfaces can be greatest. Still, under these circumstances, difference between areas of vegetation and water can be as high as 5 - 8°C, differences between open grasslands and forests can be 2 - 4°C, and differences between local highland areas and adjacent areas several tens of meters lower can be as much as 3°C.

## 4.3.2.3    Weather

The local weather in and around Chiapas, Mexico generally consists of a wet season and a dry season, with high cloudiness amounts during the wet season, as mentioned previously in the report. Regarding the VIS/IR sensing aspects of MEDSAT, the cloudiness during the wet season is capable of hindering our operations. The VIS/IR sensing system is not particularly useful under cloudy conditions, although the THIR sensor can give quite useful information on the estimation of precipitation from cumulus convection through measurement of cloud top temperature. However, what is really desired is the remote sensing of the ground.

During the dry season, from December to April, the area is generally under the influence of the "subtropical high" pressure system, thus leaving the Tapachula region under significant clouds in less than 40% of the area of coverage. Much of this is weak cumulus convection which occurs in the afternoon, and subsides in the evening. Cirrus types of clouds are also prevalent associated with the subtropical jet stream. Occasionally, a weather system from the westerlies will bring cloudiness into the region at the peak of this season, but this is not common, nor will the cloudiness be great, in most cases. The transition that occurs from the dry season to the wet is quite rapid, with average values of cloudiness becoming 50-70% in April and 65 - 90% in May - October, with a similar transition occurring as the wet season ends. In each of these cases, the cloudiness amounts are greatest in the highland regions of the Sierra Madres, and lower toward the coastal plain. Tapachula is actually located in a locally minimum region of cloudiness in the general region, with cloudiness of 74% reported in July. Figure 4.3 is a climatology of cloud cover in Chiapas over the year [4-1].

| MONTH | Cloudiness (%) | Precipitation | (amount, %, | % thunder) |
|---|---|---|---|---|
| January | 36 | .5 | 3 | 0 |
| February | 44 | .5 | 5 | 1 |
| March | 58 | 2.3 | 12 | 1 |
| April | 67 | 5.8 | 30 | 8 |
| May | 67 | 28.2 | 58 | 27 |
| June | 74 | 44.5 | 77 | 30 |
| July | 69 | 33.8 | 65 | 33 |
| August | 68 | 30.7 | 68 | 32 |
| September | 72 | 47.0 | 81 | 31 |
| October | 68 | 39.1 | 68 | 21 |
| November | 44 | 6.1 | 20 | 8 |
| December | 34 | 1.3 | 6 | 3 |

**Figure 4.3:   Cloud and precipitation climatology for Tapachula, Chiapas**

Precipitation is also a key factor in the VIS/IR sensing of Chiapas, since the mosquito habitat generally tends to respond to increases in rainfall. Of course, one exception is the *A. psuedopunctipennis* vector that is most prevalent in the highland regions during December, as swollen river valleys subside from the heavy amounts of precipitation over the Sierras Madres during the wet season. Figure 4.4 shows the average monthly precipitation in the region of study during August (one of the less wet months during the wet season) [4-2]. The maximum of 80cm over the Sierra Madres is significantly higher than the about 30cm average along the coastal plain, and the 20cm average near Tapachula. However, it still rains on about 70% of the days during the wet season at Tapachula. Figure 4.5 is representative of the dry season. Here, the only values of over 10cm are over the mountainous regions, and much of the coastal plain, including Tapachula, receives very little precipitation.
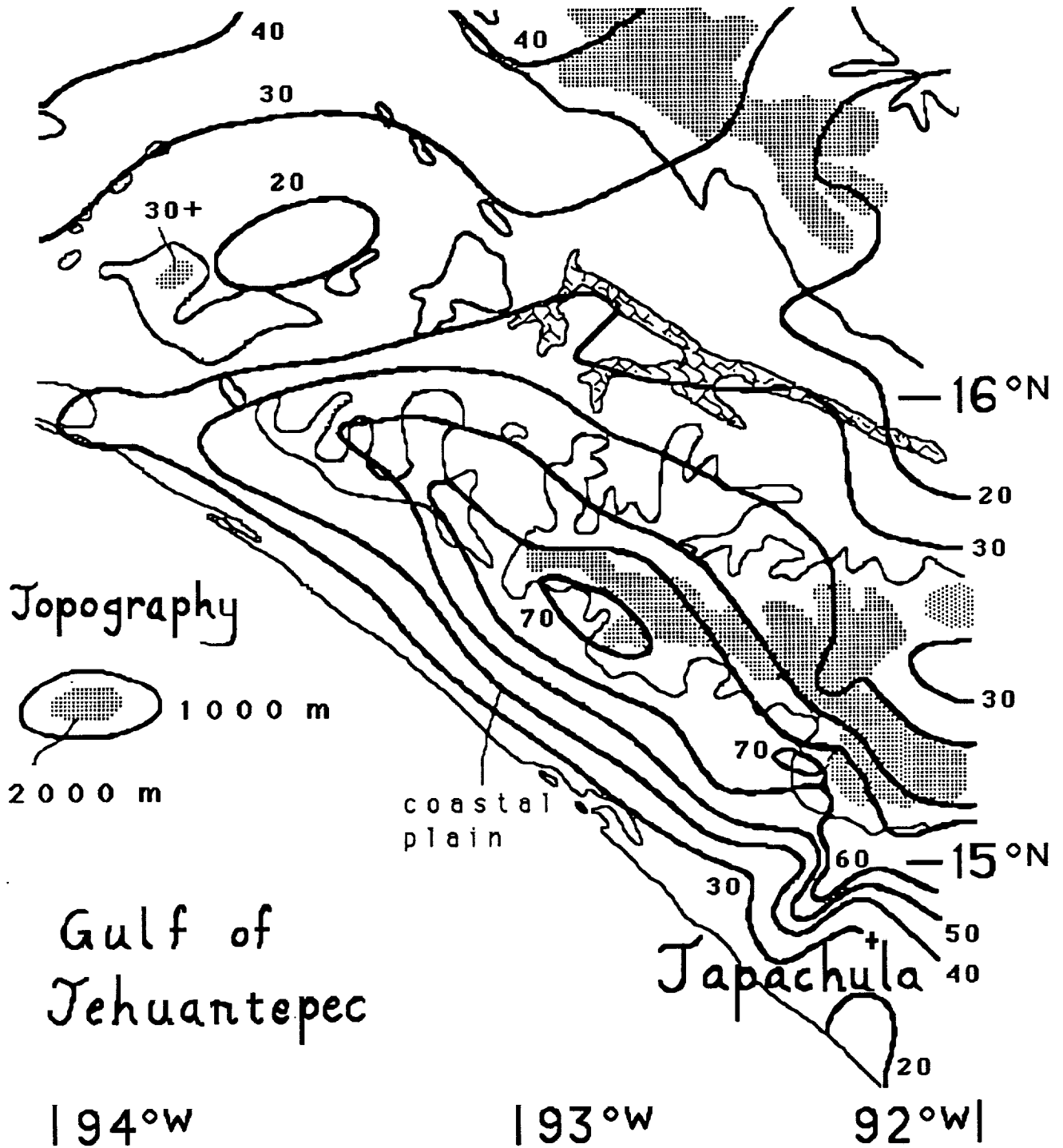
**Figure 4.4:** **Average August precipitation (cm) near MEDSAT study region**
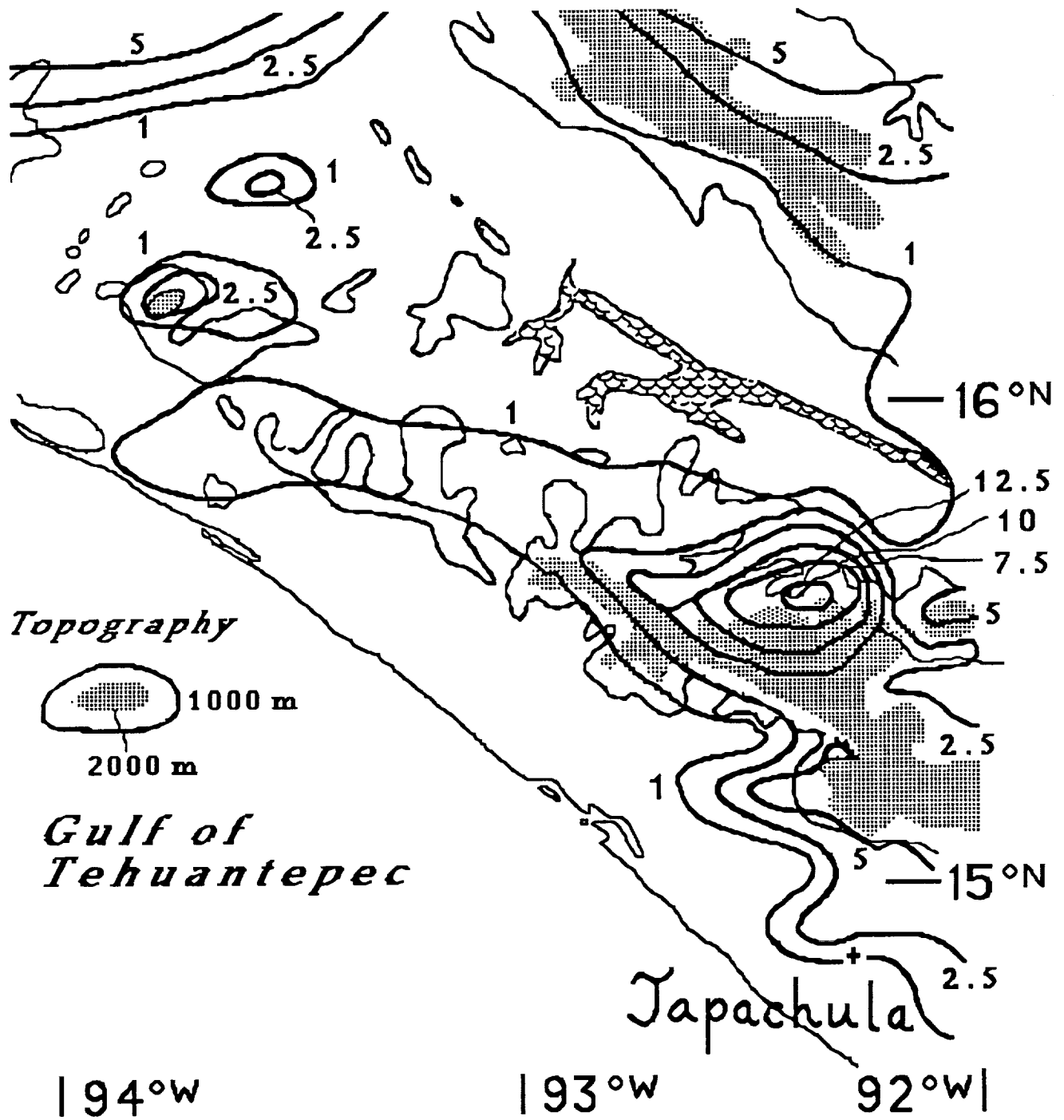
**Figure 4.5:  Average December precipitation (cm) near MEDSAT study region**

Orographic lifting and the sea breeze are important factors in determining the weather in the region of interest. Figure 4.6 illustrates this and how it generally affects the cloudiness and precipitation. Although high enough resolution cloud data was not available to study specific cloud amounts at each time of day over various places in the region of interest, nor to create a comprehensive cloud climatology, inspection of larger scale satellite photos revealed that the following pattern is often seen: Convection begins over the coastal plain and over the highlands in the late morning, and is most intense over the Sierra Madres, where orographic lifting takes place. The sea breeze can develop, as well, due to the differences in land and ocean temperature. This enhances the cumulonimbus convection and thundershowers over the highlands, and has the *tendency* to "push" the convection off the coastal plain and toward the mountains, leaving the strip very near to the shoreline clear, at times. This can be of great help to remote sensing when this occurs. However, due to the strength of the convection during the wet season, even the cumulonimbus over the Sierra Madres often spread out over the entire region, often leaving even the coastal areas under a middle or high overcast in cases where the thundershowers do not form over the coastline.



Insolation early in the day (A) can cause differential heating of land and ocean, which can sometimes cause early cumulus development (B) to develop more greatly over the Sierra Madres due to orographic lifting and be "pushed" off the coastal plain (C) by the sea breeze.
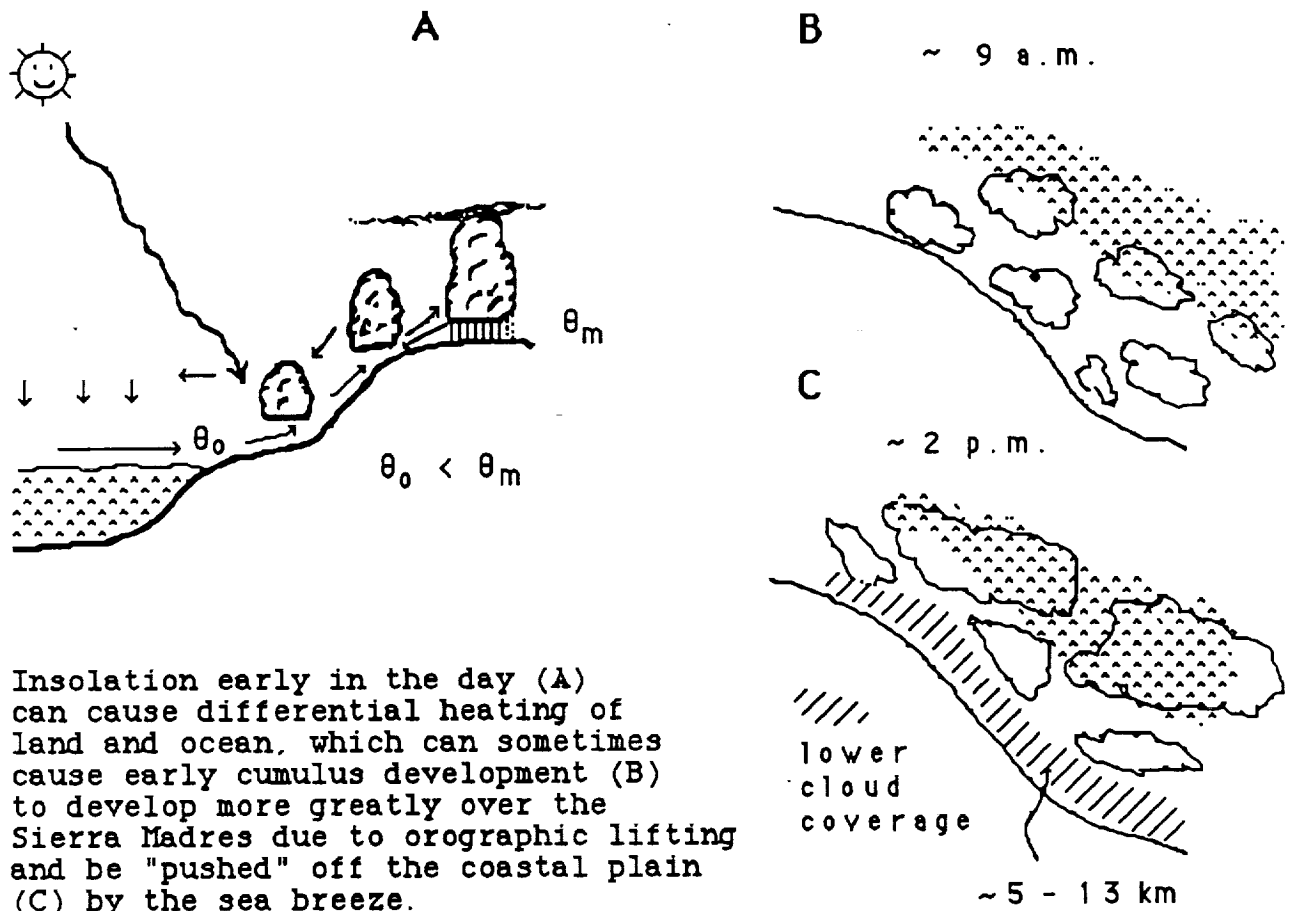
Figure 4.6: The sea breeze effect near the MEDSAT study region

Thus, the prognosis for sensing during the wet season is not good, but not hopeless either. It is expected that cloudiness will be high during the wet season, although there will be breaks, more so in the nighttime than the daytime. Nocturnal thunderstorms will occur over the Gulf of Tehuantepec, and may drift inland at any time of the day. During the nighttime, in the cases where it is clear and especially if significant rain fell the previous day, some local valley fogs will be expected to occur. However, due to variations in the convection, having an area that is always under clouds at a given time of day is quite unlikely, since the Sierra Madres are not large mountains. Easterly waves will also come by the region, causing cloudiness for one to several days, and these are more frequent in the late summer and fall than any other time of year. Obviously, during the dry season, all of this will be little or no problem.

## 4.4    Visible and Infrared Sensor

In order to determine the malaria habitat, one may use relationships between the mosquito habitat and vegetation, moisture, and temperature on the ground. Thus, detectors in four wavelength bands were considered to bring out various characteristics that we are trying to sense. These are the VNIR from 0.5-0.9um, the SWIR from 1.5-2.8um, the MWIR from 3-6um, and the THIR from 8-12um. Remote sensing of vegetation, grasslands, marshes, and crops can be done using the VNIR and the SWIR, and information on ground temperature is given by the MWIR and/or THIR. Considering each of the wavelength bands, there are advantages and disadvantages regarding the amount of valuable information given, feasibility, and cost. The consideration of wavelength bands for MEDSAT are discussed below.

### 4.4.1    Consideration of Wavelength Bands

The VIS/IR sensor on the MEDSAT platform is to be used for the remote sensing of mosquito habitat as well as other factors affecting the malaria distribution. So far we are considering five bands for the MEDSAT VIS/IR sensor. The required remote sensing information for mosquito habitats includes vegetation type and canopy, temperature, moisture, and human and animal density which provides blood meals for mosquitoes. Besides the vector, there are other factors which are important to the malaria problem such as the number of cases per certain number of people which serves as the source of malaria. We hope our VIS/IR sensor can effectively monitor the vegetation and temperature variation as well as the agricultural behavior of the area in question. We suggest four of the five bands considered, which will be able to provide the information we need.

BAND A: 0.62-0.69um, red. The lower limit is not very crucial (should be higher than 0.6um) but the upper limit is, because between 0.69 and 0.75um is a transitional region where the vegetation reflectivity increases very fast. In this band, the reflectivity of green vegetation is very low and is fairly constant at about 4% for various types of vegetation, pigmentation or cell structure. This low reflectivity in the red band is due to the chlorophyll content of green vegetation leaves.

BAND B: 0.77-0.90um. In this case, the lower limit is crucial but the upper limit is not. For wavelengths between 0.85 and 1.1um, there is very little change in the characteristics of a certain type of vegetation with certain leaf cell structure (the spectral responses are quite flat so the same information will be expected for 0.77 - 0.9um as it would extending to 1.1um). In this band the reflectivity varies dramatically among different types of vegetation as well as in different stages for a certain type of vegetation because the reflectivity in this band indicates leaf cell structure. The high ratio between the reflecting signal in band B over band A is a very definite criteria for deliniation of green vegetation, since there are almost no other major targets on the surface of the earth with a very low red reflectivity and a very high near-infrared reflectivity. And this ratio will tell us how much of the land in our field of view is covered by green vegetation leaves. From this information we can classify different vegetations and therefore find the potential malaria habitat. It seems quite obvious that we need a red and a near infrared band in order to get the vegetation information for malaria vector habitat sensing. But we should ask ourselves whether or not these two bands can provide enough information to identify the high or low malaria risk areas. The answer is almost as obvious; it is not sufficient. Researchers from the NASA Ames research center at the University of California at Davis have done research that shows in the rice fields of California that the high and low mosquito producing fields have different spectral characteristics during the early stages of their growth. Basically, the NIR-red ratios are different. Our target area is southern Mexico, and only some of the vegetation types there are rice field. Scientists from NASA Ames also did a large amount of research within this area and the results show that the mosquito habitat in the coastal area of southern Mexico is mostly transitional swamps or fresh water marshes close to pasture areas. This makes the problem more complex, so we must collect other information.

BAND C: 1.55-1.7um. The signal in this band is reflected solar infrared radiation which can be used to get vegetation moisture content information. In a wet tropical area, such as southern Mexico, especially during the rainy season when coastal malaria is transported faster, the vegetation moisture is almost always quite high and does not vary too much. Therefore the moisture is not a very important factor in this special case.

BAND D: 4.0-5.6 um. As mentioned above, another important factor in terms of mosquito habitat is temperature. And we can remotely sense the temperature using the MWIR and/or THIR band. The MWIR is more sensitive to the variation of surface temperature, with a higher quantum efficiency for the detector, and the detector is much easier to build. There is better uniformity (PtSi 512 x 512 array), but the signal level is lower because it is far from the peak of the solar blackbody radiation curve, and the cloud-reflected solar radiation would render the observations almost useless at daytime. On the other hand, the THIR band has higher signal level basically because the terrestrial blackbody radiation curve reaches its maximum in this region. However, the detector is very difficult to make and typically the detectors in this wave band have higher dark current and therefore need to be cooled to lower temperatures. Band D is likely to be from 4.0-5.6um.

The option also exists of using a sensor which yields a "continuous spectrum"; one that covers a wavelength interval with very high resolution. This is possible for any wavelength band, but is presently being considered for the VNIR region of the spectrum, from 0.5-0.9um. It is in this region where the characteristics of vegetation are sensed the best, and a look at continuous spectra may give added information, and perhaps will yield specific signatures for certain types of ground conditions. This possibility should be considered. In the worst case, the signal can likely be degraded into larger spectral channels if it were found necessary.

## 4.4.2 Visible/IR Spectrometer Design

Regarding VIS/IR imaging for MEDSAT, there are three basic spectrometer designs that can meet our needs of high spatial and possibly high spectral resolution. First, a framing camera can be used that acquires an entire scene simultaneously on a 2-dimensional detector array. Second, a line scanner, or "pushbroom" imager, can be used to acquire one line of the scene onto a one-dimensional linear array detector. And third, a point scanner, or "whiskbroom" imager, can be used to produce the image using a single detector, with a scanning system for one image axis, and vehicle motion for the other. Each of these implementations has a progressively lower sensitivity because the energy received must be shared among fewer detector elements.

There are several technical challenges in developing a system based on any one of these designs. The system must be able to achieve an adequately high signal to noise ratio in conjunction with the required spectral and spatial resolution. Also, a dynamic range of 1000 or greater is desirable, which puts certain restrictions on system design. For example, a whiskbroom scanner will work well for a few wide spectral bands, but cannot be converted to a narrow band system without making the aperture unreasonably large. In a pushbroom design, many detector elements are made adjacent to each other along the same array, and each element is independent of one another. Every element is looking at a certain field of view (FOV) at a certain time. This technique requires a larger integrated detector array, but can save weight due to a simpler optical system (without scanning mechanics, optics, and electronics). In this case, the use of broad spectral bands and a reasonable instantaneous field of view (IFOV) may reduce the need for fast large optics. In a typical modern spectrometer design, the optical system may have an effective f number between 1 and 3. We believe that for the MEDSAT design, which has a swath width of 50km, long integration times, and wide spectral bands (greater than 50nm), f can be increased to near 4. The higher f combined with a relatively low orbital altitude implies a shorter focal length so that a compact and lightweight design should be achievable.

The spectrometer design, pushbroom or otherwise, will require the following sub-assemblies: fore optics, spectrometer, collimator, dispersing optics, and detector system.

### 4.4.2.1 Optics

The fore optics images the scene over the required FOV, and the size of these optics determines the system aperture. The field stop of the fore optics is coincident with the entrance slit of the spectrometer portion of the instrument. Spectral coverage requirements in many designs, and also in the case of MEDSAT, limits the optical design to an all reflective system. A conventional fore optic design is a Schmidt Cassegrain two mirror design. An obvious drawback to this is the large obscuration created by the Cassegrain secondary mirror. One possible solution is to use one of the modified Schmidt designs where secondary and tertiary mirrors lie off-axis. A series of such designs are being developed by the EOS High Resolution Spectrometer (HIRIS) design group at the Jet Propulsion Laboratory (JPL). These designs utilize lightweight aluminum mirrors, but require some rigid support structure (e.g., an optical bench). The VIS/IR sensor proposed for MEDSAT will utilize a scaled-down version of one of these offset designs which is modified to meet our IFOV and FOV requirements. The design selected was developed for a pre-HIRIS experiment to be carried out on the low-orbiting Shuttle Imaging Spectrometer Experiment (SISEX). Although the FOV on SISEX was 2.75°, modification of the design to extend the FOV to 6° was considered quite feasible.

The all-reflecting Schmidt fore optic telescope images the earth on a slit which is curved to match the spherical focal surface produced by the primary mirror. The spectrometer portion of the instrument is also a Schmidt design with a double pass configuration. The radiation passing through the slit is both collimated and reimaged by the same optics. In addition, the radiation is separated with dichroic beamsplitters into the VNIR, SWIR, and MWIR bands. The original SISEX design has been modified in the MEDSAT design to include a second dichroic beamsplitter to separate out the MWIR energy. The collimated light received is then passed back through the spectrometer to a focus which is co-located with the VNIR and SWIR bands (see figure 4.7).
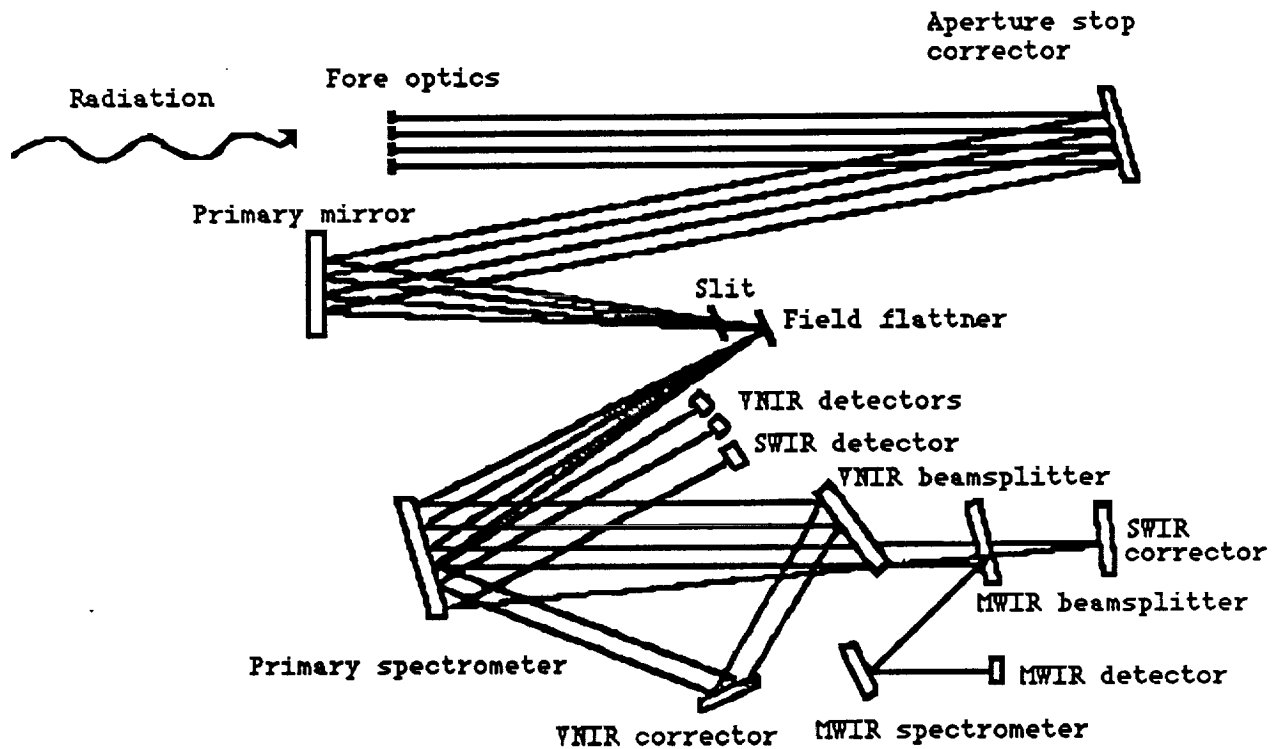


**Figure 4.7:   Optical system for VIS/IR sensing system.**

A flat spectrometer focal plane is achieved by using a field flattening mirror immediately following the slit. One very attractive feature of this design is that by changing the curvature of the field flattener, various fore optic focal lengths can be used with the same spectrometer design.

The original SISEX design called for fast optics (f = 2.3), and thus much larger optics. The projected weight savings for the slower (f = 4) MEDSAT design is nearly 50%. Theses savings are made in the weight of the aluminum optical mounts and optical bench structures. Additional savings will be realized by incorporating the existing spacecraft housing as the instrument housing with little additional weight needed for isolation of structures. For the MEDSAT design, the total instrument mass is 33kg. The total mass for the original SISEX design was about 100kg.

The optical system (lenses, filters, and spectrometer optics) requires a constant temperature environment around 0°C. Therefore thermal isolation of the optics is required, which consists of enclosing it with a blanket of insulation and using mounting supports with minimal thermal conductance.

### 4.4.3.3    Detector System

Below are discussed the detector system: the choice of detector arrays, their cooling, and their calibration.

### 4.4.3.3.1    Detector Arrays

The focal plane detectors proposed for MEDSAT utilize recently developed charge coupled device (CCD) technology. Each detector consists of a 2x1024 array with a 30umx30um pixel size. For the VNIR bands (bands A and B), a CCD detector is suggested, which has a high and flat frequency response from 0.4-0.9um, with a quantum efficiency of higher than 40%. A CCD developed for NASA by the RCA New Products Division provides spectral windows for the two desired VNIR bands, which are integral to the detector. This detector can be butted with others to form a longer area array if a wider IFOV is required. The filter technology involves stacking alternating one-quarter wavelength high and low index of refraction layers to achieve the desired passband. For MEDSAT, one of the rows will be integrated with a 0.62-0.69um passband, and the other with a 0.77-0.9um passband. These detectors have very low dark current (100e/pixel) and a large dynamic range (13000), and integration times in the 1-4msec range. Readout noise is less than 300e rms. Other VNIR passbands could be added by selecting a CCD with additional rows of array elements.

As mentioned previously, ideally it would be best to examine continuous spectra. Thus, a CCD silicon array which would have 1024 (perhaps 2x512) area sensors by 200 spectral intervals (2nm resolution) can be used. This can be done by ITRES Research in Calgary, Alberta. There would be several advantages of this sensing device, particularly the increased resolution. However, there are two problems that have to be overcome using this. First of all, to the best of our knowledge, such a high resolution sensing system would require very large fore optics, much larger than can be used to satisfy the requirements of MEDSAT. Secondly, since the total reflectance signal will be split up into so many smaller ones, the individual signal in each individual region would necessarily be quite small. Thus, this may make sensing more difficult. However, for the extra resolution to give increased knowledge of the factors that can determine mosquito habitat, it may well be worth it. This is possible in other bands, but we feel would be most useful here if employed.

For the SWIR band, we also suggest two line sensors. For these detectors, we recommend Palladium Silicide ($Pd_2Si$) Schottky Barrier arrays (2x512) developed by Walter Kosonocky at the David Sarnoff Research Center. Again, two of these arrays can be butted together to accommodate IFOV requirements. This detector operates at 125K, which can be controlled using a thermal conducting rod connected to the MEDSAT passive radiator cooler.

For the MWIR band, we suggest two line sensors as well. The detectors for this band include PtSi and HgCdTe. The PtSi detector has better uniformity, and can be made up to 512 elements as for the $Pd_2Si$. It operates best at 77K, and thus active cryogenic cooling may be necessary . However, if 95K is acceptable, this can be accomplished with the radiative cooler. The noise equivalent temperature for the PtSi array is less than 0.1K, which compares well to the performance of HgCdTe thermal detectors. With these considerations we recommend a PtSi arrays (2x512), developed by Walter Kosonocky, which can be butted together, as for the SWIR band.

A THIR band was considered, as well, and has certain advantages. Among these are that radiation in this region of the EM spectrum is almost exclusively from earth emission. Thus, this would be good for detecting surface temperature both day and night, unlike the MWIR band. However, there are disadvantages as well. The detector materials for this region (photoconductive or photovoltaic HgCdTe linear array) are difficult to make and quite expensive. The best array to our knowledge is one of photoconductive HdCdTe of 180 elements; a one-dimensional array for which a few bad elements normally exist (produced by the United States Army). Another option is copper-doped silicon or mercury-doped germanium, but these detectors require liquid helium cooling (for HgGe, a temperature of 28K is needed), which can be achieved with an active cooler with extreme difficulty and at high expense. For the 50km swath width planned for MEDSAT, the best possible IFOV for this array would be 260m, but for measurement of temperature, this should be okay for our purposes, as discussed previously. However, with all of the problems considered and the MEDSAT specifications, it does not seem possible to include the THIR band on our sensing system.

## 4.4.3.3.2    Detector Cooling

Dark current, due to the thermal movements of the electrons in a solid state sensor material, is a major noise source for the VIS/IR sensor. This can only be lowered by cooling. For bands A and B, the CCD detectors need to be cooled down to -60°C to get an acceptable signal to noise ratio. This can be done through deep space radiator cooling. The required area of the radiator is about $0.5m^2$. The radiator can be mounted facing a direction toward the north pole, so that the radiator's view can avoid the sun, earth, and moon (see figure 4.8). Since the orbit of MEDSAT is designed to be of low inclination (21°) and low altitude (475 km), the orientation of the radiator needs to be carefully designed in order to prevent the radiator from facing sun, earth, and moon. Since our orbit is not sun-synchronous, the sun angle with respect to the satellite will change from time to time, and therefore a solar shield is needed. An earth shield will also be used to shield the terrestrial radiation. These shields will be designed so that the radiation from them will not affect performance of the radiator.
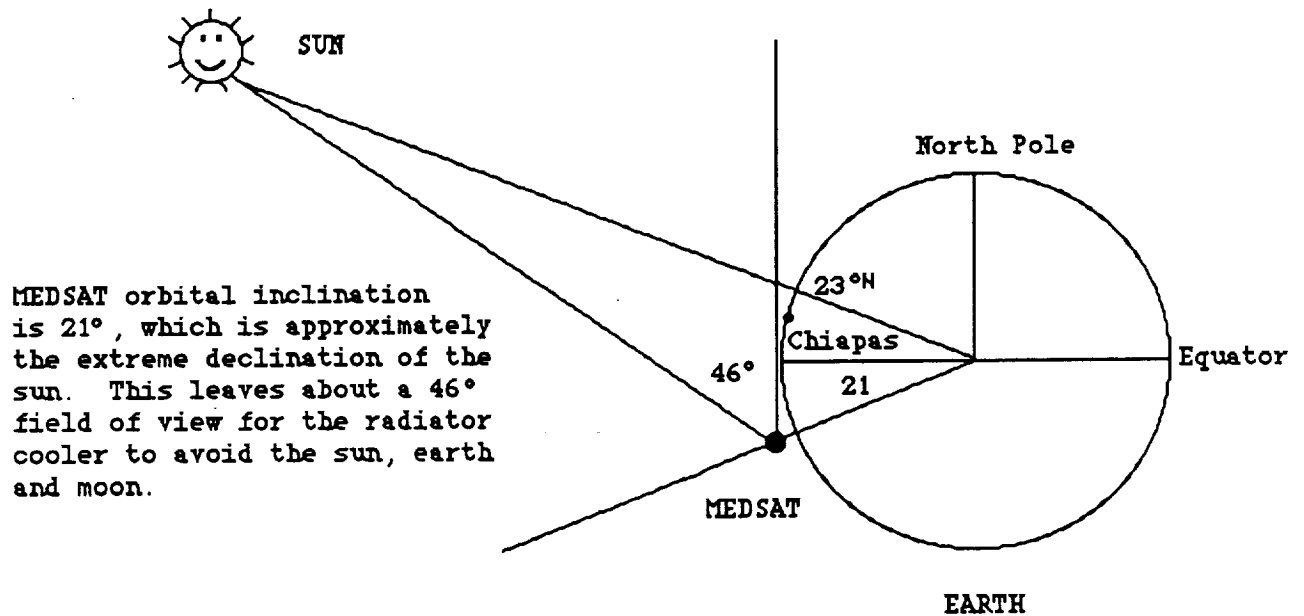
**Figure 4.8: Radiative cooler geometry for MEDSAT.**

Since the dark current for the MWIR detector is higher than that of the VNIR and SWIR detectors, a lower working temperature for the detector (image plane) is required. The temperature needed is about 77K, although a slightly higher temperature may be acceptable. If liquid nitrogen cooling is desired, the Mitsubishi closed-cycle stirling cooler can be used, which has been designed for 2000 hours of use without recharging. This cooler draws 50W of power and it is estimated that it would need to be on for a period of 10 minutes to achieve a 77K temperature from 300K. However, one may ask the question if it is realistic for a satellite with a lifetime of 3-5 years. If 95K is acceptable for cooling the MWIR array, the three stages needed are 210K, 125K, and 95K (cold stage). ITT Aerospace/Communication Division has the ability to manufacture this radiator cooler. The size of the radiator cooler is $0.5m^2$ (1.04m x 0.46m), and the thickness for the radiator is 0.1m, including the radiation shields, which can be folded.

### 4.4.3.3.3    Detector Calibration

Another important issue regarding the detectors is calibration. Since the performance of the detector, as well as the whole optical system, varies with temperature and other factors, the detector needs to be calibrated at the beginning and the end of each scan. We can use two pieces of blackbody with different temperatures to do the calibration. Calibration blackbodies should be large enough to allow for the detectors' full field of view, in order to calibrate all elements simultaneously. A chopper or pointing mirror is needed to switch the detector between looking at the ground target and the calibration blackbody. The detector calibration includes both wavelength and radiometry calibration.

### 4.4.4 Technical Specifications

Below (figure 4.9) is a list of technical specifications for the various components of the proposed MEDSAT visible and infrared sensing system.

|  | Dimensions (cm) | Mass (kg) |
|---|---|---|
| **Fore Optics** | | |
| Instrument housing | 35 x 30 x 100 | 4 |
| Optical bench | (Existing structure) | |
| Optical mounts | | 4 |
| | | |
| **Spectrometer** | | |
| Structure | | 8 |
| Optical mounts | | 8 |
| Detector structure | 3 x 5 x 5 | 2 |
| | | |
| **Electronics** | | |
| Detectors, Preamplifiers, and | | |
| Digital Multiplexing Electronics | | 1 |
| | | |
| **Coolers** | | |
| Cryogenic | 4 x 4 x 6 | (6) |
| Radiative | (Existing structure) | |
| | | |
| TOTAL | 35 x 30 x 100 | 27 - 33 |

Figure 4.9: Technical specifications of VIS/IR sensing system.

## 4.5 Summary of Parameters and Specifications for MEDSAT Visible and Infrared Sensing System

A. SYSTEM SPECIFICATIONS

| | |
|---|---|
| Orbital altitude: | 475km |
| Swath width | 50km |
| GIFOV | 50m |
| Spectral coverage: | A: 0.62-0.69um VNIR |
| | B: 0.77-0.9um, VNIR |
| | C: 1.55-1.7um, SWIR |
| | D: 4.0-5.6um, MWIR |
| Pointing: | cross track, 15° off nadir |
| Encoding: | 12 bit |

C-2

Project MEDSAT

## B. SYSTEM CONFIGURATION

1. Optical system:
IFOV: 0.05mrad
Aperture: 20cm
Effective focal length: 570mm
Effective f number: 4
FOV: 6°
Objective mirror, slit, collimator, dichroic beamsplitter,
filter, corrector, spectrometer

2. Detectors:
Bands A and B: Silicon CCD, 2x1024, 30umx30um
Band C: $Pd_2Si$, 2(2x512), 30umx30um
Band D: PtSi, 2(2x512),30umx30um

3. Radiator Cooler:
3 stages at 210K, 155K, and 95K
Heat removed from cold stage (3W)
Radiating area: $0.5m^2$
Mass: 12kg
Solar and earth shielding
Heat pipe, conducting rod or thermoelectric cooler to remove
heat from detector to radiator

4. Cryogenic Cooler:
Mitsubishi closed-cycle stirling, 77K obtained
2000 hours of usage

5. Calibration:
Blackbodies of two different temperatures used
Chopper or pointing mirror to switch the sensor between
looking at ground target and blackbody
Spectral and radiometry calibration

6. Data volume;
$5x10^8$ bits of data/overhead pass; finite spectra

7. Electronics:
Preamplifier
Encoding (high speed digitizing)
Storing and calibrating
Microprocessor control

8. Housing:
Isolating optics and image plane (detector)
Optics: 273K; detectors: 210K, 125K, 95-77K

# Chapter 5

# DATA MANAGEMENT AND PROCESSING

## 5.1    Introduction

Data management and communication is an integral part of the operation of any satellite system. For the MEDSAT design, large amounts of data must be collected from the Synthetic Aperture Radar (SAR) and Visible/IR sensors. To be of any use, this data must be transmitted to a station were the collected data can be decoded and processed into a final image. As a final step, this data may be distributed to the users and/or archived in some manner to be of further scientific use. Therefore, data management and communications must function in an efficient and timely manner.

Design constraints that could possibly limit the functionality of data management and communications are power requirements, size, weight, and time. Data management and communications must consume the least amount of power possible to afford the operation of the SAR and Visible/IR sensors. Its size must be small to insure that space is available for hardware to insure the operation of the satellite; weight must also be limited to allow for the maximum amount of scientific payload. As a final point, the data management and communications hardware must operate quickly to ensure that data can be transmitted to a ground station.

Given these design constraints, data management and communications is broken down into five different sections: data handling, data processing, communications path, data compression, and data storage. All suggestions are based on how they will affect the design constraints. Figure 5.1 gives a broad overview of the data management flow.
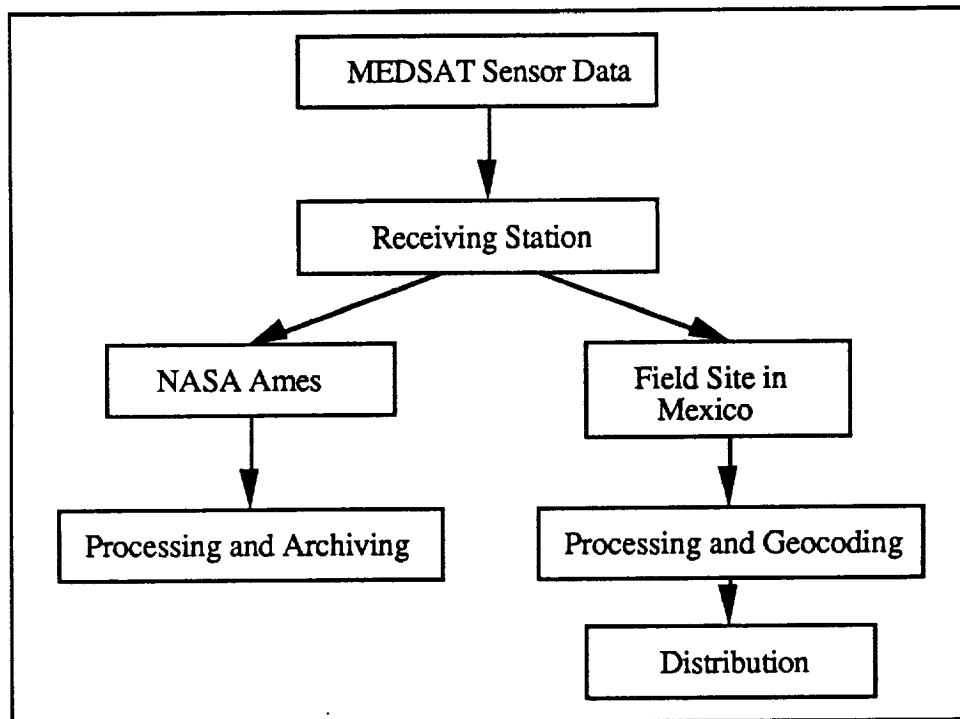


**Figure 5.1: Data Management Flow**

## 5.2 Sensor Data Handling

Raw SAR data needs to go through a great deal of processing in order to generate an image from the radar backscatter data. The SAR uses the Doppler history to produce high resolution in a spatial dimension. Many successive echoes are processed to form a single pixel thus indicating that a great deal of arithmetic operations are needed to form the image [5-1]. In addition to this, processing must also be performed along the range and azimuth directions.

On-board SAR image generation would significantly reduce the volume of data and improve data handling and on-board storage. A study of SAR image generation for Eos-type missions showed the feasibility of such a system [5-2]. The design for a SAR processor is composed of the following units:

1. Input Data Conditioner
2. Range Processor
3. Azimuth Processor
4. Multilook Processor
5. Output Data Conditioner
6. Control Processor

This proposed SAR image generation system requires 540 W of power and is expected to have an approximate mass of 100 kg.

Although such a processor improves data handling and optimizes the flow of data from the acquisition step to the dissemination of information, this system is far too large and consumes too much power for MEDSAT's on-board system. A more standard approach is to collect the sensor data, process the information for downlinking, and subsequently generate the image at a ground facility. The extent of on-board SAR data processing and handling would include conversion of the analog signal to digital signal, data compression, error correction coding and storage prior to downlinking.

The visible/IR data is converted into a digitized form when it is collected by the sensors. Hence, only compression and storage are required before transmitting the data to the ground for image registration.

A proposed design for the MEDSAT Data Handling System is shown in Figure 5.2. The data handling system is controlled by a customized microprocessor such as FRISC (Forth Reduced Instruction Set Computer), for example. FRISC was developed by the Johns Hopkins University Applied Physics Laboratory and is specifically used for light satellite applications [5-3]. Its high speed, low power, and simple programming using the Forth language, make it ideal for on-board processing applications. FRISC is also capable of collecting and digitizing housekeeping data, formatting telemetry, FFT(Fast Fourier Transform) computation, and interpreting and executing commands. The satellite's on-board computer would control the scientific instruments and direct the flow of data collected.

The raw SAR sensor data is steered into the Analog\Digital Conversion Unit to be converted into a digital format. In the next step, the information is compressed by a Data Compression Unit (Section 5.4 discusses the algorithms used for compression). After this has been completed, the Error Correction Coding System adds correction bits to the bit

stream and organizes the data into packets for transmission. The resulting data is stored by the Optical Disk Storage System and awaits transmission to the ground receiving station.

The visible/IR sensor data is handled in a similar way. The Analog/Digital Conversion is excluded since the sensor already accomplishes this step.
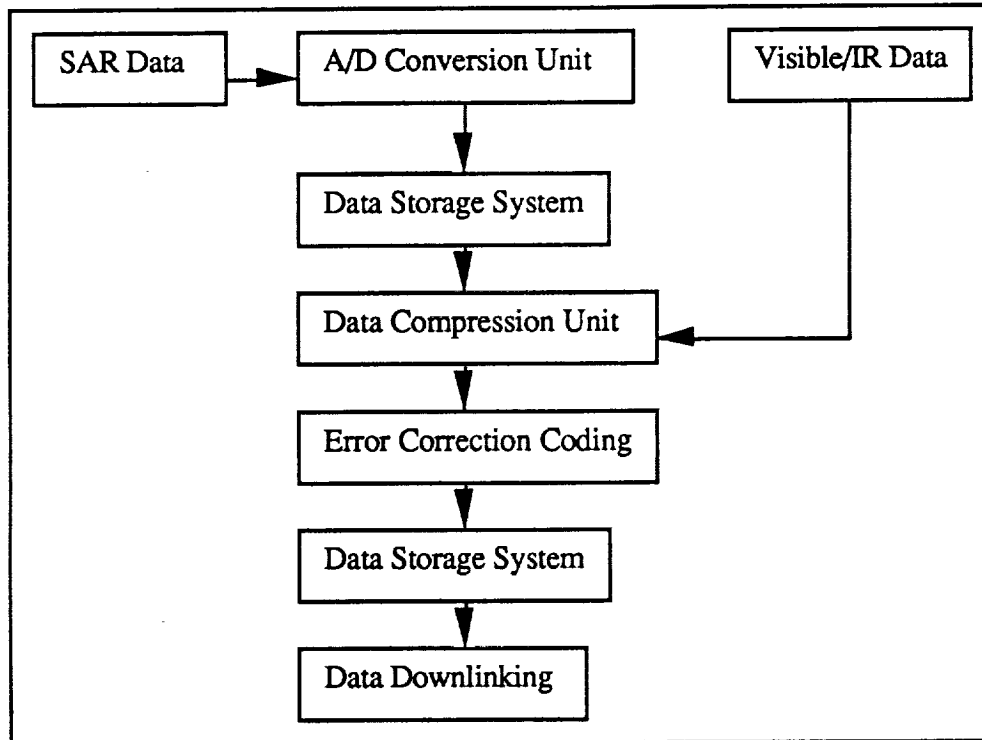


**Figure 5.2: Data Handling System**

## 5.3    Image Processing

Sensor image generation and correction is performed on the ground. If the processing station receives data directly from the satellite it would need a transcription system to go from a high downlink rate to a computer compatible tape (CCT). However, the transcription system is placed at the receiving ground station since this is where the transmission is first sent. The NASCOM system then sends the information to the processing facility where the data if first decompressed before any processing can take place. Figure 5.3 shows an overview of the processing steps.

For raw SAR data, image formation involves range and azimuth processing. Range correlation and range look extraction are performed so that range compression produces the required range resolution. Azimuth processing performs range migration correction and azimuth compression to achieve the necessary azimuth resolution. The resulting image that is generated still needs to go through image enhancement to correct for geometric and radiometric effects. Further processing can enhance the image if more analysis is needed. A SUN SPARCstation is capable of processing the raw SAR data to produce an image. This image can be further enhanced using the Meridian processing system. The image data

is turned into geographic referenced information which can be entered into a GIS (Geographic Information System) computer.

The visible/IR data requires only minimal processing. The digital image data needs to go through image registration, calibration for image correction, and enhancement. Defects that result from geometry, alterations due to haze and clouds, and solar radiation intensity need to be corrected. The SUN workstation will eliminate these errors before geographic referencing of the information.

```
┌──────────────────────────────────────────────────────────────────────┐
│   ┌────────────┐          ┌──────────────────────┐                     │
│   │  SAR Data  │─────────▶│  Range Compression   │                     │
│   └────────────┘          └──────────────────────┘                     │
│                                      │                                 │
│                                      ▼                                 │
│                           ┌──────────────────────┐                     │
│                           │  Azimuth compression │                     │
│                           └──────────────────────┘                     │
│                                      │                                 │
│                                      ▼                                 │
│                           ┌──────────────────────┐                     │
│                           │  Image Enhancement   │                     │
│                           └──────────────────────┘                     │
│                                      │                                 │
│                                      ▼                                 │
│                           ┌──────────────────────┐      ┌────────┐     │
│                           │ Geographic Referencing│────▶│  GIS   │     │
│                           └──────────────────────┘      └────────┘     │
│                                      ▲                                 │
│                           ┌──────────────────────┐                     │
│                           │  Image Enhancement   │                     │
│                           └──────────────────────┘                     │
│                                      ▲                                 │
│   ┌────────────┐          ┌──────────────────────┐                     │
│   │Visible/IR data│──────▶│  Image Registration  │                     │
│   └────────────┘          └──────────────────────┘                     │
└──────────────────────────────────────────────────────────────────────┘
```
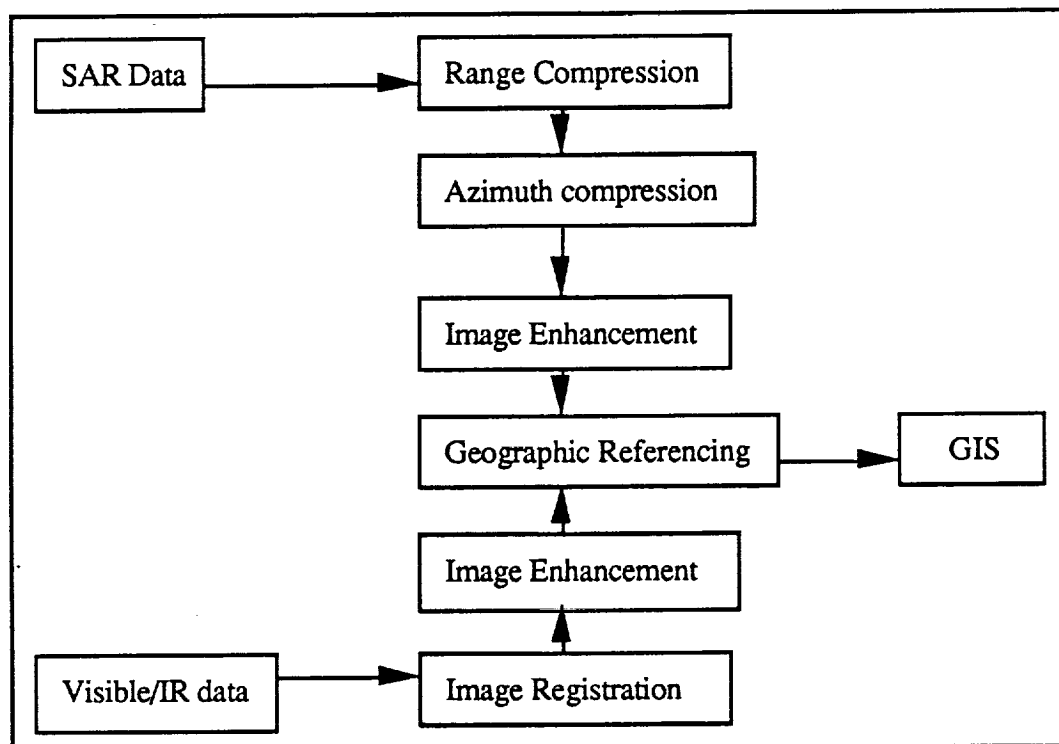
**Figure 5.3: Data Processing Steps**

## 5.4    Data Communications Path

Figure 5.1 already shows the block diagram of the flow of information. Once the data has been downlinked to the receiving ground station, the information is transferred to two sites via the NASCOM system (more information on direct downlinking to the receiving station and the NASCOM system can be found in chapter 6). One data set will be transmitted to the NASA Ames Research Center while the other set will be sent to the field site in Mexico. NASA Ames will then be able to do extensive and more sophisticated imaging using the SAR data. Ames may also want to archive the generated images since the field station will be physically limited in its ability to store the large volume of information.

The field station will be equipped with the hardware and software needed to process the SAR and visual/IR data. An alternative processing site would be the MEDVAN mobile facility which would contain custom designed hardware to generate a first order image that

can be quickly disseminated to the users. A description of the hardware used and more details on MEDVAN were discussed in Section 3.7

## 5.5 Data Compression

An important aspect of MEDSAT is its data collection capabilities. For each SAR and visible/IR image, upwards of two gigabits of information is necessary to properly define the final picture. This enormous amount of information must find its way to a processing station on Earth to be of any practical use; hence, the amount of data downlinked defines the amount of resources on the satellite necessary to communicate the information. Such resources would be power, processing capabilities, antennae size, and storage required for collected data. It can easily be seen that for more information to be processed, more resources will be necessary. Therefore, to reduce the amount of resources required for sending the data, a reduction in the size of the data set would be appropriate. To accomplish this for MEDSAT, data compression algorithms were implemented, thus reducing the amount of resources used on the satellite.

### 5.5.1 The Importance of Data Compression

The most important aspect of data management on MEDSAT is the ability to compress data. The amount of compression obtained defines three major performance parameters of the satellite - downlinking abilities, computational power, and on-line storage. Of these three, downlinking is of most concern. To transmit the collected data, the signaling antennae will use power that could otherwise be used for more important aspects of operation, such as the operation of the SAR and visible/IR sensors. Another concern during downlink is the short amount of time the satellite will be over the sight to transmit. To minimize the time required for data transmission, the collected data needs to be compressed as much as possible. The time necessary for this compression, though, is a function of the algorithm used and of the speed of the on-board processor. Therefore, a fast compression algorithm and on-board processor becomes a requirement. To help offset the expense of these requirements, on satellite storage provides a viable alternative. But again, with such a large data set, and the need to store collected information on-board, data compression has a very strong influence over on-satellite storage. To best summarize, data compression is an inherently important aspect of MEDSAT that, if used properly, can greatly increase the efficiency of operation of MEDSAT. The compression method that best suits our needs for this satellite is Vector Quantization.

### 5.5.2 Vector Quantization Algorithms and Specifications

Vector Quantization is the data compression method chosen for implementation on MEDSAT. There are various properties of Vector Quantization that lend itself easily to compressing raw imaging data. The first important property of this compression technique is that it takes advantage of the redundancy of the input data. Image collection has the inherent property that there will be a considerable amount of data repetition; therefore, Vector Quantization is a good design choice. Another important property of Vector Quantization is that the compression ratio can be defined in the algorithm used. This is a useful aspect because it allows an increased compression of data as deemed necessary by the design team. Vector Quantization can also be used with another processing technique referred to as Computational Compression Technique. This method enhances the abilities of Vector Quantization as an efficient compression algorithm.

Although there are a number of advantages Vector Quantization provides, there is an inherent disadvantage to using this method. The disadvantage is that it is a lossy method (i.e. the reconstructed image is not exactly the same as the original image). The loss in vector quantized data is determined by the amount of compression desired; the higher the compression ratio, the more noise will be found in the reconstructed image. (Note: the compression ratio is defined by $r = n*b/m$, where n is the number of element blocks, b is the number of bits defining each element in the original data set, m is the number of bits defining each element in the reconstructed data set, with r the compression ratio).

### 5.5.2.1 General Properties of Vector Quantization as Applied to SAR Data

Vector Quantization is a lossy method of data compression that can be categorized as a technique of block encoding. The reason for this is that Vector Quantization codes blocks of data with reference vectors found in a "codebook". This codebook is a statistically representative set of data taken from a sample data run. The process flow for vector quantization is as follows:
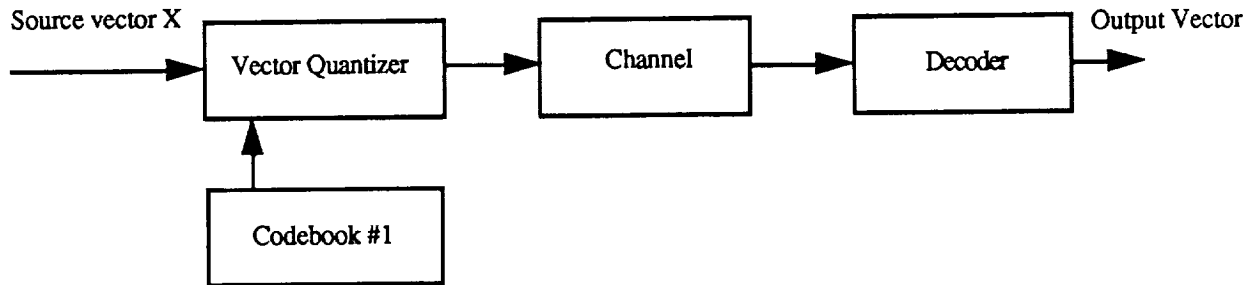


**Figure 5.4: Vector Quantizer Block Diagram**

The process for Vector Quantization is straightforward. The first step involves quantizing the original input vector X into a digital format. From there, comparisons are made to codebook vectors Y to find a best fit. It is at this stage of processing that requires a significant amount of time as well as complex circuitry. To reduce this complexity, a method of product encoding is suggested. Product encoding is a method where a "product codebook" is defined as all combinations of all components of codevectors contained within the original codebook. This more or less provides an exhaustive representation of the available codevectors to be used. After the proper vector from the codebook has been chosen, that vector is used in place of the original. The compression arises from the fact that a smaller set of vectors are used to represent a wide range of vectors.

### 5.5.2.2 Specific Properties of Vector Quantization as Applied to SAR Data

Vector Quantization is applied to the raw SAR data in either the real-imaginary plane or the magnitude-phase plane. It has been found that compressing data in the real-imaginary plane provides the best overall performance when compared to magnitude-phase data of the same bit length. To reduce the error involved in the encoding of the input data, a method referred to as Vector Residual Vector Quantization (VRVQ) is suggested. This method encodes the input vector and subtracts the result from the input vector. The result from this operation is then encoded again using another codebook. This method can be cascaded to

reduce error as much as necessary. To measure the distortion of the final image, a mean square error is suggested as being the easiest to use.

### 5.5.2.3 Decompression of Vector Quantized Data Using the Computational Compression Technique

After the compressed data set has been transmitted and received, it is necessary to decompress and perform image processing. This decompression and image processing step requires additional resources to be available at the receiving station, as well as additional time to perform the actual image processing. To reduce processing time, the CCT is suggested for use. This technique is applied at the stage of decompression where the transmitted vector is matched to a vector contained within the decoding codebook. For the standard decompression process, the transmitted vector is matched to another vector in the decoding codebook. For the Computation Compression Technique, instead of matching the input vector to another vector, the transmitted vector is matched to a preprocessed vector that is available for image display. This simply means that the decoding codebook is a processed version of the encoding codebook. It has been demonstrated that the image processing time can decrease by as much as a factor of eight. There are two methods available for performing CCT. The steps of the methods are listed as follows:

Method #1
    1. Pre-process the two dimensional vectors in the decoding codebook
    2. Compress the raw SAR data using VRVQ w/ compression ratio ~ 100:1
    3. Reconstruct the SAR image by adding all pre-correlated vectors (overlap and add)

.Method #2
    1. Pre-process the one dimensional vectors X in the decoding codebook
    2. Pre-process the one dimensional vectors Y in the decoding codebook
    3. Vector quantize raw SAR data w/ one dimensional vectors X
    4. Vector quantize raw SAR data w/ one dimensional vectors Y
    5. Reconstruct the SAR image w/ one dimensional vectors X
    6. Reconstruct the SAR image w/ one dimensional vectors Y and that of step 5.

Method #1 requires more memory and processing time to produce an image; therefore, Method #2 is suggested for use.

### 5.5.3 Block Adaptive Quantization Used in Conjunction With Vector Quantization

To assist in increasing the rate of data collection for the SAR, a method referred to as Block Adaptive Quantization (BAQ) can be used. This method is described in section 4.4.5. BAQ, by virtue of the encoding scheme, cannot be used in a vector quantization process. For this reason, it is suggested that the data compression algorithms be specified solely by VQ and CCT methods.

### 5.5.4    Compression Summary

The MEDSAT design team suggests that Vector Quantization be used as the method of data compression. VQ is a lossy method of compression that takes advantage of the redundancy of input. The compression ratio of VQ can be specified by the designer, thus easing design constraints. The MEDSAT design team also suggests that Vector Residual Vector Quantization be used to reduce error; the distortion in the final image can be measured by mean square error analysis. For decompression, CCT is the method of choice because of the reduction in processing time required for a final image.

## 5.6    Data Storage System

After the collected data is prepared for downlinking, it needs to be stored in a memory device until the scheduled linking time to transmit the compressed data to the ground station. During one pass, the on board recorder will be switched on after the uplinking command has been received, and records Synthetic Aperture Radar and Visible/Infrared sensors' data . Then on the next scheduled time the satellite passes over the receiving station, it will transmit the compressed data and receive new commands from the ground station.

### 5.6.1    Storage Capacity Requirement For One Pass

The SAR sensor will require approximately 234 Mbits of data to generate an image for a 250 km by 50 km of scanning area. The calculations of SAR data requirements are described in Chapter 3. For the visible/IR sensor, the data requirement is calculated as follows: (refer to Figure 5.5)

| | |
|---|---|
| . Area scanning------------ | 250 km x 50 km |
| Resolution--------------- | 50 m  x  50 m |
| Bits per resolution------- | 12 bits |
| No. of bands------------- | 4 bands (maximum case) |
| Calculation--------------- | 250k x 50km x 12bits x 4bands /(50m x 50m) |
| | = 240.0 Mbits |

Therefore, it will require a maximum of 240.0 Mbits of data to create one image. Storage is needed for data from the satellite on the condition of power system, battery level, and whether both sensors are fully functional. Additional storage is used for the transponder data stream, the low bandwidth auxiliary data channel used by the SAR RF system. Hence, approximately 1.0 Gbits of SAR and Vis/IR sensors' raw data need to be recorded in a storage system. The data that results from data compression needs to be stored as well. For example, if a 10:1 compression ratio is used 1Mbit of data also needs to be stored bringing the total to 1.1 Gbits.

50 m

50 m

250 km

Sensing ground
area

50 km
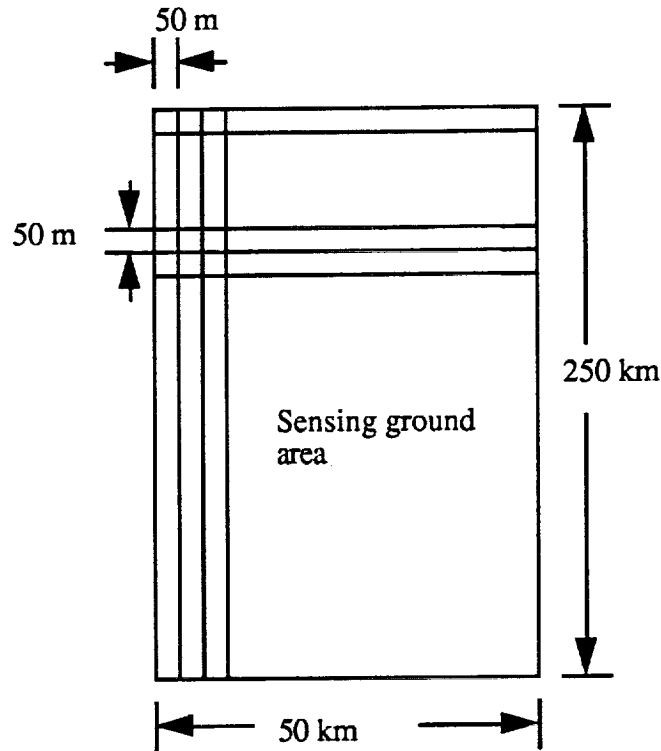
**Figure 5.5: Visible/IR Sensing Area**

### 5.6.2 System Requirement

When choosing a storage system, some of the criteria taken into account include high memory capacity, fast transfer rate, low power, and advances in technology. Devices such as magneto optical disks, magnetic tape recorders, and CD-ROM systems, were compared to find the system that satisfies the requirements of the satellite. The design team also needed to look forward into the future to determine which device will be used in the next five years after further research and development [5-4],[5-5]. In this section, two types of memory storage devices will be discussed. One device is an optical disk storage system, and the other method involves using integrated circuit technology. This section will discuss some of the criteria for system requirements and will introduce two types of storage systems.

### 5.6.2.1 Optical Disk Memory System

The optical disk memory system has the largest memory capacity, fastest data transfer rate, and lowest error rate, in comparison with other storage devices. NASA and other companies are currently researching and developing better disk storage systems. Therefore, within the next five years, the optical disk system will become more reliable and more powerful. By searching through the current market, we found out Sundstrand Data Control Inc. has developed an air borne optical disk system called Tactical Optical Disk System (TODS), which is small, light and requires low power consumption [5-6]. The basic information regarding TODS are the following:

| | |
|---|---|
| Memory capacity---------------- | 2.4 Gbits |
| Transfer Rate--------------------- | 4.0 Mbits per second |
| Error Rate------------------------ | $10^{-12}$ |
| Power consumption------------- | 35 Watt |
| Weight---------------------------- | 8.182 kg |
| Dimension------------------------ | 12.7 x 16.5 x 25.4 cm$^3$ |

The advantage of using such a system is that it satisfies the requirements of the satellite. However, this system has never been tested in a space environment before. The first test of the TODS system in space will be in May 1991 when it will be used on the space shuttle Columbia. There are also some other optical disk memory systems on the market or under research and development, and in the future there will be some systems that are better and more qualified than TODS. But at this point, we will use TODS as an example of optical disk memory system that can be implemented on the satellite [5-7],[5-8].

### 5.6.2.2    Integrated Circuit Technology

Another option available to MEDSAT is using integrated circuit technology for mass data storage. With the amount of data collected being on the order of 1.0 Gbit, an effective means of storage must be found. This includes providing storage with low power consumption and small overall size. Using space hardened 16 Mbit DRAMs would satisfy the design constraints of MEDSAT easily. Listed below are the important parameters of the mass data storage system using DRAMs.

| | |
|---|---|
| Technology----------------------- | CMOS |
| Memory Capacity --------------- | 2 Gbit |
| Organization--------------------- | 16Mb x 1b |
| Chip size------------------------- | 7.7 x 17.5 mm$^2$ |
| Access time---------------------- | 60 ns |
| Vcc------------------------------- | 3.3 V |

A reasonable amount of memory to provide for this system would be 256 Megabytes. This would require 144 chips. The power consumption for all of the chips in dynamic mode would be ~40.0 watts, a reasonable requirement.

## 5.7    Conclusion

MEDSAT's data management and communications section will use an on-board processor similar to FRISC to handle all the necessary on-satellite processing. For storage an optical disk or DRAM memory block can be used. To minimize communication and design problems, a receiving station was specified on Earth. To reduce communication time and power consumption during transmission, Vector Quantization is suggested for use, with the additional options of using VRVQ and CCT as support algorithms. With all specified options working in tandem, data management and communications will fulfill the design constraints of the MEDSAT system as a whole.

# Chapter 6

# COMMUNICATIONS

## 6.1    Summary

The communications subsystem is the link between earth and the satellite. This allows new commands to be sent to the satellite for the sensors and attitude control mechanism. In turn, the satellite can return the data collected by the sensors to stations on earth where the data can be analyzed and sent to the appropriate authorities. Uplink/downlink sites and the on-board equipment make up this subsystem. The uplink/downlink site that as been designated is Hawaii. If there is no existing station there, one will be built. The satellite subsystem will consist of an offset-fed parabolic reflector, diplexer, and two transponders. The transmit frequency of the satellite is 12 GHz and the receive frequency is 14 GHz.

## 6.2    On-Board System

The satellite's onboard subsystem is made up of the antenna, diplexer, and transponders. Each of these will be described in detail below.

The antenna is an offset-fed parabolic. The dish is constructed of a 78 sq. cm (2.5 cm thick) plate that has been carved out to form a 75 cm diameter parabolic dish. It is made from a graphite composite and lined with a thin layer of reflective material. The feed is a corrugated circular horn 9.2 cm in diameter and 8.6 cm long. This horn has an angular spread of 45 degrees. It is also made of graphite composite. This set up was chosen for its ease of deployment and the fact that the feed doesn't block any part of the reflector aperture ( Fig 6.1). Use of the corrugated feedhorn was prompted by its low sidelobes.

The diplexer allows the same antenna to be used for transmitting and receiving. It isolates the transmitting frequency from the receiving frequency by rejecting those frequencies outside a specified range. The transmitting frequencies are then sent to the transmitting transponder and to the microprocessor for processing [6-1, p.336].

MEDSAT's communication system has two transponders, one for transmitting and one for receiving. This also builds redundancy into the system. Both transponders are connected to the microprocessor for relaying data and instructions (Fig 6.2). The transmitting frequency of the satellite is 12 GHz (gigahertz) and the receiving frequency is 14 GHz, both of which are in the lower Ku-band. Most of the 12 kg weight of this system is in the transponders which weigh 4.5 kg each.

The maximum gain of the antenna aided in the choice of size for the reflector. This was determined by the following equation [6-2].

$$G_{max} = ( \frac{\pi D}{\lambda} )^2$$

where D is the diameter of the reflector and $\lambda$ is the transmit/receive wavelength. A maximum gain of 39.5 dB was found for the 75 cm reflector. Using an efficiency factor ($\eta$) of 70%, the gain turned out to be 27.7 dB. While this gain is relatively high, it is still small enough for adequate coverage.
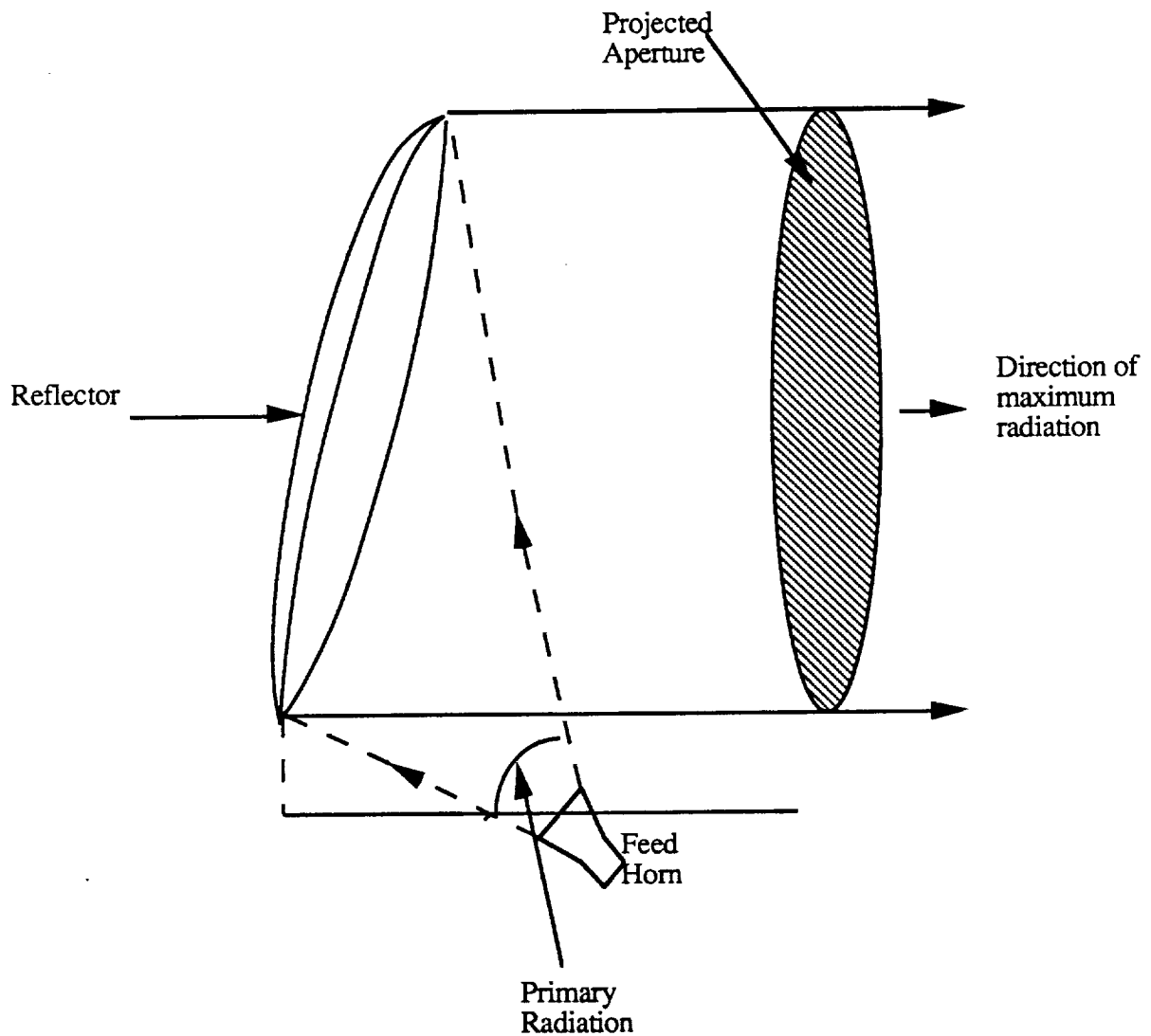
**Figure 6.1:  Antenna  Configuration**

Power was a large concern in determining the uplink/downlink capabilities of the satellite. Also tied into this was the data rate. These two factors  were related by the equation [6-1]:

$$\frac{E_B}{N_o} = \frac{PL_lG_tL_sL_aG_r}{kT_sR}$$

where

$\dfrac{E_B}{N_o}$ = ratio of received energy per bit to noise density

$P$ = transmit power

$L_l$ = transmitter to antenna line loss

$G_t$ = transmit gain

$L_s$ = space loss

$L_a$ = transmission path loss

$G_r$　　= receive gain
k　　　= Boltzmann constant  (-228.6 dBK$^{-1}$Hz$^{-1}$)
$T_s$　　= system noise temperature
R　　　= data rate
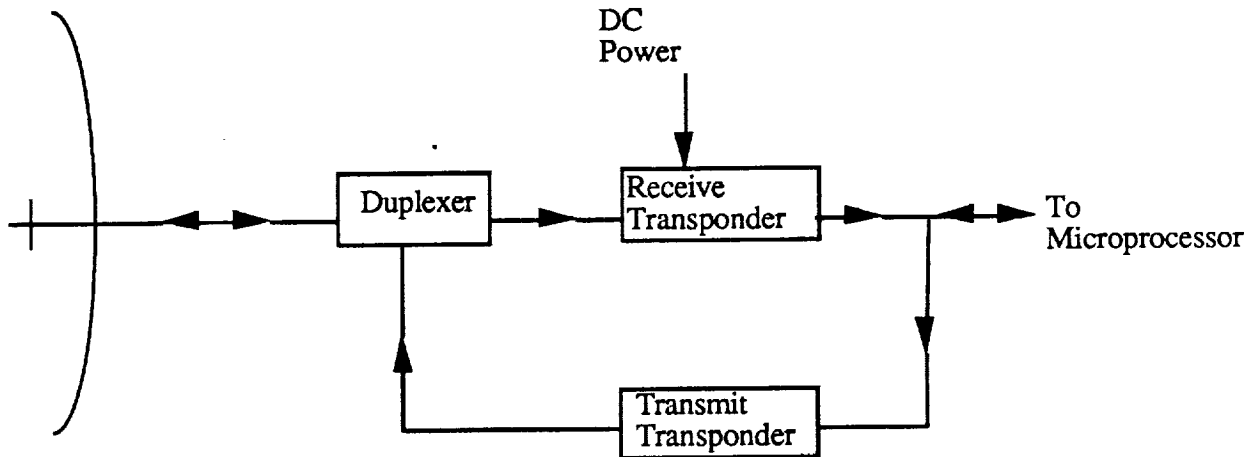


**Figure 6.2:  Communication Subsystem Schematic**

Values used for line loss, system noise temperature, and the ratio were generalized values [6-1]. The gain for the ground station receiver was determined using the maximum gain equation above and an assumed reflector diameter of 35 m. Data rate (100 Mbps) was chosen as a desired rate of transfer due to the large amount of data generated by the SAR imaging and the IR sensor. The transmission path loss is the signal attenuation due to atmospheric and climactic effects. This was determined to be 1 - 4 dB [6-1]. Space loss was calculated from the following equation

$$L_s = ( \frac{\lambda}{4\pi S} )^2$$

where S is the radius of a circle with the transmitter at the center and the receiver is on the edge. This calculation, following the transformation of all values into decibels and solving for power, yielded a value of 0.01 W required for transmission per sec. At the desired data rate, only 25 seconds would be required to transmit the estimated 2.5 Gbits of information to the ground station. The communications subsystem is provided with 15 W of power which will allow two or three transmissions of the data to ensure the accuracy of data received at the ground station.

## 6.3　Uplink/downlink Considerations

This section will discuss the considerations involved in choosing a site for the ground station and an alternative method for the data link which was researched in some detail.

## 6.3.1    Site Considerations

Sites for uplinking and downlinking information with the satellite were constrained by the inclination angle of the satellite's orbit. Another constraint was the relatively few transmitting/receiving stations located within the area covered by the orbit. Hawaii was chosen as the site for the uplink/downlink station. This site fulfilled several criteria including a sufficient amount of time between sensing and the downlink to build up power; lies within the 21 degree inclination restraint; and it is a part of the United States so that fewer political problems would be faced in establishing the site.

The estimated time within range of this ground station is five minutes. This allows sufficient time for uplink information and the data transmission at 100 Mbps (megabits per second) data rate. There is also time for the required matching of telemetry between the ground station and the satellite.
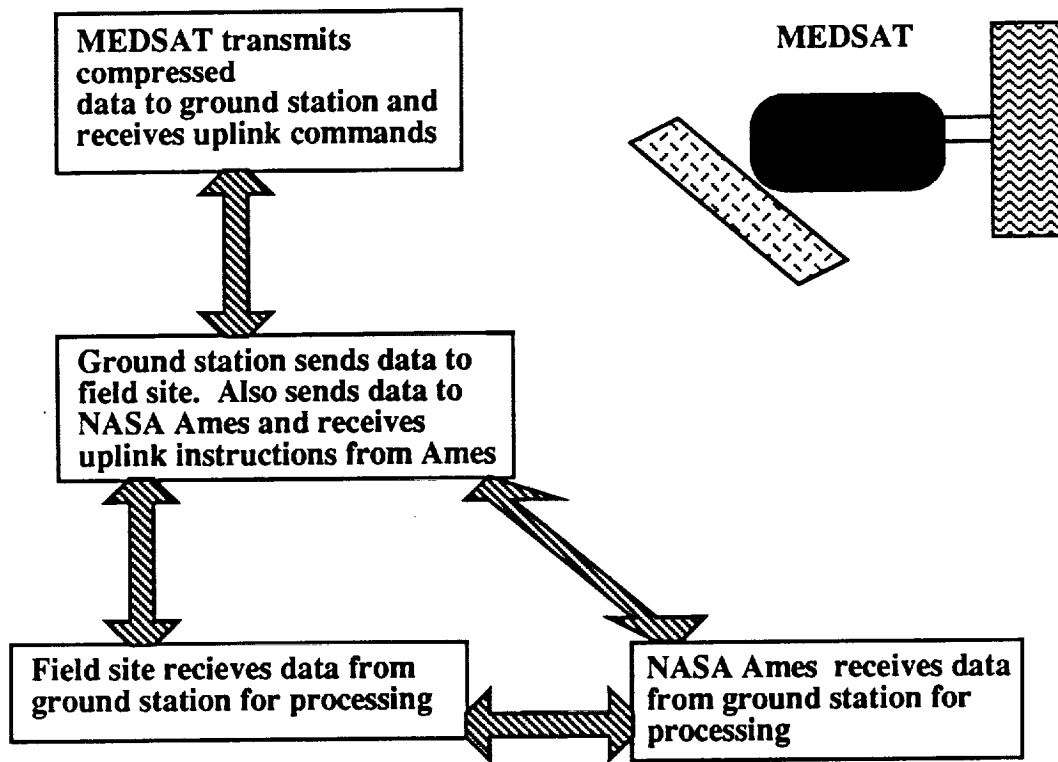


**Figure 6.3: Direct Communication Path**

The satellite passes over the Hawaii site during the fifth, sixth, and possibly seventh orbits. Sensing can be done during the first and fifth orbits of the sixteen. This means that the data can be downlinked within two to four orbits of the sensing session if there is sufficient power. If sensing is done on the first orbit and is also required on the fifth orbit, the data from the first sensing session may be downlinked as the satellite passes over Hawaii prior to reaching the target site. This is based on the minimal amount of power required for each uplink/downlink session.

NASA Ames Research Center, the sponsor of the MEDSAT project, has asked for access to the satellite as it is considered part of an experimental system. Locating the ground station within the United States guarantees NASA Ames access both to the satellite and the data it collects. It also allows for easier dissemination of the processed data to the proper agencies within Chiapas to put the information to use. This accessibility also makes the ground station and data transferral less expensive and reduces the chance of data loss.

## 6.3.2    Alternative Uplink/downlink Method

An alternative method considered for the uplink and downlink of information between MEDSAT and the ground was TDRSS ( Tracking and Data Relay Satellite System). This NASA system consists of three satellites (including a spare) in geostationary, equatorial orbit. The satellites are located at 41° west and 171° west longitude. The use of TDRSS allows satellites in low earth orbit to have continuous uplink/downlink capabilities without a ground station of its own.

| BAND | ACCESS | DATA RATE | ANTENNA |
|------|--------|-----------|---------|
| K | Single | 2 to 300 Mbps | 4.9 m gimbal |
| S | Single | 2 to 300 Mbps | 4.9 m gimbal |
| S | Multiple 20 channels | 1 to 50 Kbps | 30 element phased array |

**Figure 6.4: TDRSS Data Channel Characteristics**

TDRSS has three data access modes (Figure 6.4). Once data is received by the TDR satellite, it is transmitted to the White Sands Ground Terminal (WSGT) located in White Sands, New Mexico. From WSGT, the data can be transferred to NASA Ames, the field site, and any other location requiring access to the raw data. This is accomplished using NASCOM via modem or satellite relay (Figure 6.5).

Since TDRSS is a NASA system, it would ensure NASA Ames control over the satellite for uplinking commands and downlinking the sensor data. The system would also be very low cost as NASA users of TDRSS are not required to pay for use of the system. However, use of TDRSS requires the satellite transferring data to have a pointing antenna. Pointing antennas require more space and power than is available on a light satellite such as MEDSAT. Also, access to TDRSS's high data rate channels is extremely limited making timing for data transferral difficult to determine and guarantee. Therefore, direct downlink was chosen over TDRSS as the designated uplink/downlink system for this design.

Communications

| MEDSAT transmit the compressed data to the TDR satellite and receive uplink command from it | MEDSAT |
| The TDR satellite relay the sensors' data to ground station at White Sand, NM. Then relay the uplink to MEDSAT. | TDR SATELLITE |
| TDRSS ground station located at White Sand, NM. is the system control center. It receives data and transmit uplink command. | TDRSS GROUND STATION |

Use NASCOM system to communication between the ground stations.

NASA Ames Research Center. MEDSAT control center, it will send out the uplink command to TDRSS and receive sensors/ data.

Ground station and the field site(MEDVAN). It will receive the sensors' data, and create risk maps

communication between two ground stations

DOWNLINK

UPLINK

**Figure 6.5: TDRSS communication path**

# Chapter 7

# MISSION ANALYSIS

## 7.1    Summary

The objective of the mission analysis group was to design the optimal orbit which would satisfy the sensing and launch vehicle requirements. The specific requirements which the orbit must satisfy are: daily sensing of Chiapas, four year lifetime, low altitude, communication with groundstations and good equatorial coverage. The capabilities of the Pegasus launch system will enable the 340 kg MEDSAT to be inserted into a 477 km circular orbit with a 21 degree inclination. Precession due to the Earth's oblateness will cause the satellite to pass over Chiapas one half hour earlier than the previous day's pass. Atmospheric drag will be offset through the use of thrusters to provide the required four year lifetime. The ground track was designed to cover Chiapas twice per day to allow almost continuous daylight sensing. The ground track also passes over suitable groundstations such as Hawaii. The airborne launch of the Pegasus will allow considerable flexibility with launch windows.

At the end of the chapter a conclusion of the findings of the mission analysis group are presented and possible alternatives such as a higher altitude orbit or a sun synchronous orbit are presented.

Summary of Orbital Parameters:

> Altitude = 477 kilometers circular
> Period = 94.1 minutes
> Inclination Angle = 21 degrees
> Satellite Mass = 340 kilograms
> Revolutions/Day = 15
> Coverage Frequency = Twice per day
> (of Chiapas)

## 7.2    Requirements of the Orbit

There were five main requirements given to the mission analysis group. They are as follows:

1) At least daily coverage of target site, Chiapas.
2) Four year lifetime.
3) Low altitude
4) Ability to communicate with a suitable groundstation for uplinking and downlinking.
5) Provision for sensing over other countries with tropical disease problems in the future (i.e. good equatorial coverage).

Daily coverage of Chiapas was requested to provide a large database of information on the area and to detect small changes in the mosquito environment. The IR sensor does not function well at night or when there is cloud cover. Because of Chiapas' six month rainy season and the precession, at least daily coverage was needed to obtain good IR images of the target as often as possible. Thus, the ground track must repeat every 24 hours.

A four year lifetime is desired so that seasonal changes in the mosquito's habitat can be detected. This means that the satellite must be inserted into a high enough altitude so that atmospheric drag will not pull the satellite out of a useful orbit before the four years

expires. Another option is to use thrusters to occasionally offset the drag and keep the satellite near its desired orbit.

A low altitude was specified for three reasons. First, due to the relatively high mass of MEDSAT, only a low orbit is possible using Pegasus. (This is explored in further detail in section 7.3). Second, the lower altitude allows greater resolution of the sensors because they are closer to the surface. Finally, less power is required to communicate between the satellite and the ground station.

The ability to communicate with a suitable groundstation is necessary to downlink the data quickly and efficiently so that it may be effectively delivered to the necessary personnel. Also, timely uplink commands must be directed to the satellite from the groundstation. This means that the orbit must bring the satellite into the range of the groundstation for a suitable length of time to facilitate the uplinking and downlinking.

The final requirement was to obtain fairly complete coverage of the equatorial areas where tropical diseases are a problem. This will allow sensing of sites other than Chiapas in the future if desired. This limits the inclination angle to a range of 15 to 25 degrees.

## 7.3 Pegasus Launch System

For this mission, the Pegasus launch vehicle will be used to insert the satellite into its orbit. Specific details about the Pegasus are presented in Chapter 1. This section will address how Pegasus will launch the satellite and investigate the orbital insertion errors involved and what will be needed to correct them.

### 7.3.1 Mission Profile
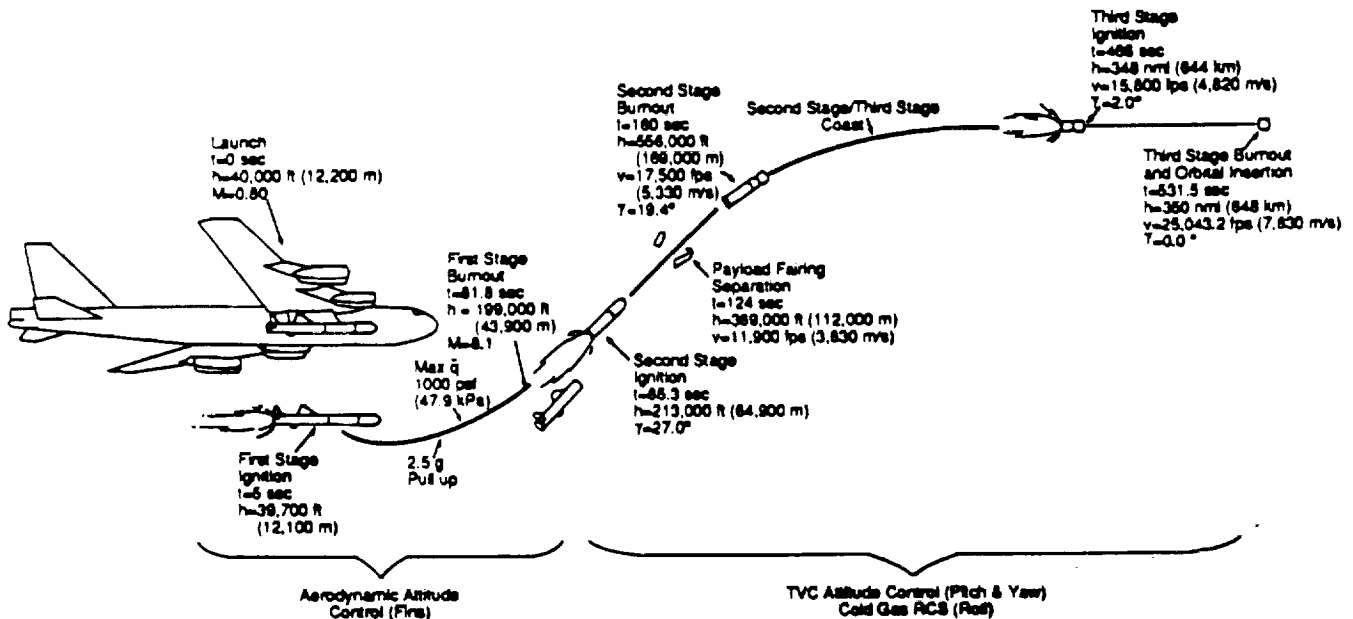


**Figure 7.1 Typical Pegasus Mission Profile (460 km Altitude)**

A typical launch sequence for a 460 km circular, polar orbit is shown in Figure 7.1 [7-1]. Although MEDSAT's orbit is different, the sequence will be similar. The Pegasus is launched at an altitude of approximately 12,200 meters with the B-52 cruising at Mach 0.8. The first stage ignites about 90 meters below the B-52 and lasts 75 seconds. During this stage, the vehicle quickly accelerates to supersonic speed and then undergoes a 2.5 g pull up maneuver. Aerodynamic fins act as attitude control devices and a 45 degree swept delta wing improves aerodynamic performance. After coasting for a short time, the second stage burns for 75 seconds using a thrust vector control system for pitch and yaw control and a cold gas nitrogen reaction control system (RCS) for roll control. The third stage burn, also using the thrust vector and RCS control systems for attitude control, completes the orbital insertion. Orbital insertion occurs approximately 530 seconds after launch 2200 km downstream.

### 7.3.2 Payload Capabilities

The main concern for the mission analysis group is the payload weight capability of the Pegasus. The payload weight is a major factor in determining the altitude which can be reached. Figure 7.2 [7-1] illustrates the Pegasus' capabilities.
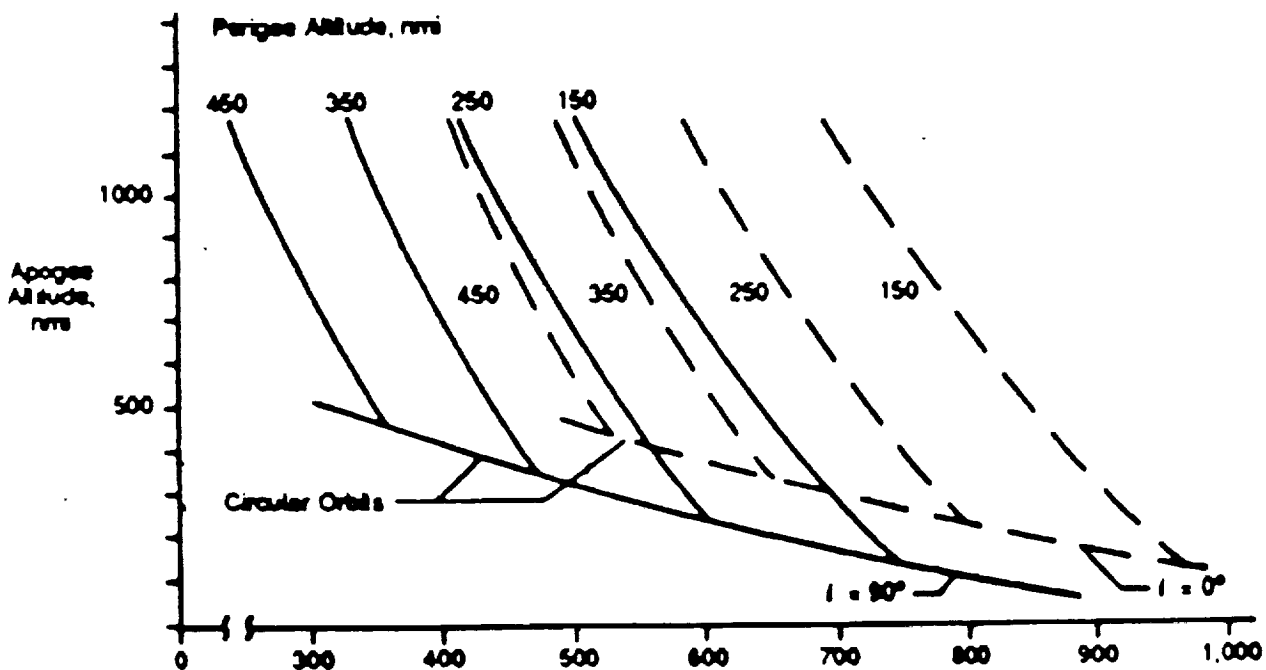


**Figure 7.2 Pegasus Payload Performance**

If the weight is increased, the altitude which can be reached with Pegasus decreases. The graph has curves for both elliptical and circular orbits at inclination angles of 0 and 90 degrees.

Since an inclination angle other than these two limits will be used, an interpolation scheme was derived to find values for different inclinations. The reason there is a difference in

payload with the inclination is that the earth's rotation affects the launch vehicle's energy [7-2]. Because the earth spins toward the east, a rocket launched to the east will have a higher kinetic energy. This is due to the fact that the rocket not only has its own velocity, but also the added velocity from the earth's rotation. It will receive the maximum velocity boost at the equator with a zero inclination angle. For a polar orbit of 90 degrees inclination, the rocket will receive no boost at all because the rocket's velocity is orthogonal to the earth's rotation. If the rocket is launched to the west, its energy will be adversely affected. For angles between the maximum and minimum curves of 0 and 90 degrees respectively, the amount of velocity boost is a function of the cosine of the inclination angle.

The more boost the rocket receives from the earth's rotation, the less energy which is required by the rocket to enter the orbit and the more payload that can be inserted into orbit. This was found to vary linearly with the amount of velocity boost. Therefore, it is also a function of the cosine of the inclination angle. Thus, the interpolation between 0 and 90 degrees is the cosine of the inclination angle.

The two altitudes considered for the mission with the inclination angle of 21 degrees are 795 km (431 nm) and 477 km (259 nm), corresponding to 14 and 15 orbits per day respectively. In Figure 7.2, these are noted and their corresponding weights are calculated using the cosine interpolation.

### 7.3.3 Insertion Errors

Because of the need for an accurate and repeatable ground track to conduct sensing, errors in the orbit must be kept to a minimum. According to Pegasus flight test data, insertion errors for Pegasus are 37 kilometers in altitude and 0.2 degrees in inclination for a 735 km, circular, polar orbit [7-5]. The orbit for MEDSAT is at a lower altitude and inclination, so the errors will be smaller. However, these values should provide reasonable maximum errors. The errors will be corrected by the use of thrusters by inducing a velocity change, $\Delta V$. The amount of $\Delta V$ was calculated along with the fuel mass and the results are shown in Figure 7.3 below.

|  | Error | Delta V | Fuel Mass |
|---|---|---|---|
| Altitude Errors | 37 km | 10.5 m/s | 1.27 kg |
| Inclination Errors | 0.2 deg | 26.8 m/s | 3.24 kg |
| Total Insertion Errors |  | 37.3 m/s | 4.51 kg |

**Figure 7.3  Orbital Insertion Errors**

## 7.4  Nominal Orbit

The nominal orbit was calculated as a first approximation assuming no precession due to oblateness. First, daily coverage requires a ground track which repeats every 24 hours. This means there must be an integer number of orbits per day. A circular orbit of fifteen revolutions per day was chosen. The period of each orbit was then found, by dividing the 24 hours by the fifteen orbits, to be 96 minutes. Next, the altitude is calculated from Equation 7-1 [7-3].

$$h = \left[ \frac{\tau\sqrt{\mu}}{2\pi} \right]^{\frac{2}{3}} - R_0 \tag{7-1}$$

where:

h = altitude in kilometers

$R_0$ = Earth's radius = 6375 km

$\tau$ = orbital period in seconds = 5760 seconds

$\mu$ = gravitational constant = $3.986 \times 10^5$ km$^3$/s$^2$

Using this equation, an altitude of 566 km is obtained. The inclination angle was chosen to be 21 degrees. This will easily cover the target site and the ground station and it provides good equatorial coverage. The choice of the inclination angle depends greatly on the precise ground track. This is examined more closely in section 7.7.

A circular orbit was chosen over an elliptical orbit for two main reasons. First, the ground track is simpler to work with, which is important when trying to design a precise orbit. Second, the main reason for using an elliptic orbit is to prolong the lifetime. However, this effect is small in our case because of the low altitude and the period constraints for ground track repeatability.

This nominal orbit is only a rough first approximation. Precession, which is studied in section 7.5, and drag, which is studied in section 7.6, perturb the orbit from these nominal values. However, the nominal orbit is still useful to gain a rough sense of the orbit and how suitable it is for the mission.

## 7.5    Precession Analysis

Precession of the nominal orbit results from the fact that the earth is not a perfect sphere, but rather oblate. Because of its rotation, mass tends to move toward the equator making the radius at the equator larger than at the poles by about 32 km.. This means the earth cannot be approximated by a point mass located at the center of a sphere. The major effect this has on a circular orbit is that the orbit will precess. In other words, the plane of the orbit will move towards the west with time.

If this is not corrected, the orbit will gradually move away from the desired coverage site. The most common way to correct for precession is to think of the precession as the earth moving to the east relative to the satellite's orbit instead of the plane of the orbit moving to the west. Then, essentially, the earth is spinning faster as viewed by the satellite. This means the earth's period will be shorter than 24 hours relative to the satellite by the same amount as the precession of the satellite.

The precession rate is calculated by using an oblate force field instead of spherical and assuming the effect is small. From this, Equation 7-2 [7-2] for the rate of precession for a circular orbit can be derived.

$$\dot{\Omega} = \frac{-3}{2r}\sqrt{\frac{\mu}{r}}\, J_2 \left( \frac{R_0}{r} \right)^2 \cos i \tag{7-2}$$

where:

$\Omega$ = precession rate, radians/revolution
r = radius of circular orbit = 6852 km
$J_2$ = coefficient of gravity potential (constant) = 1.0826 x $10^{-6}$
$R_0$ = earth's radius = 6375 km
i = inclination angle = 21 degrees

For the nominal altitude of 566 km and an inclination angle 21 degrees the precession rate is -0.00807 radians per revolutions. With 15 revolutions per day this is equivalent to 6.935 degrees per day meaning that the orbit precesses to the west at this rate. This is equivalent to 27.74 minutes per day since the earth rotates 360 degrees in one day.

Since the motion is relative, this can be thought of as the earth rotating faster with its period shortened by 27.74 minutes. For a repeatable ground track, an integer number of orbits must divide equally into this new period to account for precession. This gives a new orbital period of the satellite which will yield a new precession rate. By iteration, the values quickly converge to a period of 94.1 minutes, corresponding to an altitude of 477 km.

This period and altitude will allow the satellite to cover the target site every day. However, because the precession was taken into account when determining the period, the time of day of coverage will vary. Each day the satellite will pass over Chiapas 27.74 minutes local time before the previous day's pass. This leads to the inevitability of night time coverage of the target. This does not present a problem for the SAR because it can sense at night. However, the Visible and IR scanner has only limited capabilities.

Counteracting the precession with thrusters so MEDSAT would be able to sense at the same time of day on every pass was also considered. However, because of the low altitude and low inclination of the orbit, this would require large daily burns which are beyond the capability of a small satellite.

The problem was minimized by arranging the ground track so that the satellite will pass over Chiapas twice a day, once on the ascending node and once on the descending node. This will allow at least one of the passes to be in the daylight most of the time. This is discussed in greater detail in section 7.7 when the ground track is presented.

## 7.6    Lifetime

One of the major effects on a low earth orbit satellite during its mission is atmospheric drag. The density of the atmosphere at low orbital altitudes is quite small , on the order of $10^{-12}$ kg/m$^3$. However, this is still large enough to perturb the satellite over time.

### 7.6.1    Unassisted Lifetime

The drag force acts in the opposite direction of the motion of the satellite and gradually lowers the satellite's altitude by decreasing its energy. As the energy decreases, the altitude will decrease and the orbit will decay until the satellite eventually reenters the atmosphere and burns up. This drag force depends on the coefficient of drag, $C_D$, which is a function of the size, shape and material of the satellite. The mass of the satellite and the density of the atmosphere also affect the drag. The size affects how many molecules hit the satellite and thus cause drag. The shape and material affect the drag coefficient which in turn

affects the drag. The mass affects the inertia of the satellite which determines how much relative force the molecules will impart on the spacecraft. Finally, the density determines how many molecules hit the satellite.

The density is the major effect on the drag. At lower altitudes the density of the atmosphere is higher and the orbit will decay faster. Thus, to obtain a given lifetime, there is a lower limit on the altitude into which the satellite can be inserted.

Equation 7-3 [7-3] gives the amount of time it will take the satellite to descend from one altitude to another altitude.

$$\frac{C_D A}{m} T_{1-2} = 1.493 \times 10^{-10} \frac{h_{sc}}{R_0} \left[ \frac{1}{\rho_1} - \frac{1}{\rho_2} \right] \qquad (7\text{-}3)$$

where:

$C_D$ = drag coefficient = 1.0

A = frontal area of satellite = 2.5 m$^2$

m = mass of satellite = 300 kg

$T_{1-2}$ = time to decay from higher altitude, 1, to lower altitude, 2 in days

$h_{sc}$ = scale height = 550 km

$R_0$ = earth's radius = 6375 km

$\rho_1$ = density at higher altitude = 2 x 10$^{-12}$ kg/m$^3$

$\rho_2$ = density at lower altitude = 2 x 10$^{-11}$ kg/m$^3$

The drag coefficient is determined by the shape and material of the spacecraft and is generally accepted to be approximately 1.0. The frontal area is the projected area in the direction of motion of the satellite. For MEDSAT, this was calculated to be an average of 2.5 m$^2$ over the course of the orbit. $h_{sc}$ is a scale height, dependent on the altitude. The lifetime was determined by finding the time for the orbit to degrade from its original orbit of 477 km to 300 km. At the lower altitude, the satellite will no longer be in a useful orbit. The densities were determined from the NASA nominal density model [7-3]. Using a mass for the satellite of 300 kg, a unity drag coefficient, the respective densities for 477 km and 300 km and a scale height of 550 km, the lifetime for the satellite was determined to be 1.92 years.

This is significantly shorter than the four year lifetime required for the mission. To prolong the lifetime, the satellite could be inserted into a higher altitude. However, in order to keep a repeatable ground track, the next higher orbit would have to have a period to match fourteen revolutions per day . This altitude was found to be 795 km (431 nm). From Figure 7.2, this corresponds to a payload of only 250 kg (550 lb). This was insufficient to accommodate the scientific payload and the satellite's support systems.

## 7.6.2    Thrusters

So, instead thrusters will be employed to occasionally boost the satellite and offset the drag. This will be accomplished through a Hohmann transfer maneuver consisting of two burns, one to transfer to the higher orbit and one to recircularize the orbit. This is the lowest energy transfer maneuver and will consume the least amount of fuel. These maneuvers will use the same thrusters that are used for attitude control. So, the only additional mass is the fuel necessary to perform the maneuvers. The fuel mass, found to be

only 8.0 kg, is more than offset by the added payload of 90 kg gained over using the 14 revolutions per day orbit.

The first step in analyzing this problem involves determining how often to perform the maneuvers. This depends on how sensitive the SAR and IR sensors are to altitude changes, how exact the ground track must remain and how much acceleration the spacecraft can take. Various possibilities were studied and a tolerance of ±2 km was decided upon. So, after the satellite decays from its optimal altitude of 477 km down to 475 km, it will be boosted up to 479 km.

### 7.6.2.1 Hohmann Transfer Maneuver

A Hohmann transfer maneuver will be employed to change the satellite's altitude. This maneuver is done by using a $\Delta V$ burn to change the orbit into an ellipse with its perigee at the altitude of the lower circular orbit. After a half of a period, the satellite reaches apogee, which is at the altitude of the higher circular orbit. At this point another $\Delta V$ burn is used to recircularize the orbit. The amount of $\Delta V$ for each burn which is required for a Hohmann transfer maneuver of small altitude changes is calculated from Equation 7-4 [7-3].

$$\Delta V = \frac{1}{4}\sqrt{\frac{\mu}{r}}\frac{1}{r}\Delta h \tag{7-4}$$

where:

$\Delta V$ = change in velocity required

$\mu$ = gravitational constant = $3.986 \times 10^5$

r = radius of orbit = 6852 km for MEDSAT

$\Delta h$ = altitude change desired = 4 km

For this case, the $\Delta V$ per burn is 0.557 m/s. The total $\Delta V$ per maneuver is twice this amount.

To find the total $\Delta V$ needed for the four year mission, the number of times the maneuver must be performed was calculated. The rate of decay of the orbit is calculated from Equation 7-5 [7-3].

$$\Delta r = 9.58 \times 10^4 \frac{C_D A}{m} g_0 \rho r^2 \tag{7-5}$$

where:

$\Delta r$ = rate of decay in km/day

$C_D$ = drag coefficient = 1.0

A = frontal area = 2.5 m$^2$

m = satellite mass = 300 kg

$g_0$ = gravitational acceleration = 9.8 m/s$^2$

$\rho$ = atmospheric density = $2 \times 10^{-12}$ kg/m$^3$

r = radius of orbit = 6852 km

For MEDSAT, this value is 0.0735 km/day. Therefore, the maneuver must be done every 54 days. Over the four year mission, this will entail a total of 27 maneuvers and a total $\Delta V$ of 59.7 m/s.

### 7.6.2.2    Fuel

A special hydrazine blend fuel (which is detailed in Chapter 9) will be used to perform these maneuvers. The amount of fuel required is found from Equation 7-6 [7-4].

$$M_{fuel} = M_{initial} \left[ 1 - e^{-\Delta V/g_0 I_{sp}} \right] \qquad (7\text{-}6)$$

where:

$M_{fuel}$ = fuel mass in kg

$M_{initial}$ = initial mass of satellite including fuel in kg

$\Delta V$ = total velocity change for mission in m/s

$I_{sp}$ = specific impulse = 252 seconds for hydrazine blend

This yields a value 7.17 kg of fuel to offset the drag. There will be four 0.68 Newton hydrazine thrusters used in the $\Delta V$ maneuvers. These thrusters will also be used for attitude control maneuvers. Two thrusters will be placed on the bottom of the satellite (relative to the earth) and will burn in the direction of motion. One thruster on the top will be inclined at 20 degrees above the direction of motion so that the exhaust avoids hitting the SAR antenna. Another thruster will be placed on the bottom perpendicular to the direction of motion to offset the component of thrust on the 20 degree inclined thruster which is orthogonal to the direction of motion.

The perpendicular thruster will be regulated through valves to offset the 20 degree thruster's force. This perpendicular thruster will produce 0.23 N of thrust burning the same amount of time as the other thrusters. This will require an additional 0.83 kg of fuel over the four year mission. A summary of the fuel requirements for the mission analysis group is shown in Figure 7.4

| Orbit Correction | |
|---|---|
| Altitude | 1.27 kg |
| Inclination | 3.24 kg |
| Lifetime Sustenance | |
| Delta V Burns | 7.17 kg |
| Offset Burns | 0.83 kg |
| Total Fuel Mass | 12.51 kg |

**Figure 7.4   Fuel Requirement Summary**

Each burn will last approximately 165 seconds during which no sensing or communication may occur. Since, these times are fairly short and the maneuver is done only every 54 days, there should be minimal interference with sensing or communication. The fuel system and thrusters will also be used for attitude control. These are discussed more thoroughly in the controls section, Chapter 9.

## 7.7 Ground Track

After the nominal orbit and the perturbations were calculated an accurate ground track was produced. This was done using the ORBEL program developed by Dr. Dave Gell [7-5]. This program has as inputs of the inclination angle, the location of the desired target site, and the desired altitude. It then computes the period, location of the ascending node and the location of the satellite as a function of time, taking into account the effect of the precession. The data points for 15 orbits (one day) were then plotted and overlaid on a map of the world to produce Figure 7.6. The ground track was adjusted to cover the target site twice per day, once on the ascending node and 6 hours and 40 minutes (5.5 orbits) later on the descending node.

The mission's specific target site was determined by the Ground Segment group to be a 50 km by 50 km swath of land in the southern corner of Chiapas, near Tapachula (Figure 7.5). The sensors have swaths of 250 km long by 50 km wide. On the first pass, the satellite will be moving perpendicular to the coast of Chiapas and on the second pass, the satellite will be moving parallel to the coast. On both of these passes, the spacecraft will cover the 50 km x 50 km target site. Figure 7.5 shows a close up view of Chiapas with the target site enclosed by the square.
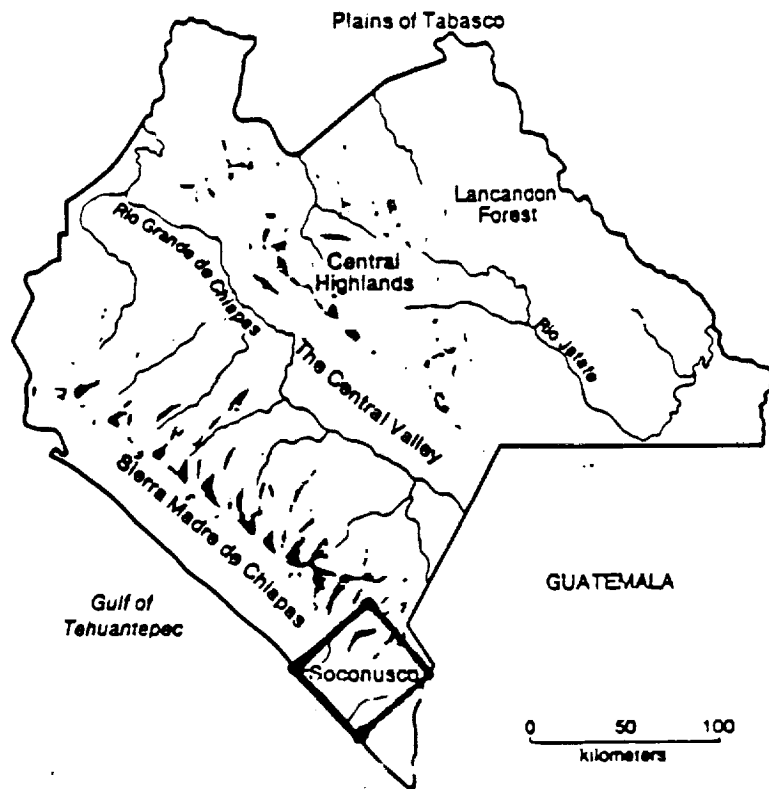


**Figure 7.5 Target Area of Chiapas**
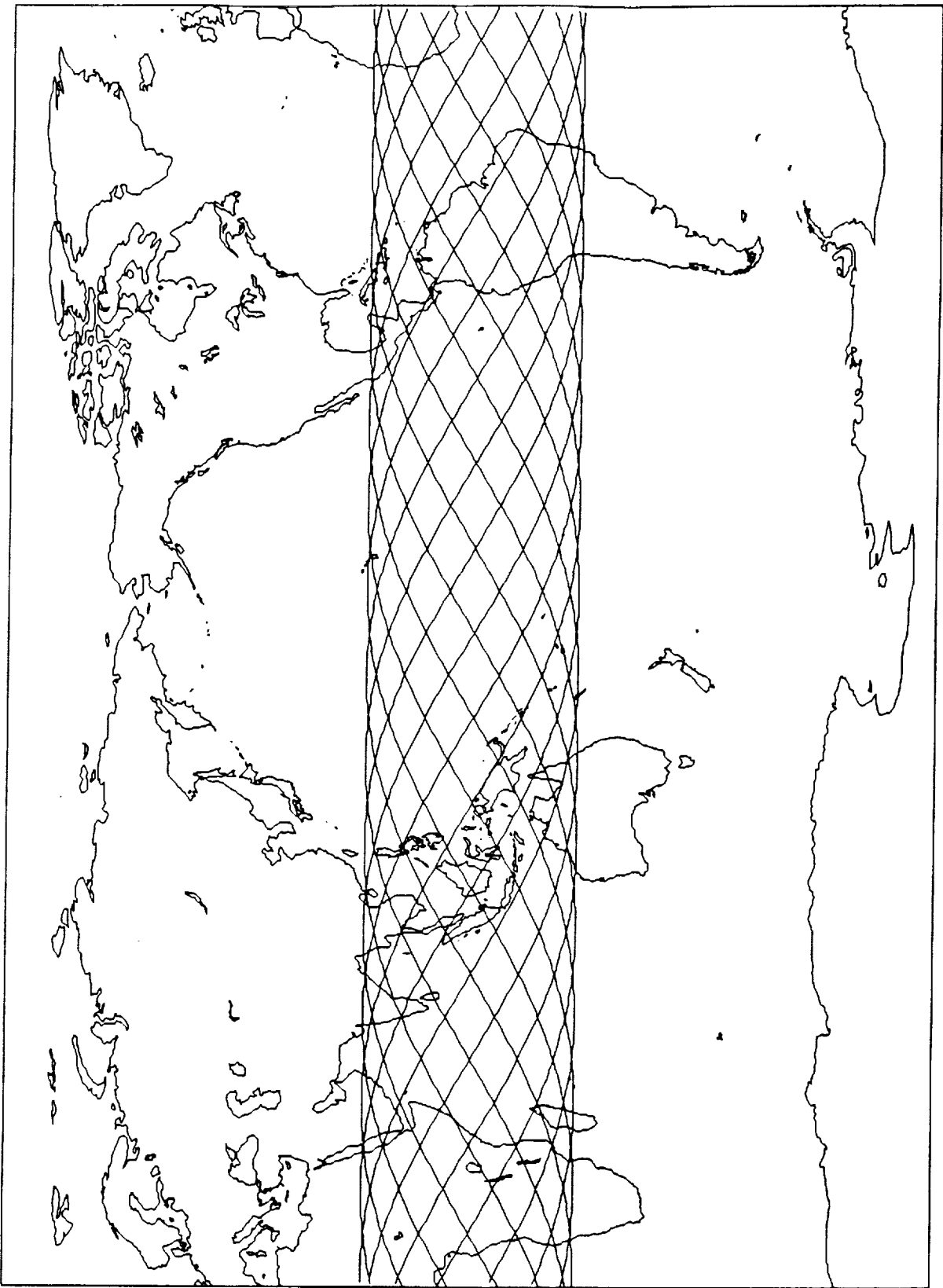
**Figure 7.6   MEDSAT Ground Track**

However, because of precession the time of day of coverage will change and each pass will have a period of several days in darkness over Chiapas limiting the usefulness of the Visible and IR scanner. The use of two passes means that sensing can be alternated between the two so that only for a few days at a time will both passes be in darkness. This will allow for the maximum benefit from the IR scanner.

The SAR needs to target the site at an angle to obtain the optimal results. An angle of 15 degrees off nadir was chosen for the SAR and IR. This offsets the ground track of the satellite from the swath which is being sensed by 1.2 degrees longitude or 125 km on the ground. This was accounted for in the ground track determination. The ascending node pass is offset to the southeast by 125 km from the target site and the descending node is offset to the southwest by 125 km. The offset can be seen in Figure 7.5.

The ground track will also cover possible groundstations such as Hawaii for downlinking. It passes over Hawaii on the fifth, sixth and seventh orbit after the ascending node sensing session. This is a viable downlink location for both the ascending node session on the first orbit and the descending node session on the fifth orbit. The time that the ground stations would be able to communicate with the satellite was determined to be at least five minutes which is sufficient to downlink the data and to uplink commands.

The ground track also offers good coverage of the equatorial regions. Since the majority of the tropical disease problem is in these areas, this will allow for the possibility of sensing over other target sites if desired.

## 7.8    Launch Window

The airborne launch of the Pegasus from beneath a B-52 offers considerable flexibility without the launch window restrictions of ground based launch facilities [7-1]. If there are poor weather conditions, the B-52 can fly over or around them and still launch. The only restriction on the launch is that it must be over open water with a clear downrange to allow for the re-entry of the first and second stages. The B-52 can be based at numerous airfields worldwide with the only limitation being the aircraft's range.

For the launch of MEDSAT the most advantageous launch site is the east coast of Florida. This will allow the Pegasus to be launched due east at 21 degrees North latitude, thus gaining the most advantage of the earth's rotation. A possible orbit in which to insert the satellite would be the orbit before the ascending node pass over Chiapas. This allows sensing one orbit after launch if desired and communication with ground stations such as Hawaii soon after launch.

To accomplish this, insertion will occur at 21 degrees North latitude and 14 degrees West longitude, just off the west coast of Africa. Insertion occurs 2200 km downrange of the launch [7-1]. So, the Pegasus will be launched due east from the B-52 at 21 degrees North latitude and 35 degrees West longitude.

The launch site is about 5000 km from where the B-52 will take off, depending on the location of the airbase. This is within the B-52's allowable range of 11000 km. A timeline of the launch sequence is shown in Figure 7.7.The recommended time of day for launch depends on the season during which the launch will occur. In general, it will be most advantageous for the satellite to have the first pass in the late afternoon or early evening, shortly before it becomes dark. This will allow a long period of sensing in the daylight on the first overpass. This means the B-52 should take off from its Florida airbase during the

| T = 0 | B-52 takes off from airbase |
| T = 5hr 43m | Launch of Pegasus |
| T = 5hr 51min | Orbital insertion completed |
| T = 7hr 12min | First pass over Chiapas |

**Figure 7.7 Possible Launch Sequence**

late-morning hours. Launch will then take place in late-afternoon local Florida time, which is mid-afternoon local Chiapas time. The first overpass, on the ascending node will occur an hour and twenty minutes later.

## 7.9 Conclusions and Future Possibilities

The orbit for the MEDSAT satellite was designed to optimally fulfill the mission requirements. It will cover Chiapas twice daily to allow almost continuous daylight sensing, thus obtaining the maximum benefit from the IR scanner. By using thrusters, the required four year lifetime is obtained. It has a low altitude to provide the best sensing and communication. The satellite will cover possible groundstations such as Hawaii several times per day to facilitate convenient communication between the satellite and the groundstation. The orbit also provides good coverage of the entire equatorial region if sensing of other sites with tropical disease problems is desired. The orbit is reachable using the Pegasus launch vehicle which eliminates the launch window restrictions of ground based launches.

During the design of the mission, several orbits were studied for their applicability to the MEDSAT project. Two were of special interest, a higher, 14 orbit/day trajectory and a sun synchronous orbit.

The first, which was also mentioned in section 7.6, involves using only 14 orbits per day. This will easily provide the four year lifetime without the use of thrusters. This will add some reliability to the mission and will eliminate logistical problems in coordinating thruster burns. The higher altitude could also allow easier attitude control because there will be less of a gravity gradient and less torque from the atmosphere. One drawback is that the resolution of the sensors would be reduced.

The second orbit considered was the use of a sun synchronous orbit. For this orbit, the precession rate of the satellite is matched to the rate of the earth's rotation with respect to the sun. Thus, the satellite would cover the target site at the same time every day. This is especially advantageous for the use of the IR scanner. The orbit could be set up so that sensing always occurs in the daylight and at an optimal time when cloud cover is less likely. One drawback of the sun synchronous orbit is that the equatorial coverage would be reduced, thus limiting the possibility of covering other sites.

However, neither of these orbits are feasible at this time because, with the current capabilities of the Pegasus, the required payload weight was too heavy. In the future, if the performance of the Pegasus is improved, these orbits may be possible and should then be investigated in detail for their applicability to this mission.

Mission Analysis

# Chapter 8

# SPACECRAFT INTEGRATION AND STRUCTURES

## 8.1 Summary

The primary responsibilities of the spacecraft integration and structures group are developing the configuration and thermally controlling the satellite. The first and most important goal is to develop both the internal and external configuration that integrates various subsystem of the satellite into a single operating system. This group is also responsible for the location of the center of gravity and keeping it within the limit of the Pegasus launch vehicle. The temperature of every component of the satellite must maintain within its operating limits.

The basic subsystems are the Synthetic Aperture Radar (SAR), Infrared sensor (IR), power system, attitude control, launch interface, and thermal control. The following are necessary considerations for the subsystems to assure the safe functioning of MEDSAT:

- Synthetic Aperture Radar
  - Antenna retracted during launch
  - Retracted subsystem support by dual shear plate
  - Support structures manufactured from aluminum
  - Dual shear plate cost justified for all electronics
- Infrared Sensor
  - IR oriented toward the Earth
  - IR thermally isolated from rest of satellite
  - Heat pipes and radiator used to cool charged couple device
- Power System
  - Solar array retracted during launch
  - Solar array design optimizes cell performance.
- Attitude Control
  - Axis located through center of gravity
  - Thruster exhaust gas directed away from the satellite and SAR
- Launch Interface
  - Adapter ring thickness minimized for location of center of gravity
  - Factor of safety of 2.0 used for the adapter ring
  - Pyrotechnics safety standards overseen to protect the manufacturer
- Thermal Control
  - Extra heat radiated to maintain components in operating temperature limits
  - Radiator surfaces shielded from sun and earth
  - Aluminum and nickel used as heat pipe materials

From a spacecraft integration standpoint of MEDSAT, the main design parameters taken into account are subsystem safety, volume, mass, and cost. There were four primary design constraints which shaped the design of the satellite. The first was the OSC/Pegasus launch vehicle which has total of 7.2 $m^3$ usable volume in its payload fairing. During launch, the satellite must fit within the dynamic envelope of the payload fairing to avoid contact with the inner wall of the payload bay. Upon reaching orbit, subsystems will deploy into their operating configurations. Second, the combination of the orbit altitude and the launch capability of the Pegasus determines the mass of MEDSAT to be 341.8 kg. Since the total mass of the satellite is limited, the mass of each subsystem must be minimized. Third, each subsystem requires adequate safety, so the malfunction or failure of any system does not hinder the performance of the other systems. Fourth, the low cost requirement of MEDSAT dictates that each subsystem be built with reasonable cost.

With the above design considerations and parameters, the final external configuration of MEDSAT main body is an octagonal cylinder attached to a conical section. The satellite

body is constructed with 8mm-thick aluminum honeycomb with two 1mm-thick aluminum face sheets. Aluminum honeycomb is chosen for its high strength-to-weight ratio. Once in orbit and separated from the Pegasus third stage, the satellite's attitude control system orients itself in which the cylindrical section pointing along the north pole axis of the earth and the conical section is pointed along the south pole axis of the earth. The SAR antenna, constructed with aluminum honeycomb and truss structures, is mounted on the north side of the satellite body while the solar array is attached to the converging conical section of the satellite facing the southern hemisphere of the earth. The communication antenna, which is constructed of graphite composite, is located on the cylindrical section of the satellite. The three radiators for the thermal control system are mounted on the converging conical section. Finally, the IR sensor utilizes a window opening positioned between the communication antenna and the SAR antenna allowing alignment with the axis of the SAR.

The remainder of this chapter discusses the system integration and structures of MEDSAT. They are divided into the following:

- Satellite configuration
- Component arrangement
- Launch interface
- Materials
- Deployment mechanisms
- Integrated Design Engineering Analysis System (I-DEAS)
- Thermal analysis

## 8.2    Satellite Configuration

The primary goal of integration is to combine every component into one single operating system while considering the design limitations. The design limitations include assembling the satellite into the Pegasus launch vehicle and integrating the scientific payloads into MEDSAT. Figure 8.1 displays the exterior shape of MEDSAT.

### 8.2.1    Integration Into Pegasus Launch Vehicle

The shape of the Pegasus payload fairing dictates a design close to a cylinder. During the design process, three body shapes were considered based on the research of existing satellites. The shapes considered were cylindrical, octagonal, and hexagonal. The octagonal body is chosen over the others for the following reasons:

- Easy to disassemble panels for access to internal components
- Efficiently utilizes the available payload bay volume
- Easy for mounting and operating of the scientific payloads
- Easy for radiator assembly
- Easy to manufacture

In order to optimize the volume available inside Pegasus, a conical section is added to utilize the converging portion of the payload fairing. The cone height is driven by the amount of volume required. Figure 8.2 displays the satellite stored inside the Pegasus payload bay.
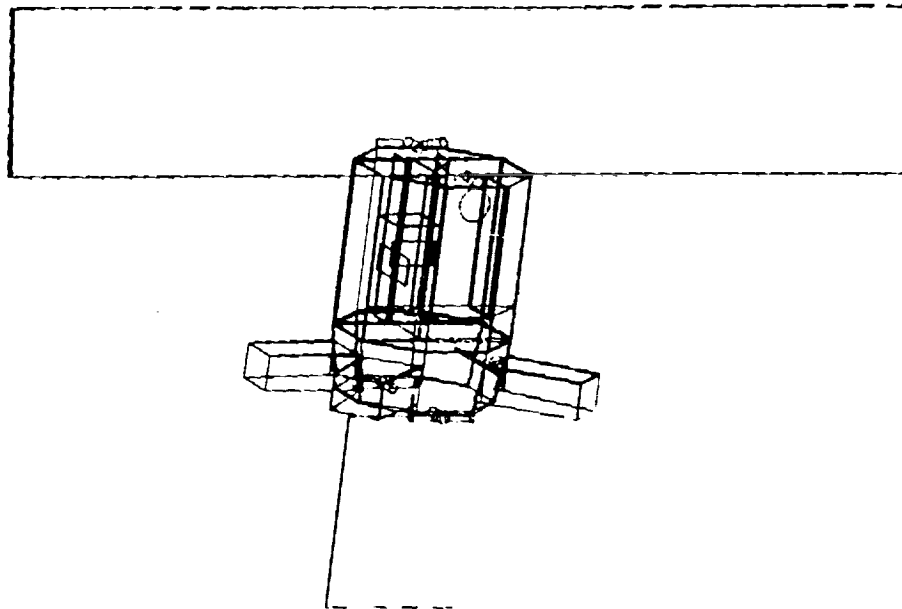
Figure 8.1    Exterior shape of MEDSAT
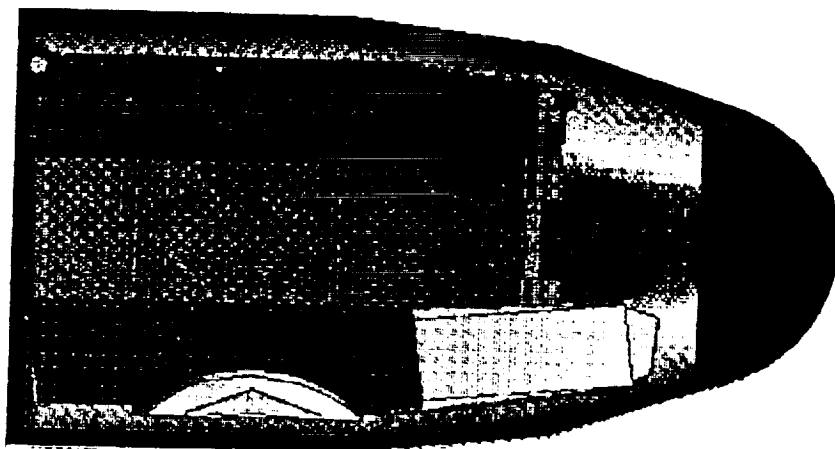


Figure 8.2    Stored Configuration inside Pegasus

### 8.2.2 Integration of Scientific Payloads into MEDSAT

The essential scientific payloads of MEDSAT are the Synthetic Aperture Radar (SAR) and the Infrared sensor (IR). The main issues of integrating these subsystems are their large weight and volume requirements. These requirements contribute to the extreme complexity of the integration tasks. Figure 8.3 shows the deployed configuration of these payloads. From the figures, it is shown that the SAR antenna and IR sensor are stored in such manner for easy deployment and proper operation.
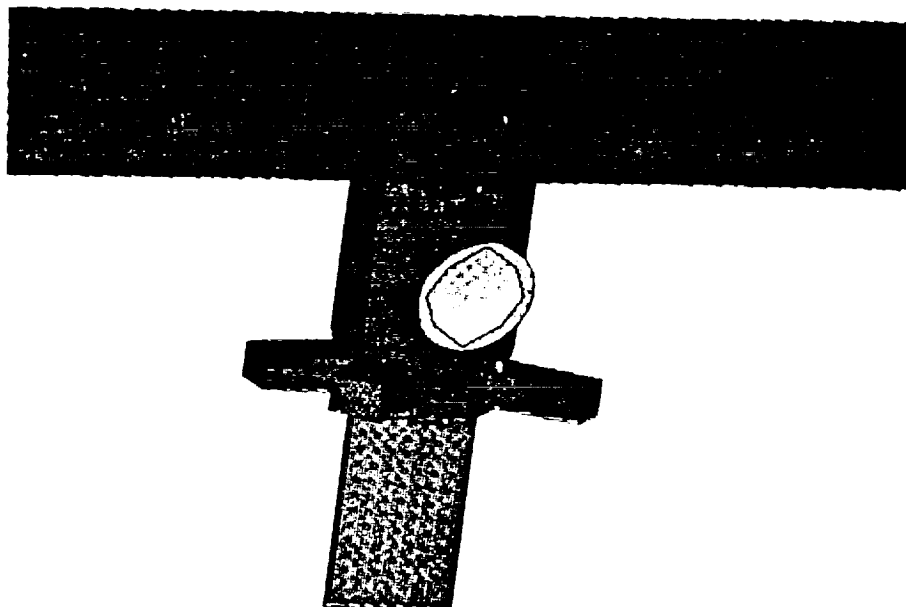


**Figure 8.3    Deployed configuration**

## 8.3    Component Integration

### 8.3.1    General Considerations

In integrating the various subsystems and components, the important considerations are the volume and mass limits and the constraint on the location of the center of gravity. Due to the small load carrying capability of the Pegasus launch vehicle, each component must be as light as possible. In addition, the limited volume of the payload bay demands an efficient packing of every component both internally and externally in the stored configuration. With the original payload interface of the Pegasus, MEDSAT must maintain its center of gravity to within 50.8 cm of the interface plane. Modifications to the third stage supporting structures can shift the center of gravity limit to 81.3 cm. The original center of gravity limit was due to the structural strength of the Pegasus third stage. An additional 1.8 kg of composite material added to the Pegasus structure would be required to raise the center of gravity limit. This is necessary to accommodate the high CG of MEDSAT. The integration analysis of the satellite was performed using the I-DEAS software on the University of Michigan Computer Aided Engineering Network (CAEN) Apollo system.

## 8.3.2 Mass and Arrangement

This section discusses the mass and the position of each subsystem within the satellite. Due to the modern technology and efficiency of the supporting subsystems, MEDSAT allows 28% of the total mass to scientific payloads. Figure 8.4 lists the weight of each subsystem.

| Systems and Components | Mass (kg) |
|---|---|
| **Primary structure** | **71.55** |
| Satellite body | 71.55 |
| **Scientific Payloads** | **121.18** |
| Synthetic Aperture Radar | 88.18 |
| Antenna | 58.18 |
| Electronics | 30.00 |
| Infrared Sensor | 33.00 |
| **Power System** | **27.35** |
| Battery | 12.75 |
| Solar array (w/ honeycomb & covers) | 8.00 |
| Solar array motor | 1.60 |
| Converter | 5.00 |
| **Attitude Sensing & Control** | **79.47** |
| Centralized logic and control unit | 3.00 |
| 3 Reaction wheels | 24.00 |
| 3 Wheel drives | 5.70 |
| 2 Trilag sensors | 1.82 |
| Sun sensor | 0.75 |
| 3 GPS systems (3 antennas and receivers) | 3.00 |
| 10 Thrusters | 3.20 |
| Propellant | 35.00 |
| Propellant Tanks | 3.00 |
| **Communication System** | **13.02** |
| Transmitter/Receiver | 2.00 |
| Feed | 1.00 |
| 2 Transponders | 8.90 |
| Diplexer | 1.12 |
| **Command & Data Handling** | **10.45** |
| Integrated circuit boards | 2.27 |
| Optical storage device | 8.18 |
| **Launch Interface** | **9.77** |
| Adapter | 9.77 |
| **Thermal Control System** | **8.99** |
| Heat pipes | 1.34 |
| 3 Radiators | 7.65 |
| **Stored Configuration** | **341.78** |
| **Deployed Configuration** | **332.01** |

**Figure 8.4    Component and subsystem Mass**

## 8.3.2.1    Synthetic Aperture Radar

The Synthetic Aperture Radar (SAR) consists of an antenna with deployed dimensions 6.0x1.0x0.0254 meters and the supporting electronics. Dual shear plates are used to mount and support the equipment during launch and operation. Operation and manufacturing safety as well cost are also considered in integrating these components

During launch, the antenna is stored into a box of dimension 1.0x0.6x0.38 meters in the octagonal section of MEDSAT. When the satellite reaches the desired orbit and orientation, the SAR antenna slides out of the bottom of the satellite, unfolds its panels, and locks into a stable and rigid position facing the northern hemisphere of the earth.

Masses of the support structures for the antenna and the electronics components are reduced by the utilization of dual shear plates. The electronics are mounted on aluminum honeycomb plates that are part of the overall structures. Instead of purchasing pre-assembled hardware and mounting them onto the satellite walls, the electronic boards are individually mounted on shear plates. This packaging method saves weight and volume required which are crucial factors in the design of MEDSAT. The dual shear plates also provide a more rigid satellite structure distributing the loads. A disadvantage of using dual shear plates is the higher manufacturing cost due to the labor-intensive packaging of electronics onto the plates. The estimated cost of repackaging the electronics is approximately $5,000 which is reasonable for the weight and volume saving.

## 8.3.2.2    Infrared Sensor

The infrared sensor system (IR) contains optical lenses, visual and thermal IR detectors, readout and interface electronics, and supporting frame. The IR has the dimensions 0.25x0.25x1.0 meters. The IR is mounted on the side of the satellite facing the earth with a 20.32 cm circular window for sensing. The window opening is regulated by a shutter to avoid direct sun light. Since the IR is a passive sensing system, it does not require any a deployment mechanism. The IR requires extreme thermal isolation from the rest of the satellite due to the low operating temperature limits of the detectors. Heat pipes and radiators are used to maintain charged-couple device at 90K. The heat pipes and the thermal control system will be discussed later in this chapter.

## 8.3.2.3    Power System

The power subsystem consists of two major components: the solar array and the battery. The solar array is constructed with silicon solar cells with aluminum honeycomb backing and laminated surfaces. The honeycomb backing reduces the mass of the support structure. Driven by the power requirements of MEDSAT, the size of the solar array is one square meter in area and 1 cm thick. During launch, the solar array is folded and stored on top of the conical octagon section of the satellite. Laminating the back side of the solar array improves the radiation into space. Lamination also eliminates the need for a radiator on the non-absorbing side of the array. Furthermore, the solar array must be thermally isolated from the satellite since the array is simply a energy absorber. A logic system will be built into the solar array motor drive to control the electrical and thermal power generated from the cells. The batteries are located close to the radiators to improve the efficiency of the heat pipes. However, considerations for the location of the center of gravity also affects the batteries location.

### 8.3.2.4 Attitude Sensing and Controls

This subsystem includes three reaction wheels and drives, a trilag sensor, a sun sensor, three Global Positioning System (GPS) receivers, ten thrusters, and hydrazine propellant. One set of reaction wheel and drive is located on each of the roll, pitch, and yaw axis of the satellite. Due to the light masses of the trilag sensor and the GPS systems, the effects of these components on the location of the center of gravity are minimal, hence they are positioned where space allows. The three GPS antennas are mounted on the side of the satellite facing away from the earth to receive data from the GPS satellites in the higher earth orbits. The sun sensor is mounted on the same side of the satellite to locate the sun once a day. Four thrusters are mounted on the SAR side and six thrusters are mounted on the solar array side of the satellite. These thrusters are oriented to give control in all three axis of rotation as well as the orbit transferring maneuver. Due to the large mass of the propellant, the propellant tanks are located in the cylindrical section of the satellite to keep the center of gravity close to the interface plane.

### 8.3.2.5 Communication, Command, and Data Handling

The communication systems includes a 0.78 m diameter graphite composite transmitter/receiver (antenna), a feed, a diplexer, and two transponders. The data handling subsystem consists of an optical storage device and a set of integrated circuit boards. All of these components, except the antenna and the feed, are mounted inside the satellite. Due to the volume constraints, they are mounted on both sides of the pitch reaction wheel. During launch, the antenna is hinged at two points and wrapped around three sides of the satellite. Since the communication will be achieve directly to and from the ground stations, both the communication antenna and the feed are located on the earth side of the satellite.

### 8.3.2.6 Launch Interface

The main component of launch interface system is the adapter ring which attaches the satellite to the Pegasus vehicle. The adapter ring is an aluminum ring that holds the satellite. The separation system and the electrical interface are used to precisely separate the satellite from the launch vehicle. A more detailed discussion regarding the specific functions of the launch interface is presented later in this chapter.

### 8.3.2.7 Thermal Control

The thermal control system is used to regulate the temperature of each component. The main components that require cooling are the IR sensor and the batteries. The system includes three radiators and three heat pipes. Two radiators are used to maintain the IR charged-couple device at 90K. These radiators are located on each side of the communication antenna on the conical section, since these sides receive the least amount of solar radiation. The third radiator is used to regulate the battery and IR optical lenses. Because the radiating surface temperature of this radiator is higher, it is located on the trailing side of the satellite which receives significant amount of solar radiation. Shields are mounted on each side of the radiating surfaces to prevent absorption of solar radiation and earth albedo.

### 8.3.3    I-DEAS Solid Modeling

The I-DEAS CAD software is used to perform the solid modelling task. By using this CAD software, the design process is extremely efficient. The I-DEAS soft also outputs the physical properties of each components and the satellite as a single system. The important physical properties are the mass, the location of center of gravity, and the mass moments of inertia. A detailed discussion of I-DEAS software is presented in a later section of this chapter.

## 8.4    Launch Interface

The launch interface consists of an adapter ring, a separation system, and an electrical interface. The payload adapter is an annular ring with an outer radius of 0.20 meters, an inner radius of 0.15 meters, and a thickness of 0.07 meters. The thickness is minimized to adhere to the center of gravity restrictions for the satellite. The design is based on a six-bolt connection with compressed helical springs to prevent plastic deformation of the adapter under 2.5G lateral and 8.0G axial compressive load during the launch sequence. The resulting mass for the adapter ring is 9.77 kg.

When the satellite is attached to the Pegasus launch vehicle, it behaves like a cantilever beam. This beam is supported by carbon graphite structures inside the third stage. The center of gravity (CG) limits are enforced due to the strength of this structure. The CG limits for MEDSAT is extended by reinforcing this graphite structure with the addition of fifty layers of carbon graphite. These carbon graphite layers weighs 1.82kg which is considered as part of the MEDSAT total weight. The original total weight of MEDSAT was 343.6kg, and after the addition of the graphite layers, the total weight becomes 341.8kg.

Another part of the launch interface is the separation system. With the use of pyrotechnics, an actuated latch separates the satellite from the Pegasus launch vehicle. Once the Pegasus launch vehicle reaches the end of its third stage burn, bolt-cutters shear the bolts and the satellite is pushed off the third stage. Since pyrotechnics are dangerous, special care must be taken with the separation system during assembly.

The last component of the launch interface system is the electrical interface which electrically links the launch vehicle and the satellite. A wiring harness is provided from the electrical connector to terminal points on the launcher. An electrical ground connect umbilical, a telemetering system, and a flight control system are the components of the electrical interface. The electrical interface transmits environmental and engineering data through the Pegasus launch vehicle to the ground control station. With this capability, a prelaunch checkout of the satellite can be achieved. This reduces the launch cost since the last minute checks can be performed with satellite attached to the Pegasus.

## 8.5    Materials

Light-weight materials such as magnesium, beryllium, or carbon fiber reinforced plastics have been used in previous satellite systems; however, these materials are toxic. Inhaling the dust particles of these materials is harmful to the human lungs. Although aluminum is relatively heavier, it is chosen for MEDSAT due to manufacturing safety considerations.

Specifically, aluminum honeycomb with face sheets is used for its high shear stiffness and low mass density. Shear plates are assembled to support the internal components and to increase the structural stiffness of the satellite body.

## 8.6 Deployment Mechanisms

There are three subsystems that require deployment mechanisms, the solar array, the communication antenna, and the SAR antenna. Each of these deployment mechanisms is discussed in this section.

### 8.6.1 Solar Array

Figure 8.5 shows both the stored configuration, and Figure 8.6 shows the deployed configuration.
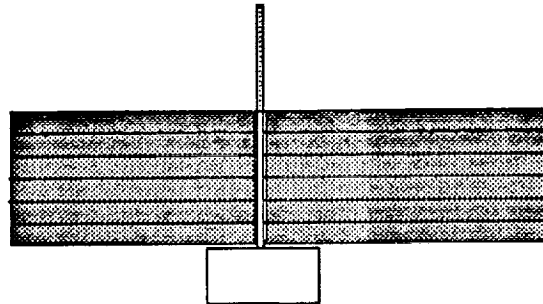


**Figure 8.5      Solar Array Stored Configuration**



Sun Synchronus Motor

6 Total Panels

.85m X 1.2m
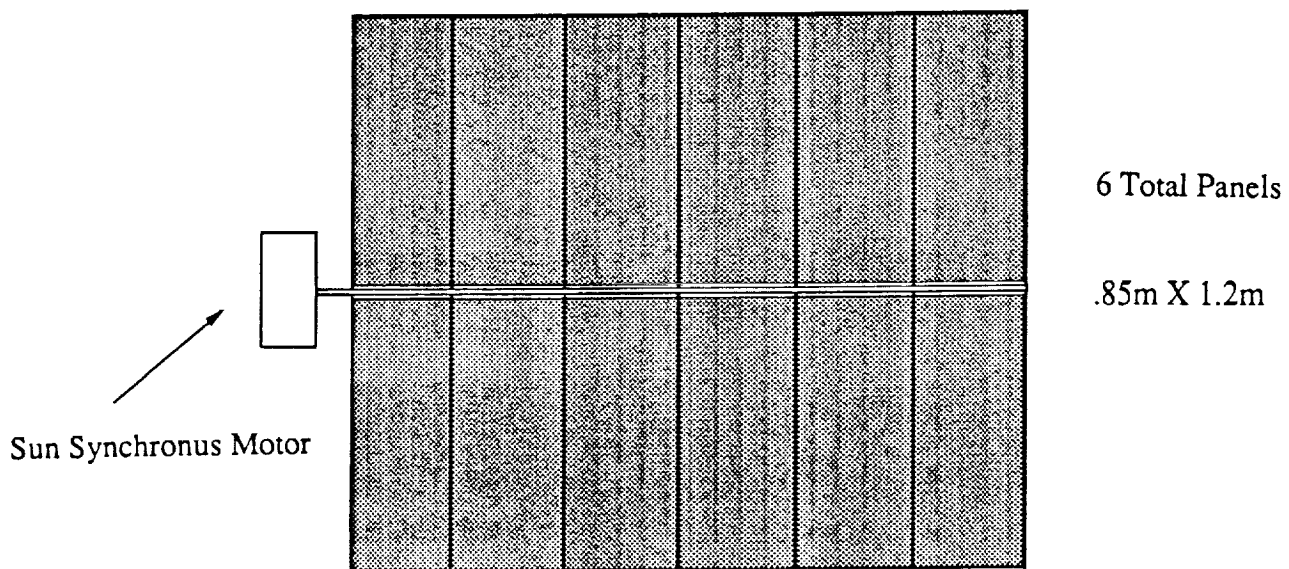
**Figure 8.6      Solar Array Deployed Configuration**

## 8.6.2 Communication Antenna

Figure 8.7 shows the deployment mechanism of the communication antenna.
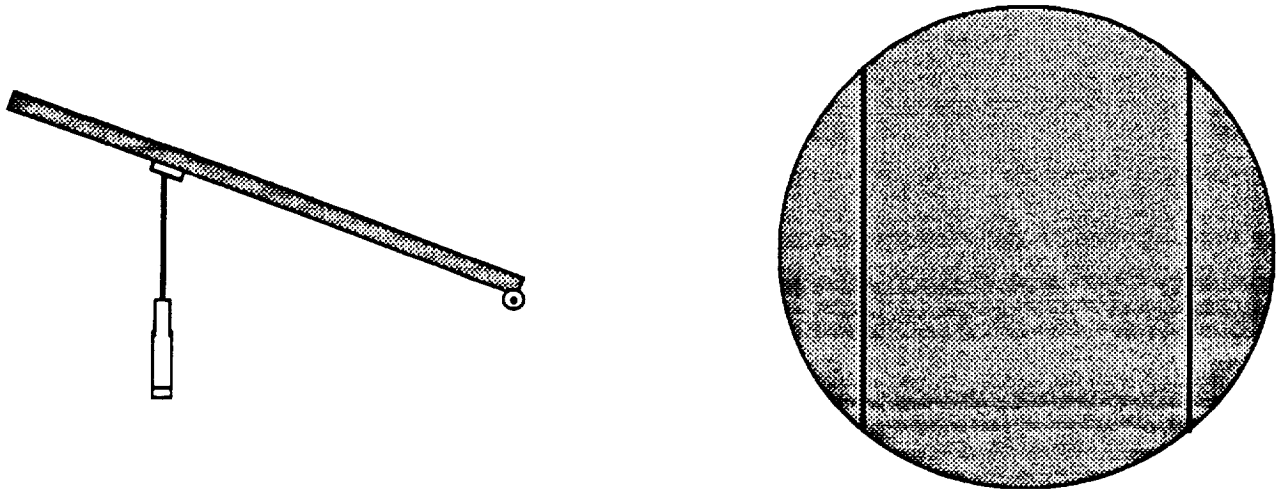


**Figure 8.7    Communications Antenna Deployment Mechanism**

The two separation joints are hinged and mounted with torsional springs. Once in orbit, the springs place the two outer sections into proper position.

## 8.6.3 SAR Antenna

Refer to Figure 8.3 for stored and deployed configuration of the SAR antenna. Figure 8.8 shows the deployment mechanism for the SAR antenna.
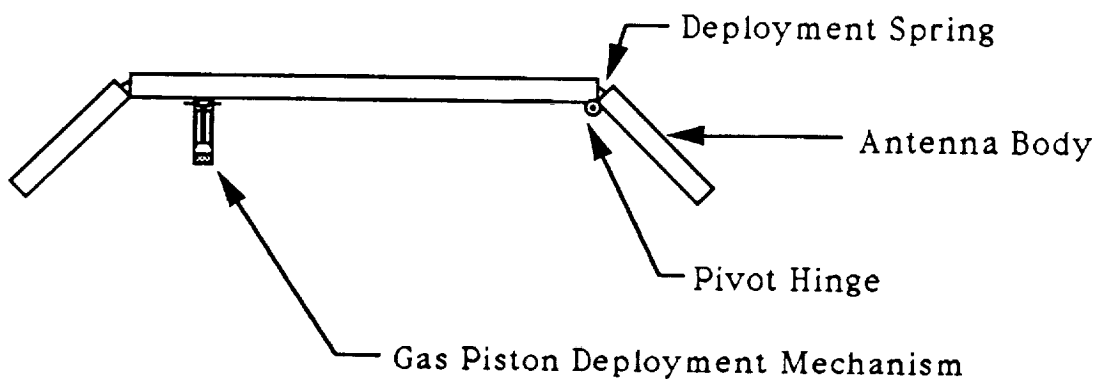


**Figure 8.8    SAR Antenna Deployment Mechanism**

## 8.7 Integrated Design Engineering Analysis System (I-DEAS)

I-DEAS (Integrated Design Engineering Analysis System) is an integrated package of mechanical engineering software tools to help facilitate a concurrent engineering approach to mechanical engineering product design. I-DEAS is made up of a number of "families" of products and functions, each subdivided into "modules", all executed from a common menu, and sharing a common database. The main families in I-DEAS areas follows:

- Solid Modeling
- Engineering Analysis
- System Dynamics
- Test Data Analysis
- Drafting
- Manufacturing

### 8.7.1 Solid Modeling

The Solid Modeling family allows one to create a geometry to represent a solid, as contrasted with surface or wire frame model programs. The geometry created can be used for mass and inertia property calculations, interference studies, finite element modeling, manufacturing, etc., as well as making engineering drawings.

There are several different methods for creating geometries. The simplest method is to use primitive shapes such as blocks, cylinders, cones and spheres. More complicated shapes can be made by extruding and revolving profiles. Even more complex sculptures surfaces can be made by skinning operation which forms surfaces between different profiles. Objects made by all of these methods can be joined or cut from each other using an object boolean operation.

Each subsystem of MEDSAT is represented by a primitive in the I-DEAS to allow for the visualization of the system interactions. Each primitive is assigned a mass density value according to its mass and volume to allow for the calculation of the satellite mass moment of inertia. From the system perspective, the Solid Modeling family provided the total mass of the satellite and the mass moment of inertia. Solid Modeling was also used to generate the shaded image of MEDSAT and MEDSAT subsystems.

## 8.8 Thermal Analysis

The thermal control problem that exists in designing the satellite is keeping each component of the satellite within its operating temperature. One difficulty for MEDSAT is that the Thermal Infrared Sensor has a Charge-Couple-Device that operates at 95K. The second problem is that there is a large discharge of heat by the batteries during the sensing time. And finally, all of the other subsystems must remain within their operating temperatures. The thermal system provided the heating, cooling, and insulation of the major components [8.1].

## 8.8.1 Component Operating Temperature Range

The major components of the satellite payload are separated into a high or a low temperature category. The IR Sensor's Charged Coupled Device (CCD) is in the low temperature category. On the other hand, the rest of the subsystems were in the high temperature category. Their temperatures varied between 285K to 318K, giving it a range of 33 degrees. The following is a table of component operating temperature ranges.

| Temperature (Kelvin) | Min | Max |
| --- | --- | --- |
| Payload | 285 | 322 |
| Telemetry and Command | 273 | 318 |
| Power Processing | 272 | 327 |
| Battery | 273 | 283 |
| Propellant Tanks | 280 | 322 |
| Infrared Electronics | 285 | 322 |
| CCD | 090 | 100 |

**Figure 8.9 Operating Temperature Ranges**

## 8.8.2 Heat Pipes

The heat pipe [8.2] is a tubular device containing an annular layer of wicking material running the length of the pipe. The core is hollow so that a working fluid may pass from the heat addition end to the heat rejection end. The heat addition end is similar to an evaporator and the heat rejection end corresponds to the condenser. Each end is connected by an insulated section. The fluid evaporates from the heat addition end, with the vapor being driven to condense (releasing its heat of vaporization) at the heat rejection end.
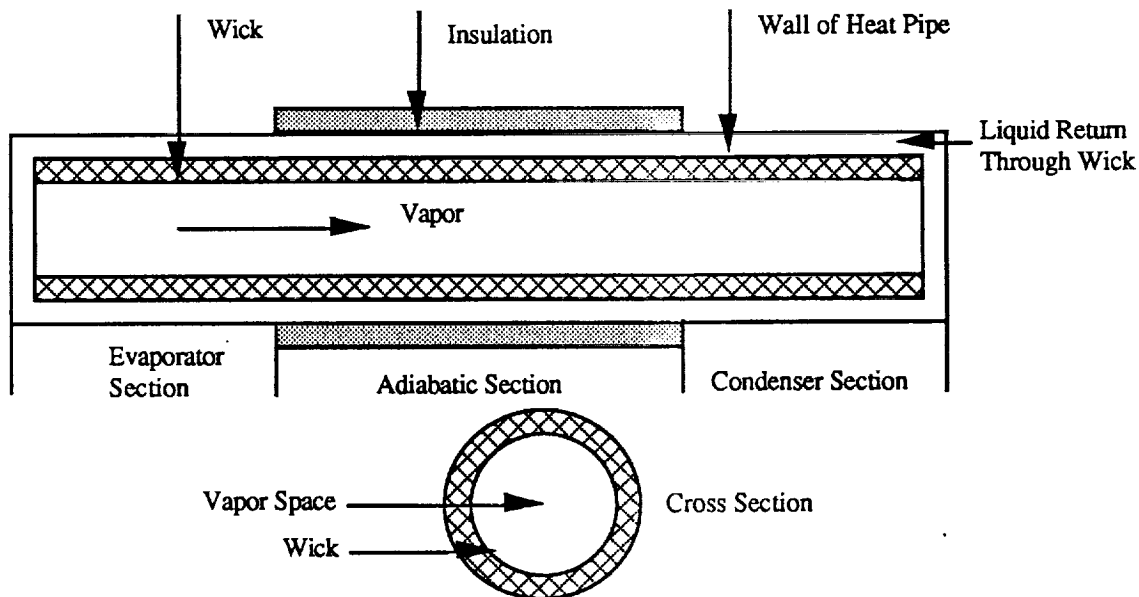


**Figure 8.10    Heat Pipe Operation**

Condensed fluid is then drawn back by capillary action through the wick to the heat addition end. The purpose of the heat pipe is to conduct energy when there is a temperature differential and cease to conduct when the differential disappears. Figure 8.10 shows the schematics of the heat pipe operation.

### 8.8.3    IR Cooling

First, the Infrared Thermal Sensor requires cooling of the Charge-Coupled Device (CCD) down to 95K. Part of the solution is to thermally isolate the area around the sensor by wrapping it with insulation. In addition, there needs to be a constant heat flux out of the sensor due to heat transfer into the system. Heat pipes and radiators cools the sensor by conduction of heat through the heat pipes and radiation of heat off of the radiators. An initial heat flux figure of 1.5 Watts was given as the amount of heat that the CCD chips produced during operation. With a factor of safety of 1.5, the following design is for two heat pipes that are able to dissipate 2.25 Watts of heat. Both heat pipes are connected to the CCD and are routed to a different deep space radiator.

For the CCD operating temperature range of 90-100K, nitrogen is the only choice of a working substance. All thermodynamic variables were for nitrogen at 93K. For the choice of wick materials and mesh size, three layers of titanium 250 mesh and three layers of nickel 100 mesh were chosen. It has been discovered that by combining materials, the maximum heat transfer increases. This is because a highly permeable but large capillary pore radius can be combined with a moderately permeable and small pore radius. Therefore, the combination of a highly permeable and small pore radius is the desired combination. The bore diameter of the heat pipes is 0.01 meter. The effective length of the heat pipes is dictated by the distance between the CCD device and the deep space radiator which is 0.224 meters. Figure 8.11 shows the relative placement of the low temperature radiators and the IR sensor.

The maximum heat transport capability is bound by wicking limitations and is in the form of the following expression [8.3]:

$$Q_{max} = 2*(\rho_1 *\sigma_1*L/ \mu_1)*(A_w*K_w/l_{eff})*(2/r_c) = \qquad 2.250 \qquad \text{Watts}$$

| | | | | |
|---|---|---|---|---|
| $\rho_1$ | = liquid density | = | 7.320E+2 | kg/m$^3$ |
| $\sigma_1$ | = surface tension | = | 0.561E-2 | N/m |
| L | = enthalpy of vaporization of liquid | = | 1.737E+5 | J/Kg |
| $\mu_1$ | = liquid viscosity | = | 0.950E-3 | Ns/m$^2$ |
| $A_w$ | = wick area | = | 0.221E-4 | m$^2$ |
| $K_w$ | = wick permeability | = | 1.520E-10 | m$^2$ |
| $l_{eff}$ | = effective length | = | 0.224 | m |
| $r_c$ | = capillary pore radius | = | 0.200E-4 | m |

In order to minimize the length of the low temperature heat pipes the radiators were near the CCD in the IR Sensor. Examination of the above equation shows why this is desirable since $Q_{max} \sim 1/l_{eff}$.
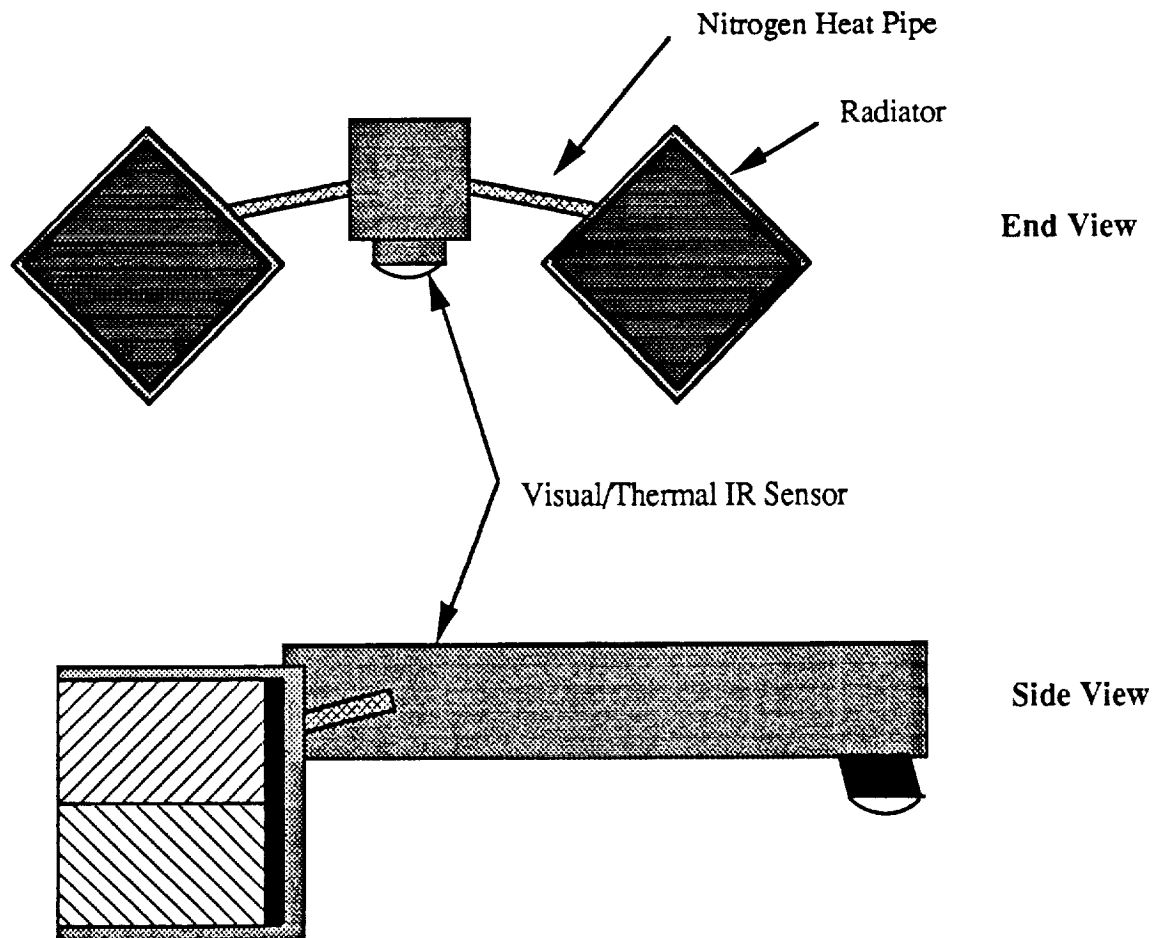
**Figure 8.11   IR Sensor and Radiator Connection**

## 8.8.4   Low Temperature Radiators

There are two deep space radiators dedicated to the CCD device. Both will be folded during the launch and be deploy when the satellite reaches orbit. As was mentioned in section 8.8.3, this location maximizes the amount of heat that can be transported as well as providing an ideal location for the storage during launch in the forward section of the Pegasus fairing. The deployed radiators will be normal to the satellite surface and point towards the south pole. Since the solar incidence angle varies with respect to the time of the year, the radiator must be shielded from both the earth and solar radiation. The solar incidence angle will be a maximum in the winter at 42° and a minimum in the summer at 2°. The solar incidence angle theta is shown in fig 8.12. The incidence of the Earth's radiation is approximately 20° as calculated from the tangent to the earth at the horizon while in a 475 km orbit. This is referred to as alpha in fig. 8.12. The heat that is radiated is calculated using the following expression [8.3].

$$Q_r = A*\varepsilon*\sigma*(T_h{}^4 - T_l{}^4) \qquad = 2.250 \quad \text{Watts}$$

$A$ = radiator surface area (2)  = 0.647  $m^2$

$\varepsilon$ = emissivity constant  = 0.935  dimensionless

$\sigma$ = Stefan-Boltzmann constant  = 5.670E-8  $\text{Watts}/(m^2*K^4)$

$T_h$ = radiator temperature            = 90.000    K
$T_l$ = deep space temperature       = 4.000     K
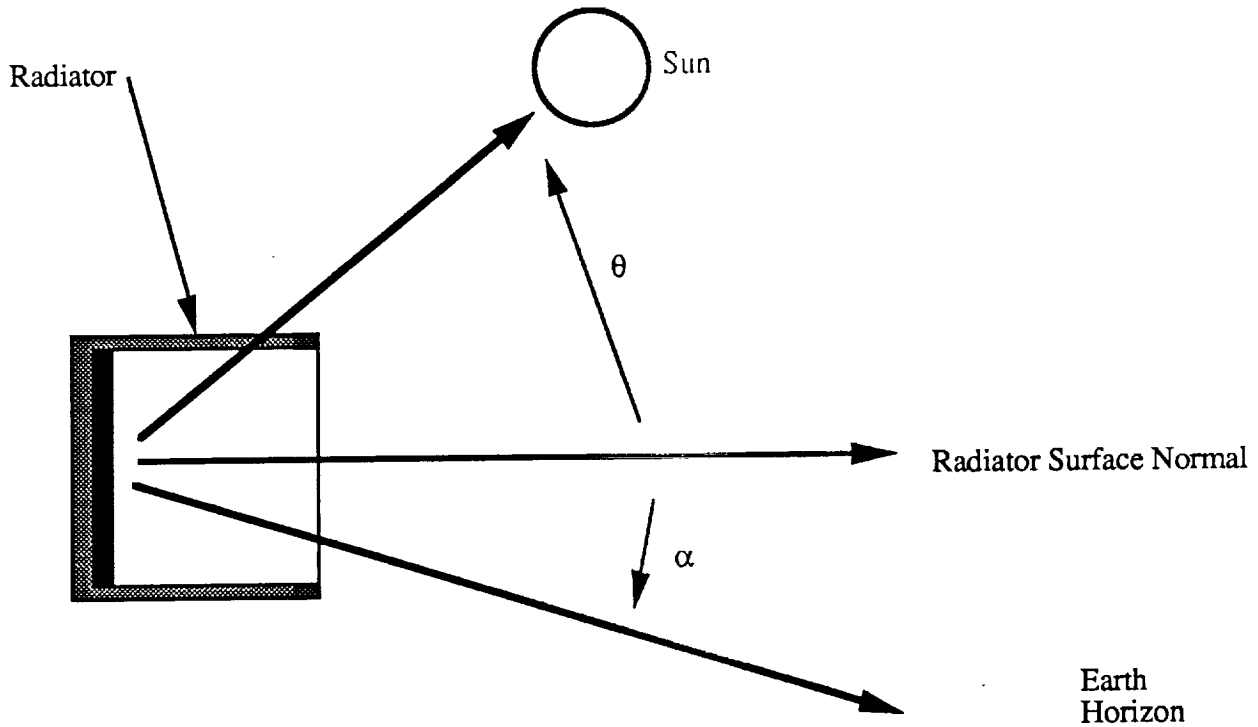


**Figure 8.12**     **Radiation Incidence Angles**

## 8.8.5   Battery Cooling

When the satellite is in the sensing mode, the batteries discharge a great amount of energy in the form of electricity and heat. Storage systems generate heat during cycling with the maximum heat load being generated during discharge. The maximum heat load is calculated using the following expression [8.3]:

$Q_l$ = P*(TN/EL-1)                      = 165.90    Watts
P   = maximum power level             = 345.60    Watts
TN  = thermo-neutral voltage           =   1.48     Volts
EL  = end-of-life cell voltage on discharge   =   1.00     Volts

The temperature of the battery will increase during discharging and decrease while charging. Since the maximum temperature change is well within the allowable temperature range, the battery will store thermal energy within itself as it cycles through its endothermal and exothermal phases. The cycling is not perfect however, and creates an increase in entropy in the system and must be accounted for. As a result each cycle needs to lose some heat through a radiator. The amount needed to be discharged is listed in the energy buildup table below. This table accounts for a worst case scenario where the SAR is sensing and the information is down-linked in the same orbit. The energy generated by the battery during the active modes is:

|  | Battery Heat Generated | Duration | Energy Buildup |
|---|---|---|---|
| Sleep Mode | 16.6 Watts | 2700 Sec. | 44.8 KJ |
| SAR Operation | 165.9 Watts | 90 Sec | 14.9 KJ |
| Info. Processing | 10.2 Watts | 600 Sec | 6.1 KJ |
| Down-link | 8.3 Watts | 300 Sec | 2.5 KJ |
| **Total** | | | 68.3 KJ |

This excess heat is dissipated through the high temperature radiator which is able to constantly radiate 55 watts into deep space. The time required to dissipate this much heat is approximately 20 minutes. The dissipation of heat due to SAR operation and down-linking will occur over several orbits.

Considering volume and mass constraints, the use of a heat pipe to conduct the excess battery heat is efficient. With a factor of safety of 1.5, the following design is for two heat pipes. Both heat pipes are connected to a single deep space radiator.

For the battery operating temperature range of 273-283 K, ammonia is the choice of the working substance. All thermodynamic variables were for ammonia at 273K. For the choice of wick materials and mesh size, two layers of titanium 250 mesh and two layers of nickel 100 mesh were chosen. The bore diameter of the heat pipe is 0.01 meter. The effective length of the heat pipes is dictated by the distance between the battery and the deep space radiator which is 1.2 meters.

The maximum heat transport capability of the ammonia heat pipes is in the form of the following expression [8.3]:

$$Q_{max} = 2*(\rho_l * \sigma_l * L / \mu_l)*(A_w * K_w / l_{eff})*(2/r_c) = 44.795 \quad \text{Watts}$$

| | | | | |
|---|---|---|---|---|
| $\rho_l$ | = liquid density | = | 6.386E+2 | Kg/m$^3$ |
| $\sigma_l$ | = surface tension | = | 2.480E-2 | N/m |
| L | = enthalpy of vaporization of liquid | = | 1.263E+6 | J/Kg |
| $\mu_l$ | = liquid viscosity | = | 0.250E-3 | Ns/m$^2$ |
| $A_w$ | = wick area | = | 0.221E-4 | m$^2$ |
| $K_w$ | = wick permeability | = | 1.520E-10 | m$^2$ |
| $l_{eff}$ | = effective length | = | 1.200 | m |
| $r_c$ | = capillary pore radius | = | 0.200E-4 | m |

## 8.8.6 High Temperature Radiator

There is one deep space radiator dedicated to the battery and other electronics. The radiator will be normal to the satellite surface and point towards the south pole. The radiation from the sun will be a 42 degrees measured from the tangent during the winter. The radiation from the Earth will be at 26 degrees. Therefore, the radiator must be shielded from the Earth and solar radiation. The heat that is radiated is calculated using the following expression [8.3].

| | | | | |
|---|---|---|---|---|
| $Q_r$ | = $A*\varepsilon*\sigma*(T_h^4 - T_l^4)$ | = | 55.000 | Watts |
| A | = radiator surface area | = | 0.218 | m$^2$ |
| $\varepsilon$ | = emissivity constant | = | 0.935 | unit-less |

$\sigma$ = Stefan-Boltzmann constant $\quad = 5.670E-8 \quad$ Watts/(m$^2$*K$^4$)
$T_h$ = radiator temperature $\quad\quad\quad\quad = 263.000 \quad$ K
$T_l$ = deep space temperature $\quad\quad = 4.000 \quad$ K

The location of the high temperature radiator was driven by the location of the major heat sources. It is located between the batteries and the electronics packages which are located at opposite ends of the satellite and produce the majority of the heat.
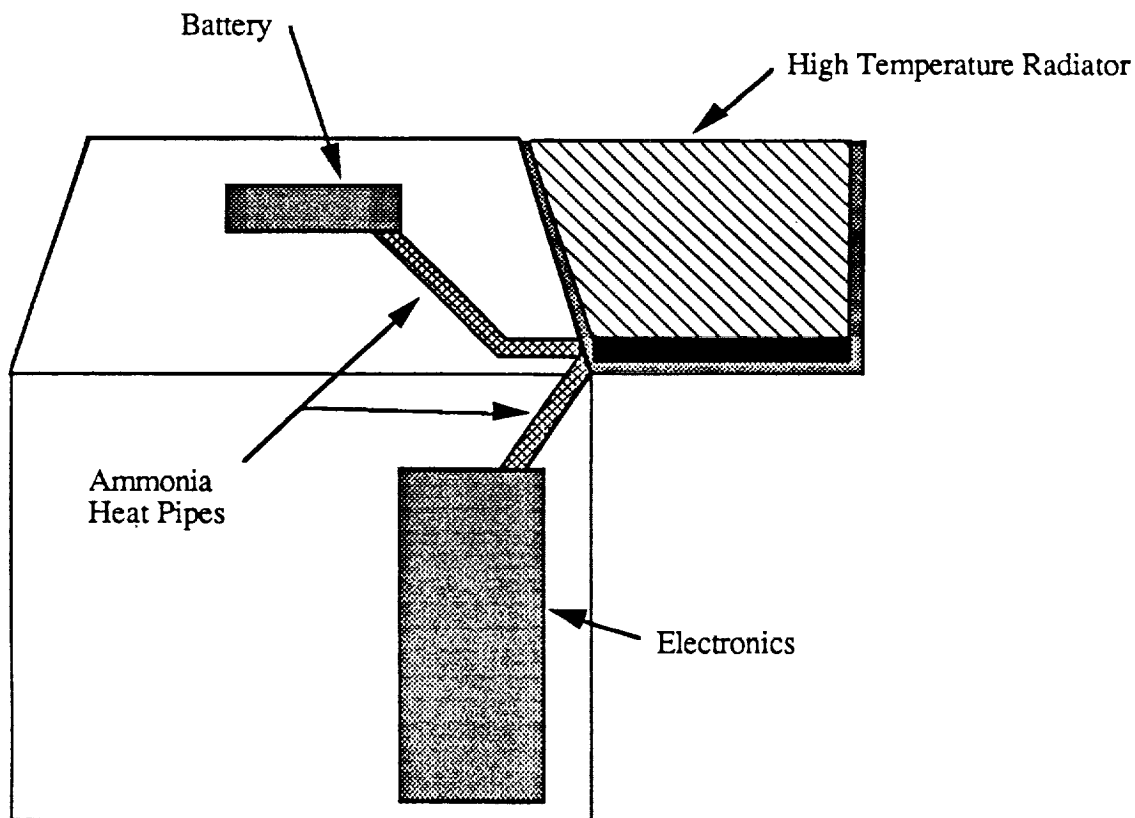


**Figure 8.13    High Temperature Radiator Location**

## 8.8.7    Satellite Insulation

The insulation shielding the components in the interior of the spacecraft from the temperature extremes generated on the outer wall of the spacecraft is aluminum Kapton. The insulation consists of a 1 cm thick blanket made up of 30 separate layers of Kapton. Each layer has a 6.35 micrometer layer of aluminum. The blanket construction is such that wrinkles in the layers hold the adjacent layers apart, minimizing the area of contact between the layers. This reduces the surface area acting as a conduction path across the entire blanket. Because the aluminum is highly reflective it also stops radiative heat transfer as well. The resulting coefficient of conductivity for the blanket is 0.00029 Watts/Meter-Kelvin. Figure 8.14 shows the Kapton blanket design and the heat transfer process.

+Q (May be Positive or Negative)

T external

Kapton Blanket

T internal

T external > T internal => +Q
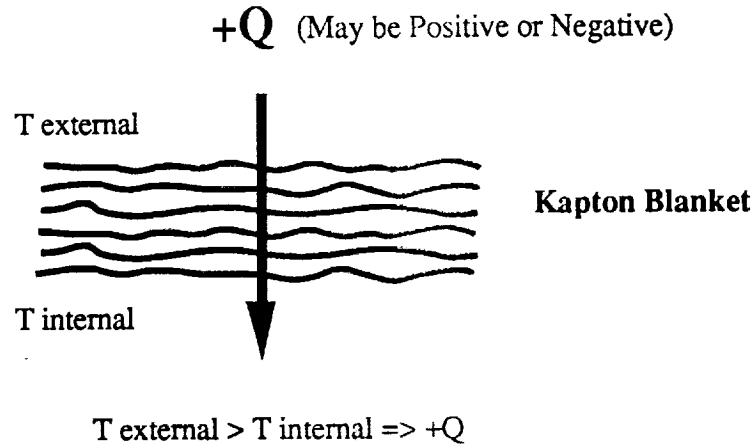
**Figure 8.14     Kapton insulation blanket**

Satellite insulation is in the form of Aluminum Kapton. Total Mass: 3.06 Kg.

In order to solve the insulation problem it was necessary to find the external temperatures of the satellite. The surface temperature of the satellite was predicted using a spreadsheet to find the transient temperature response of the panels. The temperatures were calculated using conduction, radiation, and absorption properties for unpolished aluminum. The
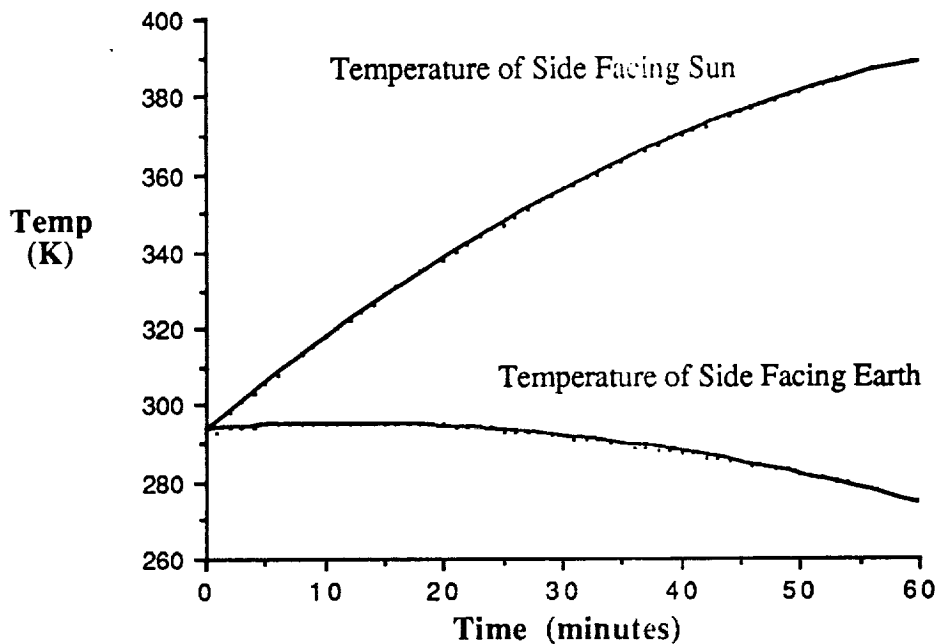


**Figure 8.15     Satellite External Temperature Transient Response**

results in figure 8.15 show the maximum and minimum temperature curves in the sunlit portion of the orbit. From the spreadsheet were able to find the maximum and minimum temperature that the satellite would experience throughout it's entire orbit.

The spreadsheet incorporated the conduction and radiation problem to find the transient response. The equations used in the balance and flow of heat are listed below [8.2].

Conduction Equation:
$Q = k * A/(DT/DX)$
$A$ = Conducting Cross Section Area
$k$ = Conduction Coefficient
$\Delta T$ = Temperature Gradient
$\Delta X$ = Distance Between Panels

Blackbody Radiation Equation:

| | | | | | |
|---|---|---|---|---|---|
| $Q_r$ | = | $A*\varepsilon*\sigma*(T_h^4 - T_l^4)$ | = | | Watts |
| $A$ | = | Surface area | | | |
| $\varepsilon$ | = | Emissivity constant | = | 0.02 | dimensionless |
| $\sigma$ | = | Stefan-Boltzmann constant | = | 5.670E-8 | Watts/(m$^2$*K$^4$) |
| $T_h$ | = | Surface temperature | = | 263.000 | K |
| $T_l$ | = | Deep space temperature | = | 4.000 | K |

Absorption Equation:
$Q = A*\alpha*\Sigma P*\cos\theta$

| | | | | | |
|---|---|---|---|---|---|
| $\alpha$ | = | Absorption coefficient | = | 0.20 | |
| $A$ | = | Surface area | = | 8.0 | m$^2$ |
| $P_{sun}$ | = | Solar radiated power density | = | 1353.0 | W/m$^2$ |
| $P_{earth}$ | = | Earth albedo power density | = | 290.0 | W/m$^2$ |
| $P_{IR}$ | = | Earth IR power density | = | 260.0 | W/m$^2$ |
| $\theta$ | = | Solar angle of incidence | = | 0° | Summer |
| | | | | 42° | Winter |
| $\sigma$ | = | Stefan-Boltzmann constant | = | 5.670E-8 | W/(m$^2$*K$^4$) |

Temperature Equation:
$T = E/(CpM)$
$E$ = Energy in Panel
$M$ = Mass of Panel
$Cp$ = Heat Capacity of Aluminum = 896 J/kg K

T max = 380 K
T min = 240 K

The spreadsheet calculated the energy absorbed by the panel from the sun and the earth. The new energy level in the panel set a new temperature from which the panel radiated energy by black body radiation. The temperature rise creates a gradient between the panel and the two neigboring panels. From this the energy conducts into or out of the panel based

upon the value of the gradient. All of these factors contribute to a net change in the energy in the panel and thus a change in temperature. The new temperature then becomes the initial temperature for the next iteration and the process begins again. The process reapeated for the time duration of a sunlit or dark period.

During the portion of the orbit when the satellite is behind the earth the exterior of the satellite begins to cool. The temperature of the side of the satellite facing earth drops and the surface becomes a radiator. The side facing away from earth does not reach as low of a temperature and thus is neglected for this part of the analysis. The heat loss due to this temperature gradient is given in the following expression.

$$Q_k = k*A/D*(T_o-T_i) \qquad = \quad 5.0 \qquad \text{Watts}$$

| | | | | | |
|---|---|---|---|---|---|
| $k$ | = | conductivity coefficient | = | 0.00029 | W/mK |
| $A$ | = | 0.5*Surface Area of satellite | = | 4.0 | $m^2$ |
| $D$ | = | Distance across insulation | = | 0.01 | m |
| $T_i$ | = | Inner wall temperature | = | 273.0 | K |
| $T_o$ | = | Outer wall temperature | = | 230.0 | K |

This energy loss is balanced by the addition of energy provided by heaters drawing energy from the battery.

A similar problem exists when the satellite passes through the sunlit portion of the orbit. The difference in the analysis is that the temperature of the Earth-side panels increases to approximately the temperature of the interior components. In addition, the sunlit panels increase in temperature and begin conducting heat through the insulation to the interior. Therefore, the temperature of the interior of the satellite increases. The heat added to the satellite is in the following expression.

$$Q_k = k*A/D*(T_o-T_i) \qquad = \quad 11.6 \qquad \text{Watts}$$

| | | | | | |
|---|---|---|---|---|---|
| $T_i$ | = | Inner wall temperature | = | 273.0 | K |
| $T_o$ | = | Outer wall temperature | = | 380.0 | K |

### 8.8.8 Heaters

When the satellite passes into the Earth's shadow, the solar energy that has collected on the outer walls begins to radiate away. As the outer surface temperature of the satellite drops below 273 K, the thermal energy in the satellite radiates to space. The Kapton insulation slows this process, but when the payload temperature decreases to a certain point, the heaters turn on to keep the payload within its operating temperature. The amount of power needed for the heater is given in the expression below [8.2].

$$P_h = q_k/\eta_h \qquad = \quad 6.25 \qquad \text{Watts}$$

| | | | | | |
|---|---|---|---|---|---|
| $q_k$ | = | Thermal heat escaping | = | 5.0 | Watts |
| $\eta_h$ | = | Heater efficiency | = | 0.8 | |

### 8.8.9 Solar Array Thermal Analysis

The temperature of the solar array must be analyzed since the performance of solar cells degrades at high temperatures. In order to estimate their performance, their thermal cycle must be examined. Since the panel orientation to the sun changes with respect to the time of year an analysis has been done at the two orientation extremes. Since the panel is of a low mass and is solar tracking it is assumed that a steady state analysis represents the cell temperature during operation. Since the solar array is attached to the satellite by a thin shaft. The system is thermally isolated from the rest of the satellite so that the heat will not conduct to the satellite's payload. To minimize the temperature the solar array operates at, the back side will be painted black. The steady state temperature analysis for the summer orbit inclination is shown below [8.3].

$$T = \left[ \frac{A(\alpha_{sc}*\cos\theta*P_{sun} + \alpha_{wp}(P_{earth} + P_{IR}))}{A\sigma(\varepsilon_{wp} + \varepsilon_{sc})} \right]^{\frac{1}{4}}$$

$T_{summer}$ = 354 K = 82 °C
$T_{winter}$ = 327 K = 45 °C

| | | | | |
|---|---|---|---|---|
| $\varepsilon_{sc}$ | = | Solar cell emittance | = | 0.8 |
| $\alpha_{sc}$ | = | Solar cell absorption | = | 0.86 |
| $\varepsilon_{wp}$ | = | Black paint emittance | = | 0.98 |
| $\alpha_{wp}$ | = | Black paint absorption | = | 0.90 |
| A | = | Solar array area | = | 1.3 m² |
| $P_{sun}$ | = | Solar radiated power density | = | 1353.0 W/m² |
| $P_{earth}$ | = | Earth albedo power density | = | 290.0 W/m² |
| $P_{IR}$ | = | Earth IR power density | = | 260.0 W/m² |
| $\theta$ | = | Solar angle of incidence | = | 0° Summer |
| | | | | 42° Winter |
| $\sigma$ | = | Stefan-Boltzmann constant | = | 5.670E-8 W/(m²*K⁴) |

## 8.9 Conclusion

This chapter has described the primary goals and tasks of the spacecraft integration and structures group which are:

- Satellite configuration and structures
- Satellite integration
- Thermal control
- Structural analysis

The main considerations for the design of the satellite are:

- Shape of the satellite body
- Material selection
- Satellite appendages and payloads

The design of the satellite shape is driven by three factors:

- Size and shape of Pegasus payload bay
- Scientific payloads of MEDSAT
- Attitude control system

With these design considerations, MEDSAT has the shape of an octagonal cylinder with a conical section on one end. In the deployed orbiting configuration, the solar array, attached to the conical section of the satellite, points toward the south pole, and SAR antenna is mounted on the opposite side of the satellite.

# Chapter 9

# ATTITUDE CONTROL

## 9.1 Summary

The Attitude Determination and Control System (ADCS) of the MEDSAT satellite must correctly position the satellite upon orbit insertion, maintain the nadir orientation of the spacecraft, point the scientific instruments to within 0.3° of the target, and provide a reference to keep the solar array pointed toward the sun. The ADCS will have to measure and counter disturbance torques while in orbit. For a satellite in low earth orbit, these torques will consist primarily of gravity gradient, aerodynamic drag, and solar radiation.

The ADCS of the MEDSAT satellite consists of many subsystems each with its own responsibilities. The three main jobs the system will perform are sensing changes in attitude, sensing changes in position, and correcting these changes. Accordingly, the main subsystems of the ADCS are the position sensing subsystem, the attitude sensing subsystem, and the actuator subsystem (which will correct changes in both attitude and position). The positioning subsystem will utilize the Global Positioning System (GPS). The attitude sensing subsystem will utilize an inertial measurement unit that will be referenced periodically by a sun sensor. The attitude actuator system will consist of three reaction wheels, one along each axis, and a ten thruster propulsion system. The thrusters will be used for orbit insertion, downloading momentum, providing redundancy for the reaction wheels, and performing the $\Delta V$ maneuvers necessary to prolong the lifetime of the satellite.

Figure 9.1 presents the proposed configuration of the MEDSAT satellite.
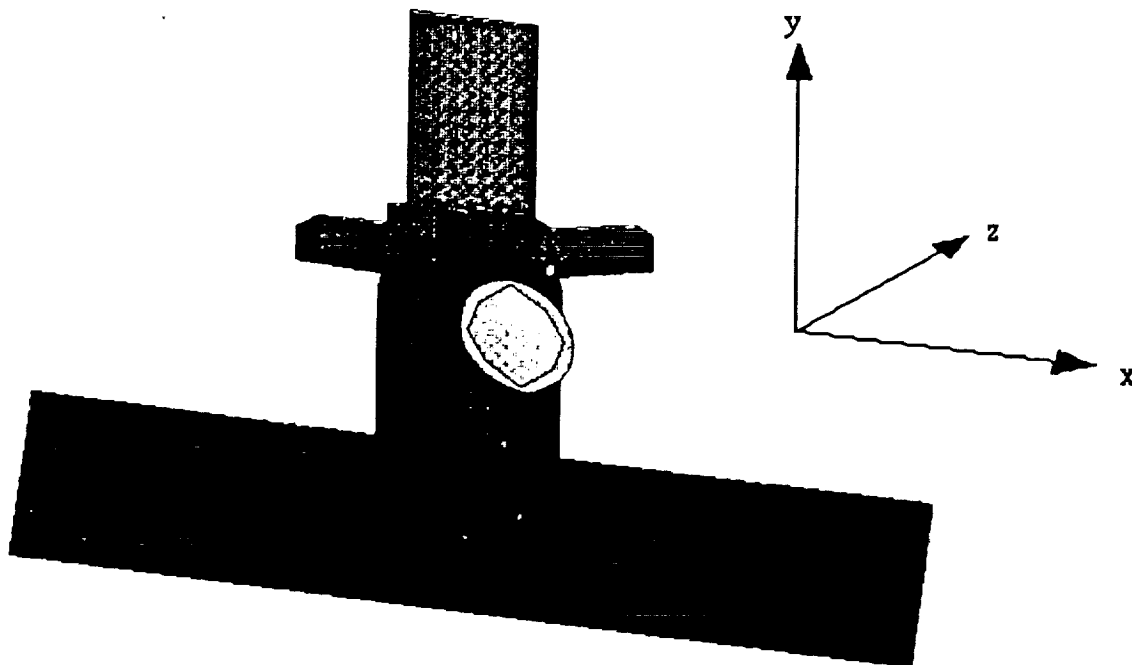


**Figure 9.1: MEDSAT Configuration in Orbit**

Attitude Control

- The z-axis points from the satellite to the center of the Earth and yaw is measured about this axis.
- The x-axis is in the direction of motion and roll is measured about this axis.
- The y-axis completes the right-handed coordinate system. It points out the solar array end of the satellite and pitch is measured about this axis.

The choice of the configuration was driven by a number of considerations. The three-axis stabilized configuration was chosen because it generally provides more stability for scientific missions. Since the satellite is carrying many scientific instruments that have to face toward the Earth, the long side of MEDSAT was placed horizontal to the plane of the ground. The satellite will rotate about the y-axis with the same rate as its revolution rate about the Earth to keep this side facing toward the ground. Another consideration was to keep the solar array out of the shadow of the SAR antenna.

## 9.2    Initial Attitude Acquisition

Because of the way MEDSAT has to be positioned inside Pegasus for launch, it will be necessary to conduct an orbit maneuver before the mission begins. The third stage of Pegasus will rotate the satellite so that the communication antenna side of the satellite is facing toward the Earth. Once the satellite has separated from the third stage, the solar aspect sensor (SAS) and the global positioning system (GPS) receiver will determine the position of the satellite in orbit. After the position of the satellite has been determined the other sensors can be referenced and the proper attitude can be acquired through a 90° rotation about the yaw axis. The reaction wheel on the pitch axis will also be started up to begin the tumbling motion of the satellite that will keep one side facing towards Earth. Further adjustments will then be made as the solar array, communications antenna, and SAR antenna are deployed.

## 9.3    Disturbance Torques

Total disturbance torques about each axis were calculated from the sum of the gravity gradient, aerodynamic drag, and solar wind torque about each axis. The total disturbance torque on the roll axis is $-2.253 \times 10^{-5}$ Nm, the total disturbance torque on the pitch axis is $-6.40 \times 10^{-6}$ Nm, and the total disturbance torque on the yaw axis is $1.797 \times 10^{-4}$ Nm. Two other torques that were not calculated were the magnetic field effect and the solar array drive torque. The electronic systems on MEDSAT will generate a magnetic field that will try to align itself with the Earth's magnetic field, generating a magnetic torque. This torque could not be calculated without a more detailed design of the installation of each of the power consuming systems. However this effect could be minimized by a proper design of the electronic components. The motor losses in the solar array drive will generate an internal torque. This torque could not be estimated without more detailed information about the specific drive to be employed.

### 9.3.1    Gravity Gradient

Gravity gradient torques arise from the gravitational attraction of the Earth applying different forces to different parts of the satellite. The gravity gradient pulls on the satellite trying to align the axis with the smallest moment of inertia of the satellite with the line to the center of the Earth. The MEDSAT configuration resulted in the unusual circumstance that

the x-axis was the axis of minimum moment of inertia, so that the gravity gradient applied a pitching torque (for most satellites of cylindrical configuration, gravity gradient tries to rotate the long axis of the cylinder toward an Earth radius). This circumstance became a problem because the short moment arm of the pitch correction made it difficult to compensate for the gravity gradient. Gravity gradient torques were calculated using the following equations [9.1]:

$$T_{xb} = (3\mu/R_o^3)(I_{zz}-I_{yy})a_{ez}a_{ey}$$
$$T_{yb} = (3\mu/R_o^3)(I_{xx}-I_{zz})a_{ex}a_{ez}$$
$$T_{zb} = (3\mu/R_o^3)(I_{yy}-I_{xx})a_{ey}a_{ex}$$

where $\mu$ is the Earth's gravitational constant, $R_o$ is the orbit radius, and $a_{ex}$, $a_{ey}$, and $a_{ez}$ are direction cosines of the angles between the spacecraft axes and a line to the center of the Earth. The direction cosines were calculated using the 0.3° accuracy our system was designed for and the rotation angles from system to principal axes. Moments of inertia,and the angles from system to principal axes were calculated on the I-DEAS solid modeling program.

## 9.3.2 Aerodynamic Drag

Aerodynamic drag is the force acting against the satellite due to the density of the atmosphere. Aerodynamic drag on a satellite is much smaller the the drag acting on something near Earth, but since all other disturbances acting on the spacecraft are also much smaller, drag has a large effect. If the satellite were symmetric about the direction of motion, the drag would not act as a torque on MEDSAT, but since the satellite has a large solar array extended out on one side, the drag acts more on that side and causes a yaw moment on the spacecraft. A pitching moment also resulted from the drag on the communications antenna. These drags had a large effect on MEDSAT because the center of gravity is not near the geometric center of the frontal area. Aerodynamic torques are calculated from the aerodynamic force and the distance the area is offset from the center of spacecraft area [9.1].

$$F_d = \tfrac{1}{2}\rho C_d AV^2 \approx \rho AV^2$$
$$T_d = L_d F_d$$

where $\rho$ is the atmospheric density, V is the spacecraft orbital velocity, A is the spacecraft area projected into a plane perpendicular to the direction of the velocity, $C_d$ is the drag coefficient (=2), and $L_d$ is the distance of center of area offset from the center of mass.

The calculations considered the solar array, the body, the SAR antenna, and the communications antenna outside of the main spacecraft area. Drag torque was calculated for the worst case condition (during sunrise and sunset when the arrays are facing bluff into the wind), but the average drag was used to calculate how long it took for the torques to saturate the reaction wheels.

### 9.3.3 Solar-radiation Torque

Solar -radiation torque arises from solar radiation pressure, which in turn arises from the transfer of linear momentum from the incident radiation as it strikes the surface of the satellite. For an Earth-oriented spacecraft, solar-radiation torque has a secular term. On MEDSAT, the solar array and the SAR antenna are absorptive, and the body is reflective. For the absorptive parts the solar-radiation pressure is collinear with the incident radiation, and for the reflective parts the solar-radiation pressure is normal to the surface [9.1]. The solar-radiation pressure is calculated normal to and in the plane of the surface.

$$P_{sn} = 4.644 \times 10^{-6}(2 - \alpha_s)\cos i$$

$$P_{sp} = 4.644 \times 10^{-6} \alpha_s \sin i$$

Where $i$ is the angle of incidence of the radiation, and $\alpha_s$ is the absorption coefficient of the surface. ($\alpha_s = 1$ for absorptive surfaces, and $\alpha_s = 0$ for reflective surfaces) Once the solar-radiation pressure on each extremity of the satellite was calculated, the solar-radiation torque was calculated from the surface area, A, the radiation pressure, $P_s$, and the moment arm from the surface to the center-of-mass of the satellite, L.

$$T_s = A(L \times P_s)$$

Solar radiation torques were once again calculated for the worst case conditions (at high noon when the Sun is directly overhead, inducing a roll, and at sunset when the back of the solar array creates a yaw torque), but only the averages were used in the time to saturation calculations.

### 9.3.4 Summary of Torques

Figure 9.2 shows the total torques acting on each axis of the satellite.

| axis | gravity gradient | aerodynamic (Nm) | solar-radiation (Nm) | total torque (Nm) |
|------|------------------|------------------|----------------------|-------------------|
| roll | $-4.03 \times 10^{-6}$ | -- | $-1.85 \times 10^{-5}$ | $-2.253 \times 10^{-5}$ |
| pitch | $-1.97 \times 10^{-5}$ | $1.33 \times 10^{-5}$ | -- | $-6.40 \times 10^{-6}$ |
| yaw | $-4.80 \times 10^{-8}$ | $1.73 \times 10^{-4}$ | $6.785 \times 10^{-6}$ | $1.797 \times 10^{-4}$ |

**Figure 9.2: Torques Affecting the Satellite Along Each Axis**

## 9.4 System Design

The main subsystems of the ADCS are the position sensor, the attitude sensor, and the attitude actuator. The data from any of these systems will go through the microprocessor to the other subsystems that rely on it. The roles of each of the subsystems in the overall ADCS system are shown in the following figure. The sun sensor is used to reference both the rate gyro and the solar array. It has been assumed that one microprocessor can conduct

all of the information transfer that will occur on the satellite. Figure 9.3 shows the flow of information throughout the satellite.
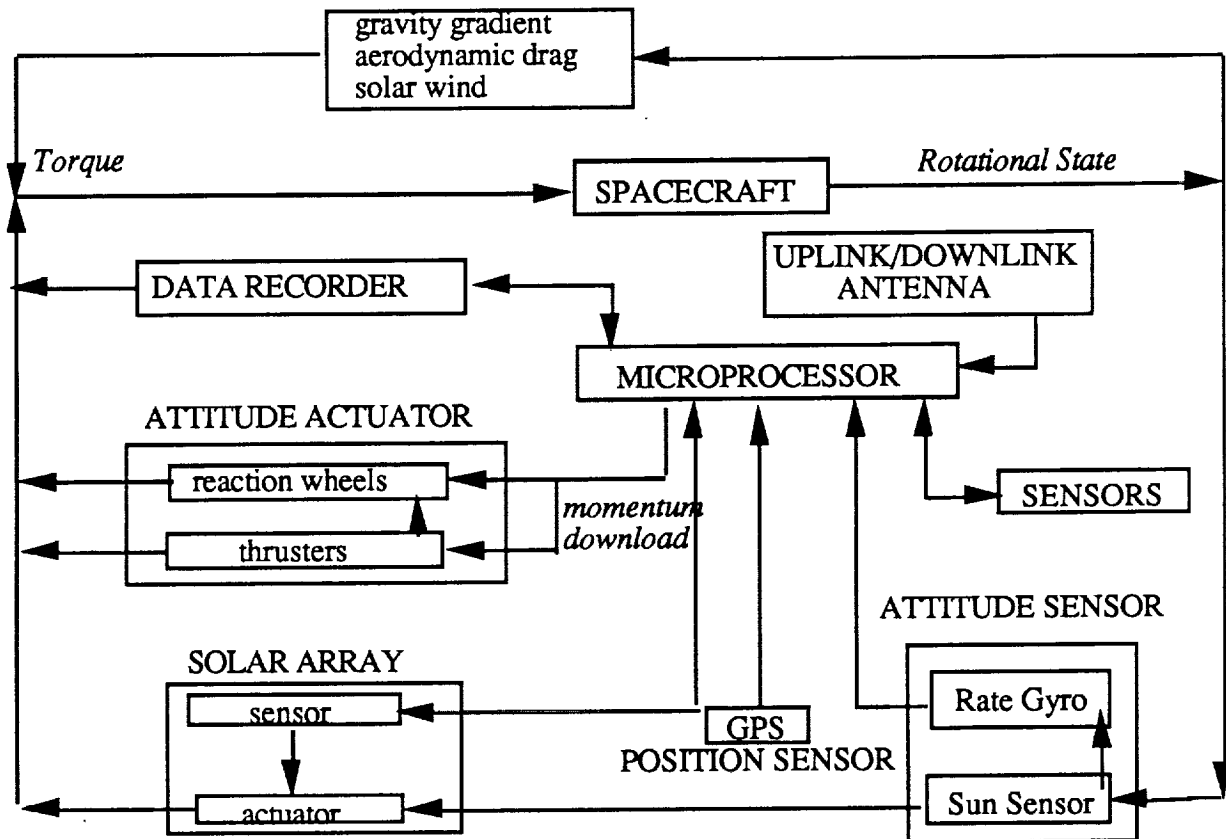


Figure 9.3: Flowchart of subsystem information

## 9.4.1 Position Sensing Subsystem

The position sensor subsystem plays two roles. The position sensor must determine when the satellite is positioned over a particular area to know when to turn on the scientific instruments or the communications antenna. Although the communications system will only expect commands when told by the position sensing system, it will be "warm" at all times in case an override command is needed. Also, the altitude must be determined by the position sensor so that when the satellite has fallen to a certain altitude a $\Delta V$ maneuver can be performed to boost the orbit.

Three Global Positioning System (GPS) receivers will be placed on the satellite. Only one will be needed for position sensing; the other two will provide redundancy in the position sensing system. Three GPS receivers can also be used as a redundant attitude sensing system. A GPS receiver tracks at least four GPS satellites and uses ranging to determine the distance from the receiver to each satellite. Knowing the position of the four GPS satellites, the receiver then determines its position in 3-dimensional space. For inertial sensing, once the position of three points on the satellite are known, the attitude of the points in relation to each other can be determined.

## 9.4.2 Attitude Sensing Subsystem

In order to determine which way the satellite is facing, it is necessary to have attitude sensors on the satellite. These sensors will have two jobs: to provide orientation information to keep the scientific instruments pointed accurately, and to provide a reference to the sun for the solar array. To perform these two duties, the attitude sensing subsystem will have an inertial sensor and a sun sensor.

### 9.4.2.1 Inertial Sensors

The role of the "inertial sensor" is to provide very accurate attitude information throughout the orbit (including the time when the satellite is in the Earth's shadow). Typically rate gyros, accelerometers and the like are used in this role. Most are accurate to about 0.1 °. Do to the small volume constraint of MEDSAT, the design currently utilizes the Kearfott TRILAG gyro rather than using three single-axis ring laser gyros (RLG). The TRILAG is a monolithic, three-axis RLG that uses a single block and six shared mirrors. The six mirrors provide a three dimensional path for the laser beam so that knowledge of attitude changes on all three axes can be obtained. The TRILAG offers many advantages to using a single RLG on each of the three axes in terms of volume and power. The TRILAG occupies two-thirds of the volume of three single-axis gyros, increasing the performance margin for a given volume. It also uses half of the piece parts of three single-axis gyros, lowering the cost and raising the reliability [9.2]. Although the system is expensive, its solid state operation for low mass, power, and volume (as well as its ten year lifetime with low failure rate) make it an attractive choice. Other systems considered included a Systron Donner rate gyro, a quartz rate sensor (also from Systron Donner), and an Earth Horizon Sensor (EHS) from Applied Research Corporation. Recent spacecraft have utilized ring laser gyros (RLG's) in which a laser beam is directed around a circular path and changes in attitude are determined when the high frequency beam misses a sensor on the path.

### 9.4.2.2 Sun Sensors

The TRILAG rate gyro provides attitude knowledge easily in fulfillment of the mission requirements (up to 0.01° accuracy), but because the mission dictates referencing to the sun not just in inertial space the attitude sensing system requires another sensor. An external reference will also be needed to initially reference the TRILAG during attitude acquisition as well as to periodically update the TRILAG.

Sun sensors are accurate from 0.04° to 0.1°. With one sun sensor on the satellite, the inertial sensor and the solar array can be referenced once an orbit. Sun sensors find the sun in a two-dimensional reference system. The Solar Aspect Sensor (SAS) [9.3] responds to solar radiation in the blue-green portion of the spectrum. The sensors consist of an entrance slit and a linear charge-coupled device array which are mutually orthogonal to the sensor axis. It contains two channels for measuring orthogonal components, $\alpha$ and $\beta$, of the sun's angle. From these measurements the location of the center of the sun's image on the array is determined.

Once the satellite finds the sun, it can expect to find the sun in approximately the same place in the next orbit. Variation in this cycle is the result of the earth's motion about the sun. Each earth day (15 satellite orbits), the sun crosses the satellite sky earlier by the angular distance that the earth travels around the sun (i.e. about 1°). For this reason, the sun sensor

only needs to be on for about 5° in each orbit. Therefore, the sun sensor will be on and off for cycles of 75 seconds on, 92 minutes and fifteen seconds off during each orbit.

### 9.4.3 Actuator Subsystem

Once changes in the attitude of the spacecraft are determined, the satellite needs to rotate back to the desired attitude. Typically, correcting the disturbance torques acting on the satellite is accomplished using reaction wheels, control moment gyros (CMG) or thrusters. MEDSAT's attitude actuator subsystem will consist of three reaction wheels, one along each axis, and a ten thruster propulsion system. The wheels will perform corrections as needed to maintain stability for the scientific mission. The thrusters will be used for orbit insertion, downloading momentum, and performing ΔV maneuvers to prolong the lifetime of the satellite.

### 9.4.3.1 Reaction Wheels

The choice between a reaction wheel system, in which changes in angular momentum about each axis are made by changing the rate of the spinning wheel on that axis, and a CMG, which corrects changes in angular momentum by changing the axis direction of a single, gimballed wheel spinning at a constant rate, was made on the basis of reliability and available space. A reaction wheel system was chosen because it does not exhibit geometric singularities like a CMG system, and there was not room for the CMG at the center of gravity (CG) of the satellite. Having three independent wheels also limits the ADCS's susceptibility to a single failure. Magnetic torquerods were not utilized because their long, thin, shape did not fit well into the spacecraft.

Reaction wheels absorb cyclic torques and temporarily store momentum produced by the spacecraft while slewing or reorienting. Reaction wheels can be operated from zero speed up the the maximum speed of the driving motor, at which time they are considered "saturated." When the wheels are saturated, thrusters must be used to counter the torque produced by slowing the wheels back down to zero in a process known as momentum downloading. Due to the volume constraints of the satellite, the reaction wheels cannot be placed on the center of gravity. Instead each reaction wheel will be positioned so that its line of action goes through the CG along the axis it is controlling. The ADCS will use 35 cm diameter reaction wheels that can store angular momentum up to 50 Nms. The reaction wheels apply a torque about the axis perpendicular to the plane in which they spin. Figure 9.4 presents the orientation of the reaction wheels.

The time period that passes until the disturbance torques saturate the wheels is important in determining how often the thrusters will have to be fired to download momentum over the lifetime of the satellite. For the disturbance torques acting on the MEDSAT satellite, the period before the reaction wheel along any axis is saturated can be determined by dividing the maximum angular momentum (50Nms) by the torque applied by the disturbances to the axis. For these calculations, the average of the aerodynamic and solar radiation torques were used instead of the worst case torques. Figure 9.5 shows the torques and the time until saturation for each axis.

These numbers are based on the use of a TELDIX DRALLRAD DR 50 momentum wheel and a WDE 1-0 wheel drive. This is a 35 cm diameter wheel that can absorb up to 50 Nms of angular momentum [9.4].
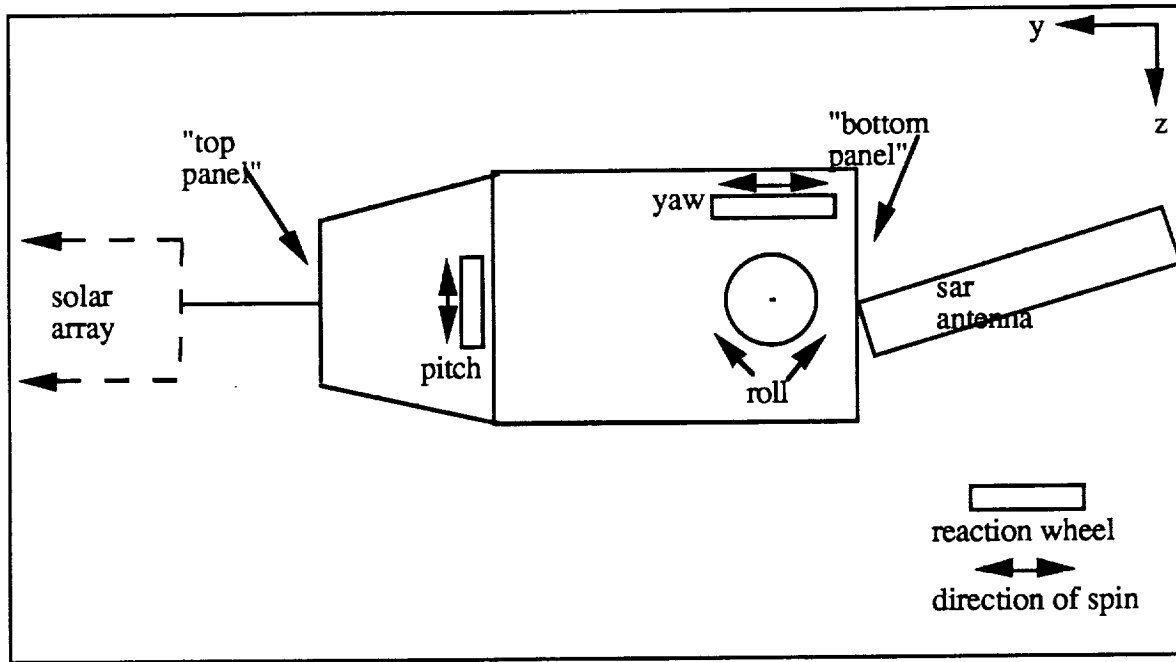
**Figure 9.4: Reaction Wheel Orientations**

| axis | disturbance torque (Nm) | time until saturation (hours) |
|------|------------------------|-------------------------------|
| roll | $-1.711 \times 10^{-5}$ | 811.74 |
| pitch | $1.029 \times 10^{-5}$ | 1349.75 |
| yaw | $1.271 \times 10^{-4}$ | 109.28 |

**Figure 9.5: Average Disturbance Torques and the Corresponding Time Until Saturation of the Corresponding Reaction Wheel**

### 9.4.3.3 Thrusters

The attitude control subsystem will use ten thrusters to download the reaction wheels when they become momentum saturated as well as perform orbit maintenance functions. It is necessary for the thrusters to be positioned so that forces can be applied to cause rotation about each of the axes without causing translational motion as well as able to cause translational motion without causing rotational motion. Because the SAR antenna is sensitive to the exhaust gases of the thrusters and the SAR antenna is mounted on the bottom panel of the satellite, the thrusters on the bottom could not be arranged as they are on the top panel. Since they are angled, thruster number 10 will be used to cancel the vertical component of the thrust produced when either 7 or 9 is fired. Figure 9.6 shows the thruster orientation on each of the end panels of MEDSAT.
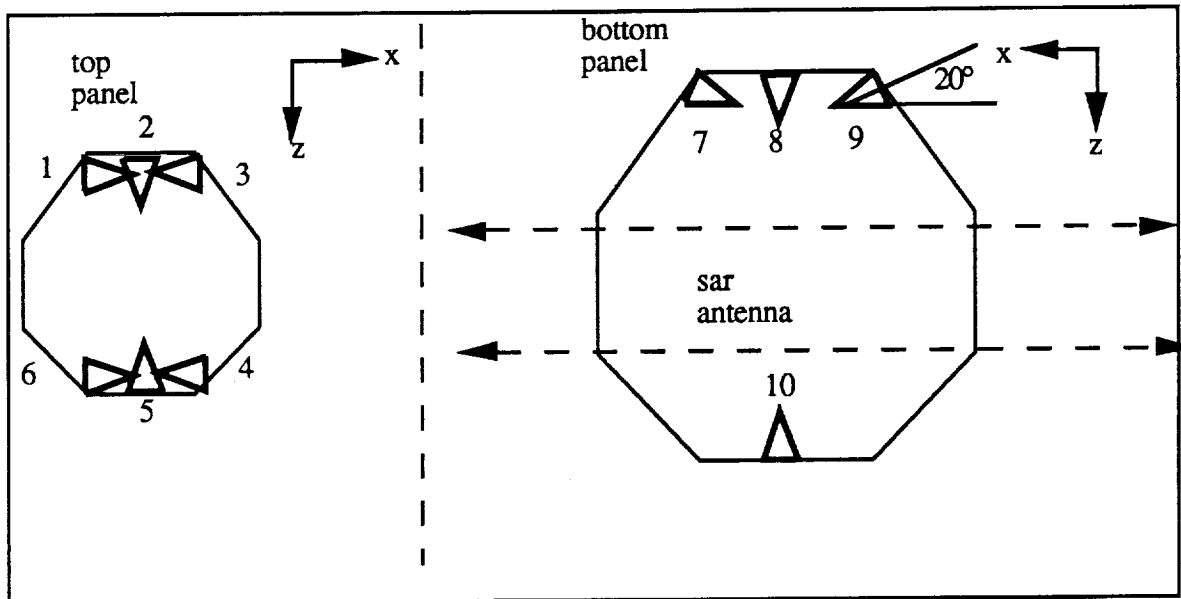
**Figure 9.6   Thruster Orientations**

To perform maneuvers rotating the satellite about an axis, thrusters coupled in pairs will be fired.

- To perform the initial maneuver, thrusters 1,6,7, and 10 will be fired to start, and thrusters 3,4, 9, and 10 will be fired to stop the rotation.
- To download momentum in the roll axis either thrusters 2 and 10 will be fired, or thrusters 5 and 8 will be fired with the other set acting as a brake for the maneuver.
- To download momentum in the pitch axis reaction wheel either thrusters 1 and 4 will be fired, or thrusters 6 and 3 will be fired with the other set acting as a brake for the maneuver.
- To download momentum in the yaw axis reaction wheel either thrusters 1,6 and 7,10 will be fired, or thrusters 3,4 and 9,10 will be fired with the other set acting as a brake for the maneuver.

To perform the $\Delta V$ maneuver thrusters 1,6,9, and 10 will be fired to increase velocity and enter an elliptical orbit to initiate the maneuver, and again to increase velocity to circularize the orbit to finish the maneuver.

To determine the total impulse necessary for attitude control, it is necessary to determine how much propellant is needed for the orbit insertion maneuver, and how long the thrusters must burn to download the reaction wheels. For the rotation of the satellite at orbit insertion, the amount of propellant can be determined from the attitude maneuver angle and the time of the maneuver [9.1]. Assuming the maneuver is completed in one minute, MEDSAT needs one gram of propellant to rotate the satellite for acquiring the initial attitude.

The amount of fuel needed for dumping momentum was calculated separately for each axis. For each reaction wheel, the moment each thruster applies about the axis can be determined, and from that the time the thruster must burn to counteract the angular momentum of the wheel is determined.

roll:    50 Nms = .888m $(F_6N)$ $t_6s$ + .522m $(F_{10}N)$ $t_{10}s$
pitch:   50 Nms = .42m $(F_1N)t_1s$ + .42m $(F_4N)$ $t_4s$

yaw: $50 \text{ Nms} = .888\text{m } (F_1 N) t_1 s + .888\text{m } (F_2 N) t_2 s + .522\text{m } (F_7 N)\cos 20° t_7 s$
$\sin(20°) t_7 s = t_{10} s$ (to counteract the vertical component of 7)

MEDSAT is designed using 0.45 lbf thrusters which produce a thrust of 2.0016 N. By summing up how long each thruster is on for downloading the momentum of one wheel, the total burn time for each download is determined. Multiplying the burntime by how many times each wheel becomes saturated (over the lifetime) will give us the total burntime required for the mission. Figure 9.7 summarizes these calculations.

| axis | individual thruster burn time (sec) | total burntime for one download | total for 4 year lifetime |
|---|---|---|---|
| roll | $t_6 = 14.06$ ; $t_{10} = 23.927$ | 37.992 sec | 1671.6 sec |
| pitch | $t_1 = 29.74$ ; $t_4 = 29.74$ | 59.48 sec | 1546.5 sec |
| yaw | $t_1 = 7.033$ ; $t_2 = 7.033$ ; $t_7 = 25.463$ ; $t_{10} = 8.709$ | 48.238 sec | 15484.4 sec |
| total | | | 18702.5 sec |

**Figure 9.7: Total Burntime for Momentum Download for Each Reaction Wheel**

The total impulse required for attitude control is the force of the thruster multiplied by the burntime $(2.0016 \text{ N})(18702.5 \text{ sec}) = 37434.9$ Ns. The specific impulse of the hydrazine propellant is 2471.1 Ns/kg (252 lbf s/lbm). Total impulse divided by specific impulse gives the total mass of propellant required for the attitude control during the mission: 15.15 kg [9.5].

The total mass of propellant on the satellite for the four year mission is 35 kg: 4.5 kg for orbit insertion correcting for Pegasus errors in altitude or inclination, 0.001 kg is needed for the initial rotation of the satellite to the correct attitude, 15.15 kg is needed for downloading the momentum from the reaction wheels, and 8.0 kg is needed for the orbit maintenance maneuvers. The 35 kg provides the satellite with an extra 7.3 kg of propellant for unexpected maneuvers.

Thruster characteristics used in these calculations are based on the MR-111 Hydrazine thruster made by Olin Rocket Research Company [9.5]. This is a 0.45 lbf (2.0016 N) thruster with a specific impulse of 252 lbf s /lbm (2471.1 Ns/kg). The thruster size was determined by the need to keep burn times reasonably small, while being able to perform both attitude corrections and orbit maintenance maneuvers. Because some of the thrusters are used in $\Delta V$ maneuvers as well as rotational maneuvers, it is not possible to have large thrusters for the $\Delta V$ and small thrusters for the rotation maneuvers. Also, the need for these thrusters to provide a back-up system for the reaction wheels limits how large the thrusters can be because the minimum impulse of large thrusters is too large to correct for small disturbances.

Aside from the thrusters themselves, a monopropellant hydrazine blowdown system has been chosen for the propellent distribution subsystem. Due to MEDSAT's volume constraints, two separate fuel tanks will be employed. Each tank will hold a pressurant (GN2) separated from the hydrazine by an ethylene propylene diaphragm. Although exact details of the subsystem have not been determined, some of the components can be mentioned. Each tank will have three service valves to fill and drain the fuel. Each will also have a latching valve to isolate the hydrazine during launch. A pressure transducer and temperature sensor will also be needed for each tank. The total volume of the fuel tanks will be 0.09 $m^3$ and they will weigh 3kg.

The fuel tanks will also provide some measure of nutation damping. When an object in inertial space spins, its axis of rotation "nods" in a circle; this process is called nutation. In order to keep one side facing the Earth, MEDSAT will rotate in inertial space with the same rotation period as its period of revolution. The "sloshing" of the hydrazine in the fuel tanks will serve to damp out the nutation due to this slow spin.

A hydrazine blend has been chosen for the propellent. The fuel, HPB-2400, contains 24% (by weight) HN and 76% hydrazine ($N_2H_4$). This fuel is marketed by Olin Rocket Research Company as a fuel with high specific impulse, a mid-range freezing point (-1°F), and high detonability. Other fuels that were considered were anhydrous hydrazine, and other mixtures of hydrazine, HN and water. If a lower freezing point is required, it may be necessary to utilize a mixture containing 8% -12% water. The addition of water will depress the freezing point but will also reduce the $I_{sp}$ [9.5].

## 9.5     System Analysis

The proposed system will provide pointing accuracy for the scientific instruments to within 0.3° and knowledge of the Sun location to within 0.1° at least once a day. The system will last at least four years with propellant being the limiting factor. The amount of fuel on board was calculated with a 25% margin of safety. The system is designed with redundancy in mind and in anticipation of a certain amount of on-board decision making ability.

### 9.5.1     Redundancy

Because failure of the ADCS is a common cause of the loss of satellites, redundancy was an important consideration in MEDSAT's ADCS design. As mentioned above, the three receiver GPS system provides position redundancy as well as redundancy for the inertial measurement. Loss of the sun sensor could be compensated for by uplinking information once a day from the ground. One advantage of GPS, TRILAG and the SAS is that they have been developed specifically for use in light satellites. As a result, they are particularly simple, reliable components that are intended to be used on systems with little redundancy.

There are three levels of actuator redundancy on each axis. Having three reaction wheels provides one level of redundancy on each axis. This is because the loss of control on one axis can be compensated for by control on the other two axes. Using successive rotations about "Euler angles" of two axes, an arbitrary orientation can be acquired by three single axis rotations, so that a system of control about two axes can provide any attitude adjustment necessary. As a result, loss of a wheel on one axis could be compensated for in three different ways. The thruster set on that axis could provide control, the wheels on the other two axes could provide control, or the thruster pairs on the other two axes could provide control [9.6].

### 9.5.2     Logic Requirements

The ADCS will require a certain amount of decision making from the on board microprocessor to coordinate sensor and actuator information. Position information from the GPS receiver must be used to determine when the scientific instruments and communications antenna must be turned on, and to determine when the $\Delta V$ maneuver is required. Attitude information must be used to determine when the reaction wheels need to change their momentum to correct attitude changes. Also, the wheel drive electronics will

measure the rate of the wheels. When this rate exceeds the saturation rate the microprocessor must control the thrusters to download momentum. The sun sensor must turn on and off for given time periods starting when it finds the sun. The solar arrays and the inertial sensor will need to reference this information every orbit.

Aside from coordinating sensor information with the actuators, the microprocessor will have a number of other decisions to make. The thrusters should not be fired when the scientific instruments are on. The satellite should be able to receive override commands from the ground. In the case of a component failure, the MEDSAT should recognize the failure and either relay the information to the ground or switch to a redundant system on its own.

### 4.5.3    Possible Improvements

There are a number of ways that the ADCS system could be improved during the later, more detailed stages of the design process. It was mentioned earlier that electronics aboard MEDSAT generate a magnetic torque. Thoughtful location of the electrical system could provide a stabilizing influence instead of a disturbance, particularly during the operation of the SAR, which is the time when the most current will be running through the satellite and also the time when the most stability is needed. Similarly, thoughtful shaping and location of the fuel tanks will allow them to serve as nutation dampers. The "sloshing" of the hydrazine in the fuel tanks will serve to damp out the nutation due to the satellite's slow spin.

Besides arranging the fuel tanks for stability, a number of improvements are possible to the propulsion system to improve performance. When the thrusters are fired to apply a torque about any axis, each thruster has a different moment arm to the center of gravity. This means that some thrusters must apply more force than other thrusters. In these calculations, variations of the forces were achieved by varying the burn times. However this method induces a certain amount of instability during the burn that could be avoided if each thruster could provide a different amount of thrust, for equal amounts of time. To do this, the thrusters would have to receive fuel at different pressurizations. This could be done either by varying the pressurization among the three fuel tanks, or using variable orifices into the fuel inlets. Either solution adds complexity to the simple, cheap system, but it is possible the savings in propellant (or increase in lifetime) would balance the added cost and risk of failure. Similarly, if more volume and weight becomes available, it is possible that the lifetime of the satellite can be extended by including a regulating valve and high pressure (~3000 psi) tank to keep the pressure in the tanks from degrading during the lifetime. The addition of this system would raise the specific impulse of the thrusters during the later stages of the lifetime, so that less propellant would be used for each maneuver. A similar savings could be achieved by utilizing a "warm gas blowdown" propellant system, in which a small hydrazine tank feeds a reactor that supplied warm gas on demand as a pressurant for the main fuel tank [9.7].

The use of resistojets was considered for MEDSAT. These thrusters add heat to the propellant, increasing the specific impulse at the cost of power. Calculations were made using Rocket Research's MR-501 Electrothermal Hydrazine Thruster, but the increase in specific impulse did not offset the longer burn times required for the lower thrust . If resistojets with higher thrust are developed, it is possible that their increased specific impulse can extend the lifetime of the satellite for the same propellant mass or lower the propellant mass for the same lifetime. Arcjets, which add heat to the fuel via an arc discharge, were found to require far too much power for MEDSAT.

# Chapter 10

# POWER

## 10.1    Summary

To achieve the project goal of low cost, the power system of MEDSAT is designed to use mostly standard satellite equipment such as gallium arsenide solar cells and nickel-cadmium batteries. However, the system includes a modern microprocessor to increase the power system efficiency, prolonging the life of the batteries and reducing the overall weight of the power system. MEDSAT's power system is faced with the unusual task of providing high power levels to the scientific instruments for short durations in the low earth orbit environment. This requires a battery with a large charge capacity, and also a pulse modulator to feed the SAR with the required short pulses of peak power.

## 10.2    Power Requirements

### 10.2.1  Power Budget

Various components on the satellite require electrical power to perform their functions. In order to detremine the power available for these devices, the following power budget was constructed. The power values are divided into two catagories - continuous and peak. The continuous values are the power levels that the component needs constantly from the power system. Examples of this include the solar array drive motor, which continously tracks the sun, or the ring laser gyro which is constantly sensing changes in satellite attitude. The peak power column represents the maximum power that the component would draw during operation. The sum of the continuous power values is termed the nominal operation power. The length of time that the peak power would be functioning is dependant on the component. For example, the SAR and the Visible/IR sensors operate at their peak power for only short periods of time (around 35 seconds) and have a continuous power of essentially zero. Figure 10.1 on the next page summarizes the power demands of MEDSAT.

To gain a visual perspective of the various power requirements of MEDSAT, a power profile for a worse case single orbit is shown in figure 10.2. From the figure it can be seen that the sensing sension draws a large amount of power from the battery in a very short time while the nominal operations continuously draw a much lower power level continuously. From a viewpoint of energy, the nominal operations draw much more energy from the power system than the scientific instruments due the longer operational time each orbit. The scientific payload is almost insignificant from the energy standpoint, but since it uses so much energy in a short period of time, the power system must be able to handle the resulting high current levels. This was an important factor in sizing the battery.

### 10.2.2   Initial Power Requirements

Although the power system was mainly designed for operations in orbit, there are several other situations when the components of MEDSAT require power. While the satellite is connected to the pegasus launch vehicle, power is drawn from Pegasus' electrical system. Immediately after the satellite is inserted into orbit, power must be provided by the battery because the solar arrays are folded up and consequently are not producing power. During this phase, power is needed for the attitude control system and the deployment of the solar array SAR antenna. A possible sequence of events could be the following : attitude control requires power to operate the thrusters in order to attain correct attitude. Once this attitude

PRECEDING PAGE BLANK NOT FILMED

| Component | Continuous Power (W) | Peak Power (W) |
|---|---|---|
| Scientific Payload | | |
| Sensors | | |
| SAR | 0 | 240 |
| IR Sensor | 0 | 25 |
| Data Management | | |
| Compression | 0 | 30 |
| Read/Write to storage device | 0 | 10 |
| Communications | | |
| Data downlink | 0 | 15 |
| Ground control communication | 2 | 15 |
| | | |
| Nominal Operations | | |
| Attitude Control | | |
| Thrusters (9W each-max 4 operating) | 0 | 36 |
| Solar Aspect Sensor | 0 | 1.6 |
| GPS (times 3) | 0 | 28 |
| Reaction Wheels (total for three) | 13 | 237 |
| TELDIX Wheel Drive | 18 | 200 |
| Trilag - Laser Ring Gyro | 10 | 10 |
| | | |
| Thermal Control | | |
| Heaters | 7 | 10 |
| | | |
| Computer - Satellite Control system | 10 | 20 |
| Solar Array Orientator | 3 | 3 |
| | | |
| Total Nominal Operations | 58 | |

**Figure 10.1   MEDSAT Power Budget**

is reached, as much as 179 watts is needed to spin up the momentum wheels in order to provide stability for the satellite. Once the satellite achieves reasonable stability, the solar array can be deployed. Depending on the nature of the deployment mechanisms and the initial attitude of the spacecraft, these initial events could severely strain the battery. Consequently, the satellite will require several orbits to recharge the batteries before the SAR antenna can be deployed and scientific operations can begin.

## 10.3   Solar Array

The first step in providing power for the satellite is to harness the energy of the sun. A solar array generates electrical power to be used by the satellite to run various components.
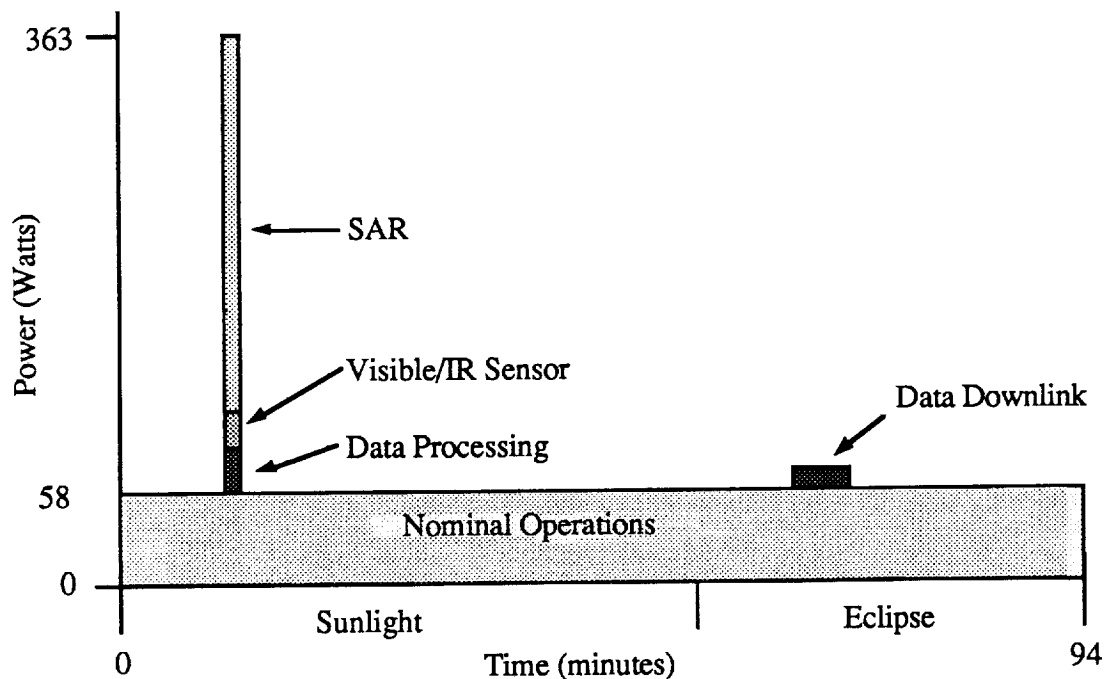
**Figure 10.2 Typical Power Requirement Profile**

## 10.3.1 Solar Cells

The solar cells convert energy from the sun into electrical energy through the photoelectric effect. Many environmental factors affect the power output of the cells, such as the temperature and angle of the cells in relation to the sun. The cells are more efficient in converting the solar energy into electrical energy at lower temperatures. The efficiency of the cells also decreases when they are not perpendicular to the sun, and this decrease is approximately proportional to the cosine of the angle between the incoming solar rays and the normal of the plane of the solar cells.

Currently, there are two types of cells being used for aerospace applications - silicon and gallium arsenide (GaAs) based cells. The more recently developed gallium arsenide based cells have several advantages over the silicon cells. At normal conditions, silicon cells have approximately a 12% efficiency versus the GaAs cells which operate near 18% efficiency. The GaAs cells have a lower temperature coefficent of efficiency which means that when the temperature increases, the efficiency of GaAs cells doesn't decrease as quickly as that of the silicon. Gallium arsenide solar cells cost approximately four to five times as much as silicon cells, but on MEDSAT this cost differential is small compared to other expenses such as the scientific instruments, and gallium arsenide cells offer a reduction in array area which significantly reduces the aerodynamic drag on the satellite. This effect substantially reduces the fuel required during MEDSAT's lifetime. In addition, the smaller array reduces the disturbance torques on the satellite, easing the problem of attitude control. The solar cells used on MEDSAT will be Galium Arsenide based cells made by SpectroLab Inc. Figure 10.3 summarizes some of the physical characteristics of the cells. In order to reduce

the effects of radiation degradation, micrometeorite damage, and to reduce the temperature of the arrays, the cells will have a 0.025 cover slide made of fused silica [10-2].
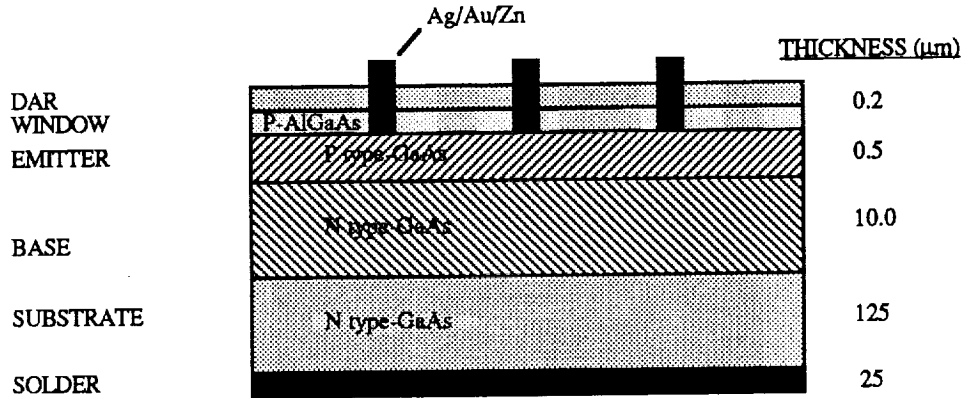


**Figure 10.3   Cross Section of 5 mil Spectrolab Gallium Arsenside Cells**

The solar array structure will consist of an aluminum honeycomb core sandwiched between aluminum facesheets. A layer of insulation is located betweent he actual cells and the aluminum. A cross section of the array is shown in Figure 10.4
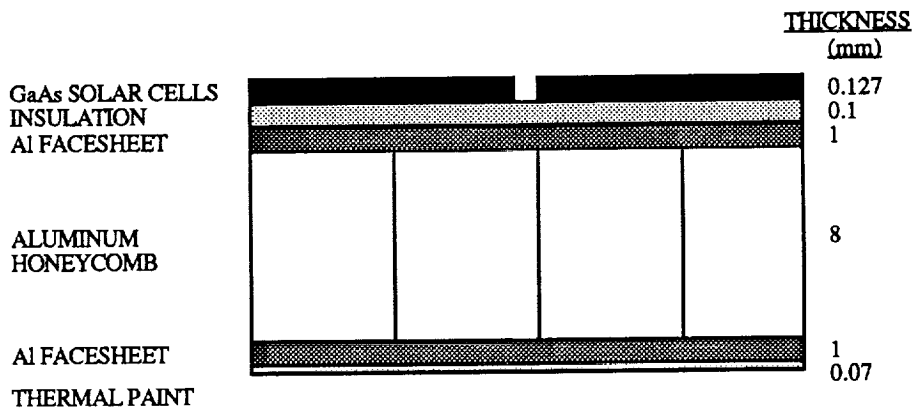


**Figure 10.4      Cross section of the array**

## 10.3.2   Configuration of the Array

There were two basic choices for the configuration of the array -- body mounted cells and panel mounted cells. In the body mounted configuration, the cells are affixed to the structure of the spacecraft. Many more cells are required in this configuration because only a portion of the cells are facing the sun at any time. Since MEDSAT has limited available surface area and also due to the high power requirements, the solar cells will be panel mounted. In order to obtain the highest efficiency of the solar panel, it must be as nearly perpendicular to the sun as possible. Therefore MEDSAT has a solar array orientation control system with one degree of freedom.

## 10.3.3 Orientation System

The array will have orientation control in only one axis - the stable axis of the spacecraft. Adding another orientation axis would increase the mass and complexity of the system and possibly lead to attitude control problems. With this single orientation axis system, the solar panels will normally be at an angle to the sun, reducing the power output of the cells. Consequently, the area of solar cells required had to increase.

Several of the factors affecting the array performance are the earth's 23° tilt (which causes the seasons) and the effects of precession on the orbit. The best case solar angle of incidence is 2° which results from the combined effect of the 21° orbital inclination and the 23° tilt of the earth (see Figure 10.5). In the worst case situation, the solar angle of incidence is 44° which results in only 72% of peak power production. This situation occurs quite often due to the precession of the orbit.

Worst Case Solar
Incidence Angle of 44°

Best Case Solar
Incidence Angle of 2°
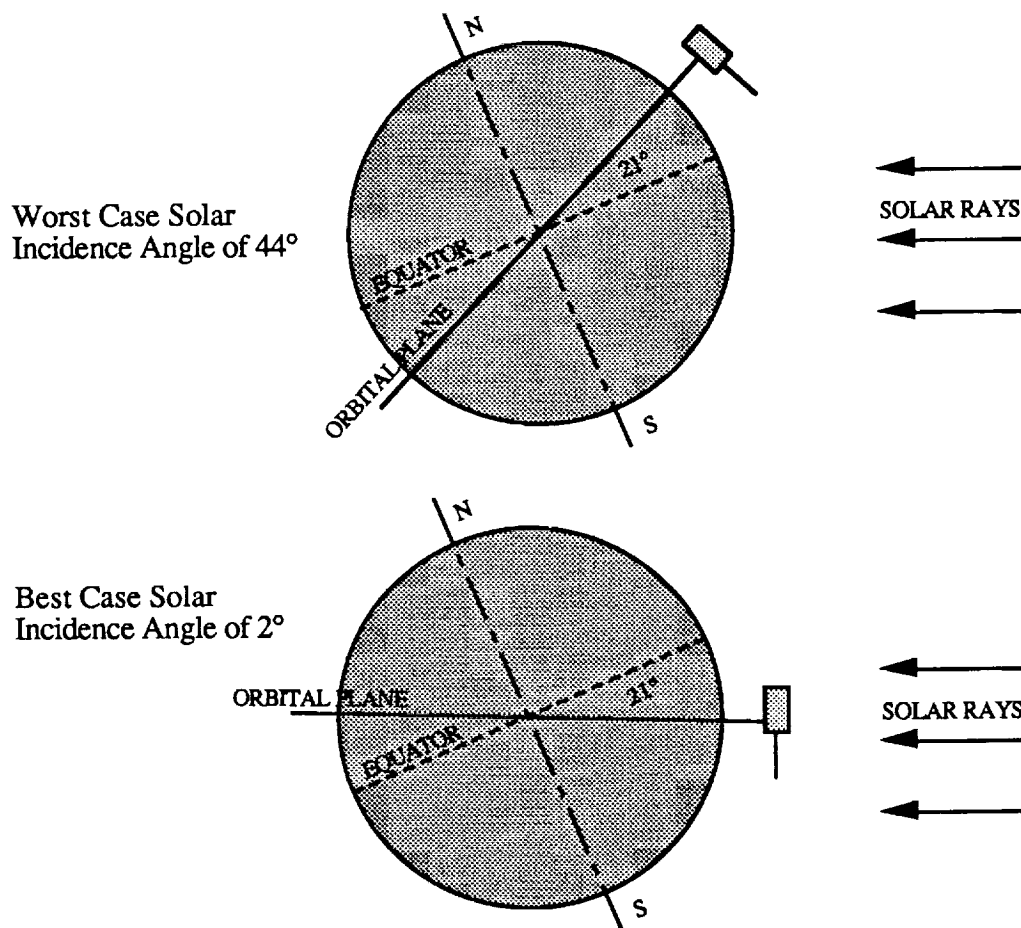
**Figure 10.5  Geometry of Solar Incidence Angles**

To reduce the effect of the incidence angle, an idea was proposed to design the solar array with a permanent tilt to compromise between the best and worst case angles pictured in Figure 10.6. This idea works fine for the case pictured in Figure 10.6 which describes the winter in the earth's northern hemisphere, but a different situation occurs when the earth is on the other side of the sun. This is summer for the earth's northern hemisphere. During this situation the added tilt actually has a negative effect on the system. Figure 10.6 shows the satellite in both the winter and summer. It can be seen that the while this seems like a viable option, the fixed angle actually increases the incidence angle and consequently reduces the power output when the earth is on the other side of the sun.
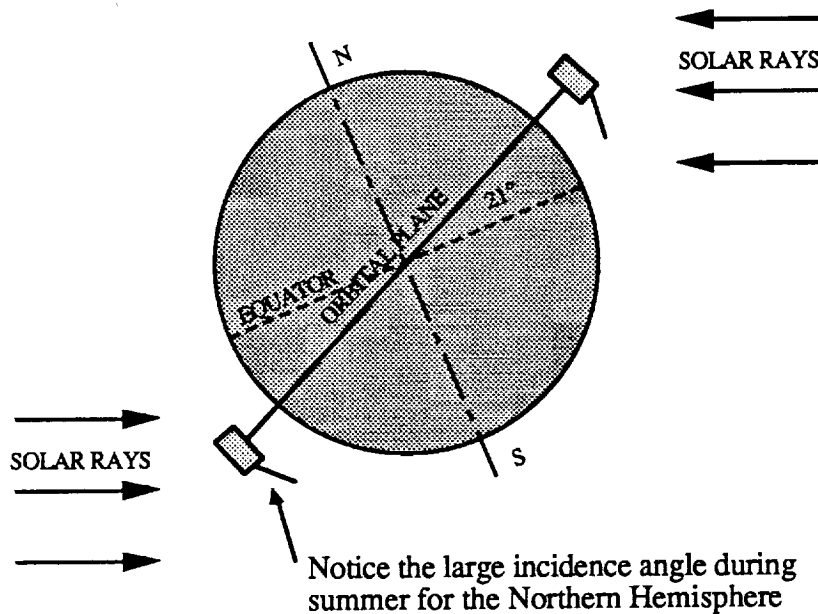
**Figure 10.6  Proof that a fixed tilt array is not feasible**

## 10.3.3   Array Performance

<u>Cell Power Output</u>

$$P_{CELLS} = [N_{EFF} - C_{TCE}(T - 28°C)]\ P_{SI}$$

where

| | | |
|---|---|---|
| $P_{CELLS}$ | = Power output of the cells (W/m$^2$) | |
| $N_{EFF}$ | = Cell Efficiency at 28°C | 18% |
| $C_{TCE}$ | = Temperature Coefficent of Efficiency (%/°C) | -0.033%/°C |
| $T$ | = Operating Temperature (°C) | |
| $P_{SI}$ | = Solar Intensity | |

The operating temperature of the array is dependent on several factors, including the incidence angle of the cells to the sun as described in the previous section. Using heat transfer properties (see Section 8.8 on thermal control) the equilibrium temperature of the array is calculated to be 82°C for 2° incidence angle and 45.5°C for a 44° incidence angle.

The decrease in power due to the higher cell temperatures is partially offset by the increased efficiency due to the lower solar incidence angle [10.1].

| Cell Power Output | |
|---|---|
| Minimum Temp | $218.94$ Watts/m$^2$ |
| Maximum Temp | $191.02$ Watts/m$^2$ |

## Other Inefficiencies

$$P_{SA} = P_{CELLS} \, P_F \, N_{TC} \, N_{RAD} \, N_{UV} \, A_F \, N_D \cos \alpha$$

where

$P_{SA}$ = Solar Array Power Output

| | | EOL Value |
|---|---|---|
| $P_{CELLS}$ | = Cell Power Output | |
| $P_F$ | = Packing Factor | 90% |
| $N_{TC}$ | = Thermal Cycling Factor | 97% |
| $N_{RAD}$ | = Radiation Degradation | 97% |
| $N_{UV}$ | = UV Degradation | 98% |
| $A_F$ | = Assembly Factor | 96% |
| $\alpha$ | = Incidence angle | $2°$ to $44°$ |

The assembly factor takes into account the decreased efficiency due to cell mismatch and losses in the cell interconnects. The radiation degradation is very small because the radiation particle fluence is very small (less than $1 \times 10^{13}$ MeV equivalent fluence) at our relatively low altitude of 477km. The coverslides also serve to reduce the radiation effects. For satellites in low earth orbit, the temperature of the array cycles every orbit. This continued cycling over a five year lifetime reduces effiency of the cells leading to the three percent decrease in power output. Ignoring the effects of incidence angle and the temperature coefficienct, the solar array initially produces only 86% of the maximum power output of the cells. After five years the inefficiencies of the array reduce this figure to 80%; again ignoring the temperature and incidence angle effects [10.1].

| | Summer | Winter |
|---|---|---|
| Nominal Temperature (°C) | 28 | |
| Efficiency at nominal temperature | 18.00% | |
| Temperature Coef of Efficiency (%/°C) | -0.033% | |
| Solar Intensity (W/m^2) | 1350 | |
| | | |
| Equilibrium Temperature (°C) | 82 | 45.5 |
| Efficiency (temperature corrected) | 16.22% | 17.42% |
| Other efficiencies | | |
| Packing factor | 90.00% | 90.00% |
| Other Losses | 88.50% | 88.50% |
| Cosine angle losses | 99.94% | 71.96% |
| | | |
| Power (one square meter) (Watts) | 174.28 | 134.81 |

**Figure 10.7   Performance Characteristics of the Solar Array**

The power values in figure 10.7 are calculated for the equilibrium temperature of the array. When the satellite leaves the earth's shadow, the temperature of the solar array increases slowly until an equilibrium is reached. During this transient period, the array is actually cooler than the equilibrium temperature and consequently is producing power in excess of the values stated in the table above.

## 10.4 Batteries

Satellites in low Earth orbit (LEO), like MEDSAT, spend a considerable portion (~45%) of their orbital period in the shadow of the earth. During this darkness or occultation, the solar array cannot produce power for the satellite subsystems. Consequently, electrical energy must be stored to provide power during this eclipse period.

### 10.4.1 Type of Cells

Of the batteries that have been used for aerospace applications, only two types were possible candidates for use on MEDSAT -- nickel cadmium and nickel hydrogen. The nickel cadmium cells are historically the most popular with satellite designers due to their proven reliability and the vast amount of technical data available. Recently, nickel hydrogen cells, which have better performance characteristics than NiCd cells, have been developed. Unfortunately, the current technology has produced nickel hydrogen cells for power and weight limits that are significantly higher than MEDSAT. Consequently, nickel cadmium cells will be used aboard MEDSAT [10.3].

The cells to be used aboard MEDSAT are General Electric low-profile sealed nickel cadmium aerospace cells. The characteristics of the cells are as follows :
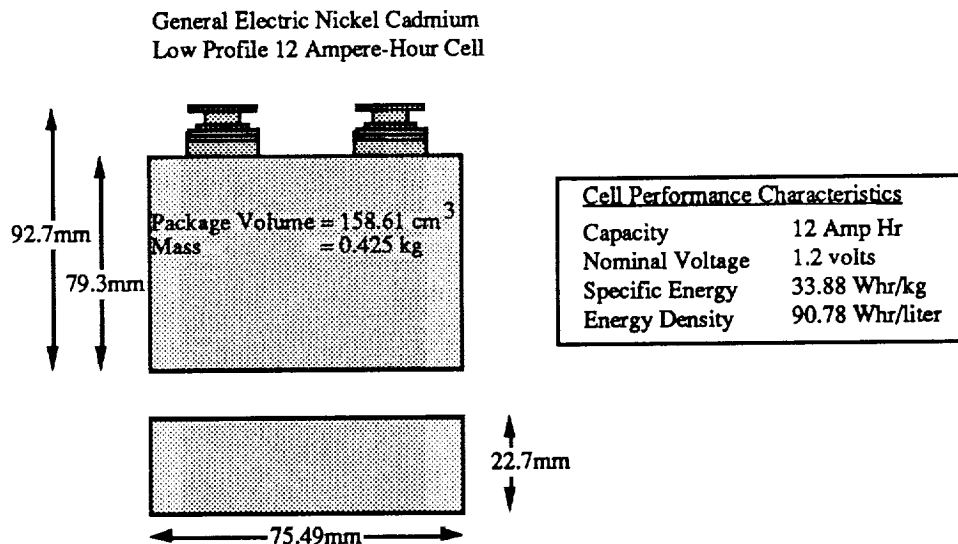


**Figure 10.8   Specifications of an individual nickel cadmium cell**

### 10.4.2 Battery Configuration

The battery chosen for the satellite must provide power at nearly 28 volts, the satellite's bus voltage. In order to reach this voltage, the battery will consist of 23 of the 1.2V cells

connected in series. The redundancy of the system will be the result of a twenty-fourth cell in the battery. If one of the cells fails, the extra cell will be switched into the series connection to continue providing power at the required voltage. The amount of charge stored in the battery is referred to as the capacity of the battery and fraction of the total charge that has been removed from the battery is referred to as the depth of discharge (DOD).

### 10.4.3   Battery Performance

One goal of the energy storage system was to be able to fully recharge the battery in one orbit after a sensing session. Figure 10.9 depicts the battery state for an orbit with a sensing session. The sensing session occurs during eclipse when the solar array isn't producing power. The system is almost able to fully recharge the battery (100% capacity) before the next orbit begins.
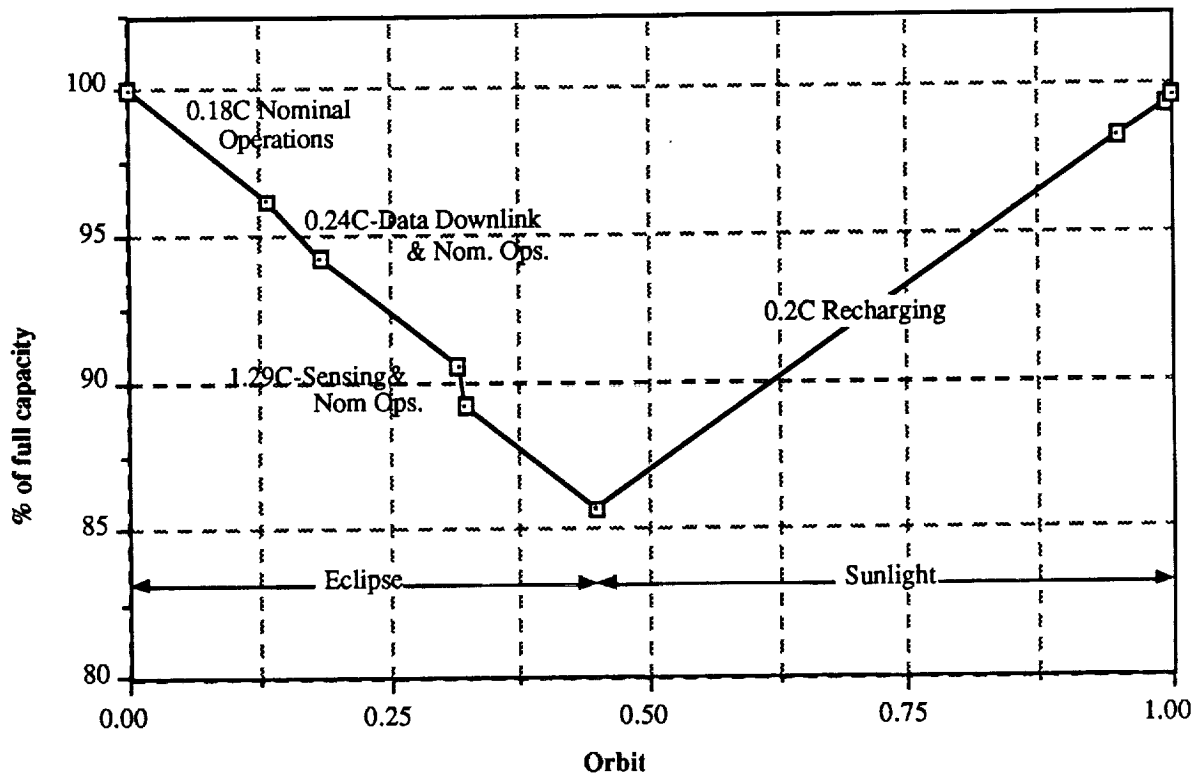


**Figure 10.9   Battery charge status for the worst case orbit**

The battery system was developed with the concept of mission flexibility in mind. Although possible sensing and downlink locations have been chosen, the power system should be able to provide power for alternate missions, such as scanning sites in other regions of the tropics. To illustrate the battery performance, a typical mission, determined from the satellite groundtrack, was chosen as an example. On the second and fifth orbits of a fifteen orbit twenty-four hour day, MEDSAT flies over the Chiapas, Mexico. During these passes (which are assumed to be in worse case conditions -- during eclipse) the

scientific instruments and the data management system draw power from the battery. On the sixth and seventh orbits, the satellite passes over Hawaii where data is downlinked to a groundstation located on one of the islands. During this mission the battery experiences various states of charge as illustrated in figure 10.10. Notice that the battery power level in the battery never decreases below 85.7% of full capacity.
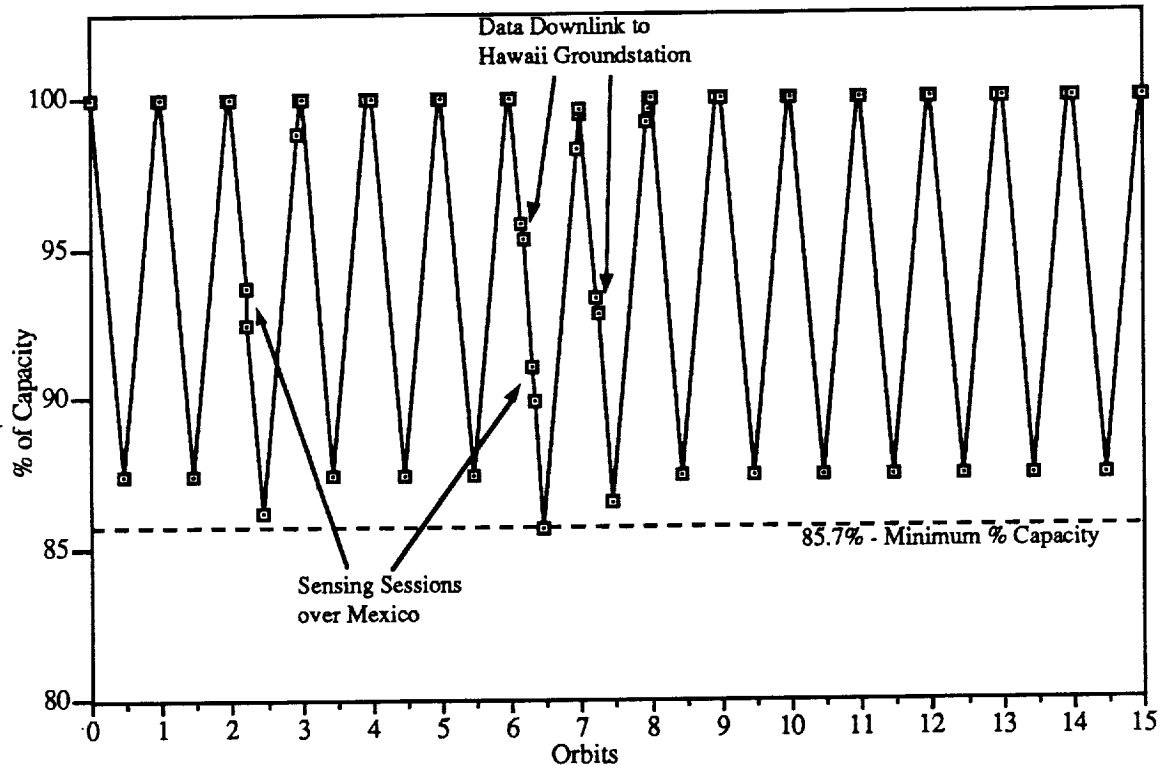


**Figure 10.10   Charge state of the battery for a typical mission day**

The previous battery capacity profiles were developed with several assumptions. The battery charge rate was assumed to be held constant at 0.2C until the battery reached 100% capacity. In the actual system, when the battery nears around 95% of full capacity the battery charge system decreases the charging to a trickle rate in order to prevent battery overcharge and reversal. Although this would slightly increase the length of time to fully charge, the battery reliability and lifetime would increase.

## 10.4.3   Reliability

The reliability of a battery system is highly dependent on the number of cycles, i.e. discharge-charge phases, the battery experiences. A Nickel Cadmium battery running at 15% DOD and 10°C has approxmiately a 27000 mean cycle life [10.4]. Since MEDSAT's battery is cycled every orbit due to the eclipse, it will experience approximately 22344 cycles during a 4 year lifetime. From this comparision, the mean lifetime of the battery is over four years. This lifetime will be decreased by several other factors such as the battery operating temperature fluctuations and the high discharge rate of the sensing sessions. On the other hand the lifetime will be increased by the redundancy introduced by the extra cell in the battery.

## 10.5   The Power Conditioning and Control System

With the advent of lightsats and improved computer technology, power control systems are becoming more flexible and efficient. The power conditioning and control system for MEDSAT is based on an independent microprocessor which resides in the central satellite computer module. This microprocessor continually monitors the satellite power system, including the battery voltage, array current, and battery charging rate, and it can also carry out instructions received from the ground.

### 10.5.1   System Overview

MEDSAT's power conditioning and control system is based on a design philosophy developed by Dunbar and Hardman [10.5]. They contend that by designing a satellite power system with the fewest possible number of power convertors effectively minimizes the mass of the power system. They have successfully applied this philosophy in combination with a microprocessor of the 80C51 family in DATASAT X.

The power conditioning and control system is in position to regulate the charging rate of the batteries, and also to regulate and direct the output from the solar array. MEDSAT uses both a fully regulated power bus and a partially regulated power bus. The fully regulated bus operates at 28 volts, and it conects to loads which require a steady and precise power supply, such as the scientific instruments. The partially regulated bus has a variable voltage which is usually higher than 28 volts, since this bus charges the battery. Many of the satellite systems can be run from this bus, eliminating the need to pass this power through additional convertors.

The microcontroller controls the input from the solar array based on what the current loads require and also what the optimal battery charging rate is. The microprocessor determines the optimal battery charging rate based on an algorithm which takes into account when the batteries will next be drained by a sensing pass. If the batteries must be recharged quickly,
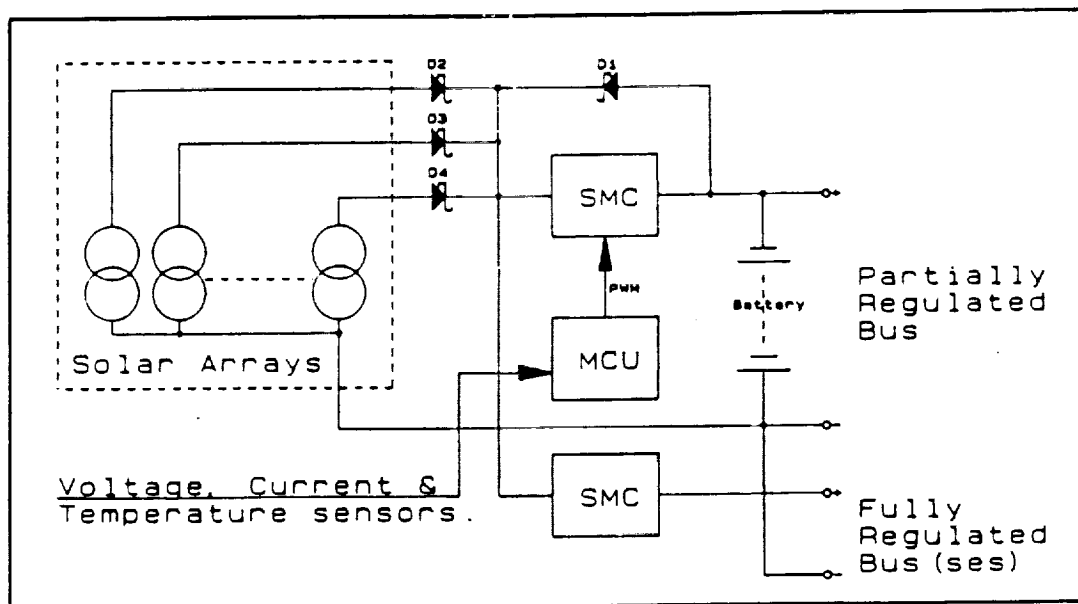


**Figure 10.11.   Power conditioning and control system**

Power

a higher charging rate is selected. If several orbits are available for charging, the controller selects a lower charging rate and disconnects some of the solar cell strings, in order to save wear on the batteries. An elementary block diagram of the power conditioning and control system is shown in Figure 10.11. In addition, the controller will phase the solar array in gradually when the satellite comes out of eclipse. This will eliminate the sudden inrush of current which would otherwise occur, and save wear on the power system.

### 10.5.2    Battery Charge Regulation

Since the lifetime of the batteries depends on their treatment and use, it is advantageous to design a power conditioning and control system which is gentle on the batteries. Although high discharge rates are occasionally unavoidable due to sensing passes during eclipse, MEDSAT's controller seeks to augment the battery lifetime by using a low charging rate whenever possible.

## 10.6    Power System Characteristics

MEDSAT's power system incorporates few advances in technology, using largely well-proven equipment with an emphasis on reducing costs. However, the power control and conditioning system exemplifies the modern trend of designing innovative satellite systems within strict weight and cost constraints.

# Chapter 11

# FIRST ORDER COST ANALYSIS

## 11.1     Summary

One advantage of the MEDSAT design is its use of many developed and proven systems. By using these tested and proven systems, the research and development costs can be reduced. For example, the Pegasus launch vehicle allows the insertion of a small satellite into low earth orbit at a much smaller cost compared to other currently available vehicles.

However, determining the costs of a lightweight satellite also involve many variables which cannot always be determined precisely. There are no "off the shelf" estimates for the sensors due to the theoretical nature of the sensor design thus far. In order to turn theory into actual working hardware, much research and development is involved.

To address the first order cost analysis, the Scientific Payload Group first organized a cost breakdown structure which divided each satellite system into its subsystems. For each subsystem, either actual industry estimations or CERs were used to estimate the costs.

By definition, an estimation involves a degree of uncertainty. Different components will, of course, have different degrees of uncertainty. The degree of uncertainty of any one component can usually be directly linked to its need for research and development. The most speculative costs, the research and development costs, are therefore tabulated separately to emphasize the specific uncertainty involved in these areas.

## 11.2     Cost Estimating Relationships

Cost Estimating Relationships (CERs) were a primary tool used in the first order cost analysis presented here. The CER model was calculated using a least squares linear regression analysis from data points of contractors estimates and past costing experience. The CERs used for this cost analysis were taken from <u>Space Mission Analysis and Design</u> by James R. Werts and Wiley J. Larson [11.1]. By using these CERs, we were able to estimate any occuring (initial launch) or reoccurring (ground station) costs that were withheld by industry.

## 11.3     Cost Breakdown

While gathering data for the Cost Breakdown several industry sources were used in addition to CERs. Representatives from NASA Lewis [11.2], NASA Ames [11.3], and Orbital Sciences Corporation [11.4] were very helpful in obtaining cost estimates for the subsystems. It was also helpful to access past University of Michigan Space Systems Design project reports [11.5], to provide an example of first order cost analysis sections.

The following is a summation of the System level cost estimates. These costs are meant to be a first order estimate. Many of the components are very complex and the price quotes are order of magnitude estimates. All costs were estimated as accurately as possible using the resources available to the Scientific Payload Group.

The system level costs were computed by summing the subsystem level component costs. The following is a more detailed list of subsystem component costs which addresses both hardware and research and development cost estimates. These cost estimates were obtained using the same methods described above.

## System Level Elements

### (Costs in thousands of 1991 U.S. dollars)

| System Element | Research and Development | Mission Hardware |
|---|---|---|
| Synthetic Aperture Radar | $ 6000 | $ 8000 |
| Visible/Infrared Sensor | $ 100 | $ 600 |
| Power | | $ 72 |
| Controls and Communications | $25 | $ 2389 |
| Structures | $ 10 | $ 253.5 |
| Launch Vehicle and Launch | | $ 8000 |
| Ground Segment | | $ 850 |
| Communications and Data Management | | $ 970 |
| Operations and Production | | $ 7880 |
| Total Costs (in 1991 U.S. dollars): | $ 6.135 million dollars | $ 29 million dollars |

**Total Estimated Project Cost (in of 1991 dollars):**     **$35 million dollars**

## Subsystem Level Elements

(Costs in thousands of 1991 dollars)

| Subsystem Element | Research and Development | Mission Hardware |
|---|---|---|
| **SAR:** | | |
| Antenna | $ 6000 | $ 8000 |
| Visible/Infrared Sensor | $ 100 | $ 600 |
| **Power:** | | |
| Batteries | | $ 57 |
| Solar Arrays | | $ 15 |
| **Controls and Communications:** | | |
| Thrusters (10) | | $ 400 |
| Fuel tanks | | $ 75 |
| Fuel | | $ 1 |
| Service valves | | $ 12 |
| Latching valve | | $ 7 |
| Transducer | | $ 7 |
| Production (Control Systems) | | $ 30 |
| Downlink Antenna | | $ 1082 |
| Solar Aspect Sensor | | $ 50 |
| TRILAG | | $ 500 |
| Global Positioning System | $ 25 | $ 75 |
| Reaction Wheels (3) | | $ 150 |
| **Structures:** | | |
| Honeycomb Aluminum Shell | | $ 200 |
| Radiators | | $ 3 |
| Heat Pipes | | $ 2 |
| Insulation | | $ 20 |
| Deployment Mechanisms | $ 10 | $ 8.5 |
| Truss | | $ 20 |
| Launch Interface | | $ 20 |
| **Launch Vehicle and Launch:** | | |
| Pegasus (including Supporting Costs) | | $ 8000 |
| **Ground Segment:** | | |
| Ground Station Hardware | | $ 240 (w/out decomp) |
| Staff | | $ 600 |
| Antenna | | $ 10 |

First Order Cost Analysis

## Subsystem Level Elements (continued)

### (Costs in thousands of 1991 dollars)

| Subsystem Element | Research and Development | Mission Hardware |
|---|---|---|
| Communications and Data Management: | | |
|     Processing Unit | | $ 550 |
|     Storage | | $ 420 |
| Operations and Production: | | |
|     NASA staff (3 people for 4 yrs) | | $ 160 |
|     Production | | $ 6000 |
|        .6(hardware cost) [11.2] | | |

### 11.3.1    Uncertainty in Cost Breakdown

The purpose of the first order cost analysis is to give a general estimate of the costs over the lifetime of the mission. A degree of uncertainty is always involved in estimates. Cost overruns, schedule restraints and the inherent speculative nature of estimating, will contribute to errors in the cost estimates.

The largest source of uncertainty involves research and development costs. It is impossible to accurately predict the resources and time needed for this type of work. The research and development needed could lead to time and cost overruns.

In the MEDSAT project, the SAR and Visual/Infrared sensors will cause the largest amount of research and development costs. The design of the SAR will include previous design work and 1991 technology. The combination of past and present knowledge will be used to produce a lighter, smaller and less power consuming device than SARs now in production. Many of the design subsystems have yet to be space tested, including the prospective Visual/Infrared sensor. This adaptation to space will also lead to added costs that are difficult to predict.

The integration of known components into a original, coherent system also requires a degree of uncertainty. Due to the experimental nature of the ground station and the fact that it is a prototype, estimates concerning the hardware and staff costs were made based on past experience provided by industry contacts. Because of the unique nature of any ground station, estimates cannot be based on previous designs. The ground station involved in the MEDSAT project will be unique and therefore the total costs are also uncertain.

## 11.4    Cost Justification

To obtain funding for a costly space mission, it is important to be able to demonstrate the anticipated benefits. Such benefits can take two forms. Humanity can be benefitted

through improvements in the quality of living, and science can advance through the development of new technologies. The cost of project MEDSAT can be justified by considering both its future benefits and cost effectiveness.

With over half the world's population living in areas of Malaria risk, the benefits of a project that could help control this disease would be significant. Through the construction of "risk maps" the severity of Malaria outbreaks could be controlled. Based on the success of MEDSAT, the next step will be to create a much larger and more versatile medical satellite. This advanced version could help fight different diseases in many parts of the world through its collection of sensory data.

The MEDSAT satellite will be breaking new ground in the area of compact lightweight remote sensing. Never before has a satellite contained both and SAR and Vis/IR systems. This new technology could be applied to other satellite designs as well. Remote sensors can be used to detect many variable characteristics. Interpretation of resulting data could help control other diseases that threaten different parts of the world. In this way, the technology gained from the MEDSAT project could be used in future endeavors in satellite design.

The design team of the MEDSAT project has made a conscious effort to make this project cost effective. By using the Pegasus launch vehicle, the satellite can be deployed into its predetermined low earth orbit without the high cost of the Space Shuttle (one hundred ninety million dollars) or other high cost launch vehicles. Developed and tested technology was used as much as possible to help eliminate the need for excessive research and development costs. By taking these two courses of action, the cost of the MEDSAT was kept at a minimum. The design team has realized that is very important in these times of economic hardship to propose a project that satisfies the mission goal while being cost effective.

First Order Cost Analysis
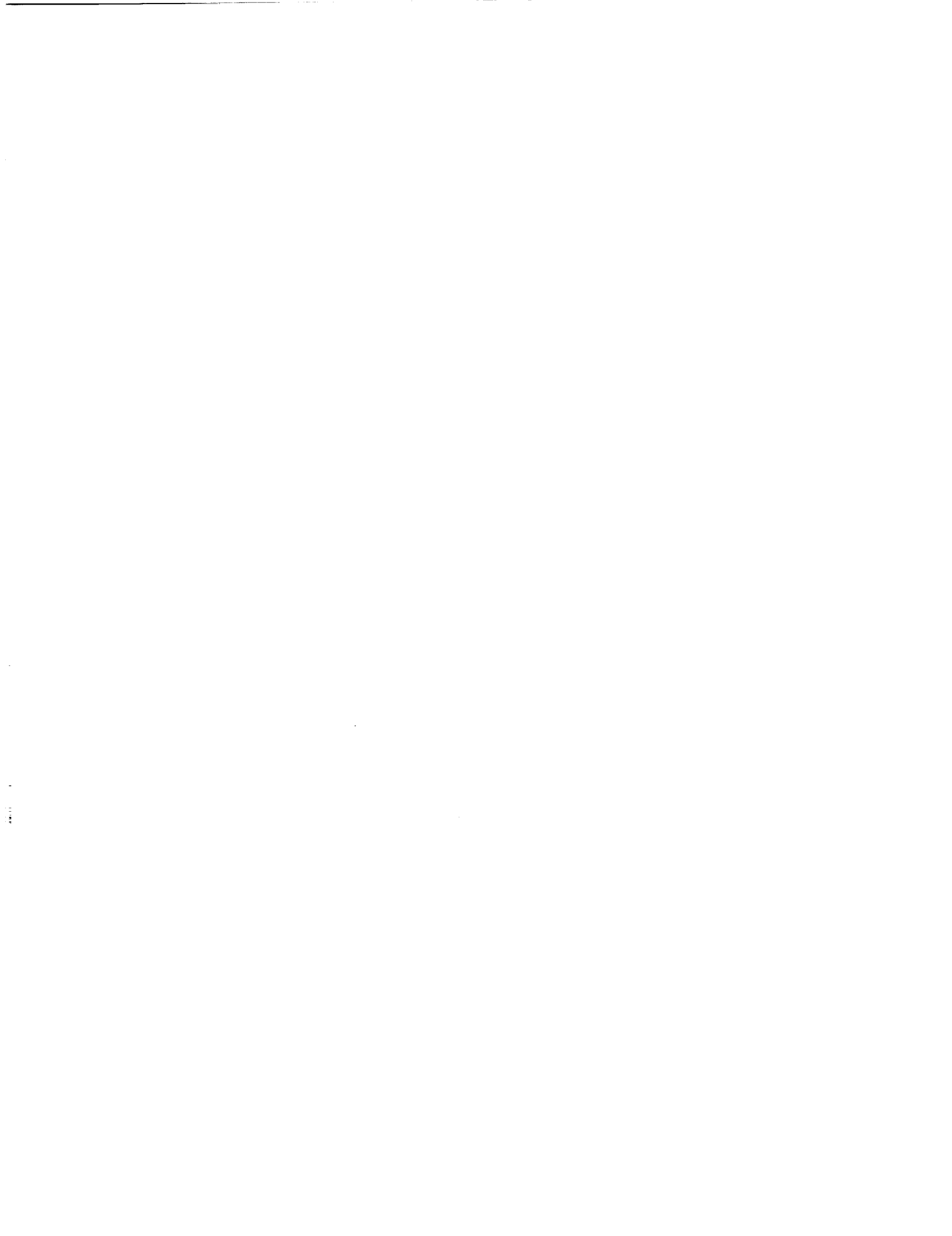
# Chapter 12

# CONCLUSION

12.1 Summary

12.2 Future Research

## 12.1 Summary

From the onset of this project it was a general understanding that NASA was looking to get approval for a medical satellite project in the next couple of years. For this reason the feasibility of MEDSAT was taken very seriously. We determined early on that two factors would make our MEDSAT pre-proposal feasible and attractive to NASA. These factors were the use of a small satellite and making the satellite cost effective. The decision to use a small satellite was seen as important because of the prevailing trend toward the use of small satellites by the space community. This trend is due in part to the flexibility and lower cost of launching a small satellite. The fact that advances in technology have made it possible for small satellites to handle the missions once carried out by larger satellites has also influenced this trend. The choice to use the Orbital Sciences Corporation Pegasus launch vehicle to launch our small satellite was made because of its initial success and its unique and flexible launch method. The use of Pegasus was also in line with our determination to make MEDSAT cost effective. At an average cost of eight million dollars for a launch, the Pegasus provides a reliable and inexpensive means of putting small satellites into low earth orbit. Not only was a cost effective launch vehicle chosen, but the design of the satellite was made to be cost effective as well. This was accomplished by using an "off the shelf" philosophy. We knew that by using proven current technology we could save money over using costly advanced technologies. We deviated from this philosophy only when it was apparent that an advanced system would be needed to meet the size and weight requirements of our small satellite. The synthetic aperture radar and visible/thermal/IR sensors were the two major sub-systems where it was necessary to rely on technology that would be developed within the next decade. All other systems are readily available and will not require costly research and development. We feel that by deciding to use a small satellite with cost effective components and launch capability the MEDSAT pre-proposal provides a very feasible design for a medical satellite. It is hoped that NASA will take our initial ideas and expand them into a working medical satellite that will improve the quality of life for the millions of people affected by malaria and other vector-borne diseases.

## 12.2 Future Research

In order to make possible the design of MEDSAT there are a few areas where advanced research and/or development must take place. While we have proposed the use of a synthetic aperture radar and visible/thermal/IR sensors, these sensors do not exist today in a form that will meet the size and weight requirements of a small satellite. Further reseach and development, which is currently underway, needs to be done to solve this problem within the decade. Another area where further research needs to be done is spacecraft integration. While the major sub-systems have been designed for the satellite, the minor systems and wiring necessary to make the satellite work have not. These areas and others will need to be addressed and researched by NASA.

Conclusion

# REFERENCES

*Chapter 1 -- Introduction*

[1.1]   Asker, J. R., "Technology Spurs Lightsat Activity in Science, Commercial, Military Sectors," *Aviation Week and Space Technology*, Jul. 30, 1990, pp. 76-78.

[1.2]   Gatland, K. W., *The Illustrated Encyclopedia of Space Technology*, 2nd ed., Orion, New York, 1989.

[1.3]   Schade, C., "Pegasus, Taurus, and Glimpses of the Future," Orbital Sciences Corp., Fairfax, VA, AIAA 90-3573, Sept. 1990.


*Chapter 2 -- Ground Segment*

[2.1]   Bailey, N.T.J., *The Biomathematics of Malaria*, Charles Griffen and Company Limited, Bath, 1982.

[2.2]   Cherfas, J., "Malaria Vaccines: The Failed Promise", *Science*, Vol. 247, 1990, pp. 402-403.

[2.3]   American Public Health Association, *Control of Communicable Diseases of Man*, 14th ed., The John D. Lucas Printing Co., 1985.

[2.4]   Foote, R. H., Cook, D.R., *Mosquitoes of Medical Importance*, Agricultural Handbook No. 152, U.S. Government Printing Office, Washington D.C., 1959.

[2.5]   "Status of Malaria Programs in the Americas," *Pan American Health Organization Bulletin*, Vol. 22(1), 1988, pp. 93-103.

[2.6]   World Health Organization, *Manual on Environmental Management for Mosquito Control*, WHO Offset Publication No. 66, Geneva, 1982.

[2.7]   Dirección General de Epidemiología y Dirección General de Medicina Preventiva, "Evolución del Paludismo en México durante 1988. Análisis Epidemiológico," *Paludismo y Otras Enfermedades Transmitidas por Vector*, Vol. 1(1), 1989, pp 1-12.

[2.8]   Benjamin, T., *A Rich Land A Poor People, Politics and Society in Modern Chiapas*, The University of New Mexico Press, 1989.

[2.9]   Dirección General de Epidemiología y Dirección General de Medicina Preventiva, "Situación Epidemiológica del Paludismo en México hasta la Semana Epidemiológica No. 22 de 1989," *Paludismo y Otras Enfermedades Transmitidas por Vector*, Vol. 1(1), 1989, pp 13-19.

[2.10]  Bustamante, M.E., "La Lucha Antipalúdica en el Mundo y en México," *Gaceta Médica de México*, Vol. 110, 1975, pp 389-418.

[2.11]  Fábregas, A., Pohlenz, J., Baez, M., Macías, G., *La Formación Histórica de la Frontera Sur*, 1st ed., Cuadernos de la Casa Chata, Tlalpan, 1985.

[2.12] Ramsey, J.M., Bown, D.N., Aron, J.L., Beaudoin, R.L., Mendez, J.F., "Field Trial in Chiapas, Mexico, of a Rapid Detection Method for Malaria in Anopheline Vectors with Low Infection Rates," *American Journal of Tropical Medicine and Hygiene*, Vol. 35, 1985, pp. 234-238.

[2.13] García, R.H., Hernández, J.P., Rangel, F.A.R., "Frecuencia del Paludismo en Inmigrantes en la Zona Fronteriza de Chiapas," *Revista Médica: Instituto Mexicano del Seguro Social*, Vol. 23, 1985, pp. 255-261.

[2.14] Hoffman, C.C., "Anopheles pseudopunctipennis y su Relación con el Paludismo en la República Mexicana," *Salud Pública de México*, Vol. 31, 1989, pp. 824-831.

[2.15] Carpenter, S.J., LaCasse, W.J., *Mosquitoes of North America*, University of California Press, Berkeley, 1955.

[2.16] Horsfall, W.R., *Mosquitoes, Their Bionomics and Relation to Disease*, The Ronald Press Company, New York, 1955.

[2.17] Warren, M., Collins, W.E., Jeffery, G.M., Skinner, J.C., "The Seroepidemiology of Malaria in Middle America. II. Studies on the Pacific Coast of Costa Rica," *The American Journal of Tropical Medicine and Hygiene*, Vol. 24(5), 1975, pp. 749-754.

[2.18] Morgan L.M., "International Politics and Primary Health Care in Costa Rica," *Social Science and Medicine*, Vol. 30, 1990, pp. 211-219.

[2.19] Beck, L.R., Palchick, S.M., Sebesta, P.D., Washino, R.K, Wood, B.L., "Spectral and Spatial Characterization of Rice Field Mosquito Habitat," NASA document.

[2.20] World Health Organization Division of Malaria and Other Parasitic Diseases, *Manual on Practical Entomology in Malaria: Part I*, WHO Offset Publication No. 13, Geneva, 197.

[2.21] Conversation with Dr. Lew Legter, Uniformed Armed Services University of Health Sciences, on April , 1991.


The following references were not directly cited:

Bhaskara, Vasudev, *GIS-An Image Processing Perspective*, Hewlett Packard Laboratories Technical Report, December, 1990.

Curran, Paul J., *Principles of Remote Sensing*, Chap.6, 1985.

NASA Goddard Space Flight Center, *UARS Project Data Book*, Sec.6, 1987.

Marble, Duane F., Hugh W. Calkins, and Donna J. Peuquet, *Basic Readings in Geographic Information Systems*, SPAD Systems, Ltd., 1984.

Tomlin, C. Dana, *Geographic Information Systems and Cartogrpghic Modeling*, Prentice-Hall, Inc., 1990.

[Mattingly, P.F., *The Biology of Mosquito-Borne Disease*, American Elsevier Publishing Company, Inc., New York, 1969.

*Chapter 3 -- Synthetic Aperture Radar Sensor*

[3-1]   Conversation with Michael DeSandoli, Marketing Manager, MacDonald Dettwiler, April 1, 1991.

[3-2]   Conversations with Craig Dobson, Electrical Engineering and Computer Science Department, University of Michigan, Jan.-Apr. 1991.

[3-3]   Conversations with Stephen L. Durden, Radar Vegetation and Rain Measurement Specialist, California Institute of Technology/Jet Propulsion Laboratory, Feb.-Mar. 1991.

[3-4]   Conversations with William T. K. Johnson, Magellan Radar System Chief Engineer, California Institute of Technology/Jet Propulsion Laboratory, Feb.-Mar. 1991.

[3-5]   Conversations with Rolando Jordan, SIR-C System Engineer, California Institute of Technology/Jet Propulsion Laboratory, Feb.-Mar. 1991.

[3-6]   Conversations with Richard W. Larson, Senior Research Engineer, Environmental Research Institute of Michigan, Jan.-Apr. 1991.

[3-7]   Conversations with Valdis Liepa, Electrical Engineering and Computer Science Department, University of Michigan, Mar.-Apr. 1991.

[3-8]   Conversations with Jack Paris, Department of Geography, California State University--Fresno, Mar. 19, 1991.

[3-9]   Conversations with Robert A. Shuchman, Director, Center for Earth Sciences, Environmental Research Institute of Michigan, Jan.-Apr. 1991.

[3-10]  Conversations with Fawwaz Ulaby, Electrical Engineering and Computer Science Department, University of Michigan, Feb.-Apr. 1991.

[3-11]  Conversation with John Volakis, Electrical Engineering and Computer Science Department, University of Michigan, Mar. 20, 1991.

[3-12]  Conversations with Charles L. Werner, Cassini Radar System Engineer, California Institute of Technology/Jet Propulsion Laboratory, Feb.-Mar. 1991.

[3-13]  Conversations with Byron Wood, TGS Technology Inc., NASA--Ames Research Center, Jan.-Apr. 1991.

[3-14]  Aguttes, J. P., D. Massonnet, O. Grosjean, "A New French Radar System for Earth Resources Monitoring," *IGARSS 1990*, pp. 2085-2088.

[3-15]  Andrewartha, R., L. E. Comtesse, P. C. Harvey, B. E. Richards, "Advanced SAR Design for Multipolarization Operation," *IGARSS 1990*, pp. 2473-2476.

[3-16] Bachman, C. G., *Radar Sensor Engineering*, D. C. Heath and Company, 1982, pp. 3-33 and 74-83.

[3-17] Bender, O., W. Gilg, H. Ottl, "X-Band Synthetic Aperture Radar for Earth Observation Satellites (X-EOS)," *IGARSS 1990*, pp. 2289-2294.

[3-18] Blom, R. G., "Effects of Look Angle and Wavelength in Radar Images for Geologic Applications: Implications for SIR-C and Magellan,"*IGARSS 1988*, pp. 731-739.

[3-19] Brown, M. A., F. G. Sawyer, "Advanced SAR Concepts,"*IGARSS 1988*, pp. 1035-1036.

[3-20] Cantafio, L. J., *Space-Based Radar Handbook*, Norwood, MA: Artech House, Inc., 1989, pp. 122-165 and 516-519.

[3-21] Carpentier, M. H., *Principles of Modern Radar Systems*, Norwood, MA: Artech House, Inc., 1988, pp. 41-43, 191-155 and 255-276.

[3-22] Carver, K., J. Cimino, C. Elachi, "SAR Synthetic Aperture Radar Earth Observing System," NASA Synthetic Aperture Radar Instrument Panel Report, Volume IIf.

[3-23] Cimino, J., A. Bradini, D. Casey, J. Rabassa and S. Wall, "Multiple incidence angle SIR-B experiment over Argentina: Mapping of Forest Units," *IEEE Trans. on Geosc. and Remote Sensing*, Vol. GE-24, No. 4, 1986, pp. 498-509.

[3-24] Cimino, J., C. Elachi, M. Settle, "SIR-B---The Second Shuttle Imaging Radar Experiment," *IEEE Trans. on Geosc. and Remote Sensing*, Vol. GE-24, July 1986, pp. 445-451.

[3-25] Colin, Robert E., *Antennas and Radiowave Propagation*, New York: McGraw-Hill Book Company, 1985, pp.107-159.

[3-26] Coll, E. C., R. G. Pettigrew, "A High Fidelity, High Throughput System for Geocoding SAR Imagery," *IGARSS 1988*, pp. 687-690.

[3-27] Dobson, M. C., and F. T. Ulaby, "Active Microwave Soil Moisture Research," *IEEE Transactions on Geoscience and Remote Sensing*, Vol. GE-24, No. 1, January 1986, pp. 23-35.

[3-28] Dobson, C., K. McDonald, and F. Ulaby. "Using MIMICS to Model L-Band Multi-angle and Multitemporal Backscatter from a Walnut Orchard." *IEEE Transactions on Geoscience and Remote Sensing* , Vol. 28, No. 4, July 1990.

[3-29] Durden, S. L., J. J. van Zyl, H. A. Zebker, "Modeling and observation of the Radar Polarization Signature of Forested Areas," *IEEE Trans. on Geosc. and Remote Sensing*, Vol. 27, No. 3, May 1989, pp. 290-301.

[3-30] Elachi, C., E. Im, L. E. Roth, C. L. Werner, "Cassini Titan Radar Mapper," Submitted to: *Proceedings of the IEEE*, Jan. 10, 1991.

[3-31] Elachi, C., T. Bicknell, R. L. Jordan, and C. Wu, "Spaceborne Synthetic-Aperture Imaging Radars: Applications, Techniques, and Technology," *Proc. IEEE*, Vol. 70, No. 10, Oct. 1982, pp. 1174-1209.

[3-32] Evans, D., C. Elachi, "Overview of the Shuttle Imaging Radar (SIR-C)," *IGARSS 1988*, Vol. 13, No. 16, Sept. 1988.pp.1015-1017.

[3-33] Evans, N., N. Denyer, "User Access and Production Control of Canada's Operational SAR Data Processing Facility," *IGARSS 1989*, pp. 222-225.

[3-34] Ferrazzoli, P., G. Luzi, et al., "Comparison Between the Microwave Emissivity and Backscatter Coefficient of Crops," *IEEE Transactions on Geoscience and Remote Sensing*, Vol. 27, No. 6, November 1989, pp. 772-778.

[3-35] Fitch, J. P., *Synthetic Aperture Radar*, New York: Springer-Verlag New York Inc., 1988, pp. 11-17, 23-30, 57-82 and 131-135.

[3-36] Ford, J. P., R. G. Blom, M. L. Bryan, M. I. Daily, T. H. Dixon, C. Elachi, E. C. Xenos, "Seasat Views North America, the Caribbean, and Western Europe With Imaging Radar," (Jet Propulsion Laboratory) *NASA Report #CR-163825*, Nov. 1, 1980.

[3-37] Hayes, R. O., E. L. Maxwell, et al., "Detection, Identification, and Classification of Mosquito Larval Habitats Using Remote Sensing Scanners in Earth-Orbiting Satellites," *World Health Organization Journal*, 1979, pp. 361-374.

[3-38] Hovanessian, S. A., *Introduction to Sensor Systems*, Norwood, MA: Artech House, Inc., 1988, pp. 6-25 and 88-148.

[3-39] Huneycutt, B. L., "Spaceborne Imaging Radar-C Instrument," *IEEE Transactions on Geoscience and Remote Sensing*, Vol. 27, No. 2, March 1989, pp.164-169.

[3-40] Huneycutt, B.L., T.J. Bicknell, B.M. Holt, C. Wu, "User's Manual for Existing EDIS Data from the SEASAT Synthetic Aperture Radar", JPL Publication, August 1, 1981.

[3-41] Jackson, T. J., and T. J. Schmugge, "Passive Microwave Remote Sensing System for Soil Moisture: Some Supporting Research,"*IEEE Transactions on Geoscience and Remote Sensing*, Vol. 27, No. 2, March 1989, pp. 225-234.

[3-42] Jensen, H., L. C. Graham, L. J. Porcello and E. N. Leith, "Side-Looking Airborne Radar," *Scientific American*, Vol. 237, No. 4, Oct. 1977, pp. 84-98.

[3-43] Johnson, W. T. K., "Radar System Design for the Magellan Radar Mission to Venus," California Institute of Technology/Jet Propulsion Laboratory, (no publishing date).

[3-44] Kasischke, E. S., G. A. Meadows, P. L. Jackson, "The Use of Synthetic Aperture Radar Imagery to Detect Hazards to Navigation," Radar Division of The Environmental Research Institute of Michigan, 1984, Chapter 2.

[3-45] Knott, E. F., Shaeffer, J. F., Tuley, M. T., *Radar Cross Section*, Dedham, MA: Artech House, Inc., 1985, pp. 155-160.

[3-46] Kwok, R., W. T. K. Johnson, "Block Adaptive Quantization of Magellan SAR Data," *IEEE Trans. on Geosc. and Remote Sensing*, Vol. 27, No. 4, July 1989, pp. 375-383.

[3-47] Le Vine, D. M., T. T. Wilheit, Jr., et al., "A Multifrequency Microwave Radiometer of the Future," *IEEE Transactions on Geoscience and Remote Sensing*, Vol. 27, No. 2, March 1989, pp. 193-198.

[3-48] Liu, K. Y, W. E Arens, "Spacecraft On-Board SAR Image Generation for EOS Type Missions," *IEEE Trans. on Geosc. and Remote Sensing*, Vol. 27, No. 2, Mar. 1989, pp. 184-192.

[3-49] Long, M. W., *Radar Reflectivity of Land and Sea*, Dedham, MA: Artech House, Inc., 1983, pp. 34-37, 59, 98-107, 143-169, 211-261 and 313-373.

[3-50] Moore, R. K., *Radar Return from the Ground*, Lawrence, Kansas: School of Engineering, University of Kansas, 1969, pp. 65, 71, and 75.

[3-51] Ott, J. S., E. S. Kasischke, et al., "Preliminary Evaluation of A Multi-Channel SAR Data Set For A Mid-Atlantic Coastal Marsh," *IGARSS 1990*, pp.453-456.

[3-52] Paris, J. F., and H. H. Kwong, "Characterization of Vegetation with Combined Thematic Mapper (TM) and Shuttle Imaging Radar (SIR-B) Image Data," *Photogrammetric Engineering And Remote Sensing*, Vol. 54, No. 8, August 1988, pp. 1187-1193.

[3-53] Pike, T. K., G. Braun, A. J. Knopf, A. P. Wolframm, P. Gudmandsen, J. M. Hermer and P. Wood, "An Advanced SAR for a European Polar Platform," *IGARSS 1990*, Vol. 3, pp. 2459-2462.

[3-54] Sabins, F. F., *Remote Sensing Principles and Interpretation*, San Francisco, CA: W. H. Freeman and Company, 1978, pp. 177-231.

[3-55] Saunders, R. S., G. H. Pettengill, R. E. Arvidson, W. L. Sjogren, W. T. K. Johnson, and L. Pieri, "The Magellan Venus Radar Mapping Mission," *Journal of Geophysical Research*, Vol. 95, No. B6, June 10. 1990, pp. 8339-8355.

[3-56] Sawyer, G., et al., "An Advanced SAR for the European Polar Orbiting Platform," *IGARSS '88*, Vol. 13, No. 16, Sept. 1988.pp.2459-2462.

[3-57] Sheen, D. R., E. S. Kasischke, L. P. Johnston, N. H. F. French, "SAR-Derived Polarimetric Scattering Properties of Terrestrial Ecosystems," *IGARSS 1990*, pp. 1675-1678.

[3-58] Skolnik, M. I., *Introduction to Radar Systems*, McGraw-Hill, Inc., 1980, pp. 18-20, 55-62, 278-310 and 462-466.

[3-59] Skolnik, M. I., *Radar Handbook*, McGraw-Hill, Inc., 1990, pp. 21.1-21.23.

[3-60] Toan, T. L., H. Laur, et al., "Multitemporal and Dual-Polarization Observations of Agricultural Vegetation Covers by X-Band SAR Images,"*IEEE Transactions on Geoscience and Remote Sensing*, Vol. 27, No. 6, November 1989, pp. 709-718.

[3-61] Touzi, R., S. Goze, T. Le Toan, A. Lopes, "Optimization of Polarimetric Discriminators in SAR Images," *IGARSS 1990*, pp. 1683-1686.

[3-62] Ulaby, F., "Introduction to Synthetic Aperture Radar," AOSS 605 Presentation Notes (not published), EECS Department of the University of Michigan, March 13, 1991.

[3-63] University of Michigan, Engineering Summer Conferences, *Principles of Imaging Radars*, Ann Arbor, MI: University of Michigan, College of Engineering, July 20-31, 1970.

[3-64] University of Michigan, Engineering Summer Conferences, *Synthetic Aperture Radar Technology and Applications*, Ann Arbor, MI: University of Michigan, College of Engineering, July 6-10, 1981.

[3-65] Velten, E. H., "X-SAR, A New Spaceborne Synthetic Aperture Radar," *IGARSS '88*, Vol. 13, No. 16, Sept. 1988.pp.1021-1024.

[3-66] Wahl, M., P. Ammendola, "Main Features of the X-SAR Project," *IGARSS '88*, Vol. 13, No. 16, Sept. 1988.pp.1018-1020.

[3-67] Wall, S. D., "The Magellan Mission: High-Resolution Radar Mapping of Venus," *IGARSS 1988*, pp. 729-730.

[3-68] Wang, J. R., E. T. Engman, et al., "The SIR-B Observations of Microwave Backscatter Dependence on Soil Moisture, Surface Roughness, and Vegetation Covers, " *IEEE Transactions on Geoscience and Remote Sensing*, Vol. GE-24, No. 4, July 1986, pp. 510-516.

[3-69] Wehner, D. R., *High Resolution Radar*, Norwood, MA: Artech House, Inc., 1987, pp. 185-271.

[3-70] Werner, C. L., E. Im, "Cassini Radar for Remote Sensing of Titan," *IGARSS 1990*, pp. 2089-2042.

[3-71] Werner, C. L. "Cassini Radar SAR Mode," California Institute of Technology/Jet Propulsion Laboratory, Interoffice Memo (3343-91-11, Rev. 1), (not published) Feb. 11, 1991.

[3-72] Wood, B. L., et al., "Spectral and Spatial Characterization of Rice Field Mosquito Habitat," NASA--Ames Report (not published), Dec. 1990.

[3-73] Zahn, R.W., E. Schmidt, "Advanced Phased-Array Technologies for Spaceborne Applications,"*IGARSS '88*, Vol. 13, No. 16, Sept. 1988.pp.1037-1038.

[3-74] Imhoff, M. L. and D. B. Gesch, "The Derivation of a Sub-Canopy Digital Terrain Model of a Flooded Forest Using Synthetic Aperture Radar,"Photogrammetric Engineering and Remote Sensing," Vol. 56, No.8,August 1990, pp.1155-1162.

[3-75] James, J.R., P.S. Hall, *Handbook of Microstrip Antennas*, London, Peter Peregrinus Ltd., 1989, pp.1112-1148.

C-3

[3-76] Way, J., E. A. Atwood, "The Evolution of Synthetic Aperture Radar Systems and Their Progression to the EOS SAR," California Institute of Technology/Jet Propulsion Laboratory, (submitted to TBD), April 6, 1990.

## Chapter 4 -- Visible and Infrared Sensing

[4-1] U. S. Navy Hydrographic Office, Weather Summary, Mexico, Publication # 532, Washington, D. C., 1949.

[4.2] Direccion General de Geografia del Territory Nacional, Carta de Precipitation Total Anual, 1981.

## Chapter 5 -- Data Management and Processing

[5-1] Elachi, C., Bicknell, T., Jordan, L., Wu, C., "Spaceborne Synthetic-Aperture Imaging Radars: Applications, Techniques, and Technology", Proceedings of the IEEE, Vol 70, No.10, October 1982.

[5-2] Liu,K., Arens,W.,"Spacecraft On-Board Image Generation for Eos-Type Missions", IEEE Transactions on Geoscience and Remote Sensing, Vol 27, No.2, March 1989.

[5-3] Henshaw,R., Ballard,B.W., Hayes,J.R.,Lohr, D.A.,"An Innovative On-Board Processor for Lightsats", Proceedings of the 4th Annual AIAA/USU Conference on Small Satellites, August 27-30, 1990.

[5-4] David K. Campbell,"Drive Issues for High Performance Magneto-optical Recording",IEEE Optical Disk Storage,1987

[5-5] Yoshitom Tsunoda, Masahiro Ojima,"Advanced Technologies for the Next Generation Optical Disks",IEEE Optical Disk Storage, 1987.

[5-6] Conversation with Steve Jurczyk, NASA Langley

[5-7] Conversation with Susan Thim, Sunstrand Data Control Inc.

[5-8] Conversation with Dan Moore, Sunstrand Data Control Inc.

## Chapter 6 -- Communications

[6-1] Space Mission Analysis and Design, James Wertz & Wiley J. Larson (editors), Kluwer Academic Publishers, 1991

[6-2] Design of Geosynchronous Spacecraft, Brij N. Agrawal, Prentice-Hall Inc., 1986

*Chapter 7 -- Mission Analysis*

[7.1]  Schade, C., "Pegasus, Taurus and Glimpses of the Future," *Proceedings of AIAA Space Programs Technologies Conference.* American Institute of Aeronautics and Astronautics 90-3573, pp. 1-5, September 25-28, 1990.

[7.2]  Ball, K.J. and Osborne, G.F., *Space Vehicle Dynamics,* Oxford University Press, London, 1967, pp. 104-105,187-188.

[7.3]  Buning, Harm, *Mission Analysis and Orbital Operations, Aerospace Engineering 542 Course Notes,* Fall 1990.

[7.4]  Wertz, James R. and Larson, Wiley J., ed., *Space Mission Analysis and Design,* Kluwer Academic Publishers, Dordrecht, The Netherlands, 1991.

[7.5]  ORBEL Ground Track Program, Dr. Dave Gell, University of Michigan Space Physics Research Laboratory.


*Chapter 8 -- Spacecraft Structures and Integration*

[8-1]  Dunn, P. and D.A. Reay, Heat Pipes, Pergamon Press Ltd., Oxford, 1976.

[8-2]  Griffin, Michael D. and James R. French, Space Vehicle Design, American Institute of Aeronautics and Astronautics, Inc., Washington D.C., 1991.

[8-3]  Kreith, Frank and Mark S. Bohn, Principles of Heat Transfer Fourth Edition, Harper& Row, New York, 1986.


*Chapter 9 -- Attitude Control*

[9.1]  Wertz, James R., and Larson, Wiley J., ed., Space Mission Analysis and Design, Kluwer Academic Publishers, Boston, MA., 1991, pp. 274, 273

[9.2]  Kearfott Guidance & Navigation Corporation, *High Performance Lightweight Inertial Measurement Unit,* Wayne, N. J.

[9.3]  Auer, S. and Von Burn, F.O., "Low Cost Attitude Sensors for Spacecraft", Applied Research Corporation, *Presented at the AIAA/USU Conference on Small Satellites Aug. 28-31, 1990*

[9.4]  Chetty, P.R.K., Satellite Technology and its Applications, TAB Books Inc., Blue Ridge Summit, PA, 1988

[9.5]  Olin Rocket Research Company, *Hydrazine Handbook,* Redmond, WA

[9.6]  Conversation with Professor Greenwood, Department of Aerospace Engineering, University of Michigan

[9.7]  Conversation with J.J. (Joe) Galbreath, Vice President, Marketing, Olin Rocket Research Company, Defense Systems Group

References

Additional references not cited in text:

"Spacecraft Attitude Control", *TRW Electronics & Defense/ Quest,* Summer 1982,
Volume5, Number 2, pp. 23-49

Stuart, J.R., and Gleave, J., "Key Small Satellite Subsystem Developments, AIAA-90-
3576

Wiesel, William E., Spaceflight Dynamics, McGraw-Hill Book Co., 1989


*Chapter 10 -- Power*

[10.1] NASA "Solar Cell Array Design Handbook" Jet Propulsion Laboratory,
California Institute of Technology, Pasedena California, October 1976

[10.2] "Satellite Technology and Application", P. Ghetty, TAB books

[10.3] Scott, W.R., Rusta, D.W., "Sealed-Cell Nickel-Cadmium Battery Applications
Manual, NASA reference publication 1052, Dec 1979

[10.4] "GaAs Solar Panel ManufacturingExperience", SPECTROLAB, Inc., June 1989

[10.5] Dunbar, R., and Hardman, G., "A Flexible Autonomous Power Management
System for Small Spacecraft", *Proceedings of the 4th Annual Utah State University
Conference on Small Satellites,* 1991.


*Chapter 11 -- First Order Cost Analysis*

[11.1] Wertz, James R., and Larson, Wiley J., (editors) "Cost Modeling", *Space Mission
Analysis and Design,* Kluwer Academic Publishers, Boston, 1991, pp. 657-682.

[11.2] Conversations with Marie Cassidy, Operations Research Analyst, NASA Lewis
Research Center,Cost Analysis, 5 Apr 91 and 15 Apr 91.

[11.3] Conversation with Bryon Wood, NASA Ames, Ground Segment Cost Estimates, 3
Apr 91.

[11.4] Conversation with Chris Schade, Orbital Sciences Corporation, Pegasus systems
support costs, 3 Apr 91.

[11.5] Space Systems Design (Aerospace 483), *Project Kepler* final report, 1987,
pp.191-198.